SOLID STATE PHOSPHATE SENSOR TECHNOLOGIES FOR ENVIRONMENTAL AND MEDICAL DIAGNOSTICS

SOLID STATE PHOSPHATE SENSOR TECHNOLOGIES FOR ENVIRONMENTAL AND MEDICAL DIAGNOSTICS

By VINAY PATEL, B.Tech.

A Thesis Submitted to the School of Graduate Studies in Partial Fulfilment of the Requirements for the Degree Doctor of Philosophy

McMaster University

DOCTOR OF PHILOSOPHY (2022)

Graduate Program in School of Biomedical Engineering

McMaster University, Hamilton, Ontario, Canada.

TITLE:	Solid-state phosphate sensor technologies for environmental and medical diagnostics
AUTHOR:	Vinay Patel
	B.Tech. (Indian Institute of Technology, Kharagpur, India)
SUPERVISOR:	Dr. P. Ravi Selvaganapathy
Pages:	xxi, 218

LAY ABSTRACT

Phosphorus is an essential element for the survival of living beings including humans and plants because it is needed in multiple physiological pathways and functions like cellular signalling, energy storage, metabolism and maintenance. Therefore, phosphate in the human body is strictly regulated and in disease conditions like chronic kidney disease, and metabolic disorders. It can increase or decrease resulting in ailments and worsening of diseases.

Phosphorus is also extensively used in the agricultural field to improve the growth and crop yield. Excess phosphorus from these fertilizers can enter our water sources via agricultural water run-offs leading to the increasing incidences of algal bloom across world.

Current phosphorus measuring systems require chemicals which generates toxic waste, needs manual sample collection and transport, and have narrow measuring ranges. There is an urgent need for sensors which would eliminate the need of sample collection and processing, do not require toxic chemicals and could work over a wide detection range. This study presents two solid-state sensor technologies which would simplify the phosphate detection for both environmental and medical diagnostics samples.

ABSTRACT

Phosphorus is needed by living organism including humans and plants, to survive. Imbalance in phosphate concentration in human body can result in numerous diseases or disorders while excess phosphorus levels in water bodies like lakes, and rivers, are responsible for the rise in incidence of algal bloom across world. Current commercial phosphate monitoring systems are dominated by colorimetric measurements while electrochemical sensors including potentiometric, amperometric and voltammetric sensors are still in the research phase. Electrochemical sensors require stable reference electrodes for reliable measurements that pose challenges for miniaturization.

Solid state potentiometric sensors are widely explored due to their rapid response, easy fabrication and simple electronic measurement system. However, the sensor miniaturization is dependent both on the working and reference electrode. Metal electrodes like cobalt offers advantages such as reagent-free detection, easy to miniaturize but the sensitivity of zero-current potentiometric sensors is limited by the theoretical Nernstian limit and cobalt sensors also require chemical pretreatment in standard solution before measurement.

Here, an *in situ* electrical pretreatment method is proposed to eliminate the need of chemical pretreatment and enhance the sensitivity of cobalt electrodes to -91.4 mV/ decade of phosphate concentration. However, this electrode still needs a reference electrode for reliable measurements.

Therefore, this study has demonstrated a chemiresistive sensing platform for solid state detection of phosphate using both enzyme and enzyme-free methods. A rapid prototyping method was developed to pattern the thin metal films (~100 nm thickness) using a bench top plotter cutter. The method was used to fabricate thin gold film contact electrodes for chemiresistors. The thin gold leaf contact electrodes exhibited low-noise and offered a robust, rapid and reproducible manufacturing process for chemiresistors. The chemiresistive sensor showed a wide measuring

range (0.5 ppm to 500 ppm) for hydrogen peroxide detection. The sensor was deposited with glucose oxidase to demonstrate the application of the sensor for peroxidase assays to detect glucose in standard buffer solution and human pooled plasma. Phosphate also is detected using pyruvate oxidase in presence of pyruvate to generate hydrogen peroxide as the detectable molecule. Finally, metal phthalocyanines were used to perform enzyme-free phosphate measurements.

This work demonstrated the sensor technologies which could be used for in-field phosphate monitoring to prevent algal bloom and it also provides phosphate monitoring methods for rapid detection in medical diagnostics for early diagnosis for diseases like chronic kidney disease and to improve the patient's outcomes for such diseases.

ACKNOWLEDGEMENT

I want to start with acknowledging the freedom and immense support provided my supervisor Dr Ravi Selvaganapathy throughout my PhD in multiple methods like polishing my ideas, allowing me to explore various projects and attending multiple conferences. I am grateful to you for being so patient and listening all my ideas and giving them due consideration throughout my PhD.

I am also grateful to Dr Peter Kruse and Dr Qiyin Fang for taking their time and guidance on my research. The constant through various has helped me throughout to think in different directions for my research.

I want to thank my family and friends, my father, mother and brother to be the strong support throughout my life. I can never thank you enough for the sacrifices you all have made to make me what I am today.

Finally, a big thanks to all my lab members starting with Nidhi, Sreekant, Rong, Fathalla, Islam, Neda, Shadi, Aydin, Mehraneh, Anand, Alireza, Sneha, Maedeh, Panashe and Hareshan for adding colors to my PhD life. I also want to thank our collaborators from Dr Peter Kruse's group, Dipankar, Ali, Maryam, Johnson, and Shayan for providing their support throughout my work.

TABLE OF CONTENTS

LIST OF FIGURES AND TABLES

LIST OF ALL ABBREVIATIONS AND SYMBOLS

LOD	Limit of Detection
EPA	Environmental Protection Agency
Mo	Molybdenum
MWCNT	Multiwalled Carbon Nanotube
SWCNT	Single walled Carbon Nanotube
DI water	Deionized water
Ag/AgCl	Silver-silver chloride
RSD	Relative Standard Deviation
K_{sp}	Solubility coefficient
PyOD	Pyruvate oxidase
PNP	Purine Nucleoside Phosphorylase
XOD	Xanthine oxidase
WE	Working electrode
RE	Reference electrode
CE	Counter electrode
SS	Stainless steel
SEM	Scanning Electro Microscopy
EIS	Electrochemical Impedance Spectroscopy
OCP	Open Circuit Potential
CV	Cyclic Voltammetry
XPS	X-ray photoelectron spectroscopy
CPE	Constant Phase Element
EDX	Energy Dispersive X-ray spectroscopy
LW	Line Width
GLC	Graphene like Carbon
PCAT	Phenyl-capped aniline tetramer

PTFE	Polytetrafluoroethylene
SAM	Self Assembled Monolayer
GA	Gluconic Acid
Glu	Glucose
UA	Uric acid

DECLARATION OF ACADEMIC ACHIEVEMENT

Vinay Patel contributed to the ideation, literature search, writing, experimental design, performing experiments, data analysis, results interpretations and creating figures for all the chapters of this thesis.

P. Ravi Selvaganapathy contributed to experimental design, data interpretation and revision of all the chapters of the thesis.

Peter Kruse contributed to data interpretation and revision of Chapter 4 and 5 of the thesis.

Dipankar Saha contributed to the Raman spectral measurements in Chapter 5.

Chapter 1

Preface

1. Introduction

Phosphate is a crucial molecule for living organisms to survive as it is a major constituent for various molecules like DNA, ATP etc. It is used extensively in agricultural fields as fertilizers to increase crop yields. Excess phosphorus from agricultural fields drains into water bodies resulting in increased algal bloom incidences across globe. Algal bloom can pose serious risk to the potable water supply and aquatic life present in the water body. Blooms puts an additional burden on the water supply due to requirement of additional purification steps to remove the potential harmful algal toxins. According to the U.S. Environmental Protection Agency (USEPA) 1986, the maximum permissible limit for phosphate in streams which do not empty into reservoirs is 0.1 mg/l (1.05×10^{-6} M), streams discharging into reservoirs is 0.05 mg/l (5.2×10^{-7} M) and reservoirs is 0.025 mg/l (2.6×10^{-7} M) [1]. Phosphorus discharge sources can be divided into two categories: point sources like wastewater treatment plants, and non-point sources like agricultural run-offs from fields. Frequent monitoring on point sources like municipal wastewater treatment plants and industrial wastewater treatment plants, would help to curb the rising levels of phosphate in the water bodies.

Phosphate is also essential for human survival. It is found mainly in skeleton (~85%) and soft tissues (~10-15%) [2]. It plays a crucial role in a variety of functions including metabolism, cellular signalling, energy storage and membrane transport [2,3]. The normal physiological serum phosphate concentration for adults is between 25 to 54 mg/l while for neonates, infants and children, it is between 37 to 82 mg/l depending on the age [2]. The normal physiological phosphate

levels are maintained by intestinal absorption, release and absorption from bone and renal excretion [3]. A decrease in kidney function results in high phosphate levels (hyperphosphatemia) in blood. Abnormal phosphate levels can result in various ailments like muscular functional impairments, cardiovascular diseases, chronic kidney diseases (CKD) and skeletal abnormalities [2,3]. Studies have shown that humans with high phosphate levels are prone to vascular calcifications resulting in increased morbidity and mortality. Low phosphate levels (hypophosphatemia) are observed in people with metabolic disorders of minerals. Hypophosphatemia affects the skeletal system, myocardium, respiratory system and nervous system because phosphate is involved in multiple physiological pathways and maintenance of several organs [2]. Humans receive phosphorus from food sources in the form of phosphates and phosphate esters. Phosphate and calcium levels in blood are related to each other, and their homeostasis is regulated by bones, kidneys and intestines. In chronic kidney disease, the phosphate levels in blood are increased due to reduced excretion of phosphate and it is related to increased mortality in end-stage chronic kidney disease [4]. Majority of the patients remains asymptomatic until the later stages of chronic kidney disease [5]. A quick and hassle-free test would enable frequent testing of phosphate leading to early detection of the ailment. Besides, it would also improve the quality of patient's life and efficacy of the interventions for CKD patients [5]. Phosphate can be measured in both plasma and serum.

Current methods for phosphate monitoring include colorimetry and electrochemical. Current commercial phosphate monitoring systems (laboratory and online monitoring systems) are based on colorimetry. This method uses color change due to molybdenum blue or vanadate/molybdate yellow in presence of phosphate under acidic conditions. Molybdenum blue method is the USEPA recommended method for orthophosphate testing. The process involves reaction of ammonium

molybdate and antimony potassium tartrate in acidic medium to generate antimony-phosphomolybdate complex which was reduced to blue color in presence of ascorbic acid. The working range of the method is 0.01 to 1.2 mg/l (P in phosphate) [6]. Colorimetric methods provide accurate measurements with good resolution within a narrow measuring range of 0.1 to 10 mg/l but it requires low pH for the formation of phosphomolybdate complex. These methods require toxic reagents, laboratory settings, sample preparation, sophisticated instruments, and skilled personnel for operation. Therefore, a reagent-free phosphate sensor is needed which could work over a wide measuring range and is simple to operate with low-cost instruments.

Electrochemical sensors offer lower cost and simple instrumentation for detection. Conventionally, electrochemical phosphate sensing was performed using amperometry, voltammetry or potentiometry. Amperometric sensors can provide low limit of detection (2×10^{-8} M) and simple fabrication processes, but these sensors require multiple enzymes [7,8] or formation of complexes like phosphomolybdic acid which requires low pH (~1-2) [9–11] or highly basic media (pH ~13) for indirect measurement of phosphate using $Ni(OH)_2$/NiO(OH) substrate [12]. Similarly, voltammetric sensing was performed by reducing the phosphomolybdate complex [13–15] or using metal electrodes [16–18]. Phosphomolybdate based electrodes can measure in sub micromolar range but these methods require operations at low pH [13,15]. Molybdenum electrode was used for phosphate detection using square wave voltammetry. The oxidized molybdenum forms a phosphomolybdate complex similar to colorimetric methods in presence of phosphate. However, it requires multiple solution compartments, one with a low pH for molybdenum oxidation and other compartment for measurement. [17]. Multiple metal based voltammetric arrays were also used to measure phosphate in bioreactors and wastewater samples [18,19].

However, this method requires multiple electrodes, needs a reliable training data set for accurate prediction of concentrations and works within a narrow working range (0.54-7.3 mg/l).

Potentiometric sensors use two different approaches: one using membrane-based electrodes and another using metal/metal oxide electrodes. Membrane based electrodes are selective due to the presence of a molecule which selectively binds to the analyte of interest. These molecules are known as ionophores. Multiple ionophores have been synthesized over the years for these electrodes including various organotin complexes [20], cyclic polyamine [21] and others complexes [22–24] but these electrodes suffer from poor selectivity due to the large size of the phosphate ion and lower free energy of hydration as compared to other oxoanions [20]. Also, the sensitivity of the ion selective membrane electrodes are within a range from -28 mV/decade to -55.7 mV/decade [20–25].

Metal/metal oxide electrodes based on different metals including silver [26], cobalt [27], molybdenum [28] and tungsten [29] have been used for phosphate measurement. Cobalt is a widely used electrode for phosphate sensing due to a rapid response and low drift. However, these electrodes require conditioning in standard solution for times that vary from 5 minutes for microelectrodes to greater than 2 hours for wire electrodes and need a buffered solution (pH~4) for measurements [27]. Further, multiple studies have used cobalt oxide electrodes for non-enzymatic glucose sensing under basic pH conditions [30–32]. Glucose present in blood or serum samples could directly impact the conversion of cobalt (II, III) oxide to cobalt (IV) oxide in alkaline solutions [31]. The blood glucose concentration (3-6 mM) while the serum phosphate levels lie between 0.25 mM to 0.5 mM (2.5 – 5.4 mg/dl). So, glucose can be a potential interference for phosphate measurement with cobalt-based electrodes. Hence, a new sensing platform is needed for detection of phosphate in blood or plasma.

An ideal sensor for *in situ* phosphate measurement should perform chemical free measurements with good specificity and selectivity, along with a wide range of detection (100 to 0.01 µM) to measure phosphate in different real water samples using the same instrument. This would eliminate the need of solution processing before measurement. Finally, the sensor should have a sub micro molar limit of detection in real samples like wastewater, surface water and tap water because the phosphate concentrations in real sample like river water and larger water bodies could be less 10^{-6} M .

2. Motivation

Colorimetric monitoring systems work in a narrow measurement range and require chemicals (like ammonium molybdate, sulphuric acid and reducing agents) for phosphate detection. Electrochemical sensors (amperometric, voltammetric and potentiometric) offer an alternative for chemical-free detection. However, both amperometric and voltammetric sensors, which rely on phosphomolybdate complex require low pH while other sensors either require high pH values or their response is affected by common interferents. Potentiometric sensors provide an alternate method for chemical-free phosphate detection, but membrane based potentiometric sensors are less selective while the cobalt-based metal electrodes have low sensitivity and require a conditioning solution before measurement. Also, the sensitivity of the potentiometric sensors is limited by the Nernst equation. Therefore, there is a need to eliminate the standard solution conditioning of cobalt sensors and also enhance the sensitivity of these sensors beyond the Nernstian limit. Glucose present in blood or serum samples could affect the phosphate measurements. Further, the phosphate measurement in medical diagnostics samples also require measurement within a narrow range of phosphate concentrations 0.25 mM to 0.5 mM (2.5 – 5.4 mg/dl) which might not be suitable for the sensitivity of cobalt-based sensors.

This thesis custom designed solid-state sensor technologies for phosphate monitoring in environmental and medical diagnostics samples. Since the design requirements are different for these applications, two different approaches are used that are well suited to the need of respective applications. The first method enhances the sensitivity of the current cobalt-based sensors using an electrical pretreatment method. The electrical pretreatment method also eliminates the need of standard solutions for sensor conditioning before measurements. The second sensing platform uses chemiresistive sensors to demonstrate a solid-state reagentless sensing electrode to measure phosphate in blood and plasma samples. Here, a low-cost sensor fabrication method was developed to manufacture low noise contact electrodes for chemiresistive sensors. A chemiresistive H_2O_2 sensor was developed to measure biomolecules like phosphate, glucose and galactose, in human plasma using various peroxidase enzymes. Finally, a non-enzymatic chemiresistive sensor was used to detect phosphate in environment samples.

3. Research Objectives

The present study aims to develop a solid-state monitoring system to measure phosphate in environmental and medical diagnostics samples. The study would demonstrate a proof-of-concept based on the following objectives:

Objective 1: Enhance the sensitivity of the metal-based solid state electrode for phosphate monitoring in environmental samples.

Objective 2: Establish a low-cost manufacturing method for electrical contact electrodes to fabricate chemiresistive electrode

Objective 3: Demonstrate a chemiresistive sensor to measure the phosphate concentration in medical diagnostics samples

(a) An electropolymerized self assembled monolayer for detection of hydrogen peroxide in plasma samples and its application in enzyme-based peroxidase sensing.

(b) A proof of concept for reagent-free phosphate detection using metal phthalocyanines.

4. Thesis outline

This thesis includes 7 chapters, and the main results are summarized in 4 journal papers. Chapter 1 includes a general overview of thesis, brief introduction to phosphate sensing, motivation and research objectives. The latter chapters are summarized below.

Chapter 2 includes detailed literature review of phosphate sensing in both environmental and medical diagnostics samples. The chapter is organized in two parts. The first part is focused on potentiometric phosphate sensing and the second part is focused on chemiresistive sensing and its use in phosphate sensing. The first part of the chapter begins with a description of zero current potentiometric and current based potentiometric methods. Then the sensing mechanism of cobalt -based electrodes are briefly discussed in detail followed by a summary of issues with current cobalt electrodes. The second part of the chapter discusses a brief overview of chemiresistive sensors and how these sensors can be used for phosphate sensing in blood or plasma.

Chapter 3 introduces an *in situ* electrical pretreatment method which is directly used in the sample to enhance the sensitivity of the cobalt-based phosphate sensor. The electrical pretreatment eliminates the need for chemical pretreatment before the measurement. No significant interference was observed for the common interferents present in water like nitrates, sulfates and chlorides. The sensor was tested with real water samples including tap water, lake water and creek water spiked with different phosphate concentrations. Sensor exhibited a good phosphate recovery for

the real water samples. The enhanced sensitivity enables phosphate sensing with cobalt based electrodes in real water samples.

Chapter 4 presents a low-cost xurography method for rapid prototyping to pattern thin metal films. The process was used to manufacture thin conductive metal films on non-conductive polymer surfaces like polyethylene terephthalate and polyester shrink films. The process was able to generate reliable patterns with a line width of 80 ± 5 µm and pitch of 92 ± 2 µm with 24K gold leaf. Five different metal leaves including silver, gold, copper, aluminum, and palladium, were used in the study to demonstrate the versatility of the process. Finally, the gold metal electrodes were fabricated for different applications like low noise contact electrodes for chemiresistive sensors with low and high surface roughness, electrochemical sensors and high surface are 3D electrodes.

Chapter 5 utilizes the low-cost xurography process developed in Chapter 4 to fabricate low noise chemiresistive sensor for hydrogen peroxide (H_2O_2) measurement. The sensors were fabricated using functionalized carbon nanotube as sensing electrode and patterned 24 K gold leaf as contact electrode. The sensing electrode was functionalized with an electropolymerized self assembled monolayer of crystal violet for selective H_2O_2 detection. The sensor exhibited a wide detection range of 0.5 to 1000 ppm H_2O_2, and no significant interference were observed for common interferents present in blood like glucose, galactose, uric acid and urea. The H_2O_2 sensors were tested with different peroxidase enzymes like glucose oxidase, to demonstrate its application for sensing molecules like glucose in human plasma.

Chapter 6 presents the proof-of-concept for a solid-state reagent-free chemiresistive sensor for phosphate detection in water. Here, the knowledge gained from the previous two sensing methods was combined to fabricate a reagent-free chemiresistive sensor with cobalt phthalocyanines for

phosphate detection. The sensor exhibited a stable response from 10^{-4} M to 10^{-2} M dihydrogen phosphate concentrations.

Chapter 7 summarizes the research contributions presented in this thesis along with the limitations of the work. Finally, a few recommendations of future work were also discussed.

References

[1] D.W. Litke, Review of Phosphorus Control Measures in the United States and Their Effects on Water Quality, Water-Resources Investig. Rep. 99-4007. (1999) 1–38. http://www.msue.msu.edu/waterqual/WQWEB/ReviewPUSGS.pdf.

[2] P. Florenzano, C. Cipriani, K.L. Roszko, S. Fukumoto, M.T. Collins, S. Minisola, J. Pepe, Approach to patients with hypophosphataemia, Lancet Diabetes Endocrinol. 8 (2020) 163–174. https://doi.org/10.1016/S2213-8587(19)30426-7.

[3] H. Komaba, M. Fukagawa, Phosphate—a poison for humans?, Kidney Int. 90 (2016) 753–763. https://doi.org/10.1016/j.kint.2016.03.039.

[4] Y. Hou, X. Li, L. Sun, Z. Qu, L. Jiang, Y. Du, Phosphorus and mortality risk in end-stage renal disease: A meta-analysis, Clin. Chim. Acta. 474 (2017) 108–113. https://doi.org/10.1016/j.cca.2017.09.005.

[5] Y.N.V. Reddy, V. Sundaram, G. Abraham, P. Nagarajan, Y.N.V. Reddy, Optimal management of hyperphosphatemia in end-stage renal disease: An Indian perspective, Int. J. Nephrol. Renovasc. Dis. 7 (2014) 391–399. https://doi.org/10.2147/IJNRD.S49933.

[6] U.S. Environmental Protection Agency, Method 365.3: Phosphorous, All Forms (Colorimetric, Ascorbic Acid, Two Reagent), Method 365.3. (1978) 3–7.

[7] L. Gilbert, A.T.A. Jenkins, S. Browning, J.P. Hart, Development of an amperometric,

screen-printed, single-enzyme phosphate ion biosensor and its application to the analysis of biomedical and environmental samples, Sensors Actuators, B Chem. 160 (2011) 1322–1327. https://doi.org/10.1016/j.snb.2011.09.069.

[8] G. Kopiec, K. Starzec, J. Kochana, T.P. Kinnunen-Skidmore, W. Schuhmann, W.H. Campbell, A. Ruff, N. Plumeré, Bioelectrocatalytic and electrochemical cascade for phosphate sensing with up to 6 electrons per analyte molecule, Biosens. Bioelectron. 117 (2018) 501–507. https://doi.org/10.1016/j.bios.2018.06.047.

[9] S. Cinti, D. Talarico, G. Palleschi, D. Moscone, F. Arduini, Novel reagentless paper-based screen-printed electrochemical sensor to detect phosphate, Anal. Chim. Acta. 919 (2016) 78–84. https://doi.org/10.1016/j.aca.2016.03.011.

[10] Y. Lu, Q. Lan, C. Zhang, B. Liu, X. Wang, X. Xu, X. Liang, Trace-Level Sensing of Phosphate for Natural Soils by a Nano-Screen-Printed Electrode, Environ. Sci. Technol. (2021). https://doi.org/10.1021/acs.est.1c05363.

[11] Y. Lu, X. Li, D. Li, R.G. Compton, Amperometric Environmental Phosphate Sensors, ACS Sensors. 6 (2021) 3284–3294. https://doi.org/10.1021/acssensors.1c01035.

[12] W.L. Cheng, J.W. Sue, W.C. Chen, J.L. Chang, J.M. Zen, Activated nickel platform for electrochemical sensing of phosphate, Anal. Chem. 82 (2010) 1157–1161. https://doi.org/10.1021/ac9025253.

[13] A. V. Kolliopoulos, D.K. Kampouris, C.E. Banks, Rapid and portable electrochemical quantification of phosphorus, Anal. Chem. 87 (2015) 4269–4274. https://doi.org/10.1021/ac504602a.

[14] M.T. Rahman, M.F. Kabir, Q. Qiao, Electrochemical Phosphate Sensors Using Silver Nanowires Treated Screen Printed Electrodes, IEEE Int. Conf. Electro Inf. Technol. 2018-May (2018) 993–997. https://doi.org/10.1109/EIT.2018.8500195.

[15] R. Zeitoun, A. Biswas, Instant and Mobile Electrochemical Quantification of Inorganic Phosphorus in Soil Extracts, J. Electrochem. Soc. 167 (2020) 167512. https://doi.org/10.1149/1945-7111/abcbaf.

[16] A. Prasad, S.P. Sahu, S.K. Figueiredo Stofela, A. Chaichi, S.M.A. Hasan, W. Bam, K. Maiti, K.M. McPeak, G.L. Liu, M.R. Gartia, Printed Electrode for Measuring Phosphate in Environmental Water, ACS Omega. 6 (2021) 11297–11306. https://doi.org/10.1021/acsomega.1c00132.

[17] C. Barus, I. Romanytsia, N. Striebig, V. Garçon, Toward an in situ phosphate sensor in seawater using Square Wave Voltammetry, Talanta. 160 (2016) 417–424. https://doi.org/10.1016/j.talanta.2016.07.057.

[18] I. Campos, M. Alcañiz, D. Aguado, R. Barat, J. Ferrer, L. Gil, M. Marrakchi, R. Martínez-Mañez, J. Soto, J.L. Vivancos, A voltammetric electronic tongue as tool for water quality monitoring in wastewater treatment plants, Water Res. 46 (2012) 2605–2614. https://doi.org/10.1016/j.watres.2012.02.029.

[19] D. Aguado, R. Barat, J. Soto, R. Martínez-Mañez, Monitoring dissolved orthophosphate in a struvite precipitation reactor with a voltammetric electronic tongue, Talanta. 159 (2016) 80–86. https://doi.org/10.1016/j.talanta.2016.06.002.

[20] J.K. Tsagatakis, N.A. Chaniotakis, K. Jurkschat, Multiorganyltin Compounds. Designing a novel phosphate-selective carrier, Helv. Chim. Acta. 77 (1994) 2191–2196.

https://doi.org/10.1002/hlca.19940770812.

[21] C.M. Carey, W.B. Riggan, Cyclic Polyamine Ionophore for Use in a Dibasic Phosphate-Selective Electrode, Anal. Chem. 66 (1994) 3587–3591. https://doi.org/10.1021/ac00093a009.

[22] W. Wróblewski, K. Wojciechowski, A. Dybko, Z. Brzózka, R.J.M. Egberink, B.H.M. Snellink-Ruël, D.N. Reinhoudt, Uranyl salophenes as ionophores for phosphate-selective electrodes, Sensors Actuators, B Chem. 68 (2000) 313–318. https://doi.org/10.1016/S0925-4005(00)00450-0.

[23] M.R. Ganjali, P. Norouzi, M. Ghomi, M. Salavati-Niasari, Highly selective and sensitive monohydrogen phosphate membrane sensor based on molybdenum acetylacetonate, Anal. Chim. Acta. 567 (2006) 196–201. https://doi.org/10.1016/j.aca.2006.03.026.

[24] J. Kim, D.M. Kang, S.C. Shin, M.Y. Choi, J. Kim, S.S. Lee, J.S. Kim, Functional polyterthiophene-appended uranyl-salophen complex: Electropolymerization and ion-selective response for monohydrogen phosphate, Anal. Chim. Acta. 614 (2008) 85–92. https://doi.org/10.1016/j.aca.2008.03.008.

[25] H. Jiang, M.A. Ali, Y. Jiao, B. Yang, L. Dong, In-situ, real-time monitoring of nutrient uptake on plant chip integrated with nutrient sensor, TRANSDUCERS 2017 - 19th Int. Conf. Solid-State Sensors, Actuators Microsystems. (2017) 289–292. https://doi.org/10.1109/TRANSDUCERS.2017.7994045.

[26] I. Vermes, E.W. Grabner, A phosphate sensor based on silver phosphate-modified electrodes, J. Electroanal. Chem. 284 (1990) 315–321. https://doi.org/10.1016/0022-0728(90)85041-3.

[27] D. Xiao, H.Y. Yuan, J. Li, R.Q. Yu, Surface-Modified Cobalt-Based Sensor as a Phosphate-Sensitive Electrode, Anal. Chem. 67 (1995) 288–291. https://doi.org/10.1021/ac00098a009.

[28] Y. Li, T. Jiang, X. Yu, H. Yang, Phosphate Sensor Using Molybdenum, J. Electrochem. Soc. 163 (2016) B479–B484. https://doi.org/10.1149/2.0161609jes.

[29] G. Chen, S. Xiao, A. Lorke, J. Liu, P. Zhang, Assessment of a Solid-State Phosphate Selective Electrode Based on Tungsten, J. Electrochem. Soc. 165 (2018) B787–B794. https://doi.org/10.1149/2.0101816jes.

[30] L. Zhang, N. Wang, P. Cao, M. Lin, L. Xu, H. Ma, Electrochemical non-enzymatic glucose sensor using ionic liquid incorporated cobalt-based metal-organic framework, Microchem. J. 159 (2020) 105343. https://doi.org/10.1016/j.microc.2020.105343.

[31] Y. Ding, Y. Wang, L. Su, M. Bellagamba, H. Zhang, Y. Lei, Electrospun Co3O4 nanofibers for sensitive and selective glucose detection, Biosens. Bioelectron. 26 (2010) 542–548. https://doi.org/10.1016/j.bios.2010.07.050.

[32] K.K. Lee, P.Y. Loh, C.H. Sow, W.S. Chin, CoOOH nanosheets on cobalt substrate as a non-enzymatic glucose sensor, Electrochem. Commun. 20 (2012) 128–132. https://doi.org/10.1016/j.elecom.2012.04.012.

Chapter 2

Background

1. Introduction

Phosphorus is an essential nutrient for plants and humans. Humans receive phosphorus from food sources, and it is applied in the form of fertilizers in agricultural fields. Phosphate is found in multiple forms in nature including orthophosphates, polyphosphates and organophosphates. Therefore, phosphate is sensed as two parameters: total phosphorus and orthophosphates (soluble reactive phosphorus). Orthophosphates represent the dissolved form of the phosphorus while total phosphorus includes solution phosphorus, and organic phosphorus. For instance, total phosphorus in natural water samples can include orthophosphates and phosphorus present in different organic fragments present in the samples. In this chapter, the term phosphate is used to represent orthophosphates. Orthophosphates can be present in three forms, dihydrogen phosphate ($H_2PO_4^-$), monohydrogen phosphate (HPO_4^{2-}) and phosphate ions (PO_4^{3-}) depending on the pH (Figure 2.1). The equilibrium reaction are as follows (Reaction 1-3):

$$H_3PO_4 \leftrightarrow H^+ + H_2PO_4^- \qquad (pK_a = 2.12) \qquad (1)$$

$$H_2PO_4^- \leftrightarrow H^+ + HPO_4^{2-} \qquad (pK_a = 7.21) \qquad (2)$$

$$HPO_4^- \leftrightarrow H^+ + PO_4^{3-} \qquad (pK_a = 12.67) \qquad (3)$$

Below pH 4, dihydrogen phosphate is the dominant species while both $H_2PO_4^-$ and HPO_4^{2-} are present at near neutral pH.

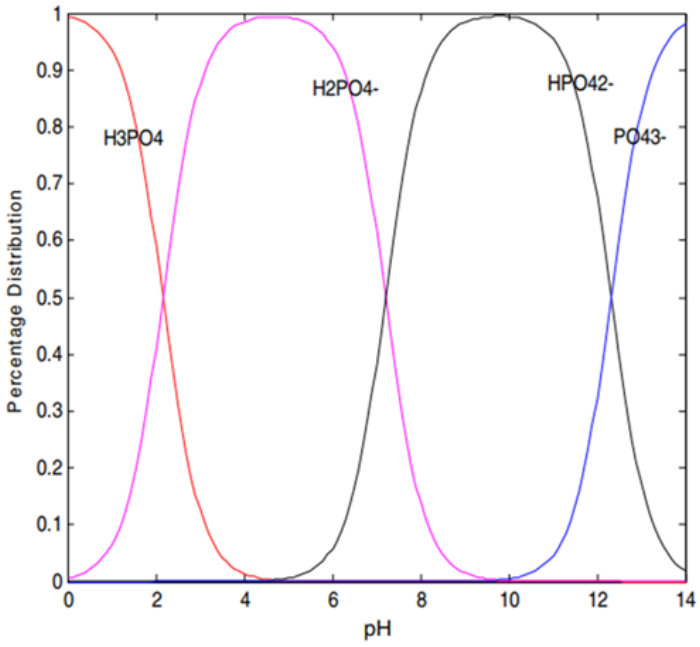

Figure 2.1 Percentage distribution of phosphate species across pH range from 0 to 14. [Adapted from [1]]

In the human body, the phosphorus is mainly present in bones (~85%) in the form of hydroxyapatite and ~10-15% in muscles associated with proteins, lipids and carbohydrates. The remaining small amount is distributed in extracellular and intracellular fluids. The total phosphate present in blood plasma is found in three forms: orthophosphates, phospholipids and phosphates bound to organic compounds [2]. The orthophosphates present dihydrogen and monohydrogen phosphates due to physiological pH (7.35 to 7.45).

An overview of phosphate sensing including the recognition elements, transducing principles and sample matrices is shown in Figure 2.2. An ideal phosphate sensor for both medical diagnostics and environment should work at near neutral pH, sensitive to both dihydrogen and monohydrogen phosphates, suitable for *in situ* monitoring, and non-sensitive to environmental conditions like pH, temperature, and dissolved oxygen.

Solid-state sensors are ideal for *in situ* monitoring for both environmental and medical diagnostics because these sensors use minimal or no reagents, require less maintenance, and are easy to miniaturize. Phosphate sensors can be broadly classified into two categories: optical and electrochemical (Figure 2). Optical sensors are widely used for phosphate sensing in commercial applications while electrochemical sensors are still in research phase.

The focus of this chapter is to critically analyze solid-state phosphate sensors. These sensors offer simple instrumentation, low-cost and rapid detection for phosphate measurements in low resource settings. The sensors are analyzed based on parameters such as measuring range, limit of detection (LOD), sensitivity and storage stability. The last section discusses few insights into the shortcomings and future research directions of solid-state sensors.

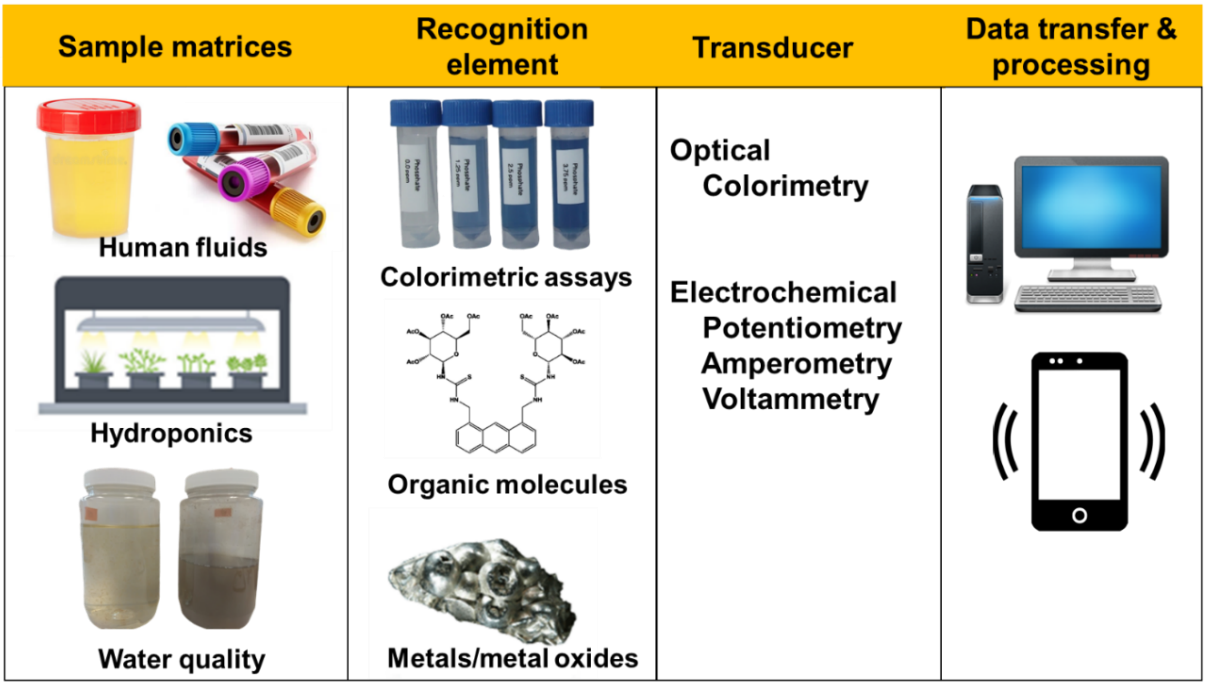

Figure 2.2 An overview of phosphate monitoring system with possible real sample matrices such as human fluids like urine, blood, and sweat, controlled agricultural system like hydroponics, and environmental samples like surface water, tap water and wastewater; recognition elements like colored dyes for

colorimetric assays, organic molecules and metal/metal oxides which selectively reacts phosphate; these changes are detected using readable signals which are transduced using transducers, then data is transferred and processed using microprocessors present in computers, mobiles etc.

2. Solid state colorimetric sensing

Colorimetric methods use two main approaches, molybdenum blue and vanadate molybdate yellow. The first approach relies on the reaction of phosphates and molybdenum in acidic medium to generate 12-molybdophosphoric acid (Reaction 4). 12-Molybdophosphoric acid in presence of reducing agents like ascorbic acid, is converted to phosphomolybdate blue (Reaction 5) which is detected using spectrophotometer at 700 or 880 nm [3].

$$H_3PO_4 + 12\ MoO_4^{2-} + 24\ H^+ \rightarrow H_3PO_4(MoO_3)_{12} + 12\ H_2O \quad (4)$$

$$H_3PO_4(MoO_3)_{12} + \text{reductant} \rightarrow [H_4PMo\ (VI)_8Mo(V)_4O_{40}]^{3-} \quad (5)$$

The phosphomolybdate blue with ascorbic acid as reducing agent is the recommended method for phosphate measurements in water samples by the Environmental Protection Agency (EPA). Phosphomolybdate blue method suffers interference from arsenate and silicate. It can also be affected in presence of sulphide, iron and fluoride [4]. The method also requires low pH (~0-1) to generate stable reduced product. A later study proposed the use of potassium tartrate to enhance rate of reaction, reduce the interference from silicate and eliminate the need of heating for formation of a stable reaction product [3]. Sulphuric acid is the preferred acid used to reduce the pH of the reaction mixture because acids like perchloric acid and nitric acids potentially interferes with reduction reaction while chloride from hydrochloric acid interferes with the development of molybdenum blue complex.

The second approach measures phosphate using ammonium vanadate and ammonium molybdate under acidic condition to generate a yellow-colored compound called ammonium phosphoric vanadomolybdate. The complex is detected from its absorption peak at 380 nm. Both colorimetric methods are sensitive and accurate for micromolar level detection of phosphates. However, both approaches require complex and toxic reagents, sophisticated instruments, sample preparation and technical experts for operation of manual bench top systems. Multiple products have been launched for automated colorimetric phosphate detection [5]. These systems are large, are expensive, need on-site reagents and waste storage system, and works within narrow detection range.

Few attempts have been made to use a solid-state colorimetric sensor using paper based devices [6–9]. A filter paper based device was fabricated with two regions to maximize the stability of the reagents used in the assay (molybdate/antimony tartrate and ascorbic acid) [8]. The reagent mixture was stable for less than 24 hours due to reduction of Mo (VI) by ascorbic acid [3]. Therefore, two reagents were stored in two different chambers in the device and the response of the device was stable for 122 days when stored at -20 ^{o}C. A later study used ethylene glycol to enhance the stability of the molybdenum reagents up to 35 weeks at <4 ^{o}C [9]. Another study fabricated reducing agent (ascorbic acid) dried strips using Whatman blotting paper for molybdenum blue assay [7]. However, the method required mixing of solution, molybdenum reagents and sulfuric acid outside in a vial and then the reducing agent dried strip was immersed in the mixed solution. All three devices were used for phosphate detection in surface water and seawater. Similar to water testing, a microfluidic chip was developed to detect phosphate in whole blood using the molybdenum blue method [10]. The device exhibited a measuring range from 0.1 to 9 mg/dl with a 12 minute reaction time and 6 µl sample volume. The device showed good

correlation with spectrophotometer measurements and linearity for whole blood samples. Later, a lateral flow device was used to detect phosphate in human serum using the malachite green assay [11]. The device exhibited an upper detection limit of 5 mg/dl, required 45 minutes reaction time for measurement and <60 µl sample volume. However, the reagents used in this assay are known to cause skin and eye irritation. Therefore, the reagents required careful handling which adds another roadblock for use of this lateral flow device as point of care device. Paper devices offer a low-cost, simple and portable method for detection, but these methods work in a narrow detection range (0.2 -10 mg/L), require a controlled sample volume, operate with toxic reagents, and need more stable reagents for long term storage [8].

3. Solid state electrochemical sensing

Electrochemical sensors offer multiple advantages over the widely used colorimetric sensors such as potential to be miniaturized, minimal interference due to solution turbidity, do not require any toxic chemicals, a longer lifetime, rapid response time, and simple fabrication. However, there is no commercial automated electrochemical phosphate detection system available at this time. Electrochemical methods including amperometric, voltammetric and potentiometric methods have been used for sensing of phosphates.

3.1 Solid state potentiometric sensors

Potentiometric sensors are suited for miniaturization because the sensors response is independent of electrode area. Potentiometric solid state phosphate sensors can be divided into two groups: Ion selective membrane-based electrodes and metal-based electrodes.

3.1.1 Solid state ion selective membranes

Ion selective electrodes have been extensively investigated over the past 60 years. Ion selective electrodes are a 2-electrode system (Figure 2.3a) consisting of a working electrode (ion selective) and a reference electrode. Ion selective electrodes generally have two layers: first layer which remains in contact with the analyte solution is selective to the ion while the second layer is used as an ion-to-electron transducer to facilitate charge conduction in the electrode (Figure 2.3b). The charge conduction is carried out by ions or electrons. Ions participate in the charge conduction in solution while electrons facilitate the charge conduction in electrode/solid conductive materials. Conventional ion selective electrodes use an inner filling solution as ion-to-electron transducer which is stable and widely used approach for tabletop devices due to their large size and the feasibility to incorporate a liquid solution. The transduction mechanism of an ion selective electrode with inner filling solution is shown in Figure 2.3c. The ion selective membrane selectively allows the analyte ions to pass through it which results in a potential difference at the interface ($\Delta\Phi_{a1}$). Similarly, ion selective membrane and inner filling solution interface will develop a potential difference due to the change in ion concentration in the membrane ($\Delta\Phi_{a2}$). Finally, the silver-silver chloride electrode interface can transduce this change in ion concentration to the electron flux ($\Delta\Phi_{a3}$). The final potential difference measured by the ion selective electrode is summation of the three potential changes ($\Delta\Phi_{a1}+ \Delta\Phi_{a2} + \Delta\Phi_{a3}$) [12].

The most accepted theory to define the membrane potential was developed using the diffusion theory of electrolyte established by Nernst [13]. According to this theory, the membrane potential has two components: Donnan and diffusion potential. The details of the theory are described here [14]. Mathematically, the membrane potential ($\Phi_{m)}$ is written as the difference between the

potential from the outer membrane side potential (Φ_{outer}) to inner membrane side potential (Φ_{inner}) (Equation 1).

$$\Phi_m = \Phi_{outer} - \Phi_{inner} \qquad (Equation\ 1)$$

From Nernst equation,

$$\Phi = \Phi^o - \frac{RT}{z_i F} ln a_i \qquad (Equation\ 2)$$

Where Φ^o and Φ are standard and actual potential, R and F are universal gas constant and Faraday's constant, T is temperature, z_i is the charge number and a_i is the activity of the target analyte (Equation 2).

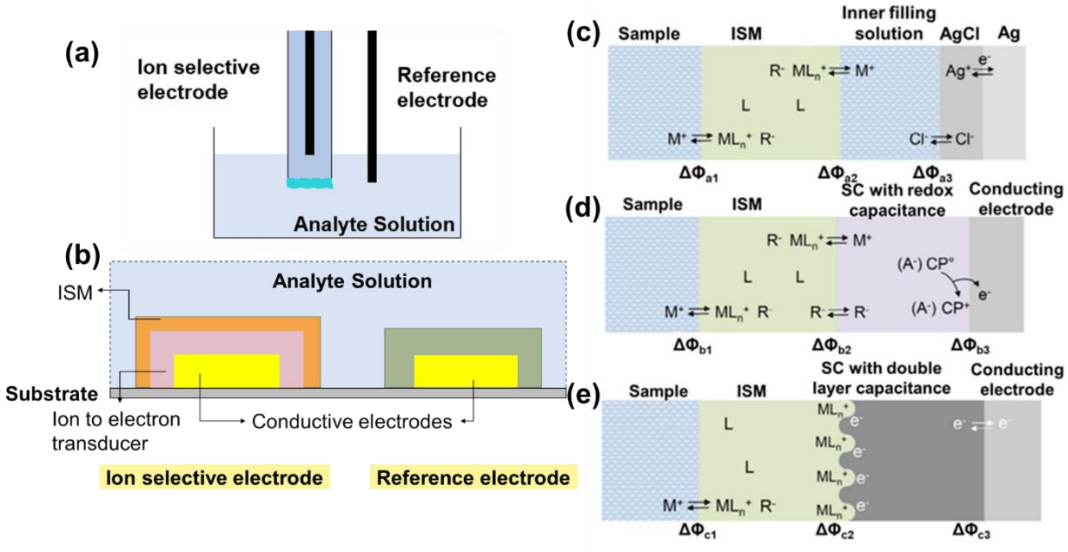

Figure 2.3 (a) A conventional ion selective electrode with a macro working electrode and reference electrode (b) A transverse section of working and reference electrode showing various layers. Working mechanism of ion selective electrode (c) Conventional ion selective electrode with inner filling solution [Adapted from [12]]. (d) and (e) Ion selective electrode with solid contact with redox capacitance and

double layer capacitance, respectively [Adapted from [12]]. Where ISM: Ion selective membrane and SC is solid contact.

Ion selective electrodes with liquid inner filling solution are difficult to miniaturize due to the risk of solution evaporation resulting in a change of the sensor response, ionic strength difference between the sample and inner filling solution resulting in osmotic pressure difference which can potentially change the inner filling solution volume, and delamination of the membrane due to change in pressure and temperature. Therefore, there are ongoing investigations into different solid materials like conducting polymers, carbon-based materials, and nanoparticles, that can replace inner filling solution as an ion-to-electron transducer [12,15]. The transduction mechanism of an ion selective electrode with solid contact with redox capacitance and double layer capacitance solution is shown in Figure 2.3d and 2.3e.

An ideal phosphate selective membrane should be able to transport phosphate ions through the membrane and should avoid interaction with the interfering ions like thiocyanate, iodide, and nitrates. A selective ionophore is difficult to design for phosphate due to its large size and hydrophilic nature. The large size of the ion makes it very difficult to accommodate in the selective cavity without any significant interference and other similar molecules like perchlorates, sulphates and arsenates [16]. Further, the four oxygen atoms present in the ion makes it highly hydrophilic. Due to these properties, phosphate lies at the bottom of Hofmeister selectivity series [17]. Therefore, to design a phosphate selective ionophore, researchers have used other properties like ability to from multiple hydrogen bond due to presence of multiple oxygen atoms and ability to form a strong metal complex with different metals like tin [16,18,19].

One of the earliest such solid membrane electrodes was fabricated with a mixture of lead sulfide, silver sulfide and lead hydrogen phosphate [20]. The electrode was used to measure phosphate down to 5 µM with a sensitivity of 13-18 mV/decade. The membrane electrode had a slow response time (~60 minutes), worked at pH >8, and suffered interference from chloride ions. A solid-state sensor based on cerium acetylacetonate as an ionophore mixed into a composite membrane made of a mixture of graphite powder, multiwalled carbon nanotube (MWCNT) and ionic liquid (1-butyl-3-methylimadazole tetrafluoroborate) was reported to detect phosphate with good selectivity against common interferents [21]. The addition of MWCNT increased the sensitivity of the electrode from -24.8 mV/dec (0% MWCNT) to -29.3 mV/dec (5% MWCNT). The increase in calibration slope can be attributed to the high conductivity of MWCNT which would have decreased the overall sensor resistance. Further, changing the binder from paraffin to ionic liquid increased the slope to -24.8 mV/dec from -19.7 mV/dec while the graphite and ionophore concentration were kept constant at 15% and 75% respectively. Another electrode was fabricated using a mixture of silver phosphate and silver sulfide with polytetrafluoroethylene (PTFE) or carbon nanotube (CNT) [22]. The active materials were mixed, and the membrane was formed by pressing the mixture at 700 MPa for 1.5 - 2 hours under room temperature. The membrane prepared with CNT improved the sensor sensitivity from 21 mV/decade (without CNT) to 32.6 mV/dec with CNT at pH 9.2. Another sensor was constructed using a macrocyclic ionophore with a PVC or polyurethane matrix [23]. A shift in lower detection limit was observed for HPO_4^{2-} when the polymer was change from polyurethane (10^{-5} M) to polyvinyl chloride (10^{-6} M). Further, the response time was reduced from 75 s (polyurethane) to 20 s (polyvinyl chloride). However, the PVC electrodes were stable for approximately 6 weeks, which was less than the polyurethane electrodes (2 months). No significant interference was reported against the common interferents

with their selectivity coefficients like sulphates (-2.51), iodide (-4.30), chlorides (-3.80), acetate (-3.15), nitrates (-3.31). Tributyltin chloride was used for real time monitoring of $H_2PO_4^-$ intake by plants [22]. The sensor was used for continuous monitoring of phosphate in the growth media at pH 5.8 for 15 days. The sensor response was linear between 5.6×10^{-6} to 1.6×10^{-2} M with a calibration slope of -55.6 mV/dec and limit of detection 2.14×10^{-6} M. However, the sensor required six hours conditioning in KH_2PO_4 solution (10^{-6} M) before measurements. A recent sensor used copper doped co-polymer and CNT to detect HPO_4^{2-} within a pH range of 7.0-9.5 [24].

Ion selective membranes offer advantages like a simple fabrication process, rapid detection, and long-term monitoring. However, these electrodes still do not have a selective ionophore that can measure phosphorus in the presence of interfering compounds at near neutral pH. In addition, most of these studies mentioned above did not perform any field experiments and the majority of these sensors work in the alkaline range which requires sample preparation before measurements. There is also a need to further study the effect of other environmental parameters like temperature fluctuations, chemical and biological fouling, on the sensor response.

3.1.2 Metal electrodes

Metal electrodes have been widely reported as potentiometric sensors in the literature for phosphate detection. The first metal electrode for measuring phosphate was fabricated using Bismuth/Bismuth phosphate [25]. However, the same group later reported that the Bismuth based electrodes were difficult to reproduce. Therefore, they proposed a new metal electrode based on silver-silver phosphate [26] but the sensor response of the silver electrode was severely affected by chloride ions. In the next decade, numerous metal-based electrodes like cadmium [27], lead [28], nickel [29], molybdenum [1,30] and cobalt [31], were proposed. But due to various limitations of other electrodes including interference, toxicity etc., only electrodes based on cobalt,

nickel, and molybdenum were continued to be investigated in subsequent studies. A more recent study has proposed a sensor based on tungsten [32].

Cobalt based phosphate sensing electrode was introduced by Xiao [31]. Multiple cobalt-based electrodes were reported in the last two decades due to it simple fabrication process, good selectivity, and long-term electrochemical stability [31,33–37]. The electrode responds to all three orthophosphate species present in the water: dihydrogen phosphate, monohydrogen phosphate and phosphate ions [37]. The first cobalt electrode was fabricated using a cobalt wire. The cobalt wire was first pretreated in distilled water followed by another pretreatment in 25 mM potassium hydrogen phthalate buffer to form a layer of cobalt oxide. The generated cobalt oxide was used for selective detection of $H_2PO_4^-$ at pH 4 [31]. The sensor reported a near Nernstian slope of 55 mV/decade and a LOD of 5×10^{-6} M. The selectivity coefficients for common anions like nitrates, chlorides, sulphates and acetates were 8×10^{-4}, 2×10^{-3}, 1×10^{-3}, 1×10^{-3}, respectively (Table 1). Advantages of the sensor include quick response time (~1- 2 minutes), chemical-free and lower sensor drift (2-3 mV in 5 days). The limitations of the sensor were its sensitivity to oxygen and pH, requirement of an acidic pH (pH 4) for detection which is not suitable for application in natural water bodies directly, need for long pretreatment time to generate a stable cobalt oxide layer (~90 minutes), high LOD (< 1 µM) and limited working range (10^{-5} to 10^{-2} M). Multiple studies have been performed after the first study, but most of the improvements were in miniaturization and robust fabrication process [38–40]. None of these studies have focused on improvement of the LOD required of the real applications like tap water, surface water, river water and/or eliminating the need of chemical pretreatment before measurements. A recent study has reported a wire based cobalt electrode with platinum wire as a quasi-reference electrode [34]. The sensor was used to detect phosphate in soil extracts. Therefore, the electrodes were tested in 0.1 M ammonium lactate

and 0.4 M acetic acid as the background electrolyte and a pH of 3.75. The sensor exhibited a linear range from 10^{-6} to 10^{-1} M with a response time of less than 300 s. The sensor response was stable for 3 days with intermittent measurement. The sensor was stored in air between measurements and was tested with modified soil samples. However, this sensor also required the pretreatment of sensor in deionized water (DI water) for 2 hours before phosphate measurement.

Cobalt electrodes have been miniaturized using microfabrication techniques. Zou and coworkers reported the first on-chip cobalt based phosphate sensor [39]. The chip was fabricated using standard microfabrication using cyclic olefin and the planar cobalt microelectrode was patterned using photolithography. The on-chip device reduced the response time to < 60s due to decreased reaction volume and sensor size. The measuring range (10^{-5} to 10^{-2} M) of the sensor was similar to the sensors reported in previous literature [31]. The sensor showed a high reproducibility (relative standard deviation (RSD) of 0.6%). A microneedle based cobalt electrode was demonstrated in a later study [41]. The microelectrode array was fabricated using microfabrication technologies. The process used diced glass probes which were etched to manufacture sharp glass tips, the glass tips were metallized, and electroplated with cobalt. The microelectrode array was connected to a printed circuit board with the electrical connectors. The electrodes were pretreated in two steps: first the electrode was immersed in DI water for 30 minutes followed by 30 minutes in 10^{-4} M $H_2PO_4^-$ solution. The sensor exhibited a super Nernstian slope of -96 mV/dec within a measuring range of 10^{-5} to 10^{-3} M and response time of ~30 s. The sensitivity of the sensor was reduced to -70 ± 4.7 mV/dec of KH_2PO_4 concentration in presence of common anions like chloride, nitrates, sulphates and acetates. However, the study did not investigate the mechanism behind the enhanced sensitivity and the sensor also require a two-step chemical pretreatment (DI water and 0.1 mM KH_2PO_4 solution in sequence for 30 minutes in each solution) before measurement. Another group

published two studies on a 400 µm cobalt microelectrode fabricated using a standard microfabrication process [42,43]. Cobalt was electroplated on a metallized glass substrate similar to previous studies. After fabrication, the electrode was chemically pretreated in DI water for 2 minutes followed by an exposure to 10^{-4} M $H_2PO_4^-$ solution for 400 s. The phosphate concentrations were measured in 25 mM potassium buffer at pH 7.5. The sensor had a wider measuring range of 10^{-6} M to 10^{-2} M with a calibration slope of –28.09 mV/dec and a response time of 200 s. The authors demonstrated a reproducible sensor fabrication process with a relative standard deviation of 2.34% (n=15). Another study fabricated a microelectrode using an UV-LIGA and metal patterning, to measure phosphate concentration for over 6 days [44]. The sensor was made using electroplated cobalt as the working electrode and Ag/AgCl as the reference electrode. The microfluidic channel was made using micro-injection molding. The sensor was chemically pretreated in 2-steps, DI water for 30 minutes followed by 25 mM of potassium hydrogen phthalate buffer until a stable potential is reached. The sensor measured phosphate within a range of 10^{-5} to 10^{-3} M with LOD of 10^{-6} M in potassium phthalate buffer (pH 6). The reported experimental repeatability showed a good precision with a relative standard deviation of 3.5% (n=8). However, the study did not report any interference, real sample measurement or chip-to-chip variability data.

Screen printing is a low-cost mass manufacturing technology for electrode fabrication. Multiple cobalt-based sensors have been manufactured using screen printing. A screen printable carbon ink was modified with cobalt powder [36]. The sensor was chemically pretreated in two steps using DI water (10 minutes) and 0.1 mM KH_2PO_4 (pH 4, 20 minutes) in sequence. With cobalt: carbon ratio of 1:99, the sensor showed a linear measuring range of 10^{-4} to 10^{-1} M with a calibration slope of 30 mV/dec at pH 4.5. The fabricated sensors also had good reproducibility with electrode-to-electrode variation (RSD of <3.2%, n=12) and with a single sensor the measurement repeatability

had RSD of 0.5% (n=10). Another electrode was fabricated by electroplating cobalt on a screen-printed carbon as base substrate [45]. The sensor was conditioned in DI water until a stable potential was reached then the electrode was put into 10^{-4} M $H_2PO_4^-$ solution until a new equilibrium potential was achieved. The sensor had a linear measurement range from 10^{-5} to 10^{-1} M with a LOD of 3.16×10^{-6} M at pH 4. The sensor had a response time of 120 s and a calibration slope of -37.51 mV/dec. The selectivity coefficients for common anions like sulphates, nitrates, chlorides and acetates for both screen printed electrodes were 8×10^{-4}, 1.5×10^{-3}, 2×10^{-3}, 4.5×10^{-4}, respectively, which are similar to cobalt wire based sensors [31]. The sensors were also tested in modified wastewater samples. However, both sensors required two step chemical pretreatment before measurements and the measurements were performed at pH 4.0 to 4.5 which is not suitable for real samples.

Moreover, a few studies have reported chemical modification of cobalt surface to improve the electrode stability. A novel cobalt phosphate-based sensor for phosphate measurement in hydroponics cultures [35]. The cobalt phosphate was electrodeposited on cobalt wire under potentiostatic mode by applying a potential bias of -0.3 V (Vs Ag/AgCl) for 2 hours in a 0.1 M NaH_2PO_4 solution. The sensor response was linear within 10^{-5} to 10^{-1} M with a calibration slope of -39 mV/dec. All the measurements were done under constant dissolved oxygen concentrations. A decrease in the sensor slope was observed when the pH was increased beyond 7 which could be due to the formation of cobalt hydroxide instead of cobalt oxide under basic conditions. The cobalt hydroxide precipitate (K_{sp}: 1.6×10^{-15} M) can degrade the sensor response. The proposed sensing mechanism for the electrode in this regime where hydroxide is present is as follows (Reaction 6-10).

$$Co^{2+} + 2e^- \leftrightarrow Co \qquad (6)$$

$$Co(OH)_2 + 2e^- \leftrightarrow Co + 2OH^- \quad (7)$$

$$Co(H_2PO_4)_2 + 2e^- \rightarrow Co + 2H_2PO_4^- \quad (8)$$

$$Co(OH)_2 \leftrightarrow CoO + H_2O \quad (9)$$

$$3\,CoO + 2\,OH^- \leftrightarrow Co_3O_4 + H_2O + 2e^- \quad (10)$$

Finally, the oxide/hydroxide/phosphate films convert to cobalt (II) phosphate as confirmed by X-ray diffraction analysis. The following reactions are believed to occur at the interface to generate cobalt (II) phosphate (Reaction 11-13) [35]:

$$2Co_3O_4 + 3Co(H_2PO_4)_2 \leftrightarrow 3\,Co_3(PO_4)_2 + 6H_2O + O_2 \quad (11)$$

$$2CoO + Co(H_2PO_4)_2 \leftrightarrow Co_3(PO_4)_2 + 2H_2O \quad (12)$$

$$2Co(OH)_2 + 3Co(H_2PO_4)_2 \leftrightarrow 3Co_3(PO_4)_2 + 4H_2O \quad (13)$$

Cobalt electrodes require a chemical pretreatment in a standard solution such as DI water and/or buffer with defined phosphate concentration before measurements. The conditioning time can vary from 5 minutes for microfabricated electrodes to greater than 2 hours for wire based electrodes [31,34,35,37,40–43,45]. For example, a two-step conditioning protocol was used for a microfabricated electrode where the electrode was first dipped into DI water for 2 minutes followed by a 200 s pretreatment in 10^{-4} M $H_2PO_4^-$ solution [43]. More importantly, many of the previous studies have required that the measurements are performed in a phthalate buffer which is not ideal for field sample measurements [31,36,37,43–45].

Molybdenum has been known to react with phosphate and this reaction is used in colorimetric sensing of phosphate [3]. A few amperometric studies with molybdenum electrodes have been used for phosphate detection [46]. Based on these studies, Li has proposed a molybdenum-based

electrode for phosphate detection [1]. The electrode was sensitive to HPO_4^{2-} in alkaline pH. The measuring range was from 10^{-5} to 10^{-1} M with a sensitivity of -26.9 mV/dec and LOD of 1.6 µM. The sensor had rapid response time of 50 s with good reproducibility (standard deviation of 2 mV). Unlike cobalt electrodes, molybdenum-based electrodes did not require any pretreatment. However, the sensor showed a better response (super Nernstian slope) for hydroxide anions and the measurements were done at pH 8.5 which is not practical for real water samples like surface water, tap water and lakes. The sensor response was also pH sensitive with a linear slope of -42.1 mV/decade (pH values tested between 6.93-8.73). The authors attributed the pH response to the change in composition of the orthophosphate species from HPO_4^{2-} at high pH to $H_2PO_4^-$ at lower pH values. However, the study did not elaborate on the sensing mechanism and the sensor was not tested with any field samples. The electrode was also stable for three months of continuous monitoring with no change in the measuring range, calibration curve slope and response time. In a different approach, molybdenum was electrochemically modified in HPO_4^{2-} at pH 9 for two hours to fabricate a phosphate sensor [30]. The modified electrode showed a linear range from 10^{-5} to 10^{-1} M and a LOD of 1 µM with a slope of -27.8 mV/dec. The sensing mechanism was explained using the Pourbaix diagram and cyclic voltammetric studies and is described below (Reaction 14-17).

$$MoO_2 \rightarrow MoO_2^+ + e^- \quad (14)$$

$$MoO_2^+ \rightarrow MoO_2^{2+} + e^- \quad (15)$$

$$MoO_2^{2+} + H_2O \rightarrow MoO_3(s) + 2H^+ \quad (16)$$

$$12MoO_3 + HPO_4^{2-} \rightarrow H^+ + PMo_{12}O_{40}^{3-} \quad (17)$$

When HPO_4^{2-} is present, two anodic current peaks were observed around 0.15 and 0.25 V in cyclic voltammetry study. These peaks can be attributed to the above two reactions (Reaction 14 and 15) which results in formation of MoO_3 (Reaction 16). MoO_3 reacts with HPO_4^{2-} to give a molybdophosphate complex (Reaction 17) which was confirmed using UV-Vis study. The sensor was tested in tap water and distilled water with 95-98% recovery as compared to colorimetric method.

Molybdenum sensors offer rapid response, a measuring range 10^{-5} to 10^{-1} M which is similar to cobalt sensors. Both the reported sensors exhibited good selectivity against common anions like sulphates, nitrates, carbonates, chlorides and acetates (Table 2.1) but the sensor response is severely affected by the presence of hydroxide anions. However, the sensor is sensitive to only HPO_4^{2-} which limits their operation to alkaline pH (pH 8-9). The divalent anions reduce the sensitivity of the sensor to theoretical maximum of ~30 mV/decade of HPO_4^{2-}concentration. The sensors also need to be tested in real surface water, wastewater and medical diagnostics samples.

Table 2.1 Summary of selectivity coefficients for different metal and modified metal based phosphate electrodes.

Interfering anions	**Co** [31]	**$Co_3(PO_4)_2$** [35]	**Modified Mo** [30]	**$Co_{63}Mo_{37}$** [47]	**Tungsten** [32]	**Modified Tungsten** [48]
Nitrates	-3.1	2.5	-3.5	-3.2	-2.3	-2.8
Sulphates	-3.0	-4.0	-2.0	-2.6	-4.0	-4.5
Chlorides	-2.7	-4.0	-3.0	-2.7	-2.1	-4.2
Acetate	-3.0	-3.2	-3.1	NR	-2.7	-3.0
Bicarbonate	NR	-2.1	-2.9	NR	-1.9	-2.8

Another transition metal, Tungsten has also been used for HPO_4^{2-} sensing [32,48]. The sensor exhibited a slope of -29.9 mV/dec similar to the theoretical Nernstian slope (29.6 mV/decade) [32]. The linear range was from 1 µM to 0.1 M with a limit of detection 0.41 µM at pH 10. The sensor had a rapid response time of < 60 s. Unlike cobalt based electrode, this electrode also did not require any pretreatment. The sensor was highly stable without any significant drift and standard deviation of ± 0.61 mV. The sensor was stable for eight weeks when used intermittently for phosphate measurement. A minor change (-29.9 mV/dec to -28.9 mV/dec) was noticed in calibration slope during the 8 weeks testing while no significant effect was observed on the measuring range. The selectivity coefficient for the interfering anions such as chlorides, sulphates and nitrates are 7.68×10^{-3}, 1.02×10^{-4}, and 5.41×10^{-3}, respectively similar to cobalt and molybdenum (Table 2.1). The sensor showed a 91% to 107% recovery with samples adjusted to pH 10 while unmodified samples showed a recovery of 74% to 85%. However, the sensor response was pH sensitive, and the sensor needs to be further explored to understand the pH dependence. Based on XPS and SEM results, the authors postulated a two-step sensing mechanism (Reaction 16 and 17). In the first step, tungsten is converted to tungsten (IV) oxide (Reaction 18) and then in presence of HPO_4^{2-}, tungsten oxide is converted to tungsten phosphate (Reaction 19).

$$\mathrm{W} + 4OH^- \rightarrow \mathrm{WO_2} + 2\mathrm{H_2O} + 4e^- \qquad (18)$$

$$3WO_2 + 4HPO_4^{2-} + 2H_2O \rightarrow W_3(PO_4)_4 + 8OH^- \qquad (19)$$

Similar to cobalt and molybdenum, metallic tungsten was electrochemically modified in a standard phosphate solution to form phosphotungstic acid [48]. The sensor showed the highest sensitivity -36.9 mV/dec at pH 10 within a measuring range of 10^{-6} M to 10^{-1} M phosphate concentration. However, the sensor was also sensitive to hydroxide ion and the sensitivity at pH 7 goes down to -19.3 mV/dec. Hence, the sensor is not suitable for most of the environmental samples.

Nickel oxide /oxyhydroxide was used to measure phosphate concentrations at pH 4.4 [29]. A screen-printed carbon electrode was electrodeposited with nickel. During electrodeposition some Ni^{2+} (NiO / $Ni(OH)_2$) gets converted to Ni^{3+} (NiOOH) as shown in the reaction (Reaction 20-21).

$$Ni(OH)_2 \leftrightarrow NiOOH + H^+ + e^- \quad (20)$$

$$NiOOH + H_2PO_4^- \leftrightarrow NiO(OH) + H^+ + e^- \quad (21)$$

Similar to cobalt, NiOOH reacts with phosphate to generate nickel phosphate (Reaction 21) which consumed the amount of NiOOH generated in Reaction 20, resulting a shift in cathodic potential. The sensor exhibited a good sensitivity -78.48 mV/decade over a wide measuring range 10^{-6} M to 10^{-1} M. However, the study did not mention the effect of dissolved oxygen and pH which is a know interference for metal electrodes like cobalt. The sensor was not tested in real samples. Therefore, further investigation is needed to establish nickel oxide sensors for environmental and medical diagnostics sensing.

Metals like cobalt and copper were mixed with other metals such as aluminum, iron, and molybdenum to reduce the interference, minimize response time, enhance sensitivity and improve stability of the electrode [47,49–52]. A solid-state electrode was fabricated using copper powder, aluminium powder, and aluminium phosphate [52]. The electrode showed a linear response from 10^{-6} -10^{-1} M with a limit of detection < 10^{-6} M. The sensor had a rapid response time of < 1 minute. The electrode was used intermittently and stored in air when not in use. The electrode was stable for 12 months with no significant change in the sensor response. However, the electrode needs 6 hours chemical pretreatment every time before measurement which can be an issue for in-field monitoring and showed interference from hydroxide and chloride ions. Another study used co-electrodeposited cobalt-iron electrode to reduce the response time and increase long-term stability

of the electrode [51]. The sensors attained the maximum sensitivity with ~ 40% iron content and further increase in iron result in reduction of sensitivity due to the reduction in more sensitive cobalt sites. The electrode showed a linear response from 10^{-5} -10^{-2} M with a limit of detection < 10^{-5} M and sensitivity of -43 mV/decade of $H_2PO_4^-$ concentration. The iron present on the electrode surface stabilizes the Co (II) and hence improve the stability and sensitivity of the sensor as compared to electrode without iron. In addition, the magnetic properties from the inter molecular interaction between cobalt and iron resulted in the increased sensitivity. However, the study did not investigate the sensing mechanism in detail and the sensor works at pH 5 which is not suited for real water testing. The electrochemical performance of electrodeposited Co-Fe electrode was improved using by electrodepositing on an annealed gold film [49]. The annealing process introduced nano scale porous holes on the gold electrode resulting a change in surface area. The annealed electrode (LOD: 2.14 × 10^{-6} M) exhibited a lower limit of detection compared to unannealed electrode (LOD: 3.41 × 10^{-5} M). However, the sensors were required to stored in potassium phthalate buffer and pretreated in the buffer before every measurement. The sensor did not exhibited any interference to common anions but the sensitivity of the sensor was -26.67 mV/decade which is ~50% than the previous reported sensitivity for electrodeposited sensors (~-43 mV/decade) [51]. The sensor was also not tested in real water samples. A different study investigated electrodeposited cobalt and molybdenum alloy as electrode to improve the working pH range of metal electrode [47]. The working range of Co-Mo alloy electrode was between pH 6-7 without any significant change in sensitivity of the sensor (~34 mV/dec). The alloy electrode showed good selectivity over common anions. However, the LOD of Co-Mo electrode (LOD: $10^{-4.9}$ M) was higher than both cobalt (LOD: $10^{-5.3}$ M) and molybdenum (LOD: $10^{-5.7}$ M) electrode and the sensor was not tested in real samples.

Cobalt and its alloy electrodes have been extensively studied, and the electrodes have high pH tolerance (pH 4 to pH 8) as compared to other metal electrodes like molybdenum (pH 8.5 to 9), tungsten (pH 10), nickel (pH 4.4). All metal electrodes have rapid response time and high selectivity for the common interfering anions like nitrates, sulphates, bicarbonates and chlorides (Table 2.1). However, cobalt electrodes need chemical pretreatment in standard solutions before measurement.

3.2. Solid state amperometric sensors

Amperometric sensors measure the rate of reaction of the analyte of interest at the electrode surface through the charge transfer occurring at the electrochemical interface. The sensors can be categorized into enzymatic and non-enzymatic solid-state sensors. Enzymatic amperometric sensors generally have a film of immobilized enzymes which converts phosphate into smaller molecules like H_2O_2, and uric acid. The concentration of smaller molecules is measured, which is correlated to the phosphate concentration. Since 1960s, multiple enzyme reactions based on glucose-6-phosphate as substrate, and enzymes like alkaline phosphatase, and glucose oxidase are used to indirectly detect phosphate and these multiple reaction detection systems are summarized in a previous review [53]. One of the earliest single enzyme sensors was based on pyruvate oxidase (PyOD) immobilized on a screen printed platinum electrode (Reaction 22) [54]. The generated H_2O_2 was oxidized at the platinum electrode. The electrode exhibited a linear response from 7.5 µM to 625 µM phosphate with a sensitivity of 0.523 µA/mM. The sensor showed a linear correlation ($y = 1.17x + 0.2$, $R^2=0.9646$) with spectrophotometric measurements in filtered human saliva samples. Later, a screen electrode modified with cobalt phthalocyanine and PyOD was used to detect phosphate in presence of pyruvate [55] (Reaction 22-24). The decarboxylation of pyruvate was done in presence of PyOD and cofactors Thiamine pyrophosphate and flavin adenine

dinucleotide (Reaction 22). The generated H_2O_2 was catalyzed by cobalt phthalocyanine at +0.4 V. The sensor exhibited a narrow range (2.5 to 15 µM) than the previous reported PyOD sensor [54] but this study has tested the sensor in diluted urine and pond water.

$$\text{Pyruvate} + \text{Phosphate} \xrightarrow{\text{PyOD}} \text{acetylphosphate} + H_2O_2 + CO_2 \quad (22)$$

$$2Co^{2+} + H_2O_2 \rightarrow 2Co^{+} + 2H^{+} + O_2 \quad (23)$$

$$2Co^{+} \rightarrow 2Co^{2+} + 2e^{-} \quad (24)$$

Another biosensor with polypyrrole-PyOD on a gold electrode was modified by rhodium nanoparticles acted as the mediator for reduction of H_2O_2 and also improve the electron transfer efficiency [56]. The biosensor exhibited a wide range of detection 0.05 to 70 mM with a sensitivity of 0.076 µA/mM under a potential bias of -0.68 V and a flow rate of 2 ml/min. The sensor was tested in artificial urine samples with a recovery of ~105% for 10 mM of phosphate concentration in the samples. The sensitivity of the PyOD biosensor was improved by modifying the electrode with aligned Gold/Platinum (Au/Pt) nanowires [57]. The sensitivity of the sensor was 3.53 mA/mM (50.5 µA/mM/cm^2) which was ~6 times better than the previous reported sensor with a screen printed platinum electrode [54]. The higher sensitivity of the sensor was due to the decrease in electron transfer resistance and overpotential for H_2O_2 reduction. The measuring range of the sensor was 0.25-1.5 mM and LOD of 45 µM under a potential bias of -0.15 V.

A bienzymatic sensor was reported where purine nucleoside phosphorylase (PNP) and xanthine oxidase (XOD) in presence of phosphate and inosine generated H_2O_2 and uric acid as the final product in a 2-step reaction [58] (Reaction 25-26). The generated H_2O_2 was used to produce the amperometric signal with ferricyanide as the mediator. The sensor exhibited a measuring range of

0.1 to 1 mM under a potential bias of +0.2 V and the sensitivity of the sensor was 6.573 µA/mM of phosphate concentration.

$$\text{Inosine} + \text{phosphate} \xrightarrow{\text{PNP}} \text{ribose} - 1 - \text{phopshate} + \text{hypoxanthine} \qquad (25)$$

$$\text{Hypoxanthine} + 2H_2O + 2O_2 \xrightarrow{\text{XOD}} \text{uric acid} + 2H_2O_2 \qquad (26)$$

It is well known that the oxidase enzymatic reactions use oxygen as the electron acceptor. Therefore, the sensitivity of the electrode suffers at low oxygen levels, which also limits the measuring range of the sensor. A recent study proposed a second generation enzymatic phosphate sensor where the enzymes PNP and XOD are coupled with a redox active Osmium complex modified polymer to minimize the oxygen interference [59]. Osmium modified polymer also acted as an immobilization matrix and facilitates the shuttling of the electrons from the oxidation reaction to the electrode. The second-generation enzyme sensors provide an alternative to improve the sensor performance by using electrode mediators. However, the sensors are still in nascent stage. Therefore, more studies will be required to establish the advantages of using the electron mediators on the sensing performance. Further, these sensors require multiple enzymes and substrates like inosine for phosphate detection which limits the use of these sensors in real applications.

Direct electrochemical oxidation of phosphate is difficult because the central phosphorus and four oxygen atoms form a hydrophilic sphere resulting in an increase in hydration enthalpy [17]. Thus multiple studies have used reduction of a phosphomolybdate complex for amperometric phosphate detection on different substrates including transition metal oxides like ZrO_2^-, TiO_2, ZnO, Al_2O_3 and nanomaterials [60–63]. The formation of a phosphomolybdate complex requires acidic conditions which is not suitable for in-field monitoring. Carbon and carbon based nanomaterials

based sensors were used in flow sensors formats and these sensors generally required external reagent mixing [61,64]. A study proposed a glassy carbon electrode modified with ammonium molybdate entrapped in chitosan to eliminate the need of acid for phosphate detection [60]. This study demonstrated that the interfacial acidity associated with the chitosan film is sufficient for phosphate and molybdate reaction. The pKa value of the amino group in chitosan is ~6.5, which makes the polymer positively charged at neutral pH. The positively charged polymer entrapped the molybdate anions via electrostatic interactions. A thin layer of PEDOT: PSS was added to stabilize the polymer film. The sensor exhibited a sensitivity of 0.044 µA/µM within a measuring range of 19-100 µM. The sensitivity and LOD was improved by adding an additional layer of an ionic liquid. The improved sensor showed a sensitivity of 0.79 µA/µM within a measuring range of 0.79-31.5 µM under a potential bias of -0.14 V. The sensitivity of the sensor can be further improved by increasing the concentration of molybdate anions. The sensor does not exhibit any significant interference for chloride and nitrate, but a significant interference was observed for silicate and sulphate was not tested in the study. The sensor was also not tested in real samples.

Multiple metal substrates have been used for both direct and indirect amperometric detection of phosphate. A nickel hydroxide/oxyhydroxide film was used in an alkaline solution for indirect detection of phosphate. The adsorption of phosphate on the nickel hydroxide film results in suppression of the current for glucose oxidation [65] which can be used as an indirect sensing method in solutions containing a constant amount of glucose. The measurements were performed under a potential bias of 0.55 V vs Ag/AgCl in 0.1 M NaOH solution. The sensor showed a linear range for phosphate up to 1 mM and LOD of 0.3 µM. A recent study used a nickel foam electrode and the nickel hydrated hydroxide for phosphate detection [66]. The 3-dimensional foam electrode increased the surface area resulting in faster electron transport, improving the sensitivity of the

sensor [66]. The sensor exhibited a sensitivity of 210 µA/µM/cm^2 for a measuring range of 0.01-14 mM and 87 µA/µM/cm^2 for a measuring range of 14-50 mM. However, the working pH of the sensor was 11 which is not suited for real sample measurements. The sensor was tested in artificial wastewater samples and diluted (10 times) wastewater samples with pH modified to pH 11.

Amperometric sensors were used for phosphate detection using enzymatic and non-enzymatic sensors. Enzymatic sensors worked well near neutral pH, but they have limited measuring range, short shelf life (12 hours to 2 weeks) and require storage at 4 ^{o}C that limits their use for in-field monitoring. Non-enzymatic sensors have better stability and higher stability but most of these sensors do not work near neutral pH except one where the acidic pH was generated using a polymer [60].

3.3. Solid state voltametric sensors

Voltammetry sensors measure the change in current with change in potential applied to the electrode. Multiple voltammetric techniques like cyclic voltammetry, linear sweep voltammetry and differential voltammetry, are used for sensing analytes. Voltammetric electronic tongues were used by multiple studies for phosphate detection [67,68]. An array of eight metal electrodes (Au, Pt, Ir, Rh, Ag, Cu, Ni and Co) was proposed for measuring phosphate along with six other wastewater parameters of an anaerobic membrane bioreactor [68]. The electronic tongue response relies on the difference in the electrochemical response of the analyte with different metal electrodes resulting in differential change in voltammetric responses between the electrodes. The electronic tongues do not necessarily need an electrochemical reaction, the array of electrode can also use non-Faradaic effects to predict the analyte concentrations. For phosphate, non-noble metal electrodes exhibited different electrochemical behavior depending on the metal species. A mathematical model was formulated using the data from metal array and the data was validated

using different samples. Even though the method is simple and rapid, but the measurements are semi-quantitative in nature and the prediction power of the model would depend significantly on the sample matrix effects and the type of data used for training the model. Later, the correlation factor of the proposed sensors was improved by developing a holistic model for both influent and effluent samples of the bioreactor [67]. Another study used a glassy carbon electrode modified with TiO_2 film to improve the LOD down to 0.1 µg/l and a measuring range of 0.1 µg/l to 50 µg/l with three-piece wise linear ranges [69]. However, the sensor requires extreme low pH to function (pH 0.6).

Phthalocyanines are organic molecules widely used due to their chemical stability and extensive redox chemistry. Recent studies have used these molecules to detect phosphorus in liquid samples [70,71]. A gold screen printed electrode was modified with copper phthalocyanine, 2,9,16,23-tetracarboxylic acid polyacrylamide to electrocatalytically reduce phosphate [71]. The sensor exhibited a linear range from 0.1 nM to 10 mM for the peak current at 1.17 V Vs Ag/AgCl. The sensor was stable for 40 days (~93% of the sensor response retention) when stored at room temperature. Another study reported a glassy carbon electrode modified with Alcian Blue 8Gx (substituted copper phthalocyanine) and Poly (sodium 4-styrene sulphonate) (PSS) [70]. The electrode exhibited a linear increase in reduction peak with increase in phosphate concentrations from 0.2 mM to 1 mM. Another study used self-assembled monolayer of dipicolyamine (II) zinc complex on gold electrode to reduce the LOD of the sensor to 0.75 fM. However, the sensor could only work for phosphate concentration lower than 10 fM. The authors did not comment on the narrow range of phosphate detection. However, the limited measuring range could be due to the low surface density of the dipicolyamine (II) zinc complex resulting in the saturation of the sensor

at phosphate concentrations higher than 10 fM. Therefore, only samples diluted within this narrow range can be used for the measurements [72].

Molybdenum blue method, the most common method used for colorimetric phosphate measurement, was adapted to measure phosphate in electrochemical format [73]. Here, a screen-printed sensor was used to measure the phosphate concentration with similar sensitivity and selectivity as spectrophotometric measurements. Moreover, the method simplifies the measuring protocol by using fewer reagents (no reducing agents like ascorbic acid or antimony potassium tartrate), faster response time and a measuring range of 0.5 to 20 µg/l. However, the method still required the addition of molybdate ions for measurement. A new solid-state sensor was proposed with screen printed electrodes on paper [74]. The molybdate ions and sulfuric acid was deposited on the paper to eliminate the need of any reagent addition during measurement. The acid facilitated the oxidation of molybdate ions in presence of phosphate. The sensor exhibited a sensitivity of 0.115 µA/µM for phosphate within a range of 10-300 µM. The storage of molybdate ions and acid together makes the sensor sensitive to light and also reduces the storage shelf life of the sensor.

Another study used silver nanowire to enhance the sensitivity of the screen printed sensor modified with ammonium molybdate tetrahydrate [75]. The faster electron transfer increased the sensitivity of the sensor from 0.1 µA/ µM (without nanowires) to 0.71 µA/ µM (with nanowires) with a measuring range of 5-1000 µM and LOD of 3 µM. However, all experiments were performed under nitrogen environment which is not feasible for in-field testing.

An enzymatic sensor with nanomolar LOD was fabricated using graphene oxide on gold electrode modified with copper oxide nanodots, gold rods and pyruvate oxidase [76]. The sensor exhibited LOD of 0.4 nM and a measuring range of 0.01 to 80 µM phosphate concentrations. was used to detect phosphate in dried milk samples. The sensor displayed good LOD and measuring range in

sub micromolar range, but the sensor performance was pH sensitive (working pH 7) and need two co-factors (Flavin adenine dinucleotide salt and Thiamine pyrophosphate chloride) for optical performance.

Voltammetric sensors enables high sensitivity and rapid detection. However, the enzymatic sensors are pH and temperature sensitive, and require multiple reagents while the non-enzymatic sensors based on molybdate ions need extreme low pH. Metal phthalocyanine are chemically stable organic molecules which offers a good alternative for phosphate measurement at neutral pH and a wide range from nano molar to milli molar phosphate concentrations. The voltammetric sensors require a three- electrode system including working, counter and reference electrode. A stable reference electrode is needed for reliable measurements which is difficult to achieve using pseudo reference electrodes like Ag/AgCl film which is known to drift over time and gets affected by presence of chlorides ions.

4. Other solid-state sensors

Alternative solid-state sensors like capacitive, impedance and resistive sensors have also been investigated due to their simple structure resulting in easy fabrication and uncomplicated electronics detection instrumentation [77,78]. A capacitive sensor was fabricated on a silicon nitride substrate modified with substituted copper phthalocyanine [78]. The sensor exhibited a detection range between 10^{-9} to 10^{-5} M with a LOD of 1 nM and sensitivity 27.7 mV/decade at 10 kHz frequency. However, the sensor fabrication requires multiple steps and sophisticated equipment like low pressure chemical vapor deposition along with multiple cleaning steps with hazardous chemicals. Even though the sensors showed some specificity over the common anions such as sulfate, chloride and carbonate, but the sensor response for sulphate was around 50% of phosphate response. Further, the interference tests were performed from 10^{-6} M to 10^{-10} M but the

concentration of interfering species present in real samples could be higher than the tested concentrations. For example, the concentration of sulphates in surface water is more than 500 ppm (5 µM). Another study used a gold microelectrode modified with substituted copper phthalocyanine to detect phosphate concentration using impedance change [77]. The sensor showed a measuring range from 10^{-8} to 10^{-3} M and a LOD of 8.32×10^{-9} M. The selectivity of the sensor was tested against 1 mM of interfering anions (nitrate, sulphate, perchlorate etc.) and sulphate could be a potential interferent. These solid-state sensors are good alternatives to the phosphate sensing for in-field monitoring due to simple fabrication process and reagent-free monitoring, but these sensors are required to be tested in real samples matrices like surface water, wastewater, or blood depending on the applications. Further, these sensors require three electrode system and miniaturized or pseudo reference electrodes are known have drift issues. Therefore, both studies have used macro reference electrodes to get reliable phosphate measurements.

5. Outlook and conclusion

Current phosphate monitoring is dominated by colorimetric devices both for bench top and real time measurements. The accuracy of bench top tests depends on the sample collection method and the collection site, sample handling and stability during transport from the collection site to laboratory, and sample preparation methods for testing. Real time monitoring systems need reagents and waste storage systems which makes these devices bulky and expensive. Solid-state sensors provide an alternative to miniaturize these conventional monitoring systems into smaller portable devices. Colorimetric sensors were transformed into paper-based sensors for reagent storage and phosphate testing. However, the long term stability of these sensors needs to be improved from days to months. Electrochemical sensors offer advantages like simple instrumentation, low-cost, no/minimal chemical requirement, easy to miniaturize, ability to mass

produce and rapid response time. However, the sensors should be improved further to reduce the LOD, enhance sensor reusability, boost the stability of the reference electrode, and devise a mass manufacturing process to produce repeatable and reproducible electrodes. The sensor also should be extensively tested in real samples to prepare them as deployable sensors for in-field continuous measurements.

Miniaturized solid-state sensors provide an opportunity to integrate these sensors with multiple other sensors to evaluate the health of water in larger water bodies, public household water systems and optimal fertilizer management. The growing Internet of Things (IoT) technology can exploit these sensors to map phosphate in different regions in the water bodies like lakes, ponds, and streams. These sensors would help to predict or prevent algal bloom which is a major problem in lakes around the world. The sensors would be useful to identify phosphate hotspots in the water bodies which would curb the phosphate input into the water bodies. The sensor networks would enable the water treatment plant to tackle the seasonal fluctuations in the phosphate levels. Public water systems add phosphate in drinking water to prevent leaching of lead and copper from the pipes and fixtures. The sensor network could also be used to manage phosphate levels in tap water. The sensor networks could aid farmers for better fertilizer management by monitoring phosphate levels in the agricultural land ruff-offs. Additionally, the sensors network could be used extensively in hydroponics to maintain the optimal phosphate levels for plant growth.

This chapter covered the recent research on solid state sensors for phosphate monitoring and their potential for on-site phosphate detection. Numerous studies showed promising low-cost solid state phosphate sensors that would work in the relevant measuring range for real sample matrices such as surface water, tap water and blood. Cobalt based phosphate sensors provide a good option for the solid-state phosphate sensing. However, current methods have demonstrated the sensor use in

acidic range (pH 4-5) which is not suitable for most of the water samples. Therefore, the sensor performance should be investigated at near neutral pH (6-7). In addition, cobalt sensors also require chemical pretreatment in standard solution before phosphate measurement which is not suitable for in-field measurement of phosphate in environmental samples. Also, cobalt-based sensors are known to be sensitive to glucose. So, cobalt-based sensors cannot be used for sensing phosphate concentration in medical diagnostic samples. Enzyme based peroxidase assays and metal phthalocyanine have been used for selective phosphate detection in previous studies on biomedical detection of phosphates. However, all the sensors reported require a stable reference electrode to provide reliable phosphate measurements. Hence, there is a need to find an alternative detection method which would work without a reference electrode.

Finally, most of the reported solid-state phosphate sensors were used within the laboratory settings. Therefore, there is a need to extensively characterize the sensor response in real settings by deploying the sensors in environmental and medical diagnostics settings. Phosphate sensing poses a unique problem due to the change of different phosphate forms with the sample pH. Therefore, an ideal sensor for real sample testing should compensate for the pH variations which can change the phosphate composition in the testing solutions.

References

[1] Y. Li, T. Jiang, X. Yu, H. Yang, Phosphate Sensor Using Molybdenum, J. Electrochem. Soc. 163 (2016) B479–B484. https://doi.org/10.1149/2.0161609jes.

[2] M. Crook, R. Swaminathan, Disorders of plasma phosphate and indications for its measurement, Ann. Clin. Biochem. 33 (1996) 376–396. https://doi.org/10.1177/000456329603300502.

[3] J. Murphy, J.P. Riley, A modified single solution method for the determination of

phosphate in natural waters, Anal. Chim. Acta. 27 (1962) 31–36. https://doi.org/10.18393/ejss.477560.

[4] E.A. Nagul, I.D. McKelvie, P. Worsfold, S.D. Kolev, The molybdenum blue reaction for the determination of orthophosphate revisited: Opening the black box, Anal. Chim. Acta. 890 (2015) 60–82. https://doi.org/10.1016/j.aca.2015.07.030.

[5] G. Duffy, F. Regan, Recent developments in sensing methods for eutrophying nutrients with a focus on automation for environmental applications, Analyst. 142 (2017) 4355–4372. https://doi.org/10.1039/c7an00840f.

[6] H. Heidari-Bafroui, B. Ribeiro, A. Charbaji, C. Anagnostopoulos, M. Faghri, Portable infrared lightbox for improving the detection limits of paper-based phosphate devices, Meas. J. Int. Meas. Confed. 173 (2021) 108607. https://doi.org/10.1016/j.measurement.2020.108607.

[7] H. Heidari-Bafroui, A. Charbaji, C. Anagnostopoulos, M. Faghri, A colorimetric dip strip assay for detection of low concentrations of phosphate in seawater, Sensors. 21 (2021). https://doi.org/10.3390/s21093125.

[8] B.M. Jayawardane, I.D. McKelvie, S.D. Kolev, A paper-based device for measurement of reactive phosphate in water, Talanta. 100 (2012) 454–460. https://doi.org/10.1016/j.talanta.2012.08.021.

[9] J.M. Racicot, T.L. Mako, A. Olivelli, M. Levine, Phosphate Detection in Seawater, (2020) 1–11.

[10] C.C. Tseng, S.J. Chen, S.Y. Lu, C.H. Ko, J.M. Wang, L.M. Fu, Y.H. Liu, Novel sliding

hybrid microchip detection system for determination of whole blood phosphorus concentration, Chem. Eng. J. 419 (2021) 129592. https://doi.org/10.1016/j.cej.2021.129592.

[11] A. Ray, S. Esparza, D. Wu, M.R. Hanudel, H.A. Joung, B. Gales, D. Tseng, I.B. Salusky, A. Ozcan, Measurement of serum phosphate levels using a mobile sensor, Analyst. 145 (2020) 1841–1848. https://doi.org/10.1039/c9an02215e.

[12] J. Hu, A. Stein, P. Bühlmann, Rational design of all-solid-state ion-selective electrodes and reference electrodes, TrAC - Trends Anal. Chem. 76 (2016) 102–114. https://doi.org/10.1016/j.trac.2015.11.004.

[13] J. Janata, Principles of Chemical Sensors, 2009. https://doi.org/10.1007/b136378.

[14] X. Chen, G. Zhou, S. Mao, J. Chen, Rapid detection of nutrients with electronic sensors: A review, Environ. Sci. Nano. 5 (2018) 837–862. https://doi.org/10.1039/c7en01160a.

[15] E. Zdrachek, E. Bakker, Potentiometric Sensing, Anal. Chem. 91 (2019) 2–26. https://doi.org/10.1021/acs.analchem.8b04681.

[16] J.K. Tsagatakis, N.A. Chaniotakis, K. Jurkschat, Multiorganyltin Compounds. Designing a novel phosphate-selective carrier, Helv. Chim. Acta. 77 (1994) 2191–2196. https://doi.org/10.1002/hlca.19940770812.

[17] M.G. Cacace, E.M. Landau, J.J. Ramsden, The Hofmeister series: Salt and solvent effects on interfacial phenomena, Q. Rev. Biophys. 30 (1997) 241–277. https://doi.org/10.1017/S0033583597003363.

[18] N.A. Chaniotakis, K. Jurkschat, A. Rühlemann, Potentiometric phosphate selective

electrode based on a multidendate-tin (IV) carrier, Anal. Chim. Acta. 282 (1993) 345–352. https://doi.org/10.1016/0003-2670(93)80220-F.

[19] V.M. Shkinev, B.Y. Spivakov, G.A. Vorob'eva, Y.A. Zolotov, Dialkyltin salts as extractants in methods for the determination of arsenic and phosphorus, Anal. Chim. Acta. 167 (1985) 145–160. https://doi.org/10.1016/S0003-2670(00)84417-7.

[20] D. Midgley, Solid-State Ion-Selective Electrodes for the potentiometric determination of phosphate, Talanta. 26 (1978) 261–266.

[21] P. Norouzi, M.R. Ganjali, F. Faridbod, S.J. Shahtaheri, H.A. Zamani, Electrochemical anion sensor for monohydrogen phosphate based on nano-composite carbon paste, Int. J. Electrochem. Sci. 7 (2012) 2633–2642.

[22] M. Bralić, A. Prkić, J. Radić, I. Pleslić, Preparation of phosphate ion-selective membrane based on silver salts mixed with PTFE or carbon nanotubes, Int. J. Electrochem. Sci. 13 (2018) 1390–1399. https://doi.org/10.20964/2018.02.49.

[23] P. Kumar, D.M. Kim, M.H. Hyun, Y.B. Shim, An all-solid-state monohydrogen phosphate sensor based on a macrocyclic ionophore, Talanta. 82 (2010) 1107–1112. https://doi.org/10.1016/j.talanta.2010.06.011.

[24] C. Topcu, F. Coldur, B. Caglar, V.. Ozdokur, O. Cubuk, Solid-state elctrochemical sensor based on a cross-linked Copper(II)-Doped Copolymer and Carbon Nanotube Material for selective and sensitive detection of Monohydrogen Phosphate, Electroanalysis. (2021).

[25] E.W. Grabner, I. Vermes, K.H. König, A phosphate-sensitive electrode based on BiPO4-modified glassy carbon, J. Electroanal. Chem. 214 (1986) 135–140.

https://doi.org/10.1016/0022-0728(86)80092-4.

[26] I. Vermes, E.W. Grabner, A phosphate sensor based on silver phosphate-modified electrodes, J. Electroanal. Chem. 284 (1990) 315–321. https://doi.org/10.1016/0022-0728(90)85041-3.

[27] D.E. Davey, D.E. Mulcahy, G.R. O'Connell, Flow-injection determination of phosphate with a cadmium ion-selective electrode, Talanta. 37 (1990) 683–687. https://doi.org/10.1016/0039-9140(90)80094-V.

[28] H. Hara, S. Kusu, Continous-flow determination of phosphate using a lead ion-selective electrode, Anal. Chim. Acta. 261 (1992) 411–417. https://doi.org/10.1016/0003-2670(92)80221-R.

[29] S. Sedaghat, S. Jeong, A. Zareei, S. Peana, N. Glassmaker, R. Rahimi, Development of a nickel oxide/oxyhydroxide-modified printed carbon electrode as an all solid-state sensor for potentiometric phosphate detection, New J. Chem. 43 (2019) 18619–18628. https://doi.org/10.1039/c9nj04502c.

[30] K. Xu, Y. Kitazumi, K. Kano, T. Sasaki, O. Shirai, Fabrication of a phosphate ion selective electrode based on modified molybdenum metal, Anal. Sci. 36 (2020) 201–206. https://doi.org/10.2116/analsci.19P296.

[31] D. Xiao, H.Y. Yuan, J. Li, R.Q. Yu, Surface-Modified Cobalt-Based Sensor as a Phosphate-Sensitive Electrode, Anal. Chem. 67 (1995) 288–291. https://doi.org/10.1021/ac00098a009.

[32] G. Chen, S. Xiao, A. Lorke, J. Liu, P. Zhang, Assessment of a Solid-State Phosphate

Selective Electrode Based on Tungsten, J. Electrochem. Soc. 165 (2018) B787–B794. https://doi.org/10.1149/2.0101816jes.

[33] F. Xu, P. Wang, S. Bian, Y. Wei, D. Kong, H. Wang, A co-nanoparticles modified electrode for on-site and rapid phosphate detection in hydroponic solutions, Sensors (Switzerland). 21 (2021) 1–22. https://doi.org/10.3390/s21010299.

[34] V.O. Ebuele, D.G. Congrave, C.D. Gwenin, V. Fitzsimmons-Thoss, Development of a Cobalt Electrode for the Determination of Phosphate in Soil Extracts and Comparison with Standard Methods, Anal. Lett. 51 (2018) 834–848. https://doi.org/10.1080/00032719.2017.1360899.

[35] K. Xu, Y. Kitazumi, K. Kano, O. Shirai, Phosphate ion sensor using a cobalt phosphate coated cobalt electrode, Electrochim. Acta. 282 (2018) 242–246. https://doi.org/10.1016/j.electacta.2018.06.021.

[36] L. Song, L. Zhu, Y. Liu, X. Zhou, H. Shi, A disposable cobalt-based phosphate sensor based on screen printing technology, Sci. China Chem. 57 (2014) 1283–1290. https://doi.org/10.1007/s11426-014-5127-6.

[37] R.K. Meruva, M.E. Meyerhoff, Mixed potential response mechanism of cobalt electrodes toward inorganic phosphate, Anal. Chem. 68 (1996) 2022–2026. https://doi.org/10.1021/ac951086v.

[38] J.J. Wang, P.L. Bishop, Development of a phosphate ion-selective microelectrode and its use in studies of the enhanced biological phosphorus removal (EBPR) process, Environ. Technol. 26 (2005) 381–388. https://doi.org/10.1080/09593332608618549.

[39] Z. Zou, J. Han, A. Jang, P.L. Bishop, C.H. Ahn, A disposable on-chip phosphate sensor with planar cobalt microelectrodes on polymer substrate, Biosens. Bioelectron. 22 (2007) 1902–1907. https://doi.org/10.1016/j.bios.2006.08.004.

[40] J.J. Wang, P.L. Bishop, Fabrication, calibration and evaluation of a phosphate ion-selective microelectrode, Environ. Pollut. 158 (2010) 3612–3617. https://doi.org/10.1016/j.envpol.2010.08.007.

[41] J.H. Lee, W.H. Lee, P.L. Bishop, I. Papautsky, A cobalt-coated needle-type microelectrode array sensor for in situ monitoring of phosphate, J. Micromechanics Microengineering. 19 (2009). https://doi.org/10.1088/0960-1317/19/2/025022.

[42] Y. Bai, J. Tong, C. Bian, G. Yan, B. Deng, H. Zhang, S. Xia, Micro cobalt electrodes for detection of total phosphorus in water, Micro Nano Lett. 7 (2012) 1176–1179. https://doi.org/10.1049/mnl.2012.0519.

[43] Y. Bai, J. Tong, C. Bian, S. Xia, Fabrication and characterization of cobalt nanostructure-based microelectrodes for phosphate detection, Key Eng. Mater. 483 (2011) 559–564. https://doi.org/10.4028/www.scientific.net/KEM.483.559.

[44] J.-Y. Han, J. Lee, Y.-G. Lee, A. Jang, Solid-state Ion Selective Lab Chip Sensor for On-site Measurement of Orthophosphate in Small Volumes of Liquid, J. Coast. Res. 79 (2017) 50–54. https://doi.org/10.2112/si79-011.1.

[45] L. Zhu, X. Zhou, H. Shi, A potentiometric cobalt-based phosphate sensor based on screen-printing technology, Front. Environ. Sci. Eng. 8 (2014) 945–951. https://doi.org/10.1007/s11783-013-0615-z.

[46] J. Jońca, W. Giraud, C. Barus, M. Comtat, N. Striebig, D. Thouron, V. Garçon, Reagentless and silicate interference free electrochemical phosphate determination in seawater, Electrochim. Acta. 88 (2013) 165–169. https://doi.org/10.1016/j.electacta.2012.10.012.

[47] R. Zeitoun, A. Biswas, Electrochemical Mechanisms in Potentiometric Phosphate Sensing Using Pure Cobalt, Molybdenum and their Alloy for Environmental Applications, Electroanalysis. 33 (2021) 421–430. https://doi.org/10.1002/elan.202060215.

[48] K. Xu, Y. Li, M. Li, Potentiometric Phosphate Ion Sensor Based on Electrochemical Modified Tungsten Electrode, ACS Omega. 6 (2021) 13795–13801. https://doi.org/10.1021/acsomega.1c00195.

[49] H. Pang, W. Cai, C. Shi, Y. Zhang, Preparation of a cobalt–Fe2+-based phosphate sensor using an annealing process and its electrochemical performance, Electrochem. Commun. 124 (2021) 106933. https://doi.org/10.1016/j.elecom.2021.106933.

[50] X. Wang, J. Church, W.H. Lee, H.J. Cho, Phosphate sensors based on Co-Cu electrodes fabricated with a sacrificial glass fiber paper template, 2015 IEEE SENSORS - Proc. (2015) 5–8. https://doi.org/10.1109/ICSENS.2015.7370475.

[51] T. Kidosaki, S. Takase, Y. Shimizu, Electrodeposited Cobalt-Iron Alloy Thin-Film for Potentiometric Hydrogen Phosphate-Ion Sensor, J. Sens. Technol. 02 (2012) 95–101. https://doi.org/10.4236/jst.2012.23014.

[52] F. Tafesse, M. Enemchukwu, Fabrication of new solid state phosphate selective electrodes for environmental monitoring, Talanta. 83 (2011) 1491–1495. https://doi.org/10.1016/j.talanta.2010.11.045.

[53] S.O. Engblom, The phosphate sensor, Biosens. Bioelectron. 13 (1998) 981–994. https://doi.org/10.1016/S0956-5663(98)00001-3.

[54] R.C.H. Kwan, H.F. Leung, P.Y.T. Hon, H.C.F. Cheung, K. Hirota, R. Renneberg, Amperometric biosensor for determining human salivary phosphate, Anal. Biochem. 343 (2005) 263–267. https://doi.org/10.1016/j.ab.2005.05.021.

[55] L. Gilbert, A.T.A. Jenkins, S. Browning, J.P. Hart, Development of an amperometric, screen-printed, single-enzyme phosphate ion biosensor and its application to the analysis of biomedical and environmental samples, Sensors Actuators, B Chem. 160 (2011) 1322–1327. https://doi.org/10.1016/j.snb.2011.09.069.

[56] M.S. Kilic, A Novel Flow-injection Rhodium Nanoparticles Modified Phosphate Biosensor and its Operation in Artificial Urine, Electroanalysis. 33 (2021) 1963–1977. https://doi.org/10.1002/elan.202100154.

[57] J. Cui, E.E. Ogabiela, J. Hui, Y. Wang, Y. Zhang, L. Tong, J. Zhang, S.B. Adeloju, X. Zhang, Y. Wu, Electrochemical Biosensor based on Pt/Au Alloy Nanowire Arrays for Phosphate Detection, J. Electrochem. Soc. 162 (2015) B62–B67. https://doi.org/10.1149/2.0701503jes.

[58] A.T. Lawal, S.B. Adeloju, Polypyrrole based amperometric and potentiometric phosphate biosensors: A comparative study B, Biosens. Bioelectron. 40 (2013) 377–384. https://doi.org/10.1016/j.bios.2012.08.012.

[59] G. Kopiec, K. Starzec, J. Kochana, T.P. Kinnunen-Skidmore, W. Schuhmann, W.H. Campbell, A. Ruff, N. Plumeré, Bioelectrocatalytic and electrochemical cascade for phosphate sensing with up to 6 electrons per analyte molecule, Biosens. Bioelectron. 117

(2018) 501–507. https://doi.org/10.1016/j.bios.2018.06.047.

[60] S. Berchmans, R. Karthikeyan, S. Gupta, G.E.J. Poinern, T.B. Issa, P. Singh, Glassy carbon electrode modified with hybrid films containing inorganic molybdate anions trapped in organic matrices of chitosan and ionic liquid for the amperometric sensing of phosphate at neutral pH, Sensors Actuators, B Chem. 160 (2011) 1224–1231. https://doi.org/10.1016/j.snb.2011.09.052.

[61] D. Talarico, S. Cinti, F. Arduini, A. Amine, D. Moscone, G. Palleschi, Phosphate Detection through a Cost-Effective Carbon Black Nanoparticle-Modified Screen-Printed Electrode Embedded in a Continuous Flow System, Environ. Sci. Technol. 49 (2015) 7934–7939. https://doi.org/10.1021/acs.est.5b00218.

[62] Y. Lu, X. Li, D. Li, R.G. Compton, Amperometric Environmental Phosphate Sensors, ACS Sensors. 6 (2021) 3284–3294. https://doi.org/10.1021/acssensors.1c01035.

[63] Y. Lu, Q. Lan, C. Zhang, B. Liu, X. Wang, X. Xu, X. Liang, Trace-Level Sensing of Phosphate for Natural Soils by a Nano-Screen-Printed Electrode, Environ. Sci. Technol. (2021). https://doi.org/10.1021/acs.est.1c05363.

[64] J.C. Quintana, L. Idrissi, G. Palleschi, P. Albertano, A. Amine, M. El Rhazi, D. Moscone, Investigation of amperometric detection of phosphate: Application in seawater and cyanobacterial biofilm samples, Talanta. 63 (2004) 567–574. https://doi.org/10.1016/j.talanta.2003.11.040.

[65] W.L. Cheng, J.W. Sue, W.C. Chen, J.L. Chang, J.M. Zen, Activated nickel platform for electrochemical sensing of phosphate, Anal. Chem. 82 (2010) 1157–1161. https://doi.org/10.1021/ac9025253.

[66] J. He, H. Sun, J. Dai, H. Wang, L. Yu, W. Zhou, Z. Shao, In situ growth of nanoflake and nanoflower-like Ni hydrated hydroxide on the surface of Ni foam as a free-standing electrode for high-performance phosphate detection, J. Hazard. Mater. 392 (2020) 122313. https://doi.org/10.1016/j.jhazmat.2020.122313.

[67] I. Campos, A. Sangrador, R. Bataller, D. Aguado, R. Barat, J. Soto, R. Martínez-Máñez, Ammonium and Phosphate Quantification in Wastewater by Using a Voltammetric Electronic Tongue, Electroanalysis. 26 (2014) 588–595. https://doi.org/10.1002/elan.201300538.

[68] I. Campos, M. Alcañiz, D. Aguado, R. Barat, J. Ferrer, L. Gil, M. Marrakchi, R. Martínez-Mañez, J. Soto, J.L. Vivancos, A voltammetric electronic tongue as tool for water quality monitoring in wastewater treatment plants, Water Res. 46 (2012) 2605–2614. https://doi.org/10.1016/j.watres.2012.02.029.

[69] Y. Jin, T. Qi, Y. Ge, J. Chen, L. Liang, J. Ju, J. Zhao, Ultrasensitive electrochemical determination of phosphate in water by using hydrophilic TiO2modified glassy carbon electrodes, Anal. Methods. 13 (2021) 996–1002. https://doi.org/10.1039/d0ay01854f.

[70] B. Ali, T. McCormac, C. Maccato, D. Barreca, G. Carraro, Multilayer assemblies of a Cu-phthalocyanine with Dawson type polyoxometalates (POMs) for the electrocatalytic reduction of phosphate, J. Electroanal. Chem. 858 (2020) 113770. https://doi.org/10.1016/j.jelechem.2019.113770.

[71] Z. Fredj, M. Ben Ali, M.N. Abbas, E. Dempsey, Determination of prostate cancer biomarker acid phosphatase at a copper phthalocyanine-modified screen printed gold transducer, Anal. Chim. Acta. 1057 (2019) 98–105.

https://doi.org/10.1016/j.aca.2018.12.058.

[72] U. Sivasankaran, L. Reinke, S.K. Anand, K. Malecka, K.G. Kumar, H. Radecka, S. Kubik, J. Radecki, Ultrasensitive electrochemical sensing of phosphate in water mediated by a dipicolylamine-zinc(II) complex, Sensors Actuators, B Chem. 321 (2020) 128474. https://doi.org/10.1016/j.snb.2020.128474.

[73] A. V. Kolliopoulos, D.K. Kampouris, C.E. Banks, Rapid and portable electrochemical quantification of phosphorus, Anal. Chem. 87 (2015) 4269–4274. https://doi.org/10.1021/ac504602a.

[74] S. Cinti, D. Talarico, G. Palleschi, D. Moscone, F. Arduini, Novel reagentless paper-based screen-printed electrochemical sensor to detect phosphate, Anal. Chim. Acta. 919 (2016) 78–84. https://doi.org/10.1016/j.aca.2016.03.011.

[75] M.T. Rahman, M.F. Kabir, Q. Qiao, Electrochemical Phosphate Sensors Using Silver Nanowires Treated Screen Printed Electrodes, IEEE Int. Conf. Electro Inf. Technol. 2018-May (2018) 993–997. https://doi.org/10.1109/EIT.2018.8500195.

[76] B. He, H. Liu, Electrochemical biosensor based on pyruvate oxidase immobilized AuNRs@Cu2O-NDs as electroactive probes loaded poly (diallyldimethylammonium chloride) functionalized graphene for the detection of phosphate, Sensors Actuators, B Chem. 304 (2020) 127303. https://doi.org/10.1016/j.snb.2019.127303.

[77] F. Zina, N.M. Nooredeen, S. Azzouzi, M. Ben Ali, M.N. Abbas, A. Errachid, Novel Sensitive Impedimetric Microsensor for Phosphate Detection Based on a Novel Copper Phthalocyanine Derivative, Anal. Lett. 51 (2018) 371–386. https://doi.org/10.1080/00032719.2017.1322096.

[78] L. Barhoumi, A. Baraket, N.M. Nooredeen, M. Ben Ali, M.N. Abbas, J. Bausells, A. Errachid, Silicon Nitride Capacitive Chemical Sensor for Phosphate Ion Detection Based on Copper Phthalocyanine – Acrylate-polymer, Electroanalysis. 29 (2017) 1586–1595. https://doi.org/10.1002/elan.201700005.

Chapter 3

Enhancing the sensitivity of cobalt based solid-state phosphate sensor using electrical pretreatment.

Vinay Patel[1], and P. Ravi Selvaganapathy[1,2*]

[1] School of Biomedical Engineering, McMaster University, Hamilton, ON, L8S 4K1, Canada

[2] Department of Mechanical Engineering, McMaster University, Hamilton, ON, L8S 4L7, Canada

Corresponding Author

P. Ravi Selvaganapathy – Department of Mechanical Engineering, McMaster University, Hamilton, ON, L8S 4K1, Canada; https://orcid.org/0000-0003-2041-7180

* selvaga@mcmaster.ca

Status: published

Full citation

Patel, Vinay, and P. Ravi Selvaganapathy. “Enhancing the sensitivity of cobalt based solid-state phosphate sensor using electrical pretreatment.” Sensors and Actuators B: Chemical 349 (2021): 130789.

KEYWORDS: *cobalt based phosphate sensor, solid state sensor, electrochemical, electrical pretreatment, phosphate sensor, phosphorus.*

Abstract

Phosphate is an important analyte to monitor in various water bodies. Cobalt based sensors are attractive for this application as they are solid-state, have a quick response time, are easy to fabricate and can perform reagent-less measurements. However, these sensors have lower sensitivity, limited dynamic range and require a chemical conditioning in a standard solution before measurement. In this study, an in situ anodic current pretreatment method in sample solution itself is used to enhance the sensitivity of the sensor and alleviate the need of chemical conditioning before measurement. With electrical pretreatment, the sensor exhibited a linear range from 10^{-6} M to 10^{-3} M with a sensitivity of -91.4 mV/decade of change in dihydrogen phosphate concentration. No significant interference was detected with common interfering anions that are typically present in field water samples such as nitrate, sulphate and chloride. Finally, the sensor was also responsive when tested on real water samples such as tap water, lake water and creek water spiked with phosphate.

1. Introduction

Phosphate is one of the major pollutants responsible for the global algal bloom in various water sources like lakes, ponds and other water bodies [1]. In order to prevent phosphate pollution, many governments have issued strict regulations to treat phosphate in wastewater before disposal [2,3]. Therefore, it is crucial to measure the phosphate concentration to maintain an optimal water quality before its disposal in natural water sources. A major source of phosphorus in the wastewater is due to agricultural run offs and industrial discharges [4]. This elevated level in phosphorus, results in eutrophication of lakes, rivers, oceans or standing water which is lethal to aquatic life and thus disturbs the ecological balance in water bodies [1]. Periodic on site field monitoring would allow

efficient use of fertilizers and limit phosphate run off onto water bodies [5,6]. Current methods for phosphate monitoring are laboratory based and the transport of samples from the field to the lab has significant costs which restrict widespread use of it for periodic monitoring. Field monitoring can also reduce the variability associated with sample collection, transport and sample degradation effects [6–8].

At present, phosphate detection is performed using optical [9–11], and electrochemical [12–17] methods . Optical sensors are the most dominant method and recommended by EPA. This method is used both for phosphate detection in both laboratory based and online monitoring systems. Here color change of a reagent (molybdenum blue or vanadate/molybdate yellow) upon reaction with phosphate in acidic medium is used to detect and quantify it [18]. The colorimetric approach provides accurate measurements but they requires toxic reagents, sophisticated instrumentation, sample preparation and skilled personnel for operation [19]. Multiple commercial online phosphorus monitoring systems use both the colorimetric methods (molybdenum blue or vanadate/molybdate yellow) mentioned above. These systems use microfluidic chips/channels, flow injection systems and pumps to automatically draw the required reagents for detection and self-cleaning protocols to remove the residuals from the channels after every measurement. However, these systems are expensive, large in dimensions, and require on-site chemical and waste storage systems [20].

Electrochemical sensors are lower in cost and complexity of instrumentation and are more amenable to field use. Traditionally, electrochemical sensing of phosphates have been performed using potentiometric [12,13], amperometric [16,17,21,22] and voltammetric sensors [23–25]. Potentiometric sensors have the advantage of being solid-state, low cost and reagent free. Amperometric sensors require multiple enzymes [17,21], a high alkaline pH (~11) [16,22] which

makes them difficult for in-field monitoring. Voltammetric tongues based semi-specific sensors are reported for phosphate measurements with an electrode panel of eight different metal electrodes [24,25]. However, the individual electrodes were not able to distinguish between different phosphate concentrations. Further, voltammetric pulses also have a significant effect on the selectivity of the metal electrodes. For example: cobalt electrodes which are known to be selective to phosphate ions were able to distinguish between different phosphate concentrations. However, the method needs multiple electrodes, training data set to predict reliable phosphate concentrations and works within a narrow range of 0.54 - 7.3 ppm. Another interesting method used cyclic voltammetry to detect phosphate using phosphomolybdate ions [23]. The method exhibited a measuring range of 0.25 to 3.08 mg/l which works well with the soil. However, the method requires a low pH (pH =1) to avoid silicate interference and works within a narrow range for other environmental samples.

Potentiometric sensors use two different approaches, one using metal/metal oxide electrodes and another using ion selective electrodes have been used. Ion selective approach has limitations as a suitable and selective ionophore that can detect phosphate in the presence of other common interferents is still under development. Alternatively, potentiometric metal/metal oxide electrode sensors are attractive but require extensive pre-conditioning. Also, most of the reported sensitivity for potentiometric sensors ranges from -19 mV/decade to -54 mV/decade) for metal based sensors [12,13,34–36,26–33] and -28 mV/decade to -55.7 mV/decade for ion selective membrane [15,37–42] based sensors.

Cobalt/Cobalt oxide system is the most common metal/metal oxide sensor used for phosphate detection. Cobalt electrodes require a chemical conditioning step in a standard solution such as DI water and/or buffer with defined phosphate concentration before measurements [12,27]. The

conditioning time can vary from 5 minutes for microfabricated electrodes to greater than 2 hours for wire based electrodes [12,13,26,27,29,32,33,43,44]. For instance, a two step conditioning protocol was used for the planar microfabricated electrode where the electrode was first immersed into DI water for 2 minutes followed by a 200 s conditioning in 10^{-4} M dihydrogen phosphate solution [33]. More importantly, many of the previous studies required that the measurements are performed in a phthalate buffer [12,13,28,29,31–33] which is not ideal for field sample measurements. Most of the previous, cobalt sensors have used 2-electrode configuration (working and reference electrode) for potentiometric measurement except one patent which proposed a counter electrode to maintain a negative polarity between working and counter electrode to prevent surface passivation of the cobalt during long term water exposure [45]. However, the study did not report any measurement data and implication of the applied potential on the measurement is unclear.

Here, we demonstrate that the long, reagent-based conditioning that is required for cobalt-based solid state sensors can be eliminated by a simple electrical pre-conditioning of the electrode just before measurement in the sample solution itself. This approach eliminates the requirement of any additional reagents needed for measurements, decreases the time for pre-conditioning and greatly improves the sensitivity to -91.4 mV/decade of concentration change within the dynamic range from 10^{-3} to 10^{-6} M of phosphate measurement. We also demonstrate that the sensors thus formed can be used for sensing phosphate in tap, lake and creek water field samples. There is minimal interference for other anionic species such as nitrates that may be present in the samples. This new electrical pre-conditioning process opens the potential for use of cobalt-based solid-state phosphate sensors in field measurements.

2. Experimental section

2.1 Materials

Cobalt wire (0.25mm in diameter, 99.995% purity, #10948) and stainless steel (SS) wire (0.25mm in diameter, type 304, #43300) were purchased from Alfa Aesar. A double junction silver-silver chloride (Ag/AgCl) reference electrode was purchased from Sigma-Aldrich (#Z113107). The screen printable dielectric paste (product# 124-18T) used was purchased from Creative Materials Inc. Sodium chloride (NaCl), potassium dihydrogen phosphate (KH_2PO_4), potassium monohydrogen phosphate (K_2HPO_4), potassium hydrogen phthalate (KHP), sodium nitrate ($NaNO_3$), potassium chloride (KCl) and sodium sulphate (Na_2SO_4) used were of analytical grade. Standard plain microscopic glass slides were used as the glass substrate for sensor fabrication.

2.2 Sensor fabrication

An overview of sensor fabrication process is illustrated in Figure 3.1a. Cobalt wire-based phosphate sensor was fabricated on a glass substrate (Step i). The cobalt and the SS wire were placed on the glass slide and were attached using double-sided conductive copper tape (Step ii). Then, a dielectric paste layer was screen printed to passivate the electrodes from the solution and exposing 2 cm of cobalt and SS wire to the sample solution (Step iii). The dielectric paste was cured at 120 ^{o}C for 60 minutes as directed by the manufacturer to remove the solvent and for optimal curing of the dielectric film (Step iv).

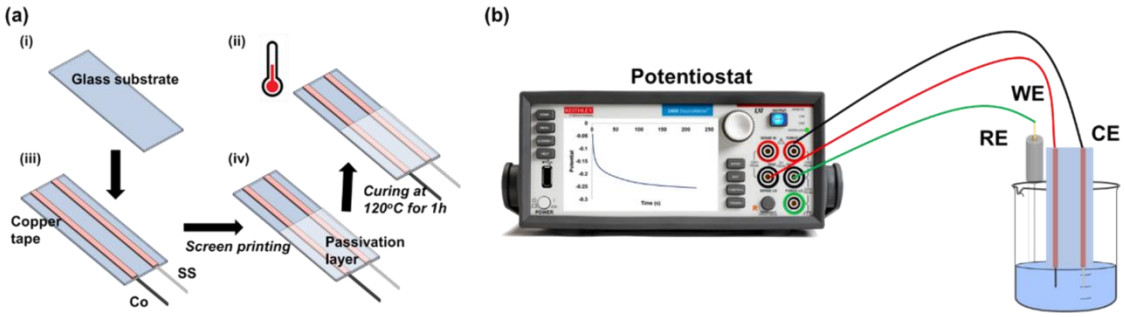

Figure 3.1 (a) Systematic overview of sensor fabrication process ((i) glass substrate, (ii) cobalt (Co) and stainless steel (SS) wire were attached using double side conductive copper tape, (iii) passivation layer and (iv) curing of passivation layer at 120°C for 60 minutes). (b) Experimental setup for measuring the sensor response of metal-based electrodes with working electrode (WE) as cobalt, stainless steel wire as the counter or auxiliary electrode and reference electrode (RE) as double junction Ag/AgCl.

2.3 Electrochemical measurements

All electrochemical measurements were done using a source measure unit (Keithley 2410) in a potentiostatic mode with cobalt wire as the working electrode (WE), Ag/AgCl as the reference electrode (RE) and a SS wire as a counter electrode (CE) (Figure 3.1b). The standard solutions were prepared by dissolving the required amount KH_2PO_4 in a 20 mM (1170 ppm) NaCl as the inert electrolyte. The salinity of the fresh water (<1000 ppm) was simulated by using 20 mM NaCl [46]. The conductivity and dissolved oxygen concentrations were measured using EXTECH handheld meters (ExStik II). The pH, and conductivity of the prepared NaCl solution was 6, and 2.26 mS respectively. The pH of the standard phosphate solutions from 10^{-8} M to 10^{-3} M was between 5.9 - 6.2. While the pH for 10^{-2} M was 5.2.

All measurements were performed in dip format in 100 ml of sample solution. Before each measurement, the electrode was polished using a silicon carbide sandpaper (Grade 600) to remove

any residual cobalt oxide or hydroxide film that may have formed due to air exposure. Prior to every measurement, the electrode was electrically pre-conditioned in the sample solution by applying a current density of -9.18 mA/cm^2 (-1.43 μA) between the WE and CE for 220 s (150-250 s) in the analyte solution. Following it, the sensor response was measured for 110s potentiometrically in open circuit mode.

2.4 Sensor characterization

Sensor surface morphology was characterized using a TESCAN Vega LSU Scanning Electron Microscope (SEM). SEM images were captured at an accelerating voltage of 5 kV and 8 mm as working distance (Figure S1, Appendix 1). The elemental composition of the samples was analyzed using the above mentioned SEM equipped with an Oxford X-Max detector and Inca software for energy dispersive X-ray spectroscopy (EDX) analysis. Line and surface mapping were used to investigate the composition of elements like carbon, phosphorus, cobalt and oxygen. The sensor-electrolyte interface was investigated by electrochemical impedance spectroscopy (EIS) using PalmSens4. EIS was performed at open circuit potential (OCP) with 5 mV AC bias with frequency from 100,000 Hz to 0.1 Hz and 15 points per decade of frequency change. EIS measurements were performed in 0.1 M KCl at open circuit potential and the sensor was equilibrated in the solution for 1 hour before the EIS measurements.

Three sensor surfaces (no pretreatment, pretreated and pretreated followed by measurement) were characterized by X-ray photoelectron spectroscopy (XPS). XPS analysis was performed using a Kratos AXIS Supra X-ray photoelectron spectrometer using a monochromatic Al K(alpha) source (15mA, 15kV). The sample were probed to a depth of 7-10 nm and the instrument can detect all elements except hydrogen and helium with a detection limit 0.1-0.5 atomic percentage. The work function of the instrument was calibrated using a Au 4f7/2 line to give a binding energy of 83.96

eV and spectrometer dispersion was adjusted using a metallic copper (Cu 2p3/2). Survey scans were performed with a pass energy of 160 eV to analyze an area of 300×700 μm^2. High resolution spectrum analysis was carried out with a pass energy of 20eV and the same analysis area as survey scan. The charge correction of the spectrum was done using the main line of carbon 1s set to 284.4 eV. Spectrum was analyzed using CasaXPS software (version 2.3.14). Cobalt (Co 2p) spectrum data was curve fitted using the procedure based on a previous study [47].

3. Results and discussion

3.1 Sensing mechanism

Metallic cobalt is covered with a passive film of its oxide (CoO) and hydroxide ($Co(OH)_2$) like other transition metals. When exposed to water, the water molecules adsorbs on the metal surface (Reaction 1-2) and potentially result in formation of multiple cobalt oxides/hydroxides such as CoO, $Co(OH)_2$ and Co_3O_4. The composition of this film depends strongly on solution pH and applied potential [48].

$$Co + H_2O \leftrightarrow Co(H_2O)_{ads} \quad (1)$$

$$Co(H_2O)_{ads} \rightarrow CoOH + H^+ + e^- \quad (2)$$

In acidic pH, the intermediate hydroxide generates cobalt (Co^{2+}) ion (Reaction 3) and continues the dissolution of cobalt metal [48].

$$CoOH^+ + H^+ \rightarrow Co^{2+} + H_2O \quad (3)$$

In neutral solution, the intermediate hydroxide generates $Co(OH)_2$ and CoO (Reaction 4-5), which would eventually stabilize the passivation film [48].

$$CoOH^+ + H_2O \rightarrow Co(OH)_2 + H^+ \quad (4)$$

$$Co(OH)_2 \rightarrow CoO + H_2O \quad (5)$$

In basic solutions, the film is further stabilized with a secondary film of mixed cobalt oxide (Co_3O_4) and cobalt oxyhydroxide (CoOOH) (Reaction 6-8) [48].

$$CoOH^+ + OH^- \rightarrow Co(OH)_2 \quad (6)$$

$$Co(OH)_2 + OH^- \rightarrow CoOOH + H_2O + e^- \quad (7)$$

$$3CoO + 2OH^- \rightarrow Co_3O_4 + H_2O + 2e^- \quad (8)$$

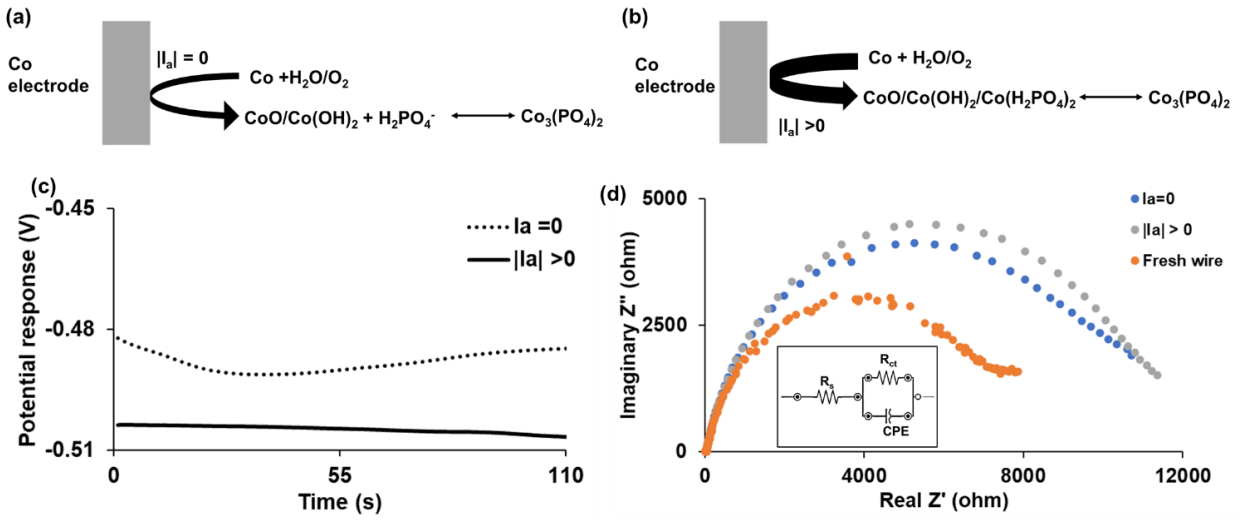

Figure 3.2 (a) Cobalt electrode with no pretreatment (I_a = 0), (b) Cobalt with electrical pretreatment ($|I_a|$ >0), (c) Sensor response with no pretreatment (I_a = 0, dotted line) and electrical pretreatment ($|I_a|$ >0, solid line) in 10^{-3} M KH_2PO_4 (d) Nyquist plot from the electrochemical impedance measurements with freshly polished cobalt wire with no phosphate exposure (orange dots), no current (blue dots) and current pretreatment (grey dots).

Here, a constant anodic-current pretreatment process was used to promote the oxidation of metallic cobalt and the measurement was performed under zero-current potentiometry (Figure 3.2a and

3.2b). This increased anodic oxidation results in formation of a more stable film of cobalt oxide resulting in a more negative potential shift [13]. The more negative potential shift was correlated to the enhanced oxidation of metallic cobalt to various oxides resulting in a higher potential with anodic current pretreatment as compared to no pretreatment (Figure 3.2c). Figure 3.2c shows the stability of the electrode potential over time, when a freshly polished sensor is exposed to 10^{-3} M KH_2PO_4 with (solid line) and without (dotted line) the current pretreatment.

In current method, the cobalt electrode was pretreated *in situ* in presence of other ions like sodium, chloride, dihydrogen phosphate, and potassium. These ions might have adsorbed on the passivation film during the pretreatment and measurement. Thus, these ions were observed in the survey spectra of the XPS measurement (Figure S2, Appendix 1). Moreover, dihydrogen phosphate is known to form complex under applied potential [27]. Therefore, another potential reaction was believed to occur in presence of dihydrogen phosphate during electrical pretreatment (Reaction 9).

$$Co(H_2PO_4)_2 + 2e^- \rightarrow Co + 2H_2PO_4^- \quad (9)$$

Finally, the oxide/hydroxide/phosphate films converts to cobalt (II) phosphate as confirmed from X-ray diffraction analysis by a previous study [27]. The following reactions are believed to occurs at the interface to generate cobalt (II) phosphate (Reaction 10-12) [27]:

$$2Co_3O_4 + 3Co(H_2PO_4)_2 \leftrightarrow 3\,Co_3(PO_4)_2 + 6H_2O + O_2 \quad (10)$$

$$2CoO + Co(H_2PO_4)_2 \leftrightarrow Co_3(PO_4)_2 + 2H_2O \quad (11)$$

$$2Co(OH)_2 + 3Co(H_2PO_4)_2 \leftrightarrow 3Co_3(PO_4)_2 + 4H_2O \quad (12)$$

EIS was performed to characterize the change in ionic and electronic charge transfer at the electrode-electrolyte interface with electrical pretreatment. The impedance data at low frequency

is related to the ionic charge transfer while the data at high frequencies provides insight in interfacial electronic transfer. EIS measurements were performed in 10^{-3} M KH_2PO_4 samples for freshly polished sensors with and without the current pretreatment. The Nyquist plots from the EIS measurements are shown in Figure 3.2d. A Randles circuit with three components: R_s representing solution resistance, R_{ct} representing charge transfer resistance and constant phase element (CPE) representing a combined effect of double layer and cobalt phosphate film on the electrode, was fitted to the experimental data (Figure 3.2d inset). The CPE was used instead of an ideal capacitive element, to capture the heterogeneity of the electrode surface. The impedance of CPE is defined as $Z\ (CPE) = [Q(j\omega)^n]^{-1}$, where Q is a constant, n is CPE power and ω is angular frequency. All fitted data had a χ_2 value in order of 10^{-3} and the error associated with all the components were <3.2%. No significant changes were observed in R_s for all the three cases. A significant increase in diameter of the semicircle was recorded for the Nyquist plot when the phosphate measurement was performed with pretreatment as compared to without pretreatment. An increase in both the Q value for CPE (21%) and R_{ct} (6%) were observed with pretreatment as compared to without pretreatment when the data was fitted to the electrical circuit. The increase in the R_{ct} and CPE for pretreated sensor can be attributed to a thicker insoluble cobalt oxide/phosphate film on the sensor resulting in the decreased electrochemical activity of cobalt oxide film.

3.1.1 XPS characterization

XPS was used to further investigate the composition of cobalt sensor before and after pretreatment followed by the measurement. Three cobalt sensors were prepared and exposed to 10^{-2} M KH_2PO_4. The first sample was untreated cobalt sensor exposed to 10^{-2} M KH_2PO_4 for potentiometric measurement. The second sample was sensor which was electrically pretreated in 10^{-2} M KH_2PO_4 while the third one has undergone electrical pretreatment followed by zero current potentiometric measurement 10^{-2} M KH_2PO_4. Survey scans were performed for all three samples (Figure S2, S3

and S4, Appendix 1). The spectra showed that the sensor surface was composed of cobalt, phosphorus, oxygen, potassium, sodium, chlorine, along with some traces of nitrogen and silicon. The sensors were sealed in nitrogen after the experiment to avoid the sensor contact with oxygen and the amount of silicon might have come from the sandpaper used for sensor cleaning. The sensor surface was further investigated using the high-resolution spectra of cobalt (Co 2p) to know the composition of cobalt species present on the surface (Supporting information, Figure S5, S6 and S7). The spectra was fitted mainly with five cobalt species: metallic cobalt (Co(0)), cobalt (II) hydroxide ($Co(OH)_2$), cobalt phosphate ($Co_3(PO_4)_2$), cobalt (II, III) oxide (Co_3O_4) and cobalt oxyhydroxide (CoOOH) [47]. The cobalt composition of three samples from the high-resolution spectra is summarized in Table 3.1.

An increase in the amount of cobalt phosphate present on the sensor surface just after the electrical pretreatment (65%) was higher as compared to a sensor without pretreatment (41%) (Table 1) (Figure S5 and S6, Appendix 1). Another study reported similar decrease in the activity of cobalt oxide film in presence of NaH_2PO_4 due to incorporation of insoluble cobalt phosphate in the film [49]. However, this increase in cobalt phosphate was reduced when the pretreatment step is followed by the measurement step (40%), but an increase in the ratio of Co^{3+}/Co^{2+} was observed as compared to untreated sensor.

Table 3.1 High resolution XPS data for three cobalt sensor samples where the number represents the atomic percentage of different forms of cobalt. The cobalt sensor was not subjected to pretreatment (No pretreatment). The cobalt sensor subjected to electrical pretreatment (Pretreated). The last sample was

subjected to electrical pretreatment and then zero current potentiometry was performed after the pretreatment (Pretreated + measurement).

Sample Identifier	**Co(0)**	**$Co(OH)_2$***	**$Co_3(PO_4)_2$***	**Co_3O_4**	**CoOOH**
No pretreatment +Measurement	2	46	41	0	12
Pretreated	5	21	65	0	9
Pretreated + Measurement	10	29	40	13	8

*A significant error was associated with $Co(OH)_2$ and Co_3PO_4 percentages due to a significant overlap in the peaks of these compounds. Therefore, the percentage of Co_3PO_4 were estimated from the total cobalt based on the stoichiometry from the survey scan results.

3.2 Effect of electrical pretreatment on phosphate sensing

The influence of the electrical pretreatment on the sensing performance of the cobalt/cobalt oxide sensor was studied. The sensors prepared were placed in sample solution (standards) with phosphate concentration between 10^{-8} M to 10^{-2} M. The electrical pretreatment was performed which was immediately followed by open circuit potential measurement. These results were compared with two control conditions. The first control experiments (Control 1) were done with sample solutions prepared in 25 mM potassium hydrogen phthalate buffer solution as used by previous studies [12,13]. These control experiments were done to investigate the influence of inert electrolyte and pH on the sensitivity of the sensor. While in second control experiments (Control 2), open circuit potential measurements were performed in the absence of electrical pretreatment in the same sample solutions. All experiments were done three times (n =3).

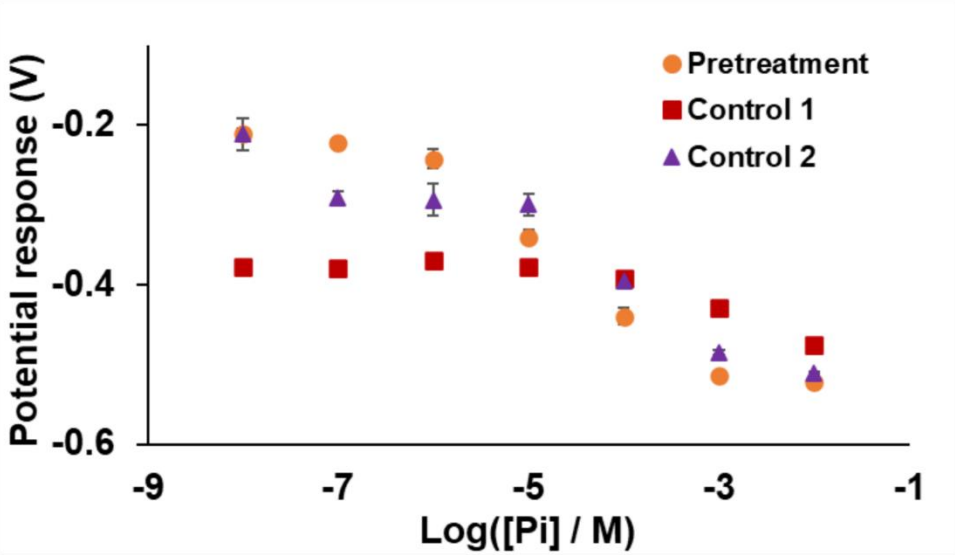

Figure 3.3 Plot showing the effect of current pretreatment when the sensor is exposed to current (circles) and two control experiments: No current with KHP (Control 1) as the inert electrolyte (rectangles) and No current with NaCl (Control 2) as inert electrolyte (triangles). All experiments were repeated three times (n=3). Pi represents phosphate concentrations.

The electrical pretreatment alleviates the need of conditioning the sensor in standard solution and it also increases the sensitivity of the sensor. As plotted on a semi-log scale, the sensors exhibited a linear response in the concentration range from 10^{-6} to 10^{-3} M with increased sensitivity of -91.4 mV/decade (Figure 3.3, circles) with electrical pretreatment. In Control 1, the sensor had a linear range from 10^{-5} to 10^{-1} M with a sensitivity of only -36.5 mV/ decade (Figure 3.3, rectangles). In Control 2, the sensors exhibited a linear range from 10^{-5} to 10^{-2} M with a sensitivity of -72.4 mV/ decade of phosphate concentration (Figure 3.3, triangles). Control 1 experiments confirmed that the increased sensitivity is not due to the change in the base electrolyte in the conventional methods (25 mM KHP buffer) to 20 mM NaCl solution. While the second control experiments demonstrated

that the current pretreatment is necessary to achieve the increased sensitivity and the extended range to the lower phosphate concentration.

The applied anodic current during the pretreatment step promotes the formation of additional cobalt oxide (Reaction 1) by promoting the forward reaction. This was supported by the observed shift in potential response with current pretreatment to more negative values as compared to without treatment within the 10^{-5} M to 10^{-3} M. In addition, the current pretreatment resulted in an early saturation of the potential response at 10^{-3} M while the potential response of Control 2 reached the saturated potential response at 10^{-2} M. In Control 1 experiments, the sensor response saturates at 10^{-1} M similar to previous studies [12,28,29,31–33]. According to the Pourbaix diagram for Co-H_2O at 25 ^{o}C, cobalt does not oxidise at negative potentials greater than -0.5 V at pH < 9, which was demonstrated by sensors in all three conditions (electrical pretreatment, Control 1, and Control 2) [50]. The upper limit of linear range for all sensors was -0.514 V (10^{-3} M phosphate solution), -0.519 V (10^{-1} M phosphate solution, data not shown here) and -0.511 V (10^{-2} M phosphate solution) with current pretreatment, control 1 and control 2 experimental conditions respectively. At the other end of the linear range, Control 1 achieved a potential of -0.378 V for 10^{-5} M phosphate solution which was lower than the sensors with electrical pretreatment (-0.340 V) and Control 2 (-0.300 V). The lower potential response might be due to more cobalt oxidation at pH 4 (25 mM KHP buffer solution) as compared to pH 6 (20mM NaCl solution) [50].

3.3 Effect of pretreatment duration

The duration of the electrical pretreatment can have a significant influence on stability of the cobalt oxide film on the electrode. In order to determine this effect, the electrical pretreatment (-1.43 μA current) was performed for five different durations (50, 100, 220, 300s and 400 s) and its influence on the sensor response was compared using the sensitivity and limit of detection obtained under

each condition, as shown in Figure 3.4a. The potential response was calculated as the average of the last 10 s of the potentiometric measurement. Three sensors were used for each pulse duration (n=3).

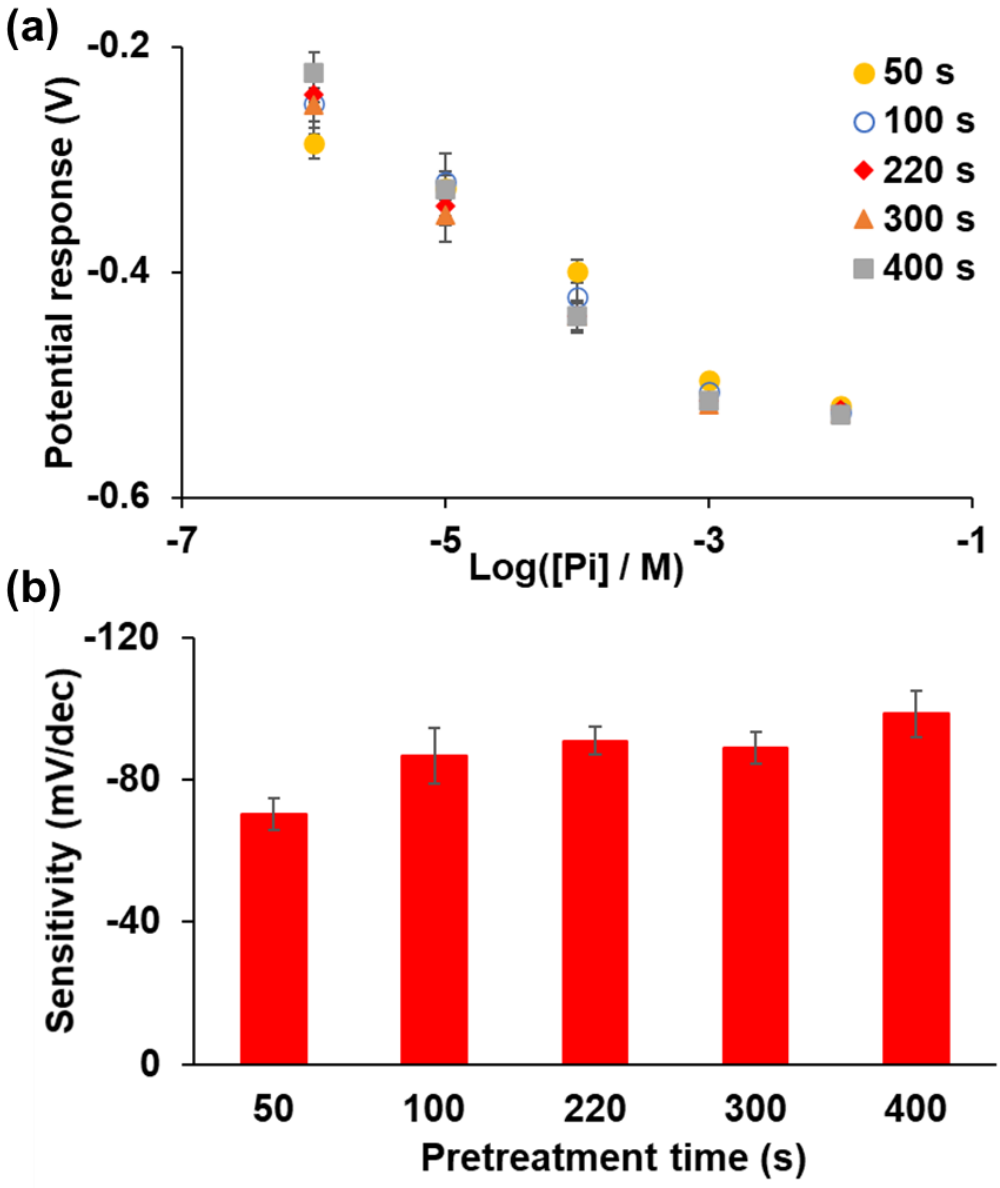

Figure 3.4 (a) Effect of pulse duration of the anodic current on the sensor response with four time durations 50 s (yellow circles), 100 s (open circles), 220 s (red diamond), 300 s (orange triangles)

and 400 s (grey rectangles). (b) Sensitivity (mV/ decade) for each pulse durations. All experiments were done using three sensors (n=3).

The results (Figure 3.4a) demonstrated that all the electrically pretreated electrodes respond linearly to a range of concentration between 10^{-6} M to 10^{-3} M of phosphate in the sample. The difference between them arises from the sensitivity as shown in Figure 3.4b.

When the electrical pretreatment was applied for short duration of time (50 s), the slope of the calibration curve was low at -70.3 mV/decade with a R^2 value of 0.955. This slope is similar in magnitude to that obtained when fresh Co wire was used as an electrode indicating that the lower time duration was not sufficient for formation of the required cobalt phosphate film to achieve the high sensitivity. With increase in the pretreatment time, the sensitivity increases to -86.83 mV/decade at 100s, -91.4 mV/decade at 220 s and -88.9 mV/decade at 300s. The variation in the sensor response was also higher for smaller pretreatment durations probably because the electrical pretreatment did not reach an equilibrium state. Therefore, 220 s was selected as the optimal time for current pretreatment and all further experiment were performed using 220 s as the pretreatment duration.

3.4 Dynamic response for standard phosphate solutions

The dynamic response of the sensor is an important parameter to define the working range of the sensor in a solution matrix. Here the dynamic sensor response was tested using seven standard phosphate solutions. The standard solutions were prepared by dissolving potassium dihydrogen phosphate in 20 mM NaCl (Section 2.3). Every measurement cycle includes current pretreatment (220 s) followed by recording the potential response of the sensor. The sensor surface was

regenerated by mechanically polishing the sensor after every measurement. The slope of the calibration curve obtained was -91.4 mV/decade of phosphate concentration change between 10^{-3} M to 10^{-6} M with a R^2 value of 0.9959, showing a good linear fit for the sensor response (Figure 3.5). The high sensitivity obtained can be due to the presence of mixed oxide on the surface of the sensor after electrical pre-treatment. X-ray photoelectron spectroscopy (XPS) measurements on the surface of the bare Co wire, electrically pre-treated sensor and sensor after measurement was performed to understand the dynamics of the surface modification due to pre-treatment. Based on the XPS data, an increase amount of cobalt phosphate was observed on the sensor surface just after the current pretreatment indicating higher phosphate incorporation in the surface film than in the sensor without pretreatment (Table 3.1) (Figure S5 and S6, Appendix 1). During the measurement step after pretreatment, the amount of Co_3O_4 on the sensor surface changed from 0% for the sensors with no pretreatment to 13% for pretreated sensors confirming that the pretreatment enhances the ratio of Co^{3+}/Co^{2+} present on the surface on the oxide/phosphate film (Figure S7, Appendix 1). The change in oxidation state of the film resulted in higher sensitivity observed for the current pretreated electrodes. The high sensitivity observed was similar to the high sensitivity reported for the pH sensors fabricated using electrodeposited iridium oxide film [51]. There again, the high sensitivity was due to the presence of multiple oxidation states of iridium (Ir^{3+} and Ir^{4+}) in the oxide film and the mixed potential response due to the non-redox reactions. In addition, other non-redox reactions can also contribute to the high pH sensitivity [51,52].

The sensor response was saturated beyond a concentration of 10^{-3} M. This can be understood from the Pourbaix diagram for Cobalt at 25 ^{o}C that also show a saturation of oxidation potential at ~ -0.5 V under current conditions [50]. Therefore, no further potential changes can occur resulting in a constant sensor response with increase in phosphate concentration. More importantly, the

electrical treatment protocol can potentially extend the lower detection range of the cobalt based phosphate sensor to phosphate concentration (~10^{-8} M) (Inset Figure 3.5). In addition, current sensor saturates for concentration >1 mM of dihydrogen phosphate which can be due to the lack of active cobalt on the surface which prevents the formation of additional cobalt oxide with phosphate concentrations beyond 1 mM.

The sensitivity of the present sensor was higher than the cobalt based wire sensors (-19 to -54 mV/decade) [27,28,32,33], molybdenum based electrodes (-26.9 to -27.8 mV/decade) [34,36] and ion selective membrane based sensors (-28 to -55.7 mV/decade) [15,38,40]. The higher sensitivity of the sensor can be attributed to the anodic current pretreatment which favors the conversion of Co to Co^{2+}. However, most of the cobalt based sensors work within a wide range from 10^{-5} to 10^{-2} M with the widest working range of 10^{-6} to 10^{-1} M [53] but the working pH reported was 3.75 to 4, which might not be suitable for most of the phosphate measurement applications. Similarly, molybdenum base sensors reported a working range of 10^{-5} to 10^{-2} M but the sensor works in alkaline pH which might not be suited to most of the phosphate measuring applications [34,36].

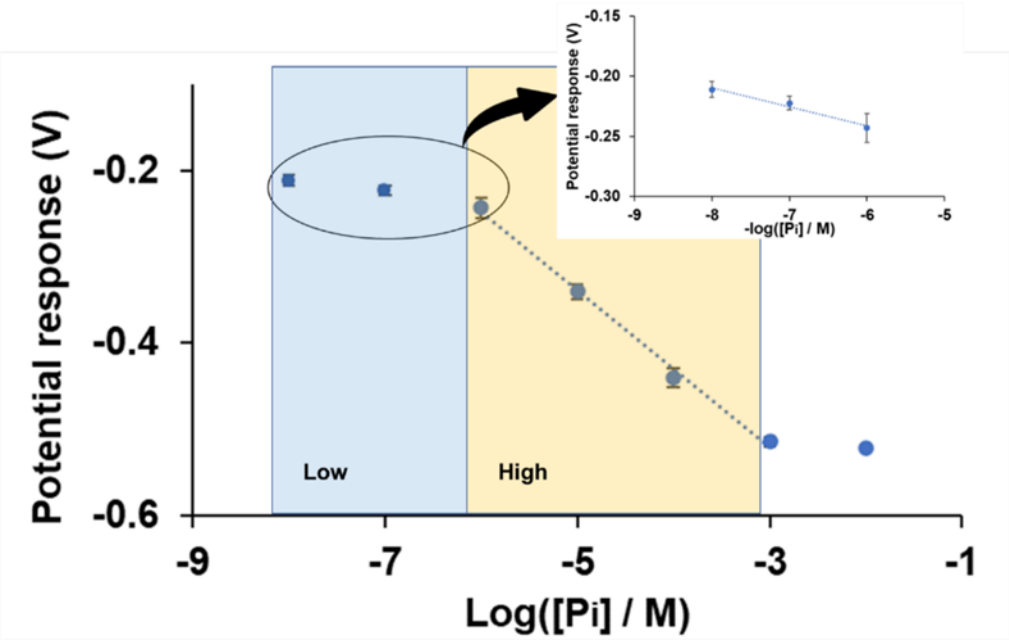

Figure 3.5 Dynamic sensor response for phosphate concentration from 10^{-2} M to 10^{-8} M. Yellow region represents the main testing range of the sensor while the blue region is the sensor response for low phosphate measurements.

3.5 Effect of electrical pretreatment on sensor-electrolyte interface

EIS was performed to understand changes at the electrode-electrolyte interface with electrical pretreatment and the influence of different phosphate concentration on the interface. Here, the measurements were performed with four standard KH_2PO_4 concentrations (0.01 µM, 1 µM, 1 mM and 10 mM) prepared as per protocol described in Section 2.3. The experimental data was fitted to a Randles circuit with three components: R_s representing solution resistance, R_{ct} representing charge transfer resistance and constant phase element (CPE) representing a combined effect of double layer and cobalt phosphate film on the electrode (Section 3.1.).

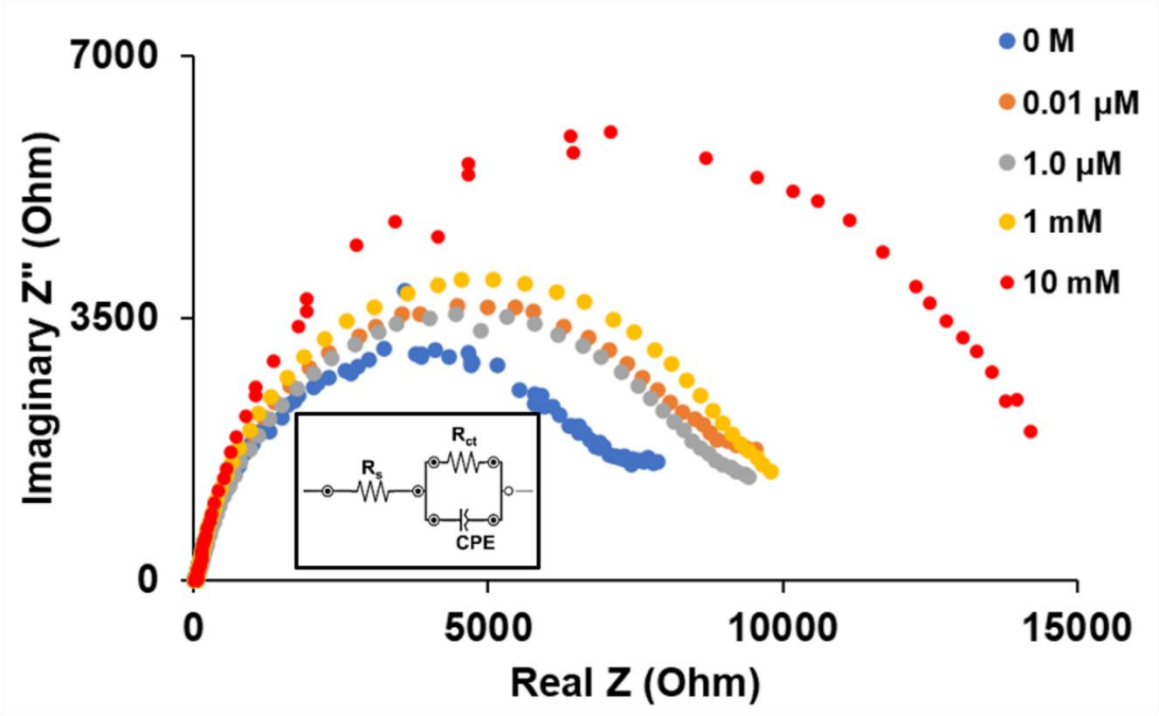

Figure 3.6 (a) EIS plot with four different KH_2PO_4 concentrations (0.01 μM (orange dots), 1 μM (grey dots), 1mM (yellow dots) and 10 mM (red dots)) and blank measurement (blue dots) were done with a fresh sensor no exposed to phosphate (blue dots). (b) Randles circuit with three components where R_s is solution resistance, R_{ct} is charge transfer resistance and CPE is constant phase element.

R_s changes depending on the spiked KH_2PO_4 concentrations where 8% resistance change was observed for 0.01 μM KH_2PO_4 and around 16% resistance change was observed for 10 mM KH_2PO_4. When the sensor was exposed to 0.01 μM KH_2PO_4 concentrations, a 26% increase in R_{ct} was observed as compared to a sensor with no phosphate exposure (Figure 3.6, orange dots). The increase in R_{ct} can be linked to the formation of the cobalt phosphate film on the surface with phosphate exposure. While a small increase in R_{ct} was observed for 1 μM and 1 mM was 28% (Figure 3.6, grey dots) and 31% (Figure 3.6, yellow dots) respectively. The small increase in R_{ct} can be related to formation of additional cobalt phosphate film but it did not seem to have a significant impact on the charge transfer on the electrode-electrolyte interface. However, a 93% increase in R_{ct} was observed for 10 mM (Figure 3.6, red dots), showing the formation of a thicker phosphate film which was further confirmed by the sensor response saturation at 10 mM KH_2PO_4. While no significant change was observed for the Q value of CPE.

3.6 Sensor repeatability and reproducibility

The repeatability of mechanical cleaning for reuse of the sensor for multiple measurements was investigated by conducting 10 repeated measurements where the electrode was polished using the sandpaper after each measurement. The sensor was tested in 10^{-5} M potassium dihydrogen solution. The sensors showed an average potential response of -0.353 V with a standard deviation of 0.7% (Figure 3.7). The relative standard deviation (R.S.D) for 10 measurements was 2.1% which was

comparable to the previous reported sensors for screen printed cobalt based sensor (R.S.D. 0.5% [31]), bulk cobalt wire (3.8% R.S.D. [54] and 3% R.S.D [55]) and on-chip phosphate sensor (0.6% [56]). The sensor surface was also investigated using SEM-EDX with a polished and unpolished surface (Figure S8, Appendix 1). EDX results confirmed the absence of oxygen on the polished cobalt electrode surface showing that the polishing can effectively regenerate the sensor surface.

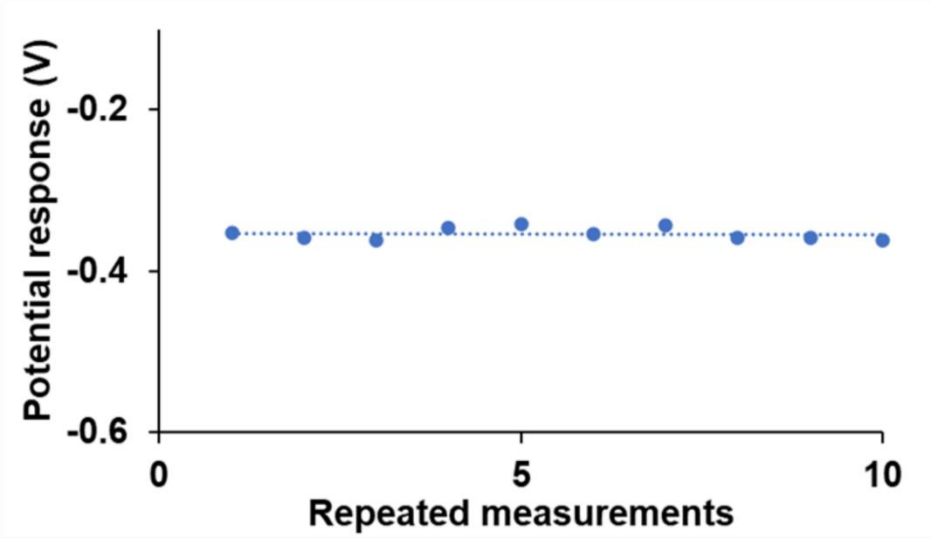

Figure 3.7 Plot showing the sensor repeatability data. The sensor was tested for 10 measurements. After every measurement, the sensor was polished using a sandpaper to regenerate the sensor surface.

The sensor-to-sensor reproducibility was evaluated by fabricating four sensors and testing the sensor with 10^{-5} M potassium dihydrogen solution. The average sensor response was -340.14 mV with a standard deviation of 0.8% and R.S.D of 2% (n=4) which is comparable to the reported sensors (on-chip sensor 2.5% R.S.D. [56] and screen printed sensors 1.9% to 3.2% R.S.D. [29]).

3.7 Interference study

The electrode response for cobalt based sensor is a mixed potential response [13]. Therefore, the sensor response depends on factors like pH, conductivity, and dissolved oxygen. The sensor was also tested with common interfering anions present in surface water like nitrates, sulphate and chlorides.

3.7.1 Effect of conductivity

Conductivity of the water varies depending on the source of water. For instance, conductivity of potable water ranges from 0.030 to 1.5 mS and conductivity range in freshwater streams is 0.1 to 2 mS [57]. Therefore, the sensor was tested in a wide range of conductivity from 0.05 mS to 10.4 mS. Five solutions of different conductivities (0.05 mS, 0.6 mS, 2.3 mS, 5.3 mS and 10.4 mS) were prepared by dissolving sodium chloride in deionized water. The effect of conductivity on sensor response is plotted in Figure 3.8a where each point on the graph represents the average of three sensors (n=3) and the error bar is the standard deviation of the response of three sensors. The calibration slope was -8.2 mV/mS with an y-intercept and R^2 value of -0.195 V and 0.9254. For potable water, a change in conductivity from 0.5 to 1 mS will result in a 4.1 mV change which is 0.045 times of the sensitivity per decade of phosphate measurements.

3.7.2 Effect of dissolved oxygen

The response of cobalt electrodes is influenced by dissolved oxygen concentration due to its mixed potential response (Reaction 2) as highlighted in previous publications [13,27]. Therefore, the sensor response is dependent on the oxygen concentration and it is positively related to the oxygen concentration unlike phosphate where the potential decreases with increase in phosphate concentration [13,27]. The effect of oxygen in this study was studied by exposing the sensor to three dissolved oxygen concentrations (0%, 48.3% and 53.1%) in presence of 10 µM of KH_2PO_4.

The calibration plot exhibited a change of 65 mV per 10% change in dissolved oxygen change (Figure 3.8b) which is a significant change as compared to the sensitivity of the sensor. The potential change was comparable to the wire based sensor reported in literature where dissolved oxygen change from 0% to 21% has resulted in a potential change from -0.58 to -0.33V in 10^{-4} M standard phosphate solution at pH 7.5 [58]. Therefore, a dissolved oxygen measurement should be performed with the sensor as reported by other cobalt based sensors [13,44,58].

3.7.3 Effect of pH

pH changes the composition of the phosphate species present in the analyte solution and the sensor response depends on pH of the solution as reported previous studies [12], [16]. In current study, the effect of pH was investigated using four different pH values 4, 6, 8 and 10 using 20mM NaCl as the inert electrolyte. The pH was adjusted using potassium hydroxide and hydrochloric acid. The sensor response at pH 4 exhibited a calibration slope of -48.1 mV/decade (R^2 value = 0.9639) for a linear range from 10^{-7} to 10^{-3} M (Figure 3.8c, red dots). The calibration slope was similar to the sensor reported previously while the current pretreatment showed an extension of the measuring range to 10^{-7} M. At pH 4, the potential response for 10^{-7} M showed a higher negative potential (-0.332 V) as compared to pH 6 (-0.222 V) and pH 8 (-0.225 V), which might be due to more cobalt oxidation at pH 4 as compared to neutral and alkaline solutions [50]. The measuring range of sensor at pH 8 was from 10^{-6} to 10^{-2} M (R^2 value = 0.965) with a calibration slope of -61.3 mV (Figure 3.8c, yellow diamonds). The decrease in slope can be attributed to the beginning of inactivation of the cobalt surface due to alkaline pH [50]. The sensor failed to perform at pH 10 (sensor response not shown here). The range of pH in typical environmental samples are quite small. Therefore, the electrical pretreatment can be used for samples with less pH fluctuations (~ ±0.5 pH changes). For larger pH variations, the sensors response should be normalized with pH values to get reliable results.

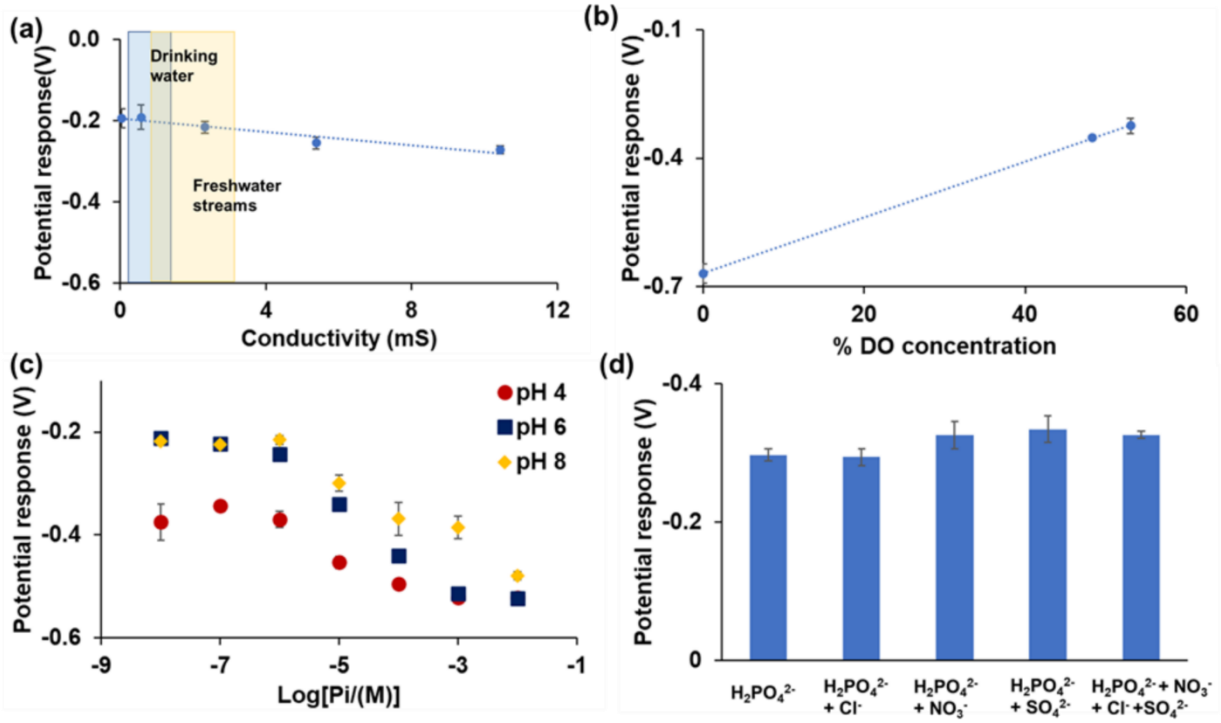

Figure 3.8 (a) Sensor response with four different conductivity solutions (0.6 mS, 2.3 mS, 5.3 mS and 10.4 mS). Experiment was performed with three sensors (n=3) and the error bars represents the standard deviation between the response of the three sensors (b) Sensor response (n=3) for three different dissolve oxygen concentrations (0%, 48.3% and 53.1%). Each point in the plot represents the average of three sensors (n=3) and error represents the standard deviation. (c) Effect of pH on the sensor response. pH= 4, 6 and 8 experiments were performed using 20mM NaCl as the inert electrolyte (n=3). The pH was adjusted using potassium hydroxide and hydrochloric acid. (d) Effect of common interferents (chloride, nitrates and sulphates) on the sensor response. The bar plot represents the average value of the sensor response from three sensors (n=3) while the error bar represents their standard deviation.

3.7.4 Effect of coexisting anions

Sensor interference was tested with common coexisting anions present in tap water and surface water like chloride, nitrate and sulphate. The interference testing was done using sodium salt of the anions mentioned above. The test was started with the current pretreatment followed by the

measurement, beginning with a KH_2PO_4 solution followed by KH_2PO_4 solution with the interferent. The concentration of surface water nitrates (0-18 mg/l)[59], sulphates (200 mg/l)[60], and chloride (<250 mg/l)[61]. Therefore, the experiment was performed with 50 mg/l of nitrate, 500 mg/l of sulphate and 500 mg/l of chloride dissolved in 10 μM of KH_2PO_4 sample solution. The results showed that there was minimal change in the potential response of the sensor to various anions species added to the background (Figure 3.8d). The selectivity coefficients calculated for chloride, nitrate and sulphate were -4.04, -1.75 and -3.58, respectively. These measurements compare well with previously reported selectivity coefficients for chloride, nitrate and sulphate which were in the range of -2.3 to -4.0, -3.1 to -3.3 and -3.0 to -3.2, respectively [12,27,58]. Therefore, the electrical pretreatment does not have a significant effect on the sensor response in presence of coexisting anions as compared to the chemical pretreatment in standard solutions. Hence, the electrical pretreatment can be used for preconditioning the sensor *in situ* before phosphate measurement.

3.8 Field sample testing

Finally, the *in situ* electrical pretreatment for cobalt electrode was tested with tap water and surface water to demonstrate its ability for phosphate measurement in real water samples. Two tap water samples were collected from Hamilton (Tap water_H) and Markham (Tap water_M). For surface water, one sample was collected from Lake Ontario, Hamilton while the other sample was collected from Spring Creek near McMaster University, Hamilton. Tap water samples were used as collected from the source while Lake water and creek water was filtered using a 0.2 μm Whatman filter paper to remove the solid particles present in the water samples before measurement. The calibration curve for real samples was generated using the collected tap water sample (Tap water_M). The Tap water_M sample was spiked with three KH_2PO_4 concentrations

(10^{-5}, 10^{-4} and 10^{-3} M) moving from low to high concentrations within a sample volume of 100 ml. The final phosphate concentrations of the spiked samples were measured using Orion Aquamate 8000, UV-Vis spectrophotometer using the Phosphomolybdic acid/ascorbic acid method (detailed protocol, Appendix 1) and the measured phosphate values were plotted against the potential response in Figure 3.9. The three measured phosphate concentrations from colorimetric methods were 3.89×10^{-5}, 1.41×10^{-4} and 1.66×10^{-3} M, respectively. The sensor was able to differentiate between real water samples spiked with the different KH_2PO_4 concentrations. The calibration slope of the curve (y (mV)=-66.6× [KH_2PO_4] -657.5) was -66.6 mV/decade of KH_2PO_4 concentrations in tap water which was 32% higher than the calibration slope (-50.6 mV/decade, Supporting information S9) for zero current potentiometry. The calibration slope for the real samples was lower than the standard solution which can be linked to the change in pH, conductivity and presence of interfering anions in the tap water samples. The pH of tap water_H and tap water_M were 7.19 and 7.47, respectively. The conductivity values were also less (0.33 mS for both tap samples) as compared to the standard phosphate solution.

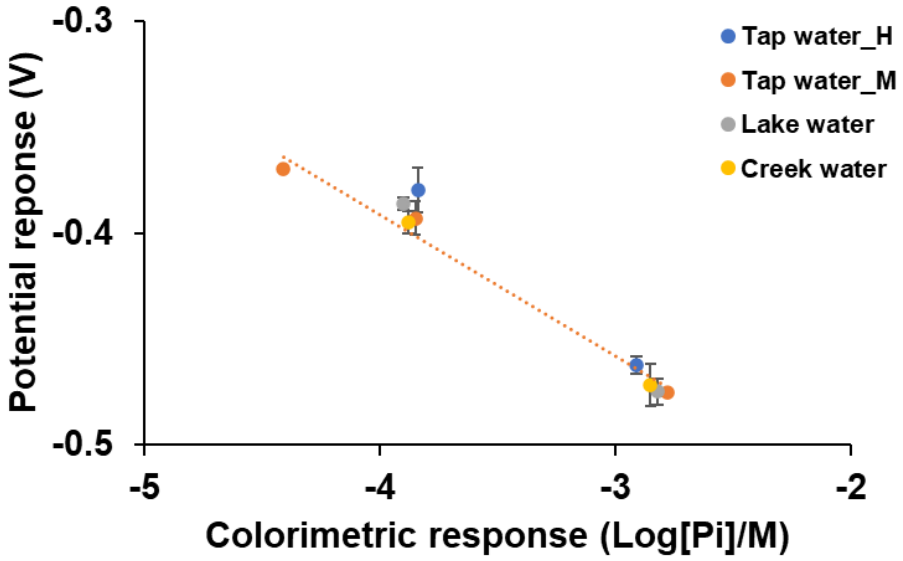

Figure 3.9 Potential response of the sensor in tap water and surface water. The samples were spiked with KH_2PO_4 to generate two different phosphate concentrations (1 mM and 0.1 mM). Each data point in the plot represents average of three sensor data (n=3) and error bar represents the standard deviation of the data.

The sensor response was validated by spiking the lake water, creek water and tap water_H with two KH_2PO_4 concentrations (10^{-4} and 10^{-3} M). For lake water and creek water, the sensor response was similar to tap water samples for concentration between 10^{-4} and 10^{-3} M. However, the sensor response was saturated between 10^{-5} and 10^{-4} M. This early sensor response saturation can be attributed to the presence of suspended solids, organic matter and chemicals in lake and creek water as compared to tap water. Further, pH of lake and creek water was 6.21 and 8.37, respectively, which can also contribute to the variation in sensor measurement.

4. Conclusions

Current study demonstrated a current treatment protocol to enhance the sensitivity of cobalt based phosphate sensor. The sensitivity of the sensor was -91.4 mV/decade which is approximately double the sensitivity reported for previous sensors. The pretreatment method does not have any effect on selectivity of the sensor to the common anions present in water. The sensor also showed a good response with spiked tap water, lake water and creek water illustrating the ability to perform phosphate measurement in real waters. The sensor measuring range is limited to 10^{-3} to 10^{-6} M. Therefore, the sensor cannot be used to measure phosphate concentration in large water bodies where the phosphate concentrations are less than 10^{-6} M.

Funding

This work was supported by the Global Water Futures program and Natural Sciences and Engineering Research Council of Canada. PRS acknowledges support from the Canada Research Chairs Program.

Acknowledgment

We would like to acknowledge Dr Peter Kruse, Department of Chemistry, McMaster University for insightful discussions and Dr Mark Biesinger, Surface science Western University for XPS characterization and its data analysis.

References

[1] C.P. Mainstone, W. Parr, Phosphorus in rivers - Ecology and management, Sci. Total Environ. 282–283 (2002) 25–47. https://doi.org/10.1016/S0048-9697(01)00937-8.

[2] U.S. Congress, Federal water pollution control act.-33 U.S.C. 1251 et seq., 2002.

[3] S. Richter, J. Völker, D. Borchardt, V. Mohaupt, The Water Framework Directive as an approach for Integrated Water Resources Management: Results from the experiences in Germany on implementation, and future perspectives, Environ. Earth Sci. 69 (2013) 719–728. https://doi.org/10.1007/s12665-013-2399-7.

[4] D.M. Anderson, P.M. Glibert, J.M. Burkholder, Harmful Algal Blooms and Eutophication: Nutrient Sources, composition and consequences, Estuaries. 25 (2002) 704–726.

[5] P.J.A. Withers, P.M. Haygarth, Agriculture, phosphorus and eutrophication: A European perspective, Soil Use Manag. 23 (2007) 1–4. https://doi.org/10.1111/j.1475-2743.2007.00116.x.

[6] R.D. Harmel, K.W. King, B.E. Haggard, D.G. Wren, J.M. Sheridan, Practical guidance for discharge and water quality data collection on small watersheds, Trans. ASABE. 49 (2006)

937–948.

[7] G.S. Toor, R.D. Harmel, B.E. Haggard, G. Schmidt, Evaluation of Regression Methodology with Low-Frequency Water Quality Sampling to Estimate Constituent Loads for Ephemeral Watersheds in Texas, J. Environ. Qual. 37 (2008) 1847–1854. https://doi.org/10.2134/jeq2007.0232.

[8] S.V. Mapare, P.L. Yu, A. Sarkar, S.C. Mukhopadhyay, A Review of sensor technology for in-field phosphate monitoring, Proc. Int. Conf. Sens. Technol. ICST. (2013) 411–418. https://doi.org/10.1109/ICSensT.2013.6727686.

[9] X. Lin, X. Wu, Z. Xie, K.Y. Wong, PVC matrix membrane sensor for fluorescent determination of phosphate, Talanta. 70 (2006) 32–36. https://doi.org/10.1016/j.talanta.2006.01.026.

[10] R.N. Fernandes, B.F. Reis, Flow system exploiting multicommutation to increase sample residence time for improved sensitivity. Simultaneous determination of ammonium and ortho-phosphate in natural water, Talanta. 58 (2002) 729–737. https://doi.org/10.1016/S0039-9140(02)00369-7.

[11] G.N. Doku, S.J. Haswell, Further studies into the development of a micro-FIA (μLIA) system based on electroosmotic flow for the determination of phosphate as orthophosphate, Anal. Chim. Acta. 382 (1999) 1–13. https://doi.org/10.1016/S0003-2670(98)00830-7.

[12] D. Xiao, H.Y. Yuan, J. Li, R.Q. Yu, Surface-Modified Cobalt-Based Sensor as a Phosphate-Sensitive Electrode, Anal. Chem. 67 (1995) 288–291. https://doi.org/10.1021/ac00098a009.

[13] R.K. Meruva, M.E. Meyerhoff, Mixed potential response mechanism of cobalt electrodes toward inorganic phosphate, Anal. Chem. 68 (1996) 2022–2026. https://doi.org/10.1021/ac951086v.

[14] N.A. Chaniotakis, K. Jurkschat, A. Rühlemann, Potentiometric phosphate selective electrode based on a multidendate-tin (IV) carrier, Anal. Chim. Acta. 282 (1993) 345–352. https://doi.org/10.1016/0003-2670(93)80220-F.

[15] T. Le Goff, J. Braven, L. Ebdon, D. Scholefield, Phosphate-selective electrodes containing immobilised ionophores, Anal. Chim. Acta. 510 (2004) 175–182. https://doi.org/10.1016/j.aca.2004.01.015.

[16] W.L. Cheng, J.W. Sue, W.C. Chen, J.L. Chang, J.M. Zen, Activated nickel platform for electrochemical sensing of phosphate, Anal. Chem. 82 (2010) 1157–1161. https://doi.org/10.1021/ac9025253.

[17] L. Gilbert, A.T.A. Jenkins, S. Browning, J.P. Hart, Development of an amperometric, screen-printed, single-enzyme phosphate ion biosensor and its application to the analysis of biomedical and environmental samples, Sensors Actuators, B Chem. 160 (2011) 1322–1327. https://doi.org/10.1016/j.snb.2011.09.069.

[18] N. Al-Dasoqi, A. Mason, R. Alkhaddar, A. Al-Shamma'a, Use of Sensors in Wastewater Quality Monitoring—A Review of Available Technologies, in: World Environ. Water Resour. Congr. 2011, American Society of Civil Engineers, Reston, VA, 2011: pp. 3379–3388. https://doi.org/10.1061/41173(414)354.

[19] A.T. Law Al, S.B. Adeloju, Progress and recent advances in phosphate sensors: A review, Talanta. 114 (2013) 191–203. https://doi.org/10.1016/j.talanta.2013.03.031.

[20] X. Zhu, J. Ma, Recent advances in the determination of phosphate in environmental water samples: Insights from practical perspectives, TrAC - Trends Anal. Chem. 127 (2020) 115908. https://doi.org/10.1016/j.trac.2020.115908.

[21] G. Kopiec, K. Starzec, J. Kochana, T.P. Kinnunen-Skidmore, W. Schuhmann, W.H. Campbell, A. Ruff, N. Plumeré, Bioelectrocatalytic and electrochemical cascade for phosphate sensing with up to 6 electrons per analyte molecule, Biosens. Bioelectron. 117 (2018) 501–507. https://doi.org/10.1016/j.bios.2018.06.047.

[22] J. He, H. Sun, J. Dai, H. Wang, L. Yu, W. Zhou, Z. Shao, In situ growth of nanoflake and nanoflower-like Ni hydrated hydroxide on the surface of Ni foam as a free-standing electrode for high-performance phosphate detection, J. Hazard. Mater. 392 (2020) 122313. https://doi.org/10.1016/j.jhazmat.2020.122313.

[23] R. Zeitoun, A. Biswas, Instant and Mobile Electrochemical Quantification of Inorganic Phosphorus in Soil Extracts, J. Electrochem. Soc. 167 (2020) 167512. https://doi.org/10.1149/1945-7111/abcbaf.

[24] D. Aguado, R. Barat, J. Soto, R. Martínez-Mañez, Monitoring dissolved orthophosphate in a struvite precipitation reactor with a voltammetric electronic tongue, Talanta. 159 (2016) 80–86. https://doi.org/10.1016/j.talanta.2016.06.002.

[25] I. Campos, A. Sangrador, R. Bataller, D. Aguado, R. Barat, J. Soto, R. Martínez-Máñez, Ammonium and Phosphate Quantification in Wastewater by Using a Voltammetric Electronic Tongue, Electroanalysis. 26 (2014) 588–595. https://doi.org/10.1002/elan.201300538.

[26] V.O. Ebuele, D.G. Congrave, C.D. Gwenin, V. Fitzsimmons-Thoss, Development of a

Cobalt Electrode for the Determination of Phosphate in Soil Extracts and Comparison with Standard Methods, Anal. Lett. 51 (2018) 834–848. https://doi.org/10.1080/00032719.2017.1360899.

[27] K. Xu, Y. Kitazumi, K. Kano, O. Shirai, Phosphate ion sensor using a cobalt phosphate coated cobalt electrode, Electrochim. Acta. 282 (2018) 242–246. https://doi.org/10.1016/j.electacta.2018.06.021.

[28] J.-Y. Han, J. Lee, Y.-G. Lee, A. Jang, Solid-state Ion Selective Lab Chip Sensor for On-site Measurement of Orthophosphate in Small Volumes of Liquid, J. Coast. Res. 79 (2017) 50–54. https://doi.org/10.2112/si79-011.1.

[29] L. Zhu, X. Zhou, H. Shi, A potentiometric cobalt-based phosphate sensor based on screen-printing technology, Front. Environ. Sci. Eng. 8 (2014) 945–951. https://doi.org/10.1007/s11783-013-0615-z.

[30] L. Hsu, P.R. Selvaganapathy, Stable and reusable electrochemical sensor for continuous monitoring of phosphate in water, Proc. IEEE Sensors. 2014-Decem (2014) 1423–1426. https://doi.org/10.1109/ICSENS.2014.6985280.

[31] L. Song, L. Zhu, Y. Liu, X. Zhou, H. Shi, A disposable cobalt-based phosphate sensor based on screen printing technology, Sci. China Chem. 57 (2014) 1283–1290. https://doi.org/10.1007/s11426-014-5127-6.

[32] Y. Bai, J. Tong, C. Bian, G. Yan, B. Deng, H. Zhang, S. Xia, Micro cobalt electrodes for detection of total phosphorus in water, Micro Nano Lett. 7 (2012) 1176–1179. https://doi.org/10.1049/mnl.2012.0519.

[33] Y. Bai, J. Tong, C. Bian, S. Xia, Fabrication and characterization of cobalt nanostructure-based microelectrodes for phosphate detection, Key Eng. Mater. 483 (2011) 559–564. https://doi.org/10.4028/www.scientific.net/KEM.483.559.

[34] K. Xu, Y. Kitazumi, K. Kano, T. Sasaki, O. Shirai, Fabrication of a phosphate ion selective electrode based on modified molybdenum metal, Anal. Sci. 36 (2020) 201–206. https://doi.org/10.2116/analsci.19P296.

[35] G. Chen, S. Xiao, A. Lorke, J. Liu, P. Zhang, Assessment of a Solid-State Phosphate Selective Electrode Based on Tungsten, J. Electrochem. Soc. 165 (2018) B787–B794. https://doi.org/10.1149/2.0101816jes.

[36] Y. Li, T. Jiang, X. Yu, H. Yang, Phosphate Sensor Using Molybdenum, J. Electrochem. Soc. 163 (2016) B479–B484. https://doi.org/10.1149/2.0161609jes.

[37] M. Bralić, A. Prkić, J. Radić, I. Pleslić, Preparation of phosphate ion-selective membrane based on silver salts mixed with PTFE or carbon nanotubes, Int. J. Electrochem. Sci. 13 (2018) 1390–1399. https://doi.org/10.20964/2018.02.49.

[38] H. Jiang, M.A. Ali, Y. Jiao, B. Yang, L. Dong, In-situ, real-time monitoring of nutrient uptake on plant chip integrated with nutrient sensor, TRANSDUCERS 2017 - 19th Int. Conf. Solid-State Sensors, Actuators Microsystems. (2017) 289–292. https://doi.org/10.1109/TRANSDUCERS.2017.7994045.

[39] P. Kumar, D.M. Kim, M.H. Hyun, M.S. Won, Y.B. Shim, An all solid state potentiometric sensor for monohydrogen phosphate ions, Electroanalysis. 25 (2013) 1864–1870. https://doi.org/10.1002/elan.201300142.

[40] P. Norouzi, M.R. Ganjali, F. Faridbod, S.J. Shahtaheri, H.A. Zamani, Electrochemical anion sensor for monohydrogen phosphate based on nano-composite carbon paste, Int. J. Electrochem. Sci. 7 (2012) 2633–2642.

[41] M.R. Ganjali, P. Norouzi, M. Ghomi, M. Salavati-Niasari, Highly selective and sensitive monohydrogen phosphate membrane sensor based on molybdenum acetylacetonate, Anal. Chim. Acta. 567 (2006) 196–201. https://doi.org/10.1016/j.aca.2006.03.026.

[42] S.A. Glazier, M.A. Arnold, Phosphate-Selective Polymer Membrane Electrode, Anal. Chem. 60 (1988) 2540–2542. https://doi.org/10.1021/ac00173a024.

[43] J.J. Wang, P.L. Bishop, Fabrication, calibration and evaluation of a phosphate ion-selective microelectrode, Environ. Pollut. 158 (2010) 3612–3617. https://doi.org/10.1016/j.envpol.2010.08.007.

[44] J.H. Lee, W.H. Lee, P.L. Bishop, I. Papautsky, A cobalt-coated needle-type microelectrode array sensor for in situ monitoring of phosphate, J. Micromechanics Microengineering. 19 (2009). https://doi.org/10.1088/0960-1317/19/2/025022.

[45] B. Jones, Phosphate detection, GB 2503689, 2014.

[46] H.A. Dugan, S.L. Bartlett, S.M. Burke, J.P. Doubek, F.E. Krivak-Tetley, N.K. Skaff, J.C. Summers, K.J. Farrell, I.M. McCullough, A.M. Morales-Williams, D.C. Roberts, Z. Ouyang, F. Scordo, P.C. Hanson, K.C. Weathers, Salting our freshwater lakes, Proc. Natl. Acad. Sci. 114 (2017) 4453–4458. https://doi.org/10.1073/PNAS.1620211114.

[47] M.C. Biesinger, B.P. Payne, A.P. Grosvenor, L.W.M. Lau, A.R. Gerson, R.S.C. Smart, Resolving surface chemical states in XPS analysis of first row transition metals, oxides and

hydroxides: Cr, Mn, Fe, Co and Ni, Appl. Surf. Sci. 257 (2011) 2717–2730. https://doi.org/10.1016/j.apsusc.2010.10.051.

[48] W.A. Badawy, F.M. Al-Kharafi, J.R. Al-Ajmi, Electrochemical behaviour of cobalt in aqueous solutions of different pH, J. Appl. Electrochem. 30 (2000) 693–704. https://doi.org/10.1023/A:1003893122201.

[49] L.D. Burke, M.E. Lyons, O.J. Murphy, Formation of hydrous oxide films on cobalt under potential cycling conditions, J. Electroanal. Chem. Interfacial Electrochem. 132 (1982) 247–261. https://doi.org/https://doi.org/10.1016/0022-0728(82)85022-5.

[50] Marcel Pourbaix, Atlas of electrochemical equilibria in aqueous solutions, (1974) 644.

[51] W. Olthuis, M.A.M. Robben, P. Bergveld, M. Bos, W.E. van der Linden, pH sensor properties of electrochemically grown iridium oxide, Sensors Actuators B. Chem. 2 (1990) 247–256. https://doi.org/10.1016/0925-4005(90)80150-X.

[52] L.D. Burke, D.P. Whelan, A voltammetric investigation of the charge storage reactions of hydrous iridium oxide layers, J. Electroanal. Chem. Interfacial Electrochem. 162 (1984) 121–141. https://doi.org/https://doi.org/10.1016/S0022-0728(84)80159-X.

[53] V.O. Ebuele, D.G. Congrave, C.D. Gwenin, V. Fitzsimmons-Thoss, Development of a Cobalt Electrode for the Determination of Phosphate in Soil Extracts and Comparison with Standard Methods, Anal. Lett. 51 (2018) 834–848. https://doi.org/10.1080/00032719.2017.1360899.

[54] R. De Marco, C. Phan, Determination of phosphate in hydroponic nutrient solutions using flow injection potentiometry and a cobalt-wire phosphate ion-selective electrode, Talanta.

60 (2003) 1215–1221. https://doi.org/10.1016/S0039-9140(03)00229-7.

[55] Z. Chen, R. De Marco, P.W. Alexander, Flow-injection Potentiometric Detection of Phosphates Using a Metallic Cobalt Wire Ion-selective Electrode, Anal. Commun. 34 (1997) 93–95. https://doi.org/10.1039/a700771j.

[56] Z. Zou, J. Han, A. Jang, P.L. Bishop, C.H. Ahn, A disposable on-chip phosphate sensor with planar cobalt microelectrodes on polymer substrate, Biosens. Bioelectron. 22 (2007) 1902–1907. https://doi.org/10.1016/j.bios.2006.08.004.

[57] C.W. Team, The clean water team guidance compendium for watershed monitoring and assessment, Version 2.0, 2004.

[58] W.H. Lee, Y. Seo, P.L. Bishop, Characteristics of a cobalt-based phosphate microelectrode for in situ monitoring of phosphate and its biological application, Sensors Actuators, B Chem. 137 (2009) 121–128. https://doi.org/10.1016/j.snb.2008.10.032.

[59] World Health Organization, Nitrate and nitrite in drinking water, WHO Guidel. Drink. Qual. 37 (2011) 227–231. https://doi.org/10.1159/000225441.

[60] WHO, Sulfate in Drinking-water Background document for development of WHO Guidelines for Drinking-water Quality. Available at http://www.who.int/water_sanitation_health/dwq/chemicals/sulfate.pdf (December 2015), (2004).

[61] WHO. SDE. WSH, Chloride in Drinking-water Background document for development, Guidel. Drink. Qual. - World Heal. Organ. 2 (2003) 9. http://www.who.int/water_sanitation_health/dwq/chloride.pdf.

Chapter 4

A xurography based rapid prototyping method to fabricate low-cost and high quality metal thin film micropatterns using metal leaves.

Vinay Patel [1], Peter Kruse [2], and P. Ravi Selvaganapathy [1,3*]

[1] School of Biomedical Engineering, McMaster University, Hamilton, ON, L8S 4K1, Canada

[2] Department of Chemistry and Chemical Biology, McMaster University, Hamilton, ON, L8S 4M1, Canada

[3]Department of Mechanical Engineering, McMaster University, Hamilton, ON, L8S 4K1, Canada

Corresponding author

P. Ravi Selvaganapathy – Department of Mechanical Engineering, McMaster University, Hamilton, ON, L8S 4K1, Canada; https://orcid.org/0000-0003-2041-7180

* selvaga@mcmaster.ca

Status: published

Full citation

Patel, Vinay, Peter Kruse, and P. Ravi Selvaganapathy. "A xurography based rapid prototyping method to fabricate and low-cost high quality metal thin film micropatterns using metal leaves." *Materials Today Communications* (2022): 103132.

KEYWORDS: *Xurography, Metal leaf thin film electrodes, rapid prototyping, chemiresistors, high surface area electrodes*

Abstract

Metal leaves are commercially available for decoration purposes and offers a low-cost alternative to sputtering thin metal films. Although thin metal leaves have been sparingly used in physical and chemical sensing and solar cells, their application has been limited primarily due to lack of a simple patterning methods and to form microscale features with them. Here, a low-cost, rapid and simple xurography based cutting method has been developed for direct pattering of metal leaves. The method was able to pattern features with line width of <100 µm and it was also able to cut patterns with a pitch of <100 µm. Conductive lines <250 µm were also achieved which is a sufficient resolution for application in sensors and most biomedical devices. The versatile capability of this method to cut various geometric shapes like circle, rectangle, triangles and hexagons was also demonstrated. The method is robust and can be applied to pattern leaves made of several materials or which gold, silver, palladium, aluminum and copper were demonstrated. This patterning method was used to fabricate contact electrodes for chemiresistive sensors with low and high surface roughness. These sensors were evaluated using the resistance and noise characteristics. The peak-to-peak noise for gold contact electrodes (11.5 nA) for chemiresistive sensors was significantly lower than the copper tape contact electrodes (18.2 nA). The process was also used to fabricate gold interdigitated electrodes for biamperometric glucose sensing at low potential (~10 mV). Finally, the method was used to indirectly pattern gold leaf on a shrink film to fabricate high surface 3D electrodes costing around one-fifth (~20%) of a sputtered gold electrode.

1. Introduction

Metal leaves are used as gilding material for decorative purposes dating back to 3 BC [1]. They are manufactured from metals like gold, silver, platinum, copper, aluminum, and palladium that are highly ductile and can be plastically deformed to form thin sheets. The gold sheets/foils are

hammered to convert into thin gold films with thicknesses down to ~140 nm which can subsequently be attached to surfaces like glass, and polymers. Metal leaves have been applied to various non porous substrates like glass using adhesive coatings such as butyl methacrylate and dibutyl phthalate as adhesives [2] and adhesive films [3]. Multiple studies have also generated nanoporous gold surface using 12K gold leaf [4–10] for different applications like electrochemical sensing [4–6,10], electroanalysis [8] and anti-biofouling surfaces [9].

Metal leaf offers a simple and low-cost method to form thin metal films on non-conducting surfaces such as on polymers or glass. Conventionally, sputter coating is used to coat thin metal films of nanoscale thickness. However, it requires a complex process and expensive vacuum equipment to coat thin metal films and it also produces a lot of metal residual waste adding further to the cost. Metal leaves provides a scalable and low-cost alternative for thin film metal coatings along with minimum material wastage as compared to sputter coating. The cost of gold leaf (24K triple transfer leaf, dimensions 80mm × 80 mm, $2.85/leaf) compares favourably to $4.30 /electrode for sputtered gold electrodes [11].

Multiple studies have used gold leaf to fabricate thin metal layers by using different adhesive films. However, these studies have either used unpatterned or indirectly patterned metal leaves that use a mask with adhesive coatings inspired from the traditional gilding process on a selective area [6,12–17] primarily due to the difficulty in handling and directly patterning these fragile films. More specifically, unpatterned metal leaves were used for fabricating electrodes for solar cells [17], electrochemical sensing electrodes [13] and microfluidic devices [12]. Although useful, they do not allow intricate features such as heaters or closely spaced electrodes to be integrated. Another study used an indirect 3-step patterning process starting with creating a stencil and spraying adhesive on top to attach gold leaf [14]. The use of stencil restricts this method to simple patterns,

and the failure rate for more complex and large connected patterns increases with the size of the pattern. Alternatively, a recent study has demonstrated metal leaf patterning by using a selective chemical etching process. However, this process uses multiple steps including polymer passivation to protect the pattern from etching followed by a chemical etching step to pattern the metal leaves [6]. Therefore, a simple method that can directly pattern metal leaves and integrate them with other functional materials for sensing would be quite useful.

Here, a xurography based cutting process is developed for direct patterning of metal leaves. The metal leaf was attached to a single sided adhesive tape. The xurographic patterning was performed using a low-cost cutting plotter to cut metal leaves into different shapes, sizes and linear patterns. The ability of the xurographic process to produce different line width and pitch for linear patterns was investigated. The surface morphology of the patterns was analyzed using scanning electron microscopy (SEM) and white light interferometry. Direct patterning offers flexibility to use metal leaves in applications like contact electrodes for chemiresistive sensors where it is difficult to use masking tapes to define the contact electrode. The process was used to fabricate low noise contact electrodes for chemiresistive sensors with active sensing films with different surface roughness. In addition, the process was used to fabricate low-cost electrochemical sensing electrodes using gold leaf. Finally, the process was combined with patterning double-sided tape and gold leaf to fabricate three dimensional electrodes with high surface area.

2. Materials and methods

2.1 Materials

Kapton double-sided tape (catalog# PIT2SD) was purchased from Caplinq Inc. A Cricut craft cutter, a low-cost cutting plotter (Provo Craft & Novelty Inc.) was used to pattern the metal leaves and the double-sided adhesive tape. Transfer tape and roller were purchased from Uline Canada.

Standard plain microscopic glass slides were used as the glass substrate. 24K gold transfer leaf, silver transfer leaf, imitation silver (aluminum) and copper leaf were purchased from L.A. Gold Leaf Wholesaler, Palladium leaf was purchased from Golden leaf products, U.S.A. All chemicals used were of analytical grade. Single walled Carbon nanotube ink dispersion was supplied by Nano-C, US (#CINK-200-P010100). Graphene Like Carbon (GLC) sheets were supplied by 3M, Canada [18].

2.2 Patterning method

Transfer metal leaves are commercially sold with a paper backing to facilitate handling of the thin leaf. Here, gold leaf is used as example to describe the entire xurographic cutting process. The gold leaf was first transferred on a thin translucent single sided tape using a roller (Figure 4.1a and 4.1b). Then the gold leaf was covered with parafilm to ensure minimal deformation and to obtain smooth cut lines during the cutting process (Figure 4.1c). Next, the combined sheet was transferred to a glue pad (Figure 4.1d) and then cut using plotter cutter (Cricut, Figure 4.1e). Finally, the unwanted material in the cut patterns were removed manually using a pair of tweezers to obtain the designed metal pattern. The final manufactured structures in the form of serpentine heater as well as electrode patterns are shown in Figure 4.1f.

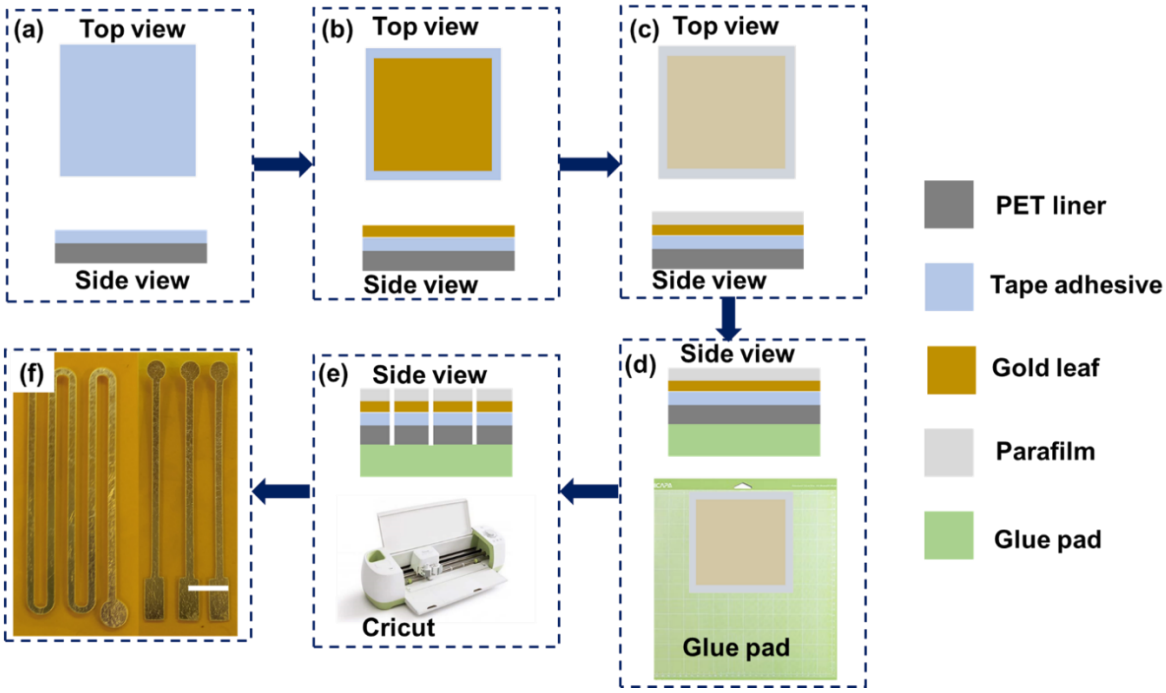

Figure 4.1 Overview of the xurographic process (a)-(c) Top view and side view of tape, gold leaf and parafilm prepared to cut different patterns of gold leaf. (d)-(e) Cutting process of the combined sheet (Tape-Gold leaf-Parafilm) using Cricut, a low-cost cutting plotter (f) Patterns generated after the cutting process (Scale bar 1 cm).

2.3 Characterization techniques

Cyclic voltammetry (CV) was performed using a PalmSens4 (Palmsens BV, Netherlands) controlled by PSTrace 5.8 software. The voltammograms were analyzed using PSTrace 5.8 software. A 3-electrode setup was used for CV with gold leaf electrode as the working electrode, graphite rod as the counter electrode and double junction Ag/AgCl as the reference electrode. The gold leaf patterns were imaged using a USB optical microscope and the optical images were analyzed using ImageJ software. In addition, the metal film morphology was characterized using a TESCAN Vega LSU SEM at an accelerating voltage of 5 kV. The surface morphology was investigated using white light interferometry with a Alicona infinite focus G5 optical microscope.

The thickness of all the films was measured using a Tencor Alphastep 200 profilometer. The samples for the thickness measurement were prepared on a silicon water and the thickness measurements were done at three different spots on each film (n=3). The measured thickness for all films gold, silver, palladium, aluminum and copper were 120 ± 18 nm, 403 ± 12 nm, 212 ± 12 nm, 1055 ± 95 nm, and 661 ± 3 nm, respectively.

3. Results and discussion

3.1 Xurographic patterning of metal leaf

Xurography provides a low-cost alternative method to directly pattern thin metal leaves. The cutting method was evaluated to determine the cutting parameters like minimum line width (LW) and pitch required to get reliable patterns from the xurographic cutting process. Five different metal leaves (gold, silver, aluminum, copper and palladium) were used to evaluate the cutting process. Metal leaf was transferred onto translucent single sided tape using a roller. Then, the metal leaf was patterned without parafilm using the process described in Section 2.2. The minimum LW and pitch were determined by cutting multiple straight lines with the design width ranging from 0.1 to 0.3 mm. Curling was observed for all the thin straight lines (Figure S1, Appendix 2). Therefore, two square blocks (side length 0.5 mm) were added to the design to avoid curling of the patterned straight lines. The minimum achieved LW for different leaf is summarized in Table 1. The cutting process failed to cut the pattern for design LW of 100 µm. Hence, the minimum achieved LW (design LW 200 µm, n ≥12) for the five metal leaves gold, palladium, silver, aluminum and copper were 80 ± 5 µm, 90 ± 17 µm), 111 ± 6.4 µm, 113 ± 14 µm) and 142 ± 3 µm, simultaneously.

The achieved pitch was investigated using four straight lines with 1 mm design LW and three design pitches of 100 µm, 200 µm and 250 µm. The minimum achieved pitch for gold leaf is

summarized in Table 4.1. The minimum achieved pitches (design pitch 100 µm, n ≥12) for the five metal leaves gold, palladium, silver, aluminum and copper were 92 ± 2 µm, 100 ± 10 µm, 101 ± 2 µm, 121 ± 10 µm and 114 ± 10 µm, respectively.

A previous study has demonstrated the use of xurography to pattern copper polyimide composite foils (thickness 9 µm) with a minimum LW of 100 µm. However, that process can only generate consistent patterns with LW greater than 200 µm [19]. This is because the metal foil used in the study was 64 times thicker than the gold leaf (thickness 140 nm) reported in the current study.

Table 4.1 Summary of minimum achieved LW and pitch for different metal leaves.

Metal leaves	Minimum achieved LW (µm)	Minimum achieved Pitch (µm)
Gold	80 ± 5	92 ± 2
Silver	111 ± 6.4	101 ± 2
Aluminum	113 ± 14	121 ± 10
Palladium	90 ± 17	100 ± 10
Copper	142 ± 3	114 ± 10

Even though our process is capable of patterning the gold leaf down to a LW of ~80 µm, these lines were found not to be conductive, likely due to tearing of the gold leaf during the patterning process. Gold leaf was used to further investigate the capability of the cutting process to pattern reliable conductive patterns. Gold leaf was also selected due to its high stability in various electrochemical conditions. Direct cutting of gold leaf on a polymeric substrate was prone to tearing due to its fragile nature. However, coverage of the gold leaf by parafilm enabled reliable cutting of the metal film (Figure 4.1). Parafilm was chosen as the coverage material due to its ability to withstand the cutting force without getting directly attached to the gold leaf surface. Hence, it was easy to remove after cutting without damaging the patterns. The combined sheet

(Tape-Gold leaf-parafilm) was attached to a polyimide tape to fix the positions of the patterned shapes (Figure 4.2a). The optical images of gold leaf with paper backing and white light interferometry image is shown in Appendix 2 (Figure S2). SEM images showed that most of the pristine gold leaf surface remained intact during the cutting process (Figure 4.2b) while deformation was observed at the edges (Figure 4.2b). Sputtered patterned electrodes generally have smooth edges. However, the edge deformation can vary depending on the patterning method. In case of mask-based patterning, tearing on the edges are reported while lifting off the mask [20]. Analysis of the optical image using ImageJ showed that the affected region extended to a width of 83 ± 3.7 µm from the edge (n=8), consistent with the lack of conductivity for straight lines with LW less than 100 µm. The linear patterns were further analyzed using white light interferometry to analyze the surface features at the center and the edges (Figure S3, Appendix 2). A rectangular area (n=4) of 60 × 600 μm^2 was analyzed both in the center and at the edges of the linear pattern. The average surface roughness of the pattern at four different spots (n=4) in the middle of the pattern was 4.36 ± 5.7 µm within 95% confidence interval while the average surface roughness of the edges was 1.21 ± 1.51 µm. The reduced surface roughness showed that the edges were squeezed during cutting.

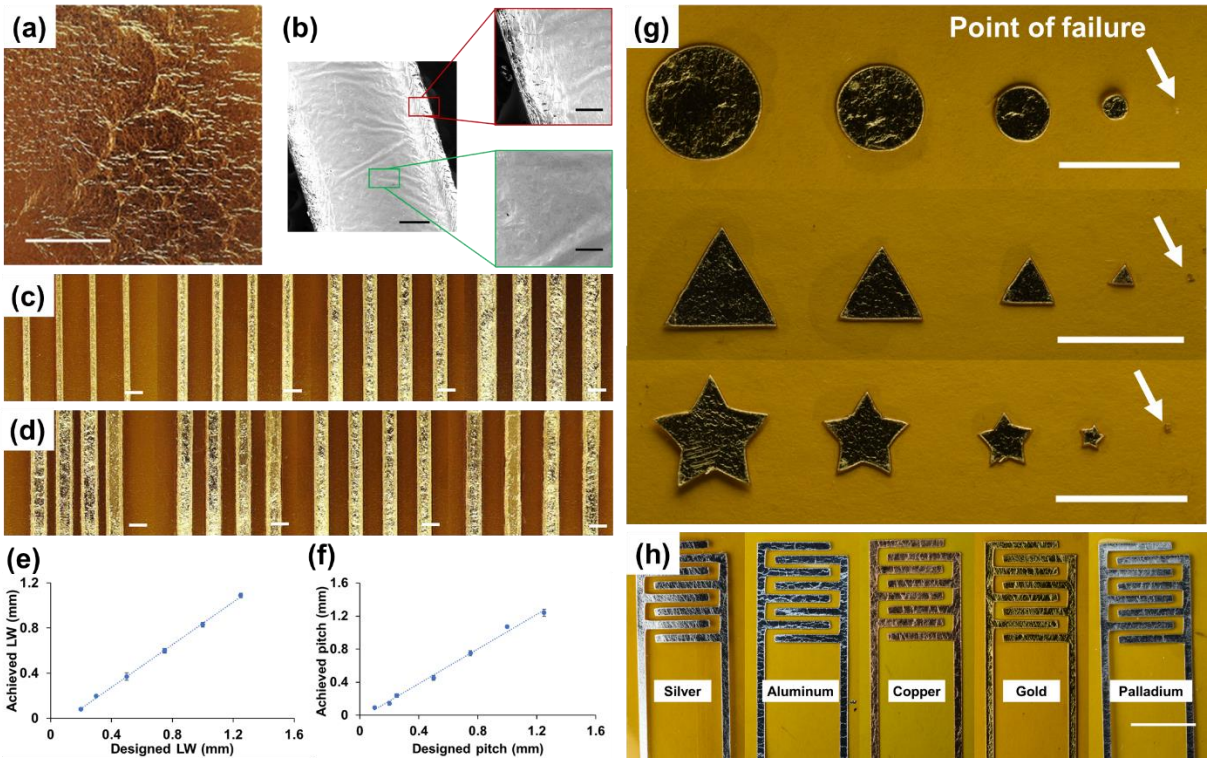

Figure 4.2 (a) Optical images of gold leaf attached on the single-sided tape (Scale bar 5mm). (b) SEM image of gold leaf patterned in a 8 cm ×1 mm rectangular pattern (200 µm as the scale bar). Inset shows two images: Red box showing zoomed image of the edge of the cut (Scale bar 100 µm) and green box showing the centre of gold with 50 µm as the scale bar. (c) Four images each with 1 mm pitch and four different design LW (Left to right: 0.5 mm, 0.75 mm, 1 mm and 1.25 mm). (d) Four images each with 1 mm LW and four different design pitches (Left to right: 0.5 mm, 0.75 mm, 1 mm and 1.25 mm). (e) & (f) Plots showing the correlation between achieved and designed (e) Line width (LW) (f) Pitch with 1 mm line width for all pitches. (g) Image showing different geometric shapes cut using xurography (Scale bar 1 cm). The point of failure is indicated using the white arrow in the figure (circular pattern, the diameter is 1.25 mm). (h) Interdigitated electrodes patterned on Kapton tape with five different metal leaves: (Left to right) Silver, Aluminium, Copper, Gold and Palladium (Scale bar 1 cm).

The minimum achieved LW and pitch was determined by cutting multiple straight lines with the design width ranging from 0.1 to 1.25 mm. Four lines each spaced by 1 mm pitch and four different line widths 0.5 mm, 0.75 mm, 1 mm and 1.25 mm were patterned using the current process (Figure 4.2c). Similarly, four straight lines of 1 mm design LW and four different pitches 0.5 mm, 0.75 mm, 1 mm and 1.25 mm were patterned using the process (Figure 4.2d). The pictures of electrodes were analyzed using ImageJ and the final dimensions are summarized in Table T1 and T2 (Appendix 2). Fabrication of conductive linear patterns below 0.228 mm achieved LW (design LW 0.3 mm) was not reproducible and resulted in a non-conductive pattern for an achieved LW of 0.198 mm (0.25 mm design). In addition, the resistance of lines with different LW was measured using a multimeter.

All the patterned straight lines had a significant but consistent offset of 65-150 µm between the achieved and designed CAD dimensions. For example, the design LW of 500 µm produced an actual gold line pattern that was 429 µm in width. This kind of a constant offset between the designed and the realized patterns is known in xurography [19]. The achieved and designed LWs were correlated linearly with a R^2 value of 0.995 (Figure 4.2e). Therefore, the offset between the designed width and achieved width can be corrected using a correction factor to incorporate the desired width into the design. A lesser variation in pitches was observed between the achieved and designed CAD patterns for the four tested values. The pitch also had an offset of 10-60 µm between the designed and achieved patterns. The desired and achieved pitch values were linearly correlated with a R^2 value 0.9941 (Figure 4.2f) between the design range of 0.1 mm to 1.25 mm. Therefore, this offset can be corrected by introducing a correction factor. The minimum reliable conductive line pattern that could be created was ~ 230 µm in width. A decrease in resistivity was observed with increase in LW till 600 µm (Figure S4, Appendix 2). The resistivity of 600 µm line pattern

was ~4 × 10^{-8} Ω.m which is 1.5 times the bulk resistivity of gold (4 × 10^{-8} Ω.m). Therefore, the process can generate highly conductive patterns with LW higher than 230 µm.

The process was also used to pattern various geometric shapes such as circles, triangles, star, hexagons, and rectangles, to demonstrate the versatility of the cutting process (Figure 4.2g). Images of hexagonal and rectangular patterns are shown in Appendix 2 (Figure S5). Five circular patterns with different diameter starting from 10 mm to 1.25 mm (10 mm, 7.5 mm, 5 mm, 2.5 mm and 1.25 mm) were patterned. The cutting process can result in reliable patterning of gold leaf down to 2.5 mm, but it failed to pattern the shapes at 1.25 mm. Similar to circular patterns, the cutting process also failed to pattern triangular pattern with a side length of 1.25 mm indicated by a white arrow shown in Figure 4.2g. Therefore, the highest resolution achievable for patterning different geometric shapes lies between 1.25 mm to 2.5 mm. Moreover, the process can pattern reliable geometric shapes above 2.5mm (diameter or side length).

The xurographic process can be used not only to pattern gold leaves but also leaves of other materials as demonstrated above. Interdigitated electrodes with 4 pair of digits and dimensions 10 mm × 1 mm and 0.75 mm spacing between the electrodes were fabricated using metal leaves from five different materials: silver, aluminum, copper, gold and palladium (Figure 4.2h). Interestingly, the top parafilm cover was not needed for patterning aluminum, palladium and copper leaves unlike gold and silver. These metal leaves did not exhibit any significant deformation or cracks during the cutting process even without the top parafilm cover which can be associated with the ductility of these materials as well as their thickness.

The xurography based direct cutting process can be used to pattern metal leaf into various patterns in a versatile manner. The smallest line width achieved was 80 µm while we get more reliable conductive linear patterns ~228 µm and the best conductivity was obtained for line width of ≥ 600

μm where the resistivity of the electrodes (4×10^{-8} Ω.m) were similar to bulk resistivity of the gold (2.5×10^{-8} Ω.m). A study with CO_2 laser patterning of a double sided Kapton tape followed by attachment of gold leaf, demonstrated a line width of 100 μm (50% reliability). However, the method was used to pattern the adhesive tape not the gold leaf directly and requires a 2-step process adhesive film patterning followed by attachment of gold leaf on the patterned substrate [15]. Further, direct patterning used in our method resulted in resistances of ~ 4.6 Ω/cm for 600 μm LW which was a quarter of the resistance obtained in the previous study (16.3 Ω/cm for 600 μm LW) [15].

3.2 Electrochemical behaviour

Metal sensing electrodes are widely used for applications like physical sensing [14] and chemical sensing [6,13]. The electrochemical performance of the fabricated electrodes was evaluated using electrochemical techniques including cyclic voltammetry and chronoamperometry. Three circular electrodes were patterned from gold leaf and the area of the working electrode of 12.56 mm^2 was defined using a parafilm film with a circular opening of diameter 4 mm. The cyclic voltammetry was performed in a solution containing 2 mM $K_4Fe(CN)_6$ and 0.1 M KCl from -0.1 to 0.5 V with a scan rate of 0.08 V/s. All three electrodes resulted in a similar cyclic voltammogram (Figure 4.3a) with distinct oxidation and reduction peaks for $K_4Fe(CN)_6$. The oxidation and reduction peak potentials were separated by 106 ± 14 mV was similar to sputtered gold electrodes (100 ± 5 mV) [21].

Moreover, the fast electrode kinetics was evident from the ratio of oxidation and reduction current (I_O/I_R) of 1.1 ± 0.06 which was similar to that of a sputtered gold electrode (1.2) [21]. The oxidation and reduction peak currents densities were 495.19 ± 24.4 μA/cm^2 (62.2 ± 3.07 μA) and -451.96 ± 10.87 μA/cm^2 (-56 ± 1.37 μA), respectively. The metal sensing electrodes also showed a good

electrode to electrode reproducibility as the variations in peak current and peak potential were within a range of 2-5% relative standard deviation (RSD) and 3.2-3.8% RSD, respectively.

The electrodes were also used to perform chronoamperometric measurements in five different concentration of potassium ferrocyanide (2 mM, 20 mM, 40 mM, 80 mM and 100 mM). The electrodes exhibited a linear increase in current with increase in ferrocyanide concentration from 2 mM to 100 mM with a slope of 8.78 µA/mM (69.95 µA/mM×cm^2) and R^2 value of 0.9987 (Figure 4.3b).

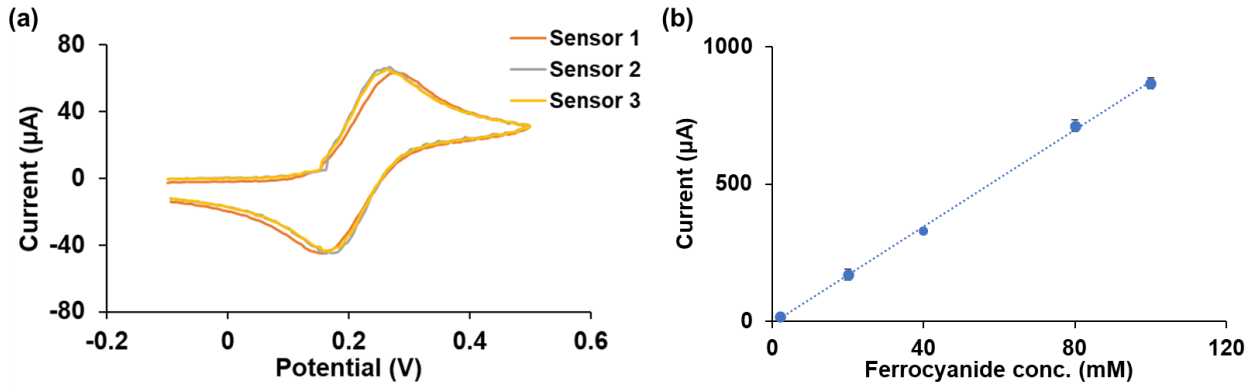

Figure 4.3 (a) Cyclic voltammetric measurements were performed using three gold leaf electrodes patterned by xurography (n=3). The CV was performed from -0.1 to 0.5 V with 0.08 V/s scan in a solution containing 2mM $K_4Fe(CN)_6$ and 0.1M KCl. (b) Gold leaf electrodes were used to perform chronoamperometric measurements with five concentrations of $K_4Fe(CN)_6$ (2 mM, 20 mM, 40 mM, 80 mM and 100 mM) in 1M KCl at 0.5V. Each data point in the plot is the current value at the end of 10s. Error bar represents the standard deviation from three measurements (n=3).

3.3 Device flexibility

Flexible sensing electrodes are used in various applications like healthcare, food and environment monitoring where they can conform to the three-dimensional topographical features while

providing the necessary analyte measurements. Xurography offers a low-cost method to fabricate thin metal leaf electrodes made of materials such as gold, silver, platinum, palladium and aluminum which can be directly integrated into flexible devices. Here, gold leaf was used to demonstrate the ability of the patterning process to fabricate robust, repeatable and reproducible flexible electrodes. Three gold electrodes were fabricated by patterning the gold leaf on a double sided Kapton tape. The electrode was passivated using parafilm with a circular hole cut using the cutting tool (Cricut) to define the active working area (circle with diameter 5 mm) of the electrodes (Figure 4.4a (i)). CV measurements were performed before and after bending to evaluate the changes in electrode after bending and its effect on sensing performance. The CV was performed from -0.1 to 0.5 V with 0.08 V/s scan in a solution containing 2 mM $K_4Fe(CN)_6$ and 0.1 M KCl using a protocol similar to Section 3.2. The electrodes were tested for 120 bending cycles and the cyclic voltammetry was performed at various bending cycles (Figure 4.4b). No significant changes were observed in the electrochemical characteristics of the sensor even after 120 bending cycles. This demonstrates that the sensor can withstand multiple bending cycles without a significant change in its electrochemical properties. In addition, there was very little change noted in the CV curves for all three sensors between the first bending cycle (Figure 4.4c) and the 100^{th} bending cycle (Figure 4.4d) showing the robustness of the fabrication process. Further, the gold leaf electrodes showed low resistivity which was around 1.5 the bulk resistivity of gold (Section 3.1) which is superior to the resistivity achieved for screen printed electrode (13.2 times the bulk resistivity for silver) [22].

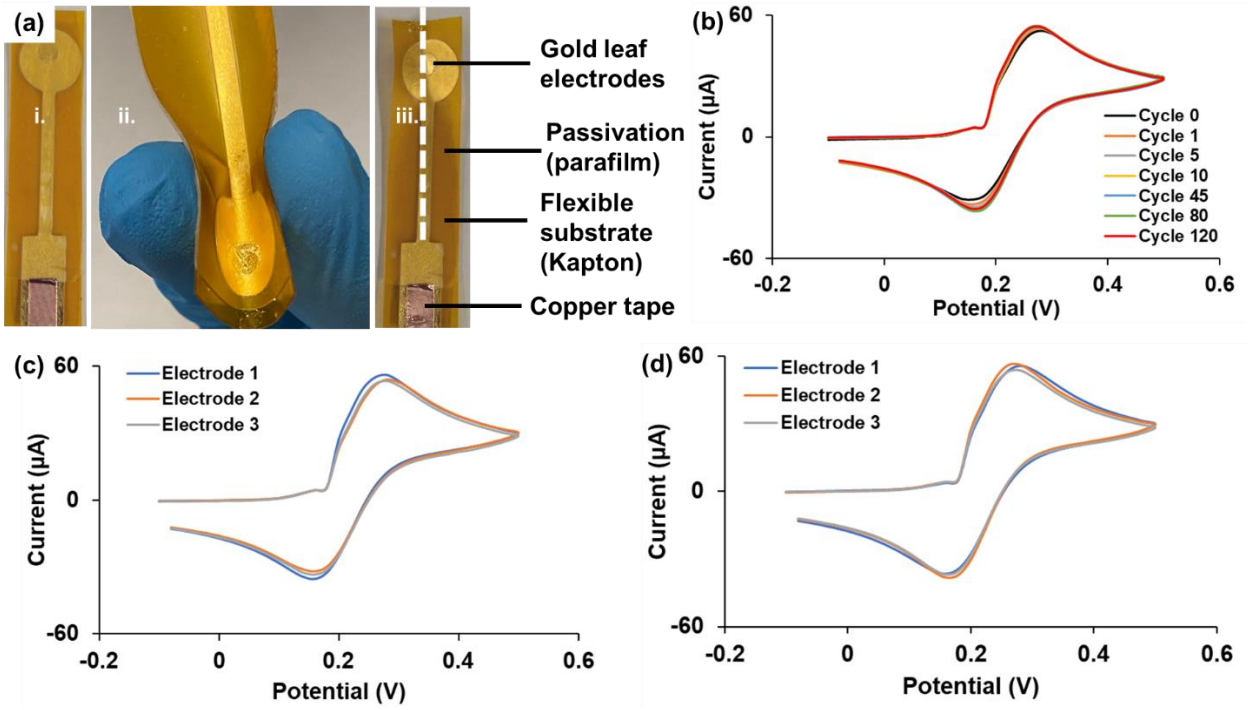

Figure 4.4 (a) Gold leaf electrode with an active circular working electrode of diameter 5 mm. i. Gold leaf electrode before bending ii. During bending iii. After 100 bending cycles (dotted line showing the bending axis). (b) Cyclic voltammogram of the gold leaf electrode before (Cycle 0, black) and after bending for multiple cycles: Cycle 1 (Orange), Cycle 5 (Grey), Cycle 10 (Yellow), Cycle 45 (Blue), Cycle 80 (Green) and Cycle 120 (Red). (c) Cyclic voltammogram for three electrodes after one bending cycle. (d) Cyclic voltammogram for three electrodes after 100 bending cycles.

4. Application

Patterned metal leaves can be used to fabricate thin metal interconnects, contacts and sensing electrodes for various applications including energy storage [16], environmental monitoring [6,23] and medical diagnostics [8]. Here the xurographically patterned metal leaves are used to demonstrate three applications: contact electrodes for nanomaterials to fabricate robust chemiresistive sensors, electrochemical sensing electrodes and 3D electrodes with high surface area.

4.1 Contact electrodes for chemiresistive sensors.

Chemiresistive sensors consist of a sensing film and two contact electrodes. The sensing film detects the change in analyte concentration through an alteration of resistance in the film. This resistance change across the sensing film is measured using the contact electrodes which are connected to the electronic systems. Therefore, contact electrodes and their bonding with the sensing film are an essential part of the chemiresistors sensors. In the past, contact electrodes of chemiresistive sensors have been fabricated using conducting materials including metals like platinum [24], gold [25,26], and silver [27], conductive carbon [28], and copper tape [29]. However, some contact electrodes require sophisticated processing like sputtering, and vapor deposition for fabrication. Simple contact electrodes like conductive tapes can result in noisy or unreliable contacts, and screen-printed contact electrodes have higher resistance and require multiple fabrication steps. Most importantly, these techniques are not versatile enough to provide high quality contacts over a range of surface roughness encountered with nanomaterial based sensors and to provide robust contacts even when undergoing mechanical deformation when flexed. On the other hand, metal leaf electrodes provide a low-cost and simple method to fabricate such robust contact electrodes for nanomaterial sensing films with wide range of surface roughness such as graphene like carbon (GLC) sheets and drop casted carbon nanotubes (CNT) on frosted glass substrates. They are also robust and maintain contact with the nanomaterial films even upon repeated flexion. Here, two nanomaterial sensing films were used to demonstrate the versatility of metal leaf contact electrodes to form high quality contacts. For comparison, contact electrodes were also fabricated using screen printed carbon ink and copper tape.

4.1.1 Chemiresistive sensors with polymer backed sensing film

Graphene like carbon (GLC) sheets used are prepared using a few layers of graphene (20-30 nm in thickness) without any binder on a polyester substrate [30]. Four GLC chemiresistive sensors were prepared using a 2 cm × 2 cm GLC sheet by cutting using xurography. The sensor fabrication process is summarized in Figure 4.5a. First, the GLC sheet was placed on a glass substrate that was previously covered with Kapton tape and parafilm (Step i). Copper tape was attached on the glass substrate at the edges to make contact pads for external clip contacts (Step ii). Then, the xurographically patterned GLC sheet was assembled on the substrate (Step iii) followed by the gold leaf contact electrodes which connect the GLC sensitive layer to copper contact pads and serve as the electrical contacts (Step iv). Finally, a patterned parafilm film with a rectangular opening of 1.5 cm × 0.7 cm that aligns with the center of the GLC layer, was assembled. The assembled sensor was heated to 70 ^{o}C for 20 to 30 s with a slight pressure to reflow the parafilm and seal the sensor (Steps v & vi). In addition, chemiresistors with copper tape and screen printable carbon as contact electrodes were also fabricated to compare the sensor performance with the metal leaf electrodes (Figure S6, Appendix 2). The fabricated sensors were dipped in a methanolic solution of phenyl-capped aniline tetramer (PCAT) for 90 minutes. PCAT serves as the ligand that makes the chemiresistive sensor selective to certain analytes in solution.

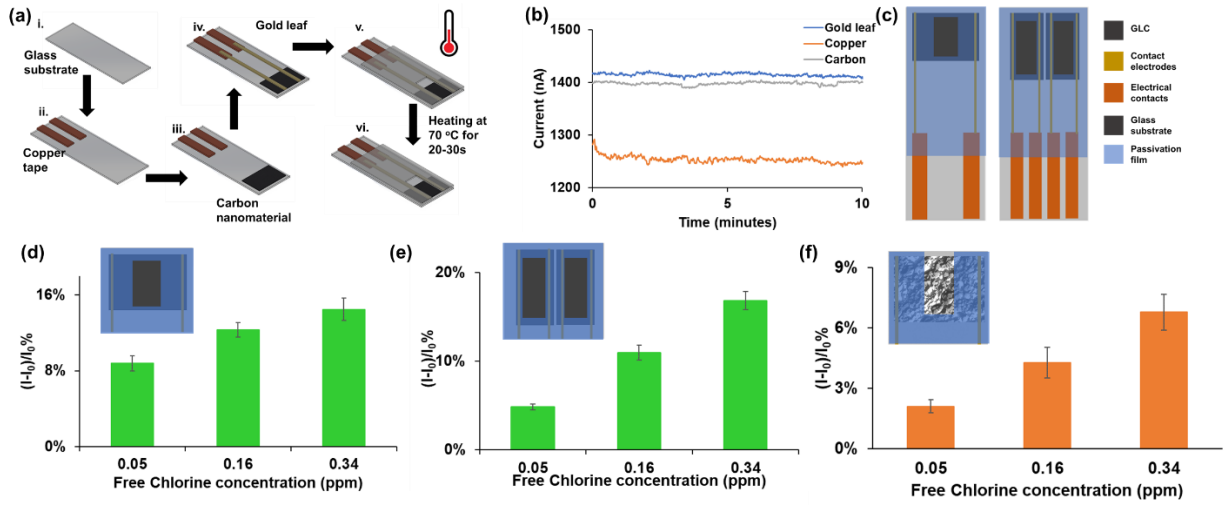

Figure 4.5 (a) Overview of chemiresistor fabrication process. (b) Plot showing the noise levels for chemiresistors with three different contact electrodes: gold leaf (blue), copper tape (orange) and screen printed carbon electrode (grey). (c) Schematics showing fabricated chemiresistive sensors with GLC as active material. The sensor can be fabricated in single and array of two electrodes within the same area. (d) Sensor response for a single electrode GLC chemiresistive sensor for three free chlorine concentration (0.05, 0.16 and 0.34 ppm). Error bar represents the standard deviation of three different sensors (n=3). Inset showing the sensor schematics. (e) Sensor response for two GLC electrode arrays with two chemiresistive sensors in each array for three free chlorine concentration (0.05, 0.16 and 0.34 ppm). Error bar represents the standard deviation of two arrays with two sensors each (n=4). Inset showing the sensor schematics. (f) Sensor response for chemiresistive sensors with drop casted CNT as active layer and gold leaf as the contact electrodes three free chlorine concentration (0.05, 0.16 and 0.34 ppm). Error bar represents the standard deviation of three different sensors (n=3). Inset showing the sensor schematics.

The PCAT functionalized sensors were dipped in DI water for noise measurements, followed by three different free chlorine concentrations (0.05, 0.16 and 0.34 ppm) to assess their sensing performance. The sensors were first allowed to stabilize for 50 min in DI water and then the stability of their response was assessed by measuring their resistance over the next 10 min. The

noise in the signal for all three types of chemiresistors (with gold leaf, copper tape and screen printed contacts) is shown in Figure 4.5b. The peak-to-peak noise for copper tape, carbon and gold leaf electrode was 18.2 nA, 10.2 nA and 11.5 nA, respectively. The standard deviation of the noise for copper tape, carbon electrode and gold leaf 2.28 nA, 1.53 nA and 1.52 nA, respectively. It was interesting to note that the noise levels of the gold leaf were similar to the screen printed carbon electrodes that have a very conformal contact and significantly better than the sensors that used copper tape as the contact electrodes. This may be due to the order of magnitude difference in the thickness of the metal layer between the gold leaf and the copper tape that enables a greater conformal contact with the sensing substrate. The sensor response for 0.05, 0.16 and 0.34 ppm free chlorine concentration was then measured by exposing the sensors to the analyte for 30 mins and then measuring their response. PCAT functionalized on the GLC gets oxidized in presence of free chlorine resulting a change in the doping level of GLC which can be read out as a change in resistance [26]. The sensors with gold leaf contacts were found to provide a 8.8% ± 0.8%, 12.3% ± 0.8% and 14.5% ± 1.3% change in their current respectively in comparison to their response in DI water (Figure 4.5d). The process was also used to fabricate flexible chemiresistive sensors described in Section 4.3.

The fabrication of the gold leaf contact electrodes can be parallelized and miniaturized to enable fabrication of not just single sensors but also chemiresistive sensing arrays [31]. Chemiresistive sensing arrays are very useful to detect multiple analytes using a single sensing chip. Xurography can be used to cut a large film of the sensitive substrate such as GLC and contact materials such as the gold leaf and assemble them close to each other to form a sensing array. Such assembly can be performed either manually or using an automated tool such as a pick and place machine. To demonstrate this versatility, an array of two chemiresistive sensors were fabricated by assembling

the GLC and the gold leaf contact electrodes cut xurographically close to each other in the same form factor as the previously described single sensor. (Figure 4.5c). The fabricated sensors were loaded with PCAT and then tested with three different free chlorine concentrations (0.05, 0.16 and 0.34 ppm). Sensor response of the individual electrodes for three free chlorine concentrations 0.05, 0.16 and 0.34 ppm as 4.8% ± 0.3%, 10.9 % ± 0.8%, and 16.8% ± 1%, respectively (n=4 electrodes on two sensing arrays). The higher sensitivity (4.05% per 0.1 ppm change in free chlorine concentration) in the case sensor array was due to the higher percentage of electrode area exposed as compared to single electrode (1.9% per 0.1 ppm change free chlorine concentration). The observed standard deviation for the three free chlorine concentrations was <1%, showing high reproducibility of the fabrication process (Figure 4.5e). These paired sensing arrays are useful to monitor and normalize for environmental effects such as humidity or temperature by functionalizing only one sensor of the pair with the selective ligand[32]. Similarly, chemiresistive sensor arrays with multiple sensitive ligands functionalized on different sensors could also be used to quantify the effect of different interfering analytes that may be present in a sample.

4.1.2 Chemiresistive sensors with drop casted sensing films

Solvent based nanomaterials deposition is a simple, rapid and widely used method to deposit nanomaterials like graphene, CNT on different substrates like glass, polymer substrates etc. Numerous chemiresistive sensors have been fabricated using drop casting methods to form sensing film [29,33]. Typically, the metal contact electrodes are fabricated either by sputtering or screen printing. Therefore, drop casted CNT films on glass were used as an example to demonstrate the suitability of metal leaf contact electrodes for integration with sensing surfaces with drop casted nanomaterial films.

Here, we fabricated the chemiresistive sensors with drop casted active films like CNT, on frosted glass substrate (with frosted area 2.5 × 2.5 cm^2) using a previous protocol [33]. Nine chemiresistive sensors were fabricated, three for each type of the contact electrodes, gold leaf, copper tape and screen printed carbon. The resistance of the sensors with screen printed, copper tape and gold leaf contact electrodes were 9.31 ± 0.91 kΩ, 5.34 ± 0.28 kΩ and 4.2 ± 0.39 kΩ, respectively. The fabricated sensors were functionalized with PCAT and then sensor was dipped in DI water for noise measurements and followed by exposure to three different free chlorine concentrations (0.05, 0.16 and 0.34 ppm) for sensing measurements. The sensors were first allowed to stabilize for 50 min in DI water and then the stability of their response assessed by measuring their resistance over the next 10 min. The peak-to-peak noise for copper tape, carbon and gold leaf electrode was 11.8 nA, 9.5 nA and 9.5 nA, respectively. The standard deviation of the signal (noise) for copper tape, carbon electrode and gold leaf 1.6 nA, 1.4 nA and 1.4 nA, respectively. Even though the noise levels for all three sensors were statistically similar, the sensor resistances for gold leaf electrodes were lower than those for copper tape and screen printed carbon electrodes. Next, the sensor with gold leaf electrodes was tested with three different free chlorine concentrations (Figure 4.5f) and the response obtained for free chlorine concentrations of 0.05, 0.16 and 0.34 ppm was 2.1% ± 0.3%, 4.3 % ± 0.8%, and 6.8% ± 0.9%, respectively (n=3). The observed standard deviation showed that the sensor fabrication process resulted in reproducible sensors.

This series of experiments confirmed that the gold leaf electrodes patterned using the current process can be used to fabricate reproducible contact electrodes (standard deviation <1% sensor response, n=3) even for nanomaterial films with drop casted films with low peak-to-peak noise. With the xurography process, not only can gold be patterned but the same process can also be used

to pattern other metal leaves like platinum, palladium, and copper as the electrical characteristics of the metal-CNT/graphene interface depend on the contact metal used for fabrication [34].

4.1.3 Flexible chemiresistive sensors

In many applications such as food monitoring, medical diagnostics and environmental monitoring, the substrates to which the sensors are to be attached are usually nonplanar and bend during the course of operation. Therefore, the ability of these sensors to operate even during and after mechanical flexion and for the contacts to remain stable is important. Here, a flexible chemiresistive sensor was fabricated with GLC sheet as the sensing layer and gold leaf or screen printed carbon as the contact electrodes on a double sided Kapton tape as the substrate. The fabrication process was similar to the process described in Figure 4.6a except that the glass substrate was replaced by a double sided Kapton tape as the base substrate. The sensor resistance was 3.5 ± 0.42 kΩ (n=3). The flexible sensor peak to peak noise and standard deviation of the signal (noise) was 10.8 nA and 1.7 nA, respectively, before bending which was similar to the noise of GLC sensors on glass substrate (peak to peak noise 11.5 nA and 1.52 nA). The sensors were loaded with PCAT using the protocol and tested with different free chlorine concentrations (0.05 ppm, 0.16 ppm, and 0.34 ppm). The current change was calculated with DI water as the baseline similar to the procedure described in Section 4.1.1. The sensors responses for 0.05 ppm, 0.16 ppm, and 0.34 ppm free chlorine concentration were 3% ± 0.6%, 11% ± 0.5%, and 20% ± 0.7%, respectively (Figure 4.6a). Before bending the sensors were chemically reset using 0.1 M ascorbic acid [35]. The average sensor responses after four chemical resets were 2% ± 0.7%, 9% ± 1.2%, and 22% ± 0.7%, respectively (Figure S7, Appendix 2). The sensitivity of the sensor was better than the sensor on the glass substrate probably due to the change in percentage of area exposed to the analyte for the flexible sensors.

The effect of bending on the sensors were evaluated by bending the sensor at different angles 30°, 45°, 75°, 90° and 120° followed by 15 bending cycles at 120° along an axis parallel to the contact electrodes. The peak-to-peak noise and standard deviation of noise was 9.5 nA and 1.7 nA, respectively, which was not statistically different from the noise before the bending. The sensor response was measured before and after all bending cycles for three different free chlorine concentrations of 0.05, 0.16 and 0.34 ppm. A small change in the sensitivity of the sensor was observed before (slope of calibration curve = 7.1% per 0.1 ppm of free chlorine change) and after the bending (slope of calibration curve = 6.9% per 0.1 ppm of free chlorine concentration change) within the measuring range of 0.05-0.34 ppm. No significant change in response was observed for the sensor between, before, and after bending (Figure 4.6b). In addition, the variation between the three sensors was similar to before bending showing that all the sensors were able to withstand the multiple bending cycles (n=15) till 120°.

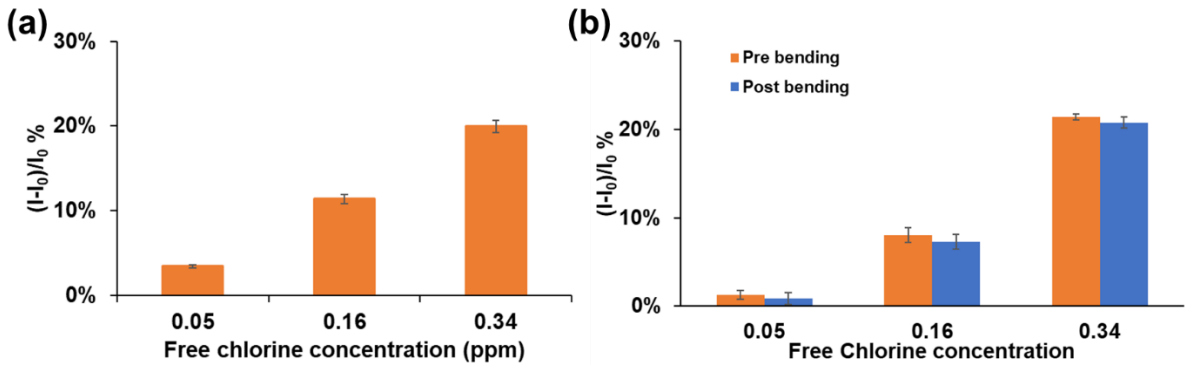

Figure 4.6 (a) Sensor response with three different free chlorine concentrations (0.05, 0.16, and 0.34ppm) (b) Sensor response with three free chlorine concentration pre (Orange) and post bending (Blue).

Chemiresistive sensors with screen printed electrodes were fabricated similar to gold leaf contact electrodes. The resistance of the sensors was 5.58 ± 0.13 kΩ which was around 60% higher than

the sensors with gold leaf contacts. The higher sensor resistance can be linked to lower conductivity of carbon-based screen printed ink. In addition, these screen printed sensors were also tested with three different free chlorine concentrations similar to sensors with gold leaf contact. The sensitivity of the sensor with screen printed contacts was 4.12% per 0.1 ppm of free chlorine change which was around 58% of the sensitivity with the gold leaf contacts (7.1% per 0.1 ppm of free chlorine change). In addition, after the bending cycle one of the screen printed sensor failed while no significant change was observed in the other two sensors (Figure S8, Appendix 2). The failure of the sensor of the screen printed contact electrode can be due to the cracks developed during the bending while the thin gold leaf electrodes were able to maintain the structural integrity due to the better adhesion of the gold on the thin tape and the resulting in the flexibility.

4.2 Biamperometric glucose sensor

Biamperometric sensors are fabricated using noble metals (wire or film electrodes) [36,37] or screen printed carbon electrodes. Noble metal like gold, platinum and palladium, are generally expensive [36,37] and the films usually are deposited by sputtering which requires complex instruments and controlled environments [37]. Screen printed electrodes are low-cost and easy to fabricate but the ink curing requires heating the substrate for 1-2 hours which is problematic for certain polymer substrates [38]. Here, we demonstrate that bioamperometric sensors can also be fabricated using xurography applied to metal leaf. Three interdigitated sensors were patterned using xurography on a Kapton tape (Figure 4.7a). The fabrication process is described in Section 3.1. The sensors were passivated with a parafilm that had a circular opening of 1.3 cm to define the exposed area of the electrodes. Double-sided conductive copper tape was used for the electrical contacts of the sensor. Potassium ferricyanide was used as the mediator and a 100 µl of 250 mM potassium ferricyanide was drop casted on the electrode. Then, the sensor was coated with 100 µl

of 2 mg/ml of glucose oxidase solution prepared in 0.1 M phosphate buffer with pH 7.4. The sensors were dried overnight at room temperature. The sensors were tested with seven different glucose concentrations (5 mM, 10 mM, 15 mM, 20 mM, 25 mM, 30 mM and 35 mM). All measurements were performed at a small potential bias of 10 mV for 100 s. Each measurement was started with a 150 µL drop of DI water which was subsequently spiked with 0.676 µl of glucose stock solution (equivalent to 5mM of glucose concentration) resulting in an increase of 5 mM in glucose concentration after every addition. A high mediator concentration (potassium ferricyanide ~167 mM) was used in the experiment. So, the current is independent of the mediator concentration, and the glucose oxidation is the limiting reaction resulting in the current controlled by the glucose concentrations [37]. The calibration curve was plotted using the current response at 10 s for each glucose concentrations. All experiments were done in triplicates (n=3). The sensor exhibited a linear range from 0 to 35 mM of glucose concentration with a slope of 1.14 µA/mM (Figure 4.7b) which is less than the slope reported by a previous study (1.8 µA/mM for a measuring range of 0-33.33 mM glucose concentration, calculated from the plot) [37]. The reduced slope used in the current study may be due to the lower potential bias (10 mV) used for the measurement as compared to the previous study (150 mV) [38]. The lower potential serves to reduce the interferences due to common interferent molecules like ascorbic acid and uric acid, present in blood [38]. A R^2 value of 0.9961 showed a high correlation between the current response and glucose concentrations.

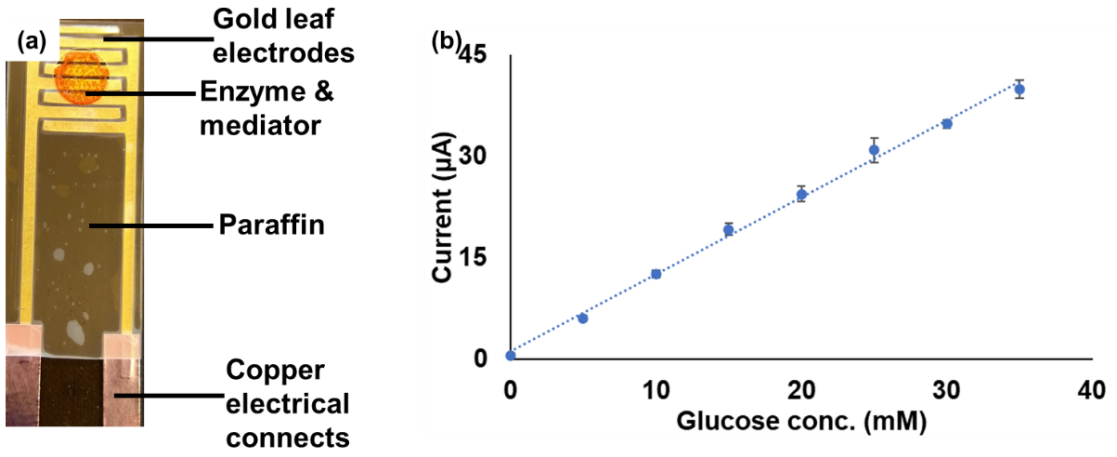

Figure 4.7 (a) An image of biamperometric glucose sensor fabricated using gold leaf. The working area was defined using a paraffin passivation film with a circular opening of 1.3 cm. The interdigitated electrode was coated with potassium ferricyanide (electron mediator) and glucose oxidase (enzyme). (b) Current response of the sensor with seven different glucose concentrations (ranging from 5 mM to 35 mM) working under an applied potential of 10 mV.

4.3 3D electrodes with high surface area

High surface area electrodes are used for various applications like electrochemical sensing to improve sensitivity, tissue engineering scaffolds to enhance cell proliferation, and to improve the performance of energy storage devices. Here, high surface area metal electrodes with microscale features were fabricated using metal leaf adhered on top of the polystyrene shrink film. Gold leaf was used to fabricate electrodes with high electrochemical surface area. The polystyrene shrink films were cleaned using isopropanol. 3M double sided adhesive transfer tape (#7952 MP, adhesive thickness of 60 µm) was patterned using xurography. The patterned double sides tape was adhered to the shrink film with the help of a roller. Finally, gold leaf was applied to the patterned adhesive layer and unattached gold leaf was removed from the shrink film to form the

gold electrode pattern (Figure 4.8a). After shrinking, all electrodes were reduced to 40% of their original size (Figure 4.8a). The electrode shrinking was performed in a hot air oven at 130 ^{o}C and 160 ^{o}C. Shrinking duration is a critical parameter for fabricating repeatable electrodes with high surface area. Therefore, shrinking duration was optimized for both the shrinking temperature. At 130 ^{o}C, the shrinking was performed for three durations 5, 10 and 15 minutes. While 160 ^{o}C, the shrinking was performed for three durations 2, 5 and 10 minutes. At 160 ^{o}C, the electrodes were deformed for 15 minutes. Therefore, the maximum shrinking duration was reduced to 10 minutes for 160 ^{o}C.

The surface topography of wrinkled surfaces was analyzed using an Alicona optical microscope (Figure S9, Appendix 2). All samples were analyzed using the same magnification which covered a spot size of 1.62×1.62 mm^2. Each sample was analyzed at four different spots (n=4). The average surface roughness of wrinkled gold leaf at 130 ^{o}C for shrinking time of 5, 10 and 15 minutes were 32.17 ± 1.12 µm, 36.79 ± 1.31 µm and 39.95 ± 5.53 µm, respectively. An increase in surface roughness was observed with an increase in shrinking time at 130 ^{o}C. Moreover, the increased surface roughness was also associated with an increased variation in surface roughness while there was no significant difference in surface roughness variation between 5 minutes and 10 minutes. However, there was a significant increase in variation for 15 minutes (5 times) samples as compared to 5 minutes samples which can be due to the deformation of adhesive film or the shrink film. The average surface roughness of wrinkled gold leaf at 160 ^{o}C for shrinking time of 2, 5, and 10 minutes were 31.45 ± 1.76 µm, 27.49 ± 4.99 µm and 27.4 ± 2.27 µm, respectively. The overall average surface roughness at shrinking temperature 160 ^{o}C was less than 130 ^{o}C but there is a significant increase in variation between different spots for 160 ^{o}C. Therefore, all further characterizations were performed with samples shrunk at 130 ^{o}C for 5 minutes.

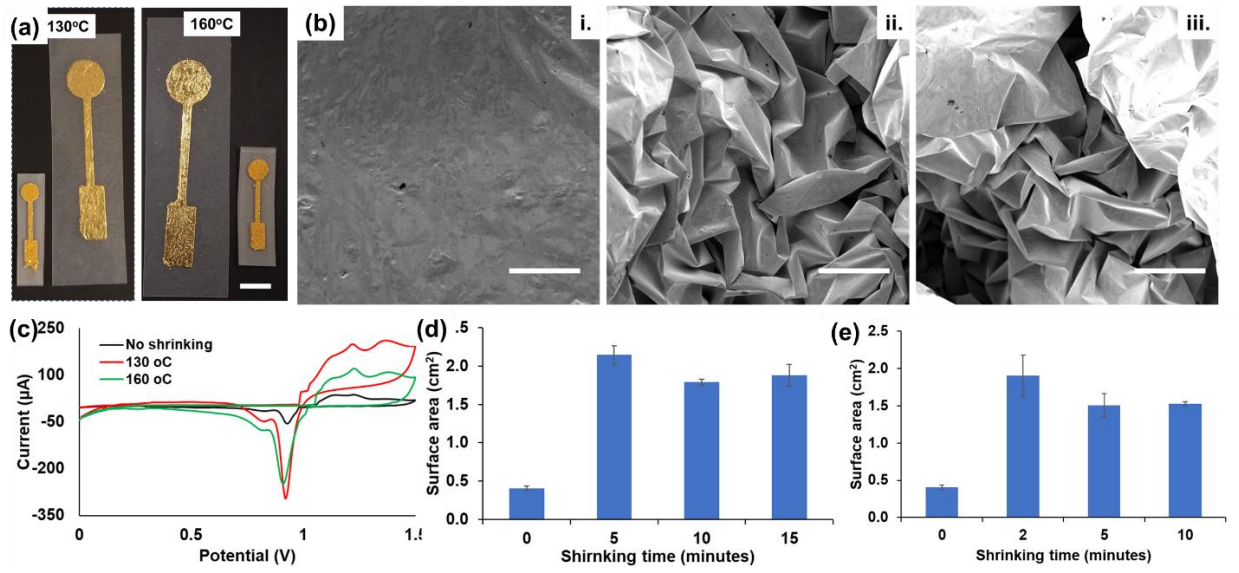

Figure 4.8 (a) Images of gold metal leaf electrodes in the original size and after shrinking at 130 °C for 5 minutes and at 160 °C for 2 minutes (Scale bar 1cm). (b) SEM images with a scale bar of 100 µm showing (i) pristine gold leaf (ii) gold leaf shrunk at 130 °C for 5 minutes (iii) and 160 °C for 5 minutes (c) Cyclic voltammogram for unshrunk (black line) and shrunk electrodes at 130 °C (red line) and 160 °C (green line) for 5 minutes each. (d) Change in surface area of the electrodes after shrinking at 130 °C for three different durations (5, 10 and 15 minutes). Error bar represents the standard deviation of three electrodes (n=3). (e) Change in surface area of the electrodes after shrinking at 160 °C for three different durations (2, 5 and 10 minutes). Error bar represents the standard deviation of three electrodes (n=3).

All the shrunken surfaces were analyzed using SEM. SEM images showed a significant difference in surface morphology of pristine and shrunken surfaces for both 130°C and 160°C shrinking temperature (Figure 4.8b, Scale bar 100 µm). Both the shrunken surfaces exhibited surface features of 10-100 µm for both shrinking temperature 130 °C and 160 °C, which matches with the surface analysis by Alicona microscope. Multiple shrunken surfaces were analyzed with SEM to investigate the effect of shrinking time and temperature (SEM images, Appendix 2, Figures S10

and S11). The surfaces shrunken at 130 ^{o}C showed uniform wrinkling features with minimum secondary features except for the longer shrinking time (15 minutes) which is supported by the surface roughness obtained from interferometry (Figure S8, Appendix 2). Further, the surfaces shrunken at 160^{o}C showed more non-uniformity with a higher number of secondary features which is supported by the higher variation in surface roughness obtained from white light interferometry (Figure S8, Appendix 2). In addition, an increase in secondary features was also observed for the longer shrinking time (5 minutes and 10 minutes) which again explains the higher spot to spot variation in these samples.

The electrochemical surface area of the electrode after shrinking was estimated using cyclic voltammetry [39]. The cyclic voltammetry was performed in a 0.1 M H_2SO_4 solution with a potential range of 0 to 1.5 V at a scan rate of 0.05 V/s used in a previous study [20]. The oxidation process has multiple anodic peaks while the reduction generally has a single peak. Therefore, the reduction peak of the cyclic voltammogram was used for surface area calculations (Figure 4.8c). All experiments were performed in triplicates (n=3). Total charge was calculated by integrating the reduction peak using PSTrace 5.8 software and the surface area was determined by dividing the charge by surface charge density of monolayer gold film (386 μC/cm^2) [20]. For 130 ^{o}C, the largest surface area enhancement was observed for a shrinking time of 5 minutes where the area change was 5.3 times (2.1 cm^2) the surface area of the pristine gold electrode (Figure 4.8d). For 160 ^{o}C, the largest surface area increase was observed for a shrinking time of 2 minutes with an area of 1.9 cm^2 (4.7 times the pristine gold surface, Figure 4.8e). At higher shrinking temperature (160 ^{o}C), a larger deformation of the gold leaf along with the polystyrene sheet was observed resulting in a higher standard deviation (Figure 4.8d and 4.8e) which aligns with the data from white light interferometry and SEM analysis. The largest change in area for shrunken surfaces at

130 ºC and 160 ºC was less than reported by a previous study where for 100 nm thick sputtered gold film exhibited 6.3 times and 6.6 times increase in surface area for 130 ºC and 160 ºC, respectively. In our study, the smaller change in surface area can be attributed to the presence of adhesive film present beneath the gold leaf while the previous study used gold films sputtered directly on the pre-stressed polymer films [20]. Nevertheless, these experiments show that metal leaf can be used to fabricate compact high surface area electrodes with heat shrink polymers.

The performance of wrinkled electrodes as 3D metal electrodes with high surface area was investigated using electrochemical methods such as CV and chronoamperometry. Six gold leaf electrodes were shrunk at 130 ºC for 5 minutes and these electrodes were characterized using the protocol described in Section 3.2. Three electrodes were used to perform CV measurements. The peak oxidation and reduction currents observed were 1448.67 ± 61.27 µA and -593 ± 79.63 µA, respectively (Figure 4.9a). The chronoamperometric measurement at 0.5 V potential bias was performed using the protocol described in Section 3.2. Similar to non-wrinkled gold leaf, a linear curve was observed with a slope of 26.17 µA/mM Fe^{2+} concentration which is ~3 times the slope obtained for a pristine gold leaf electrode (8.78 µA/mM). A R^2 value of 0.9916 showed that the current values are highly correlated with the Fe^{2+} concentration (Figure 4.7b). The slope (26.17 µA/mM Fe^{2+} concentration) was less than reported by a previous study (37 µA/mM Fe^{2+} concentration) within a similar range of measurement (0.05 to 100 mM) [20]. This can be attributed to the increased area in the previous study as the sputtered gold films where directly in contact with the pre-stressed films. This provides a greater resistance to shrinkage and therefore greater degree of wrinkling and higher surface area. The use of adhesive as an intermediate layer between the gold leaf and the pre-stressed film, as in our case, provides a slightly smaller constraint and

therefore a reduction in the change in surface area which manifests itself as a smaller slope in the sensing experiment.

The electrodes also had smaller error bars resulting from the similar surface roughness as observed in white light interferometry and SEM images. This shows that the current fabrication process can manufacture reproducible 3D metal electrodes with high surface area.

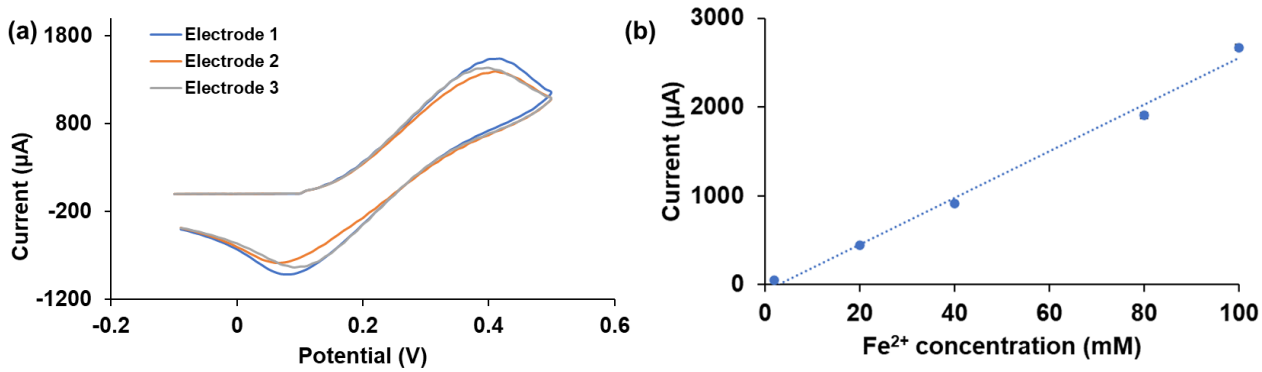

Figure 4.9 (a) Cyclic voltammogram of wrinkled gold leaf electrodes. The CV measurements were performed within the potential range of -0.1 to 0.5 V with 0.08 V/s scan in a solution containing 2mM $K_4Fe(CN)_6$ and 0.1M KCl. (b) Chronoamperometric measurements were also measured five different $K_4Fe(CN)_6$ solutions (2 mM, 20 mM, 40 mM, 80 mM and 100 mM) prepared in 1 M KCl. All experiments were done in triplicates (n=3).

The process was used to fabricate three electrodes using one gold leaf which cost around $2.85 /leaf (cost of one booklet was $71.15/25 gold leaves). Therefore, the cost of a single electrode was $0.95/electrode which is 15 cents more than the cost reported for solution-based gold nanoparticles electrodes [11]. However, this is significantly cheaper compared to sputter coated electrodes which cost around $4.30 USD /electrode [11] and screen printed gold electrodes (~$2.60 USD/electrode) [38].

5. Conclusion

A simple, rapid and low-cost patterning process was demonstrated using a low-cost bench top cutter (price ~ $ 399 CAD). The cutting was able to pattern thin lines with a line width up to <100 µm and generate reliable patterns with a pitch as small as ~100 µm. The conductive linear patterns of LW ~230 µm was obtained using xurography. The process was used to fabricate patterned electrodes for various applications like contact electrodes for chemiresistors, high surface area structures and electrochemical sensors. The fabricated contact electrodes for chemiresistors displayed low noise and were easy to manufacture chemiresistors arrays. The gold leaf was used to fabricate a biamperometric glucose sensor which measured the glucose concentration from 5 mM to 35 mM with a small potential bias of 10 mV. The low potential bias could potentially facilitate reduced interference from common compounds like ascorbic acid and uric acid. The patterning method was also used to reproducibly manufacture high surface area electrodes on shrink films with 5.3 times area increases as compared to pristine gold leaf on shrink film. The cost of fabricating a high surface gold leaf electrodes was around $0.95/ electrode which is ~around 20% of the cost for sputter coated electrodes. Apart from the three listed applications, the method could be used to integrate thin film electrodes in microfluidics channels to manufacture lab-on-a-chip devices and these patterned thin metal films could be used as seed layer for electrodepositing other metals on non-conductive substrates.

Funding

This work was supported by the Global Water Futures program and Natural Sciences and Engineering Research Council of Canada. PRS acknowledges support from the Canada Research Chairs Program.

Acknowledgment

We would like to acknowledge Dr. Ranjith Divigalpitiya from 3M Canada for providing the GLC sheets. The PCAT used in this study was synthesized by Md. Omar Sharif, Department of Chemistry, McMaster University. We would also like to acknowledge Dr Marcia Reid, Research Technician, Canadian Centre for Electron microscopy, McMaster University for helping with electron microscopy imaging and Mohammad Shariful Islam Chowdhury, McMaster Manufacturing Research Institute, McMaster University for white light interferometry imaging.

References

[1] G.P. Mastrotheodoros, K.G. Beltsios, Y. Bassiakos, V. Papadopoulou, On the Metal-Leaf Decorations of Post-Byzantine Greek Icons, Archaeometry. 60 (2018) 269–289. https://doi.org/10.1111/arcm.12287.

[2] M. Wenig, Application of metal leaf, 1960. https://doi.org/10.1145/178951.178972.

[3] R.S. Zemel, Method of transferring metal leaf to a substrate, 1999.

[4] X. Ge, L. Wang, Z. Liu, Y. Ding, Nanoporous Gold Leaf for Amperometric Determination of Nitrite, Electroanalysis. 23 (2011) 381–386. https://doi.org/10.1002/elan.201000320.

[5] Y. Li, L. Zhang, J. Liu, S.F. Zhou, K.A. Al-Ghanim, S. Mahboob, B.C. Ye, X. Zhang, A novel sensitive and selective electrochemical sensor based on molecularly imprinted polymer on a nanoporous gold leaf modified electrode for warfarin sodium determination, RSC Adv. 6 (2016) 43724–43731. https://doi.org/10.1039/c6ra05553b.

[6] J.A. Hondred, Z.T. Johnson, J.C. Claussen, Nanoporous gold peel-and-stick biosensors created with etching inkjet maskless lithography for electrochemical pesticide monitoring

with microfluidics, J. Mater. Chem. C. 8 (2020) 11376–11388. https://doi.org/10.1039/d0tc01423k.

[7] Y. Ding, Y.J. Kim, J. Erlebacher, Nanoporous gold leaf: "Ancient technology "/advanced material, Adv. Mater. 16 (2004) 1897–1900. https://doi.org/10.1002/adma.200400792.

[8] R.K. Khan, V.K. Yadavalli, M.M. Collinson, Flexible Nanoporous Gold Electrodes for Electroanalysis in Complex Matrices, ChemElectroChem. 6 (2019) 4660–4665. https://doi.org/10.1002/celc.201900894.

[9] J. Patel, L. Radhakrishnan, B. Zhao, B. Uppalapati, R.C. Daniels, K.R. Ward, M.M. Collinson, Electrochemical properties of nanostructured porous gold electrodes in biofouling solutions, Anal. Chem. 85 (2013) 11610–11618. https://doi.org/10.1021/ac403013r.

[10] M.D. Scanlon, U. Salaj-Kosla, S. Belochapkine, D. MacAodha, D. Leech, Y. Ding, E. Magner, Characterization of nanoporous gold electrodes for bioelectrochemical applications, Langmuir. 28 (2012) 2251–2261. https://doi.org/10.1021/la202945s.

[11] E. Gonzalez-Martinez, S. (Kevin) Saem, N.E. Beganovic, J. Moran-Mirabal, Fabrication of microstructured electrodes via electroless metal deposition onto polydopamine-coated polystyrene substrates and thermal shrinking, Nano Sel. (2021) 1–15. https://doi.org/10.1002/nano.202100022.

[12] B.L. Thompson, C. Birch, D.A. Nelson, J. Li, J.A. DuVall, D. Le Roux, A.C. Tsuei, D.L. Mills, B.E. Root, J.P. Landers, A centrifugal microfluidic device with integrated gold leaf electrodes for the electrophoretic separation of DNA, Lab Chip. 16 (2016) 4569–4580. https://doi.org/10.1039/C6LC00953K.

[13] M.S.F. Santos, W.A. Ameku, I.G.R. Gutz, T.R.L.C. Paixão, Gold leaf: From gilding to the fabrication of disposable, wearable and low-cost electrodes, Talanta. 179 (2018) 507–511. https://doi.org/10.1016/j.talanta.2017.11.021.

[14] C. Kao, Hsin-Lin (Cindy); Holz, Christian; Roseway, Asta; Calvo, Andres; Schmandt, DuoSkin: Rapidly Prototyping On-Skin User Interfaces Using Skin-Friendly Materials, in: 2016: pp. 16–23.

[15] H. Jeong, J.M. Seo, Electrode design on plastic substrates using laser patterned double-sided tape and gold leaf, Proc. Annu. Int. Conf. IEEE Eng. Med. Biol. Soc. EMBS. (2019) 1286–1289. https://doi.org/10.1109/EMBC.2019.8857635.

[16] Y. Huang, Y. Huang, Y. Wang, Z. Pei, M. Zhu, Z. Liu, Z. Ruan, Y. Zhao, S. Du, C. Zhi, A Wearable Supercapacitor Engaged with Gold Leaf Gilding Cloth Toward Enhanced Practicability, ACS Appl. Mater. Interfaces. 10 (2018) 21297–21305. https://doi.org/10.1021/acsami.8b03780.

[17] K. Shimada, T. Toyoda, Gold leaf counter electrodes for dye-sensitized solar cells, Jpn. J. Appl. Phys. 57 (2018) 03EJ04. https://doi.org/10.7567/1347-4065/ab5ccf.

[18] M.S. Ahmed, S. Ezugwu, R. Divigalpitiya, G. Fanchini, Relationship between electrical and thermal conductivity in graphene-based transparent and conducting thin films, Carbon N. Y. 61 (2013) 595–601. https://doi.org/10.1016/j.carbon.2013.05.041.

[19] A. Mohammadzadeh, A.E.F. Robichaud, P.R. Selvaganapathy, Rapid and Inexpensive Method for Fabrication and Integration of Electrodes in Microfluidic Devices, J. Microelectromechanical Syst. 28 (2019) 597–605. https://doi.org/10.1109/JMEMS.2019.2914110.

[20] C.M. Gabardo, Y. Zhu, L. Soleymani, J.M. Moran-Mirabal, Bench-top fabrication of hierarchically structured high-surface-area electrodes, Adv. Funct. Mater. 23 (2013) 3030–3039. https://doi.org/10.1002/adfm.201203220.

[21] M. Libansky, J. Zima, J. Barek, A. Reznickova, V. Svorcik, H. Dejmkova, Basic electrochemical properties of sputtered gold film electrodes, Electrochim. Acta. 251 (2017) 452–460. https://doi.org/10.1016/j.electacta.2017.08.048.

[22] T. Zhong, N. Jin, W. Yuan, C. Zhou, W. Gu, Z. Cui, Printable stretchable silver ink and application to printed RFID tags for wearable electronics, Materials (Basel). 12 (2019) 1–14. https://doi.org/10.3390/ma12183036.

[23] P. Prasertying, N. Jantawong, T. Sonsa-Ard, T. Wongpakdee, N. Khoonrueng, S. Buking, D. Nacapricha, Gold leaf electrochemical sensors: Applications and nanostructure modification, Analyst. 146 (2021) 1579–1589. https://doi.org/10.1039/d0an02455d.

[24] K.S. Teh, L. Lin, MEMS sensor material based on polypyrrole-carbon nanotube nanocomposite: Film deposition and characterization, J. Micromechanics Microengineering. 15 (2005) 2019–2027. https://doi.org/10.1088/0960-1317/15/11/005.

[25] A. Mohtasebi, A.D. Broomfield, T. Chowdhury, P.R. Selvaganapathy, P. Kruse, Reagent-Free Quantification of Aqueous Free Chlorine via Electrical Readout of Colorimetrically Functionalized Pencil Lines, ACS Appl. Mater. Interfaces. 9 (2017) 20748–20761. https://doi.org/10.1021/acsami.7b03968.

[26] L.H.H. Hsu, E. Hoque, P. Kruse, P. Ravi Selvaganapathy, A carbon nanotube based resettable sensor for measuring free chlorine in drinking water, Appl. Phys. Lett. 106 (2015). https://doi.org/10.1063/1.4907631.

[27] H.K. Salila Vijayalal Mohan, R. Hansen Varghese, C.H. Wong, L. Zheng, J. Yang, Epigallocatechin gallate decorated carbon nanotube chemiresistors for ultrasensitive glucose detection, Org. Electron. 28 (2016) 210–216. https://doi.org/10.1016/j.orgel.2015.10.032.

[28] E. Song, T.H. da Costa, J.W. Choi, A chemiresistive glucose sensor fabricated by inkjet printing, Microsyst. Technol. 23 (2017) 3505–3511. https://doi.org/10.1007/s00542-016-3160-4.

[29] J. Dalmieda, A. Zubiarrain-Laserna, D. Ganepola, P.R. Selvaganapathy, P. Kruse, Chemiresistive detection of silver ions in aqueous media, Sensors Actuators, B Chem. 328 (2021) 129023. https://doi.org/10.1016/j.snb.2020.129023.

[30] S.S. Ling, R. Divigalpitiya, K.P. Chia, A. Marek, C. Park, G.A. Marra, Multi-layer cover tape constructions with graphite coatings, 2017.

[31] E. Song, J.W. Choi, Multi-analyte detection of chemical species using a conducting polymer nanowire-based sensor array platform, Sensors Actuators, B Chem. 215 (2015) 99–106. https://doi.org/10.1016/j.snb.2015.03.039.

[32] S. Ishihara, J. Labuta, T. Nakanishi, T. Tanaka, H. Kataura, Amperometric Detection of Sub-ppm Formaldehyde Using Single-Walled Carbon Nanotubes and Hydroxylamines: A Referenced Chemiresistive System, ACS Sensors. 2 (2017) 1405–1409. https://doi.org/10.1021/acssensors.7b00591.

[33] V. Patel, P. Kruse, P.R. Selvaganapathy, Hydrogen peroxide chemiresistive detection platform with wide range of detection, Proc. IEEE Sensors. 2019-Octob (2019) 2019–2022. https://doi.org/10.1109/SENSORS43011.2019.8956932.

[34] Y. Matsuda, W.Q. Deng, W.A. Goddard, Contact resistance for “end-contacted” metal-graphene and metal-nanotube interfaces from quantum mechanics, J. Phys. Chem. C. 114 (2010) 17845–17850. https://doi.org/10.1021/jp806437y.

[35] V. Patel, P. Kruse, P.R. Selvaganapathy, Flexible chemiresistive sensor with xurographically patterned gold leaf as contact electrodes for measuring free chlorine, (2021) 1–4. https://doi.org/10.1109/fleps51544.2021.9469787.

[36] C. Zhao, J. Song, Flow-injection biamperometry for direct determination of hydroxylamine at two pretreated platinum electrodes, Anal. Chim. Acta. 434 (2001) 261–267. https://doi.org/10.1016/S0003-2670(01)00846-7.

[37] L.S. Kuhn, Biosensors: Blockbuster or bomb? Electrochemical biosensors for diabetes monitoring, Electrochem. Soc. Interface. 7 (1998) 26–31.

[38] C. Zhang, J. Li, Disposable biamperometric capillary-fill device for glucose, Microchim. Acta. 144 (2004) 119–124. https://doi.org/10.1007/s00604-003-0084-3.

[39] S. Trasatti, O.A. Petrii, International Union of Pure and Applied Chemistry Physical Chemistry Division Commission on Electrochemistry: Real Surface Area Measurements in Electrochemistry, Pure Appl. Chem. 63 (1991) 711–734. https://doi.org/10.1351/pac199163050711.

Chapter 5

Reagent-free hydrogen peroxide sensing using carbon nanotube chemiresistors with electropolymerized crystal violet and its applications in biological samples

Vinay Patel [1], Dipankar Saha[2], Peter Kruse [2], and P. Ravi Selvaganapathy [1,3*]

[1] School of Biomedical Engineering, McMaster University, Hamilton, ON, L8S 4K1, Canada

[2] Department of Chemistry and Chemical Biology, McMaster University, Hamilton, ON, L8S 4M1, Canada

[3]Department of Mechanical Engineering, McMaster University, Hamilton, ON, L8S 4K1, Canada

Corresponding Author

P. Ravi Selvaganapathy – Department of Mechanical Engineering, McMaster University, Hamilton, ON, L8S 4K1, Canada; https://orcid.org/0000-0003-2041-7180

* selvaga@mcmaster.ca

Status: accepted

Keywords: Hydrogen peroxide, Chemiresistive biosensor, solid-state sensor, crystal violet, electropolymerized self assembled monolayer

Abstract

Hydrogen peroxide (H_2O_2) is an intermediate molecule generated in numerous peroxidase assays used to measure concentrations of biomolecules such as glucose, galactose and lactate. At present, H_2O_2 is measured using colorimetric and electrochemical sensors (mainly amperometric). However, colorimetric sensors require reagents while amperometric sensors need multiple electrodes and are often prone to interference due to high potential bias applied. Here, we develop a solid-state, reagent-free chemiresistive H_2O_2 sensor which can measure H_2O_2 over a wide measuring range of 0.5 to 1000 ppm (0.015 mM to 29.4 mM). The sensors were fabricated using a network of functionalized single walled carbon nanotubes (SWCNTs) as the sensitive layer and xurographically patterned gold leaf as contacts. The SWCNTs were functionalized with crystal violet to impart selective detection of H_2O_2. The crystal violet was self assembled on the SWCNT film and subsequently polymerized via cyclic voltammetry to improve its retention on the sensing layer. The functionalized sensor exhibited a good selectivity against common interferents such as uric acid, urea, glucose, and galactose. In addition, the sensor was used to measure in situ H_2O_2 generated during peroxidase assays performed using enzymes like glucose oxidase. The sensor was tested in standard buffer solutions for both enzymes. The glucose oxidase assay was also demonstrated in spiked human pooled plasma solutions. The glucose oxidase coated sensor exhibited a glucose detection range of 2 mM to 20 mM in standard buffer and blood plasma solutions, with a good recovery rate (~95% to 107%) for glucose measurements in blood plasma.

1. Introduction

H_2O_2 is a crucial molecule, and its measurement is essential in a number of sectors such as textile, food processing, paper and pulp bleaching, medical diagnostics, environmental, disinfection and pharmaceutical industry[1]. It is also an intermediate compound formed during intracellular

reactions and facilitates the detection of numerous analytes like glucose, lactose, and galactose, via. peroxidase assays. Current H_2O_2 sensors can be broadly classified based on their working principle into two categories: colorimetric or electrochemical. Colorimetric sensors are highly accurate but require reagents, are unsuitable for in-field use, need sophisticated processes for manufacturing and detection, and require trained personnel for operations. Electrochemical sensors can be further divided into two main sub-categories: potentiometric and amperometric. Potentiometric sensors are easy to fabricate and are conducive to miniaturization, but they require a highly stable reference electrode for reliable measurements. Similarly, amperometric sensors are simple to fabricate and easy to miniaturize but they are more common due to their high selectivity [2]. Enzyme-free amperometric sensors for H_2O_2 measurements were also reported using numerous molecules like Prussian blue [3], ferrocene [4], conducting polymers [5], and metal nanomaterials [6]. However, they require a potential bias which requires a reference electrode to obtain reliable measurements.

Chemiresistive sensors offer a simpler sensing platform to detect the analyte and its concentration through resistance change in the sensing layer [1]. In the past, several H_2O_2 vapor and liquid chemiresistive sensors have been developed using organic molecules [7,8], metal or metal oxide nanoparticles [9–11], conducting polymers [12,13] and carbon nanomaterials like graphene and carbon nanotubes (CNT) [14,15]. A polypyrrole doped multi-walled CNT (MWCNT) sensor was developed that was capable of H_2O_2 detection within a range of 0 to 20 mM in standard buffer solutions [12]. Other conducting polymers such as polyaniline nanowires modified with silver nanoparticles [11] and poly(3,4-ethylenedioxythiophene) polystyrene sulfonate (PEDOT: PSS) along with horseradish peroxidase [13] have been used for H_2O_2 detection. The reported measuring range of polyaniline nanowire with silver nanoparticles was 2 mM to 40 mM. However, the sensor-to-

sensor reproducibility for concentrations beyond 10 mM was poor. The concentration range beyond 10 mM is important for measuring glucose levels in diabetic patients [16]. The PEDOT: PSS sensor was able to detect over a measuring range from 61.3 nM to 61.3 µM but needed an enzyme for H_2O_2 detection. Moreover, none of the three sensors were tested against any common interfering agents and real samples for medical diagnostics. Specific organic molecules such as Epigallocatechin gallate [8] react with H_2O_2. This molecule along with CNT was used in a chemiresistive sensor to measure H_2O_2 in the sub micromolar range. Although these approaches show promise, they have limitations such as a very limited range of detection, requirement for additional enzymes for H_2O_2 detection and often require multiple fabrication steps. None of the sensors were tested in real matrices used for medical diagnostics such as blood, and plasma.

Crystal violet is a water soluble triphenylmethane dye that is widely available and low-cost. It is extensively used in the paper and textile industries. It is also used as biological stain for bacterial classification, dermatological agent, poultry feed additive for prevention of mold propagation, intestinal parasites, and veterinary medicine. In past, it was used as antiseptic due to its antifungal, antibacterial and antihelmintic properties. The reduced form of the dye is colorless, known as leuco crystal violet while the oxidised form is blue in color. Leuco crystal violet in presence of horseradish peroxidase has been used to measure H_2O_2 spectrophotometrically in natural water and wastewater [17]. Multiple electrochemical studies have electrodeposited crystal violet for electrocatalytic oxidation of molecules like hydroquinone [18], catechol [19] and bisphenol [20]. The molecule is used in electrochemical sensors due to its conjugated π-electron system which makes it easier to electropolymerized on variety of substrates including graphene [19], glassy carbon [18], and CNT [20].

Here we report for the first time a solid state carbon nanotube based chemiresistive sensor functionalized with crystal violet for H_2O_2 detection over a wide range from 0.5 to 1000 ppm (0.015 mM to 29.4 mM). The study uses a simple fabrication method and demonstrates use of the dye molecule to fabricate a chemiresistive sensor. Crystal violet was used due to its low-cost, easy availability and open ionized structure. The conjugated π-electron system of the molecule facilitates π-π interactions with single-walled CNTs (SWCNTs) which promotes a simple functionalization process of the molecule on SWCNT films. Self assembled thin films of crystal violet were deposited on the SWCNT electrode. The self assembled film was potentiodynamically electropolymerized and its effect of polymerization was investigated by comparing the sensitivity of the sensor in both cases. We also demonstrate the application of the H_2O_2 sensor by coating it with glucose oxidase to detect glucose in the standard buffer solution and human pooled plasma spiked with different glucose concentrations (2 mM to 20 mM).

2. Materials and methods

2.1 Materials

Gold leaf (24 K transfer leaf) was purchased from L. A. gold leaf wholesaler, USA. A bench top craft cutter (Cricut, Provo Craft & Novelty Inc.) was used for patterning tapes and gold leaf used in the fabrication process. Crystal violet was purchased from Sigma-Aldrich, Canada (Dye content ≥ 90%) and was used without any modifications. H_2O_2 solution (30%, reagent grade, catalog # 167306) was purchased from Fischer Scientific, Canada. DI water was used for all sample preparations. Frosted glass slides (VWR, catalog# 89085-399), and H_2O_2 colorimetric reagents (item# HR-051) were ordered from LaMotte, USA. Transfer tape and roller were purchased from Uline Canada. SWCNT ink dispersion was supplied by Nano-C, US (#CINK-200-P010100).

2.2 Sensor fabrication

The sensor fabrication process is shown as a process schematic diagram (Figure 5.1). The sensors were fabricated on a glass substrate with a single sided frosted area (2.5 cm × 2 cm). The frosted area was cleaned using acetone followed by methanol before use (Step 1). A PET-parafilm mask was placed to contain the drop casted SWCNT ink on the frosted area. The SWCNT ink supplied by Nano-C was diluted to 4% (v/v) using a methanol DI water mixture (1:1, v/v). The glass substrate was placed on a hot plate at 120 ^{o}C. The SWCNT ink was drop casted in two steps (300 µl drop volume every time) to get a thin uniform SWCNT film coated on the exposed frosted area (2.1 cm x 1.8 cm) (Step 2). The SWCNT film was cured at 120 ^{o}C for 60 minutes to remove the traces of surfactants present in the SWCNT dispersion (as per the manufacturer instructions). Copper tape was fixed on the other end of the glass substrate to make the contact pads for external electrical connections (Step 3). Gold leaf was patterned using xurography [21]. The patterned gold leaf was aligned and placed on top of the SWCNT film and copper contacts to form the contact electrodes (Step 4). Parafilm was patterned using xurography to define the electrode area and passivate the contact electrodes (Step 5). The assembled sensor was sealed by applying a slight pressure after heating at 70 ^{o}C for 20-30 s to partially melt the parafilm (Step 6).

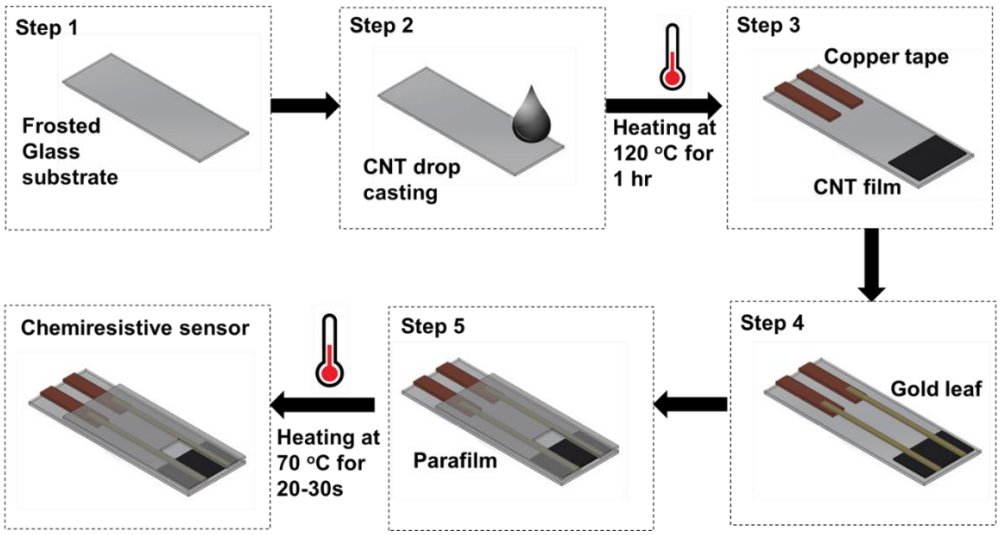

Figure 5.1 Schematics showing the overview of sensor fabrication process Step 1: cleaning the frosted glass substrate, Step 2: CNT drop casted on the heated glass substrate, Step 3: Attaching copper tape to make contact pads for external connections, Step 4: Xurographically patterned gold leaf electrodes was aligned to form the connection between CNT film and copper tape, Step 5: The electrode was passivated using a xurographically patterned parafilm with a rectangular opening (0.3 cm × 2 cm) to define the working electrode area Step 6: The electrode was sealed by applying a slight pressure after heating it at 70 °C for 20-30s.

2.3 Crystal violet functionalization and its electropolymerization

The fabricated sensors were functionalized with crystal violet by immersing the sensors in 0.6 mM crystal violet prepared in 0.1 M phosphate buffer. pH is known to influence the adsorption of crystal violet on SWCNT [22]. In acidic pH, H^+ competes with the cationic molecule for the binding sites and the adsorption saturates between pH 6 and pH 8 [22]. Therefore, phosphate buffer (pH 7) was used for sensor functionalization. The current was recorded under a small potential bias of 10 mV, and the saturation point was determined based on the current saturation (~ 90 minutes). A self

assembled layer of crystal violet was formed on top of the sensor, then this layer was electropolymerized by cycling the potential between 0 to 2 V at a scan rate of 0.1 V/s.

2.4 Sensor testing and response calculations

All sensors were tested in dip sensor format and the measurements were performed with a QUAD ISOPOD e-DAQ system. Cyclic voltammetry was performed using a Palmsens 4 potentiostat and the peak data was analyzed using PSTrace software (Ver 5.8).

The measured data was fitted to Langmuir (Equation 1) [23], Freundlich adsorption isotherm [22] (Equation 2) and first-order exponential decay (Equation 3).

$$q = K_L \times \frac{K\,C}{1+KC} \quad (1)$$

$$q = K_F \times C^{1/n} \quad (2)$$

$$q = K_e \times (1 - \exp(-kC)) \quad (3)$$

where q is the relative sensor response, K_L is the maximum theoretical adsorption on the film, K is the Langmuir constant and C is the concentration of H_2O_2 in the solution. K_F is the maximum adsorption capacity and n shows the favourability of the adsorption on the SWCNT-crystal films. K_e is the maximum amount of the H_2O_2 adsorbed and k is the equilibrium constant.

2.5 Characterization techniques

Scanning electron microscopy was used to characterize the morphology of the SWCNT film and crystal violet layer deposited on top of the film. Both SWCNT and crystal violet films were also characterized using Raman spectroscopy. A Renishaw inVia laser Raman spectrometer was used to perform the Raman spectroscopic measurements at 514 nm and 633 nm excitation wavelengths,

over a range of 500-3000 cm^{-1} and a spectral resolution of 2 cm^{-1}. A 20x objective was used in the backscattering configuration for all spectra. For Raman spectra, the samples were drop casted on a PTFE filter paper. UV-Vis spectroscopy was performed in a quartz cuvette using an Orion Aquamate 8000 UV-Vis spectrophotometer.

The surfaces of SWCNT and SWCNT-crystal violet films were analyzed using X-ray photoelectron spectroscopy. The samples were prepared on a frosted glass slide similar to the sensor fabrication process (Section 2.2). The XPS analysis was carried out on a Kratos AXIS Supra X-ray photoelectron spectrometer using a monochromatic Al K(alpha) source (15 mA, 15 kV). The work function of the instrument was calibrated for the Au 4f7/2 line to give a binding energy of 83.96 eV and the dispersion of spectrometer was adjusted using metallic copper (Cu 2p3/2) to give a binding energy of 932.62 eV. All survey scan analyses were performed on a 300 µm × 700 µm area with a pass energy of 160 eV and the high-resolution spectral analyses were done in the same area as the survey spectra with a 20 eV pass energy. All spectra were charge corrected to the main line of the carbon 1s spectrum set to 285.0 eV. The data was analyzed using CasaXPS software (version 2.3.14).

3. Results and discussion

3.1 Sensing mechanism

SWCNTs are amphoteric in nature which makes them suitable for both p- and n-doping. Reversible switching of SWCNT functionalized with oligomers from doped to undoped state have been reported previously [24]. The doping characteristics of crystal violet functionalization was investigated by exposing two sensors to 0.1 M phosphate buffer. One of the sensors was immersed in a crystal violet solution (0.6 mM crystal violet solution prepared in 0.1 M phosphate buffer) while the other sensors remained in the phosphate buffer solution after 5 minutes. When dry

unfunctionalized sensors were immersed in phosphate buffer the sensor exhibited a decrease in current due to wetting of the SWCNT films and it stabilized quickly. The decrease in current observed was due to n-doping of the SWCNT film when exposed to water. Multiple studies have shown that a mixture of semiconducting and metallic SWCNT exhibits a p-type behavior [25,26]. In presence of excess water molecules, the holes of the SWCNT film are compensated by water doping and resulted in a shifted Fermi level leading to n-doping which is shown by the decrease in current (Figure 5.2a) [27]. When the bare SWCNT sensor is functionalized with crystal violet it also showed a decrease in current, and the current started to stabilize around 60 minutes (Figure 2a). The reduction in current indicates the crystal violet molecules n-dope the SWCNT films. The adsorption of crystal violet on the SWCNT was rapid initially (within 10-15 minutes) due to the large number of vacant sites that were available on the SWCNT film. Then, the adsorption process slows down due to a reduction in the number of sites available for functionalization. Finally, the adsorption reached an equilibrium at around 60 minutes. The adsorption behavior was found to be similar to a previous study performed with MWCNT dispersion and crystal violet [22] and can be used to identify the time for process completion.

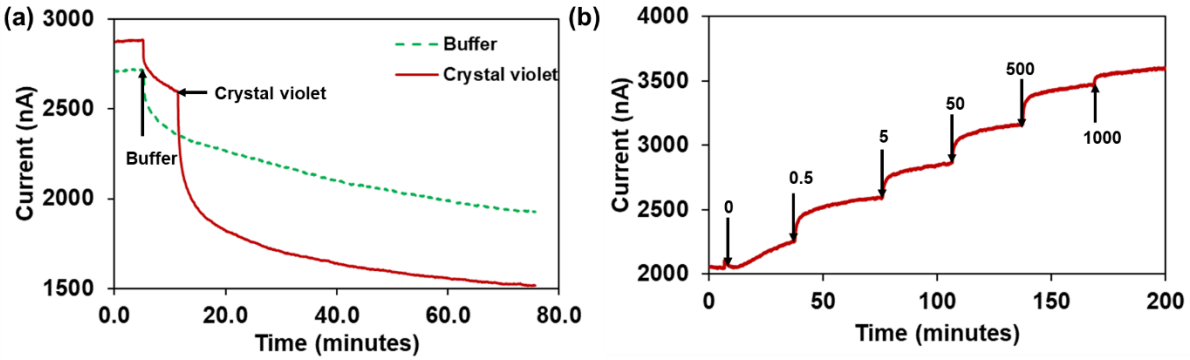

Figure 5.2 (a) Doping characteristics of SAM of crystal violet on SWCNT thin film. The current response of film in 0.1 M phosphate buffer (green, dashed line) and the current response in 0.2 mM crystal violet

prepared in 0.1 M phosphate buffer (red, solid line). (b) Sensor response for five different concentrations of H_2O_2 0.5 ppm, 5 ppm, 50 ppm, 500 ppm and 1000 ppm indicated by arrows.

The functionalized film (SWCNT-crystal violet) was exposed to acetate buffer and a sharp increase in current was observed due to wetting of the film (Figure 5.2b). Once the current stabilizes (~30 minutes), the sensor was exposed to five different concentrations of H_2O_2 (0.5 ppm, 5 ppm, 50ppm, 500 ppm and 1000 ppm) for 30 minutes in each concentration. An increase in current was observed for increase in H_2O_2 concentrations from 0.5 ppm to 1000 ppm. H_2O_2 present in solution undergoes oxidation that generates two protons, two electrons and one oxygen molecule (Figure 5.3). The generated protons and electrons reduce the crystal violet to leucocrystal violet. The reduction in amount of crystal violet in presence of dissolved H_2O_2 was confirmed using UV-Vis spectroscopy (Figure S1, Appendix 3). The UV-Vis spectrum of crystal violet showed maximum absorption peak at 590 nm. The intensity of the peak was decreased in presence of H_2O_2 and the peak intensity was reduced further with increase in H_2O_2 concentration [28]. The oxygen generated in the process p-dopes the SWCNT films resulting in the increase in the current. When SWCNT-crystal violet is exposed to H_2O_2, crystal violet gets oxidized resulting in some charge transfer from SWCNT film resulting in p-doping the SWCNT film. Hence, SWCNT functionalized with crystal violet can be used to determine H_2O_2 concentrations.

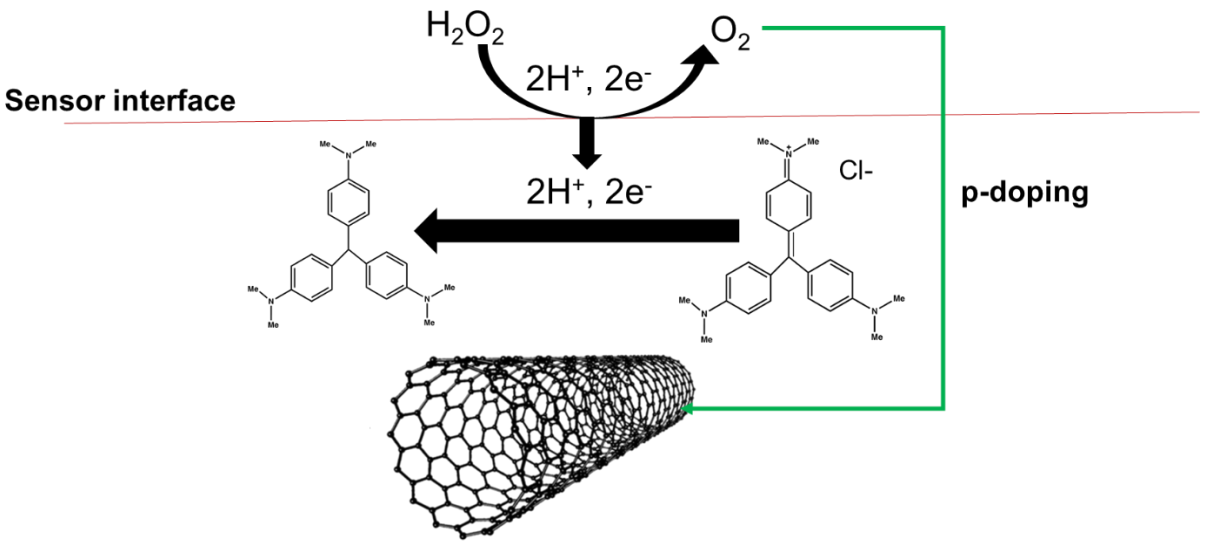

Figure 5.3 Sensing mechanism for H_2O_2 on a functionalized SWCNT-crystal violet film.

3.2 CNT functionalization

The method of functionalization of the ligand and its thickness can have a significant effect on the performance of chemiresistive sensors. In order to investigate these effects, various types of functionalization were carried out. The previously used method of formation of a self assembled monolayer (SAM) was compared with direct *in situ* electropolymerization and a hybrid process where the material was first self assembled on the SWCNT and then electropolymerized in a crystal violet free buffer solution. The first type was *in situ* electropolymerization of crystal violet from 0 to 2 V and a scan rate of 0.1 V/s (Group A) which resulted in a multimolecular thick layer of electropolymerized crystal violet on the SWCNT chemiresistors (Figure S2a, Appendix 3). The second type was performed by immersing the sensors in crystal violet solution for 90 minutes to form a thin SAM (Group B). The third type was to electropolymerize the SAM in a 0.1 M phosphate buffer solution (Group C) forming an extremely thin electropolymerized monolayer (Figure 5.4a). The effect of deposition method was assessed based on the sensitivity of the

functionalized sensors towards H_2O_2. The sensors were exposed to five concentrations of H_2O_2 (0.5 ppm, 5 ppm, 50 ppm, 500 ppm and 1000 ppm). All experiments were done in triplicates (n=3).

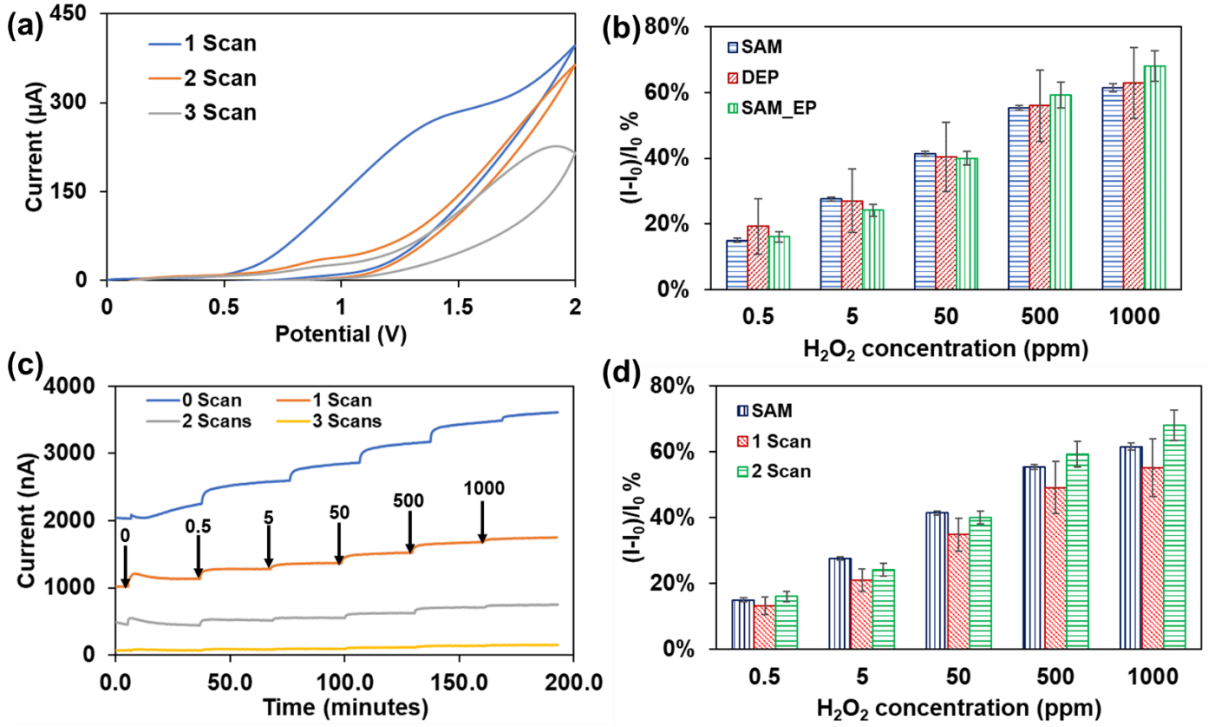

Figure 5.4 (a) Cyclic voltammetric run for a CNT electrode functionalized with self assembled layer of crystal violet with multiple scans within a potential range of 0 to 2 V and scan rate of 0.1 V/s. (b) A plot with current change for SAM (blue, horizontal stripes), direct electropolymerization in crystal violet solution (red, diagonal stripes) and SAM followed by 2 scans in crystal violet free buffer solutions (green, vertical stripes). (c) Sensor response for SAM layer of crystal violet exposed to different cyclic voltammetric scans 0 scan (blue), 1 scan (orange), 2 scans (gray) and 3 scans (yellow). All cyclic voltammetry scans were from 0 to 2V and a scan rate of 0.1 V/s. All sensors were exposed to five concentrations of H_2O_2 (0.5 ppm, 5 ppm, 50 ppm, 500 ppm and 1000 ppm) showed in the figure by arrows. (d) Sensor response for 0 scan (SAM, blue vertical stripes), SAM followed by 1 scan (red diagonal stripes) and 2 scans (green horizontal stripes) in a crystal violet free solution.

An increase in sensitivity was observed for the sensors of group B and C as compared to Group A sensors (Figure 5.4b). This can be attributed to the thinner film of crystal violet formed as a self assembled monolayer than by direct polymerization. Further, there was no statistically significant difference in sensitivity between the sensors from group B and C. However, the sensors from group C were stable over multiple chemical resets of the sensor using 0.1 M ascorbic acid solution ($n > 5$ cycles) than sensor B ($n < 3$ cycles). Therefore, the electropolymerization process can be used to stabilize the self assembled monolayer crystal violet for multi use sensors. Moreover, the *in situ* electropolymerized sensors (group A) showed the highest sensor to sensor variation in sensitivity while the sensors functionalized with a SAM showed the least variation. This can be due the ordered deposition of crystal violet monomer in case of SAM. In addition, the SAM-modified electrodes showed higher current drifts as compared electropolymerized SAMs (Figure S2b, Appendix 3). Hence, self assembled films of crystal violet are suitable for sensing applications as they introduce less sensor variability. Further, electropolymerization of these self assembled films can stabilize the sensing film for multiple use.

3.2.1 Effect of number of electropolymerization cycles

Potentiodynamic electropolymerization has been shown to result in a thinner and more stable polymerized film as compared to the potentiostatic method [29]. Therefore, self assembled crystal violet films were electropolymerized by cycling the potential within a potential range from 0 to 2 V and a scan rate of 0.1 V/s. Electropolymerization of SAM enhanced the stability of the thin crystal violet film. In order to determine the optimal conditions for electropolymerization the effect of number of electropolymerization scan cycles on sensor performance was investigated. Twelve sensors were fabricated to explore the effect of four scan cycles (0 scan, 1 scan, 2 scans, and 3 scans). The potential range and scan rate of cyclic voltammetry were the same as in Section 2.1.

The cyclic voltammogram showed a clear peak shift for first three cycles (Figure 5.4a) while the response becomes nearly flat for higher scan cycles indicating the completion of polymerization over 4 scan cycles (Figure S3, Appendix 3). During in situ electropolymerization, an irreversible oxidation peak (current 253 µA) was observed at +1.3 V for the first scan (Figure S3, Appendix 3). A peak with lower current (84.9 µA) was observed for the next scan followed by a further decrease in peak current for subsequent scan cycles. A similar oxidation peak was observed for the electropolymerized SAM for the first scan and subsequent scans. The reduction in peak current of subsequent scans could be due to a decrease in monomer concentration on the sensor surface which eventually disappears upon continued cycling (Figure S3, Appendix 3). In a previous study similar behaviour was reported for methylene blue [30].

The number of cyclic voltammetry scans can directly impact the resistance of the SWCNT film resulting in the increased resistance of the sensor film (Figure 5.4c). In addition, the sensitivity of the sensor was also affected by the number of scans. An increase in sensitivity was observed for the first two scans while it goes down with subsequent scan cycles (Figure 5.4d). The increase in sensitivity can be due to changes in the proportion of adsorbed monomers of crystal violet that has polymerized.

A decrease in sensor resistance was observed with each scan cycle which could be due to changes introduced either on the crystal violet or SWCNT film (Figure 5.4c). This was further investigated in a control experiment with non-functionalized CNT electrodes (Figure S4, Appendix 3). A similar decrease in resistance was observed for non-functionalized CNT showing that the decrease in resistance could be attributed to the change in SWCNT percolation network. Further, the sensors were characterized with XPS to investigate the presence of crystal violet on the surface after cyclic voltammetry. Four types of electrodes were prepared for the experiment. The first was non-

functionalized SWCNT (Sample 1), the second was functionalized with SAM of crystal violet (Sample 2), the third was functionalized with SAM of crystal violet followed by 4 electropolymerization scan cycles (Sample 3), and final sample was functionalized with SAM of crystal violet followed by 10 electropolymerization scan cycles (Sample 4). The survey spectra results are summarized in Table 1 and all four survey spectra are given in Appendix 3 (Figure S5-S8). An increase in nitrogen was observed in all three samples (Sample 2, 3 and 4) functionalized with crystal violet as compared to bare SWCNT films (Sample 1). This confirmed the presence of crystal violet on the sensor surface after the cyclic voltammetry scans. All samples were stored in nitrogen after preparation which might be the reason for the presence of small amount of nitrogen in sample 1 (bare SWCNT films).

Table 5.1 Summary of XPS survey spectrum. Sample 1: SWCNT film, Sample 2: SWCNT film functionalized with SAM of crystal violet, Sample 3: SWCNT film functionalized with electropolymerized (4 scan cycles) SAM of crystal violet and Sample 4: SWCNT film functionalized with electropolymerized (10 scan cycles) SAM of crystal violet.

Sample identifier	**C**	**N**	**Na**	**O**	**P**	**Si**
Sample 1	76.5	0.2	1.8	16.1		3.7
Sample 2	81.3	4.1	0.2	11.9	0.2	2.1
Sample 3	73.8	4.8	1.5	17.0	1.3	1.3
Sample 4	71.1	4.5	1.9	19.0	1.6	1.5

3.3 Dynamic sensor response in standard H_2O_2 solutions

The electropolymerized SAM sensor response was investigated with five different H_2O_2 concentrations (0.5 ppm, 5 ppm, 50 ppm, 500 ppm and 1000 ppm). The standard solutions were prepared by diluting a stock solution in 39 mM acetate buffer. The measurement was initiated in a 39 mM acetate buffer solution followed by exposure to the standard solution (from low concentration to high concentrations). Each measurement was performed over 30 minutes and then the solution was spiked with the next higher concentration. Each point in the calibration curve is the average of the last 30 seconds of the current -time response (Drift < 2 nA/minute for all H_2O_2 concentrations). All experiments were performed in triplicates (n=3).

The sensor response for unfunctionalized sensors for the five H_2O_2 concentrations 0.5 ppm, 5 ppm, 50 ppm, 500 ppm and 1000 ppm was 12%, 17%, 25%, 33% and 35%, respectively. While the sensor response for functionalized sensors for the five H_2O_2 concentrations 0.5 ppm, 5 ppm, 50 ppm, 500 ppm and 1000 ppm was 16% ± 1.6%, 24% ± 1.9%, 40 % ± 2%, 59% ± 4% and 68% ± 4.8%, respectively (Figure 5.5a). An increase in current was observed for an increase in H_2O_2 concentration for both functionalized and unfunctionalized sensors. However, the functionalized sensors exhibited a higher sensitivity compared to the unfunctionalized.

The experimental data was fitted into three mathematical models: Langmuir adsorption isotherm (Equation 1), Freundlich adsorption isotherm (Equation 2) and first-order exponential decay model (Equation 3). The calculated constant values for first-order exponential decay K_e and k were 55.75% and 0.1229 $ppm^{-1}s^{-1}$, respectively. The R^2 value for the fit was 0.8327 with a root mean squared error (RMSE) 11.91. For Langmuir isotherm, the calculated constant values K_L and K were 60.84% and 0.1 ppm^{-1}, respectively. The R^2 value for the fit was 0.8938 with a RMSE 9.49.

For Freundlich isotherm, the calculated constant values K_f and n were 18.4 and 5.29, respectively. The R^2 value for the fit was 0.999 with a RMSE 0.9156.

Based on the statistical parameters, the Freundlich model was the best fit to the experimental data, followed by Langmuir and first order exponential curve (Figure 5.5b). Langmuir adsorption assumes that a monolayer of the molecules is adsorbed on a homogenous surface with identical adsorption sites. According to the Langmuir curve, the sensor response would saturate at 60.84% while the experimental current value for 500 ppm H_2O_2 was 59% ± 4%. Therefore, the sensor should saturate beyond 500 pm of H_2O_2 concentration. The Freundlich model assumes an exponential distribution of active sites and heterogeneous adsorption surface which could be better suited to model the SWCNT-crystal violet film surface. Similar to electropolymerized SAM electrodes, the sensor response of the electrodes functionalized with SAM of crystal violet and bare CNT electrodes were best fitted with the Freundlich model. The constant n signifies the favourability index for adsorption on the surface. A n-value between 0 to 1 represents poor adsorption [22], while n>1, denotes a stronger interaction between the adsorbent and adsorbate. For our fitted data, the value of n was 5.29, which showed that the adsorption was favorable for the analyte.

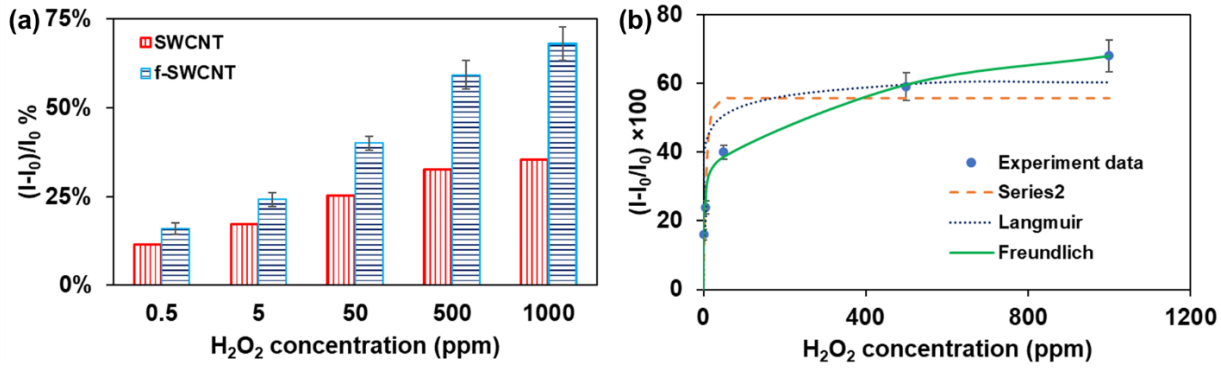

Figure 5.5 (a) Sensor response for five different concentrations of H_2O_2 0.5 ppm, 5 ppm, 50 ppm, 500 ppm and 1000 ppm. (b) The plot showing the experimental data fitted to the three mathematical model: First order exponential decay (Orange dashes), Langmuir adsorption isotherm (Blue dots) and Freundlich adsorption isotherm (Solid green line).

3.4 Effect of conductivity and pH

Peroxide measurements in biosensors are typically conducted in blood whose conductivity can vary slightly based on hematocrit between 0.6 to 0.8 S/m [31]. The conductivity of blood plasma which is devoid of cells is approximately 1.57 S/m [31]. Therefore, the effect of conductivity was tested with three solutions (0.28 S/m, 0.67 S/m and 1.21 S/m) prepared from acetate buffer with different buffer strengths of 39 mM, 100 mM and 200 mM. The conductivity of the prepared solutions was measured using ExStick II EC400. The sensor response was calculated relative to the current recorded for a reference with 0.67 S/m conductivity. The sensor response for conductivity 0.28 S/m and 1.21 S/m was 5% ± 3% and -2% ± 1%, respectively, relative to current recorded for 0.67 S/m solution (Figure 5.6a). Further, the sensor response for 50 ppm H_2O_2 was 44% ± 8% relative to pH 7.4. Hence, the variation in sensor response over the conductivity range

for blood (0.6 -0.8 S/m) was found to be insignificant (~1%) as compared to the H_2O_2 response and conductivity is not a major interferent at least in blood.

Crystal violet loses H^+ ions as the pH is increased and its pK_{a1} and pK_{a2}, are 0.91 and 2.39, respectively [32]. The normal range of arterial and venous pH for human blood lies between 7.35 to 7.45 [33]. Therefore, the effect of pH on the sensor response was investigated using a 39 mM acetate buffer and the pH was adjusted to pH 7.26, pH 7.42 and pH 7.62. The change in current was calculated with pH 7.4 as the baseline. The sensor response drifted downwards with increase in pH (Figure S9, Appendix 3). The sensor response for pH 7.26 and pH 7.62 was 2.9% and -2.7%, respectively, relative to pH 7.4 (Figure 5.6b). Moreover, the sensor response for 50 ppm H_2O_2 was 45.2% relative to the baseline (pH 7.4). Therefore, larger pH variations could have a direct impact on sensor response. However, human blood is a controlled buffered solution with pH 7.4. Hence, the sensor can be used for reliable H_2O_2 measurements.

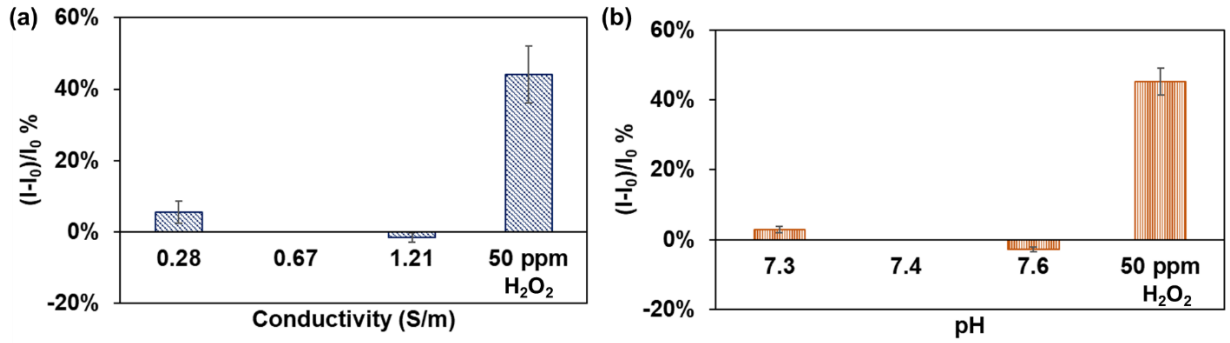

Figure 5.6 (a) Effect of conductivity on sensor response (b) Effect of pH on sensor response in 39 mM acetate adjusted to various pH using potassium hydroxide. The sensor response was calculated relative to the current at pH 7.4.

3.5 Interferences

The sensor performance was assessed in presence of common interferents present in blood plasma like glucose, uric acid, galactose and urea. Gluconic acid was included in the interference test because glucose is converted to gluconic acid and H_2O_2 in presence of glucose oxidase. Four sensors were fabricated and three were functionalized with crystal violet while the unfunctionalized SWCNT sensor was used as a control for the study (Figure S10, Appendix 3). The interference was tested in presence of 5 ppm (0.15 mM) of H_2O_2 (Figure 5.7a). The test was initiated by immersing the sensors in 39 mM acetate buffer. The buffer solution was spiked with 5 ppm H_2O_2, and the solution was subsequently spiked with the five interferents in the given order galactose (4 mg/dl), glucose (90 mg/dl), urea (22 mg/dl), uric acid (8 mg/dl) and gluconic acid (122 mg/dl). The functionalized sensors exhibited much smaller responses to the interferent than unfunctionalized ones (Figure 5.7b). The response of the functionalized sensor for galactose, glucose, urea, uric acid and gluconic acid was 2%, 1.8%, 0.4%, 3.4% and -10%, respectively, relative to the sensor response for 5 ppm H_2O_2 (Figure 5.7b, inset, green). Moreover, the response for the unfunctionalized SWCNT sensor for galactose, glucose, urea, uric acid and gluconic acid was 23.3%, 18.9%, 15.1%, 9.7% and -7.7%, respectively, to the sensor response for 5ppm H_2O_2 (Figure 5.7b, inset, red) Hence, the functionalized sensors did not exhibit any significant interference for all the compounds except gluconic acid.

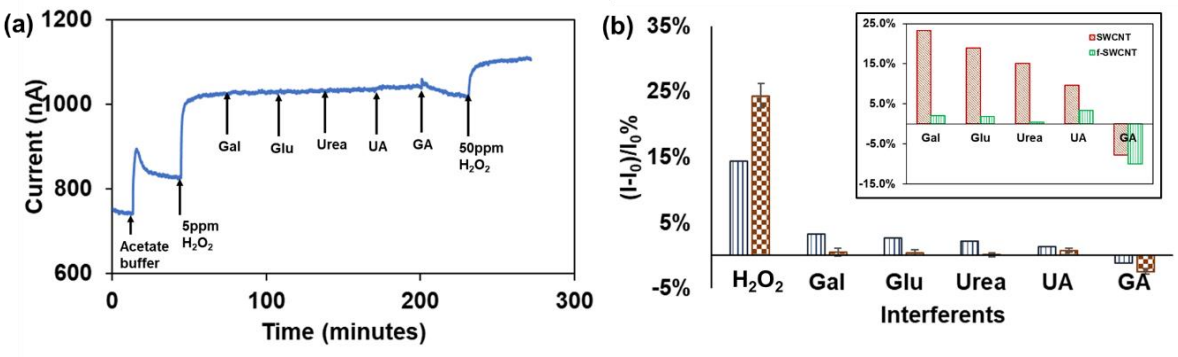

Figure 5.7 (a) Effect of interfering species on sensor response in presence of 5 ppm (0.15 mM) of H_2O_2. GA: Gluconic acid, Gal: Galactose, Glu: Glucose, and UA: Uric acid (n=3). (b) Calibration plot showing the sensor response for different interfering response for SWCNT sensor without crystal violet (blue vertical lines) and with crystal violet (Brown mosaic pattern). Inset: Sensor response to interferents relative to the sensor response for 5 ppm (0.15 mM) of H_2O_2. SWCNT sensor without crystal violet (red mosaic pattern) and with crystal violet (green vertical lines).

3.6 Application: glucose testing in human pooled plasma

The H_2O_2 sensor was converted into a biosensor by coupling it with glucose oxidase as a model enzyme for glucose detection in buffer and blood plasma. Three sensors were fabricated and functionalized with a SAM of crystal violet (Section 2.3). The sensor was then coated with 100 µl of 25 mg/ml of glucose oxidase solution prepared in 39 mM acetate buffer with pH 5.9. The sensors were dried overnight at 4 ^{o}C. The sensors were tested with four different glucose concentrations (6.2 mM, 12.5 mM, 18.7 mM, and 24.9 mM). All chemiresistive measurements were performed at a small potential bias of 10 mV for 30 minutes. A sample volume of 100 µl was used for all measurements. For standard buffered measurements, a 100 µl drop of acetate buffer (pH 5.9) mixed with 25 mg/ml of glucose oxidase was dropped on the sensor. The sample was subsequently spiked with 0.9 µl of glucose stock solution (equivalent to 6.25 mM of glucose concentration)

resulting in an increase of 6.25 mM in glucose concentration after every addition, resulting in four different glucose concentrations 6.2 mM, 12.5 mM, 18.7 mM and 24.9 mM, respectively. The sensor was exposed to each glucose concentration for 30 minutes. Each point in the calibration curve is an average of the last 30 s of a 30-minute measurement (Figure 5.8a). All experiments were done in triplicates (n=3). Similar to the H_2O_2 sensor, the sensor responses for glucose concentrations were fitted with a Freundlich isotherm; the calculated constant values K_f and n were 10.93 and 2.74, respectively. The R^2 value for the fit was 0.9908 with a RMSE 1.5627, showing a good fit of the isotherm to the experimental data.

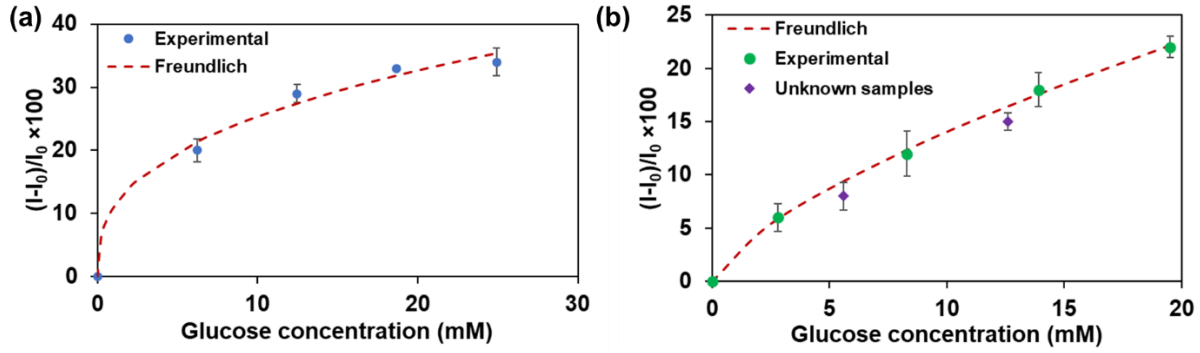

Figure 5.8 (a) Sensor response for four different glucose concentrations (6.2 mM, 12.5 mM, 18.7 mM, and 24.9 mM) in standard buffer solution. (b) Sensor response for four different glucose concentrations (2.8 mM, 8.3 mM, 13.9 mM and 19.5 mM) in human pooled plasma (green circles) and two unknown plasma samples spiked with glucose (purple diamonds).

Similar to standard buffered measurements, three SWCNT sensors were prepared and functionalized with a self assembled crystal violet film. The sensors were then coated with 100 µl of 25 mg/ml of glucose oxidase solution prepared in 39 mM acetate buffer with pH 5.9 and dried overnight at 4 ^{o}C. The sensors were tested with four different glucose concentrations (2.8 mM, 8.3 mM, 13.9 mM, and 19.5 mM). The concentration range was decreased for the plasma experiment

based on the saturation point for the standard buffer solution measurements. The measurement process and calibration curve were done following the same procedure as the standard buffer measurements (Figure 5.8b). The sensor response was fitted to a Freundlich isotherm; the calculated constant values K_f and n were 2.91 and 1.46, respectively. The R^2 value for the fit was 0.99089 with a RMSE 0.3384, showing a good fit of the isotherm to the experimental data. The calculated constant (n = 1.46) was reduced for blood plasma measurement compared to the buffer measurement (n = 2.74).

Fresh SWCNT-crystal violet sensors were prepared to investigate the glucose recovery with the glucose oxidase coated sensors (n=2). The sensor fabrication and response calculation were done same as the previous protocol. The sensor response for two spiked glucose concentrations (5.6 mM and 12.6 mM) was 8% ± 1.3 % and 15% ± 0.8 % relative to human pooled plasma, respectively. The estimated recovery for 5.6 mM and 12.6 mM was 95% and 107%, showing that the sensors could be used for reliable glucose measurement in human plasma.

4. Conclusion

A solid-state reagent-free chemiresistive H_2O_2 sensor was demonstrated for a wide range of detection from 0.5 to 1000 ppm for the first time. Both electropolymerized and non-electropolymerized SAM of crystal violet exhibited similar detection ranges for H_2O_2 and the electropolymerized sensors showed slightly higher sensitivity and lower sensor drift than the non-electropolymerized SAM. However, the electropolymerized SAM sensor was more stable for multiple chemical resets. The sensor response was fitted to Freundlich isotherm showing that the adsorption of the molecule occurred at heterogenous sites on the SWCNT-crystal violet film. No significant effect of common interfering compounds like glucose, galactose, urea, and uric acid were observed. Further, the sensor was used for *in situ* H_2O_2 generated during peroxidase assays.

Here, we have demonstrated a proof of concept with glucose oxidase in standard buffer solutions and spiked human plasma samples. The wide range of detection would enable the use of this sensor for multiple peroxide assays like glucose oxidase, galactose oxidase and cholesterol oxidase. In addition, the sensor could be used for glucose measurements in various sample matrices like blood, and urine. However, the enzyme immobilization and long-term stability of the sensors need to be investigated in future studies.

Funding

This work was supported by the Global Water Futures program and Natural Sciences and Engineering Research Council of Canada. PRS acknowledges support from the Canada Research Chairs Program.

Acknowledgment

We would like to acknowledge Paul Brookes from Nano-C, Inc. for providing the SWCNT dispersion. We would also like to acknowledge Dr Marcia Reid, Research Technician, Canadian Centre for Electron microscopy, McMaster University for helping with electron microscopy imaging, and Mohammad Shariful Islam Chowdhury, McMaster Manufacturing Research Institute, McMaster University for white light interferometry imaging.

References

(1) Patel, V.; Kruse, P.; Selvaganapathy, P. R. Solid State Sensors for Hydrogen Peroxide Detection. *Biosensors* **2020**, *11* (1), 1–32. https://doi.org/10.3390/bios11010009.

(2) Shamkhalichenar, H.; Choi, J.-W. Review—Non-Enzymatic Hydrogen Peroxide Electrochemical Sensors Based on Reduced Graphene Oxide. *J. Electrochem. Soc.* **2020**, *167* (3), 037531. https://doi.org/10.1149/1945-7111/ab644a.

(3) Rojas, D.; Della Pelle, F.; Del Carlo, M.; d'Angelo, M.; Dominguez-Benot, R.; Cimini, A.; Escarpa, A.; Compagnone, D. Electrodeposited Prussian Blue on Carbon Black Modified Disposable Electrodes for Direct Enzyme-Free H2O2 Sensing in a Parkinson's Disease in Vitro Model. *Sensors Actuators, B Chem.* **2018**, *275* (August), 402–408. https://doi.org/10.1016/j.snb.2018.08.040.

(4) Mattoussi, M.; Matoussi, F.; Raouafi, N. Non-Enzymatic Amperometric Sensor for Hydrogen Peroxide Detection Based on a Ferrocene-Containing Cross-Linked Redox-Active Polymer. *Sensors Actuators, B Chem.* **2018**, *274* (February), 412–418. https://doi.org/10.1016/j.snb.2018.07.145.

(5) Borràs-Brull, M.; Blondeau, P.; Riu, J. The Use of Conducting Polymers for Enhanced Electrochemical Determination of Hydrogen Peroxide. *Crit. Rev. Anal. Chem.* **2021**, *51* (3), 204–217. https://doi.org/10.1080/10408347.2020.1718482.

(6) Gao, Y.; Li, B.; Zhang, Z.; Zhang, X.; Deng, Z.; Huo, L.; Gao, S. CuMn2O4Spinel Nanoflakes for Amperometric Detection of Hydrogen Peroxide. *ACS Appl. Nano Mater.* **2021**, *4* (7), 6832–6843. https://doi.org/10.1021/acsanm.1c00898.

(7) Wu, N.; Wang, C.; Bunes, B. R.; Zhang, Y.; Slattum, P. M.; Yang, X.; Zang, L. Chemical Self-Doping of Organic Nanoribbons for High Conductivity and Potential Application as Chemiresistive Sensor. *ACS Appl. Mater. Interfaces* **2016**, *8* (19), 12360–12368. https://doi.org/10.1021/acsami.6b03151.

(8) Salila Vijayalal Mohan, H. K.; Hansen Varghese, R.; Wong, C. H.; Zheng, L.; Yang, J. Epigallocatechin Gallate Decorated Carbon Nanotube Chemiresistors for Ultrasensitive Glucose Detection. *Org. Electron.* **2016**, *28*, 210–216. https://doi.org/10.1016/j.orgel.2015.10.032.

(9) Aroutiounian, V.; Arakelyan, V.; Aleksanyan, M.; Shahnazaryan, G.; Kacer, P.; Picha, P.; Kovarik, J.; Pekarek, J.; Joost, B. Thin-Film SnO2 and ZnO Detectors of Hydrogen Peroxide

Vapors. *J. Sensors Sens. Syst.* **2018**, *7* (1), 281–288. https://doi.org/10.5194/jsss-7-281-2018.

(10) Song, E.; da Costa, T. H.; Choi, J. W. A Chemiresistive Glucose Sensor Fabricated by Inkjet Printing. *Microsyst. Technol.* **2017**, *23* (8), 3505–3511. https://doi.org/10.1007/s00542-016-3160-4.

(11) Song, E.; Choi, J. W. A Selective Hydrogen Peroxide Sensor Based on Chemiresistive Polyaniline Nanowires Modified with Silver Catalytic Nanoparticles. *J. Micromechanics Microengineering* **2014**, *24* (6). https://doi.org/10.1088/0960-1317/24/6/065004.

(12) Teh, K. S.; Lin, L. MEMS Sensor Material Based on Polypyrrole-Carbon Nanotube Nanocomposite: Film Deposition and Characterization. *J. Micromechanics Microengineering* **2005**, *15* (11), 2019–2027. https://doi.org/10.1088/0960-1317/15/11/005.

(13) Giaretta, J. E.; Oveissi, F.; Dehghani, F.; Naficy, S. Paper-Based, Chemiresistive Sensor for Hydrogen Peroxide Detection. *Adv. Mater. Technol.* **2021**, *6* (4), 1–8. https://doi.org/10.1002/admt.202001148.

(14) Ranjan, P.; Tiwary, P.; Chakraborty, A. K.; Mahapatra, R.; Thakur, A. D. Graphene Oxide Based Free-Standing Films for Humidity and Hydrogen Peroxide Sensing. *J. Mater. Sci. Mater. Electron.* **2018**, *29* (18), 15946–15956. https://doi.org/10.1007/s10854-018-9680-1.

(15) Soylemez, S.; Yoon, B.; Toppare, L.; Swager, T. M. Quaternized Polymer-Single-Walled Carbon Nanotube Scaffolds for a Chemiresistive Glucose Sensor. *ACS Sensors* **2017**, *2* (8), 1123–1127. https://doi.org/10.1021/acssensors.7b00323.

(16) Martin, S.; Schneider, B.; Heinemann, L.; Lodwig, V.; Kurth, H. J.; Kolb, H.; Scherbaum, W. A. Self-Monitoring of Blood Glucose in Type 2 Diabetes and Long-Term Outcome: An Epidemiological Cohort Study. *Diabetologia* **2006**, *49* (2), 271–278. https://doi.org/10.1007/s00125-005-0083-5.

(17) Mottola, H. A.; Simpson, B. E.; Gorin, G. Absorptiometric Determination of Hydrogen Peroxide in Submicrogram Amounts with Leuco Crystal Violet and Peroxidase as Catalyst. *Anal. Chem.* **1970**, *42* (3), 410–411. https://doi.org/10.1021/ac60285a017.

(18) Zhang, Y.; Zhuang, H.; Lu, H. Electrocatalytic Oxidation of Hydroquinone at Poly(Crystal-Violet) Film-Modified Electrode and Its Selective Determination in the Presence of o-Hydroquinone and m-Hydroquinone. *Anal. Lett.* **2009**, *42* (2), 339–351. https://doi.org/10.1080/00032710802507885.

(19) Sun, W.; Wang, Y.; Lu, Y.; Hu, A.; Shi, F.; Sun, Z. High Sensitive Simultaneously Electrochemical Detection of Hydroquinone and Catechol with a Poly(Crystal Violet) Functionalized Graphene Modified Carbon Ionic Liquid Electrode. *Sensors Actuators, B Chem.* **2013**, *188*, 564–570. https://doi.org/10.1016/j.snb.2013.07.032.

(20) Wang, W.; Tang, J.; Zheng, S.; Ma, X.; Zhu, J.; Li, F.; Wang, J. Electrochemical Determination of Bisphenol A at Multi-Walled Carbon Nanotubes/Poly (Crystal Violet) Modified Glassy Carbon Electrode. *Food Anal. Methods* **2017**, *10* (12), 3815–3824. https://doi.org/10.1007/s12161-017-0944-9.

(21) Mohammadzadeh, A.; Robichaud, A. E. F.; Selvaganapathy, P. R. Rapid and Inexpensive Method for Fabrication and Integration of Electrodes in Microfluidic Devices. *J. Microelectromechanical Syst.* **2019**, *28* (4), 597–605. https://doi.org/10.1109/JMEMS.2019.2914110.

(22) Sabna, V.; Thampi, S. G.; Chandrakaran, S. Adsorption of Crystal Violet onto Functionalised Multi-Walled Carbon Nanotubes: Equilibrium and Kinetic Studies. *Ecotoxicol. Environ. Saf.* **2016**, *134*, 390–397. https://doi.org/10.1016/j.ecoenv.2015.09.018.

(23) Langmuir, I. The Constitution and Fundamental Properties of Solids and Liquids. Part I Solids. *Jounal Am. Chem. Soc.* **1916**, *38* (11), 2221–2295.

(24) Hoque, E.; Chowdhury, T.; Kruse, P. Chemical in Situ Modulation of Doping Interactions between

Oligoanilines and Nanocarbon Films. *Surf. Sci.* **2018**, *676* (January), 61–70. https://doi.org/10.1016/j.susc.2018.01.003.

(25) Kong, J.; Franklin, N. R.; Zhou, C.; Chapline, M. G.; Peng, S.; Cho, K.; Dai, H. Nanotube Molecular Wires as Chemical Sensors. *Science (80-.).* **2000**, *287* (5453), 622–625. https://doi.org/10.1126/science.287.5453.622.

(26) Tans, S. J.; Verschueren, A. R. M.; Dekker, C. Room-Temperature Transistor Based on a Single Carbon Nanotube. *Nature* **1988**, *393*, 49–51.

(27) Zahab, A.; Spina, L.; Poncharal, P.; Marlière, C. Water-Vapor Effect on the Electrical Conductivity of a Single-Walled Carbon Nanotube Mat. *Phys. Rev. B - Condens. Matter Mater. Phys.* **2000**, *62* (15), 10000–10003. https://doi.org/10.1103/PhysRevB.62.10000.

(28) Miyamoto, S.; Sano, S.; Takahashi, K.; Jikihara, T. Method for Colorimetric Detection of Double-Stranded Nucleic Acid Using Leuco Triphenylmethane Dyes. *Anal. Biochem.* **2015**, *473*, 28–33. https://doi.org/10.1016/j.ab.2014.12.016.

(29) Ghica, M. E.; Wintersteller, Y.; Brett, C. M. A. Poly(Brilliant Green)/Carbon Nanotube-Modified Carbon Film Electrodes and Application as Sensors. *J. Solid State Electrochem.* **2013**, *17* (6), 1571–1580. https://doi.org/10.1007/s10008-013-2040-4.

(30) Dağci, K.; Alanyalioğlu, M. Surface-Confined Electropolymerization of Methylene Blue on Gold Electrodes. *Electroanalysis* **2011**, *23* (3), 777–783. https://doi.org/10.1002/elan.201000622.

(31) Visser, K. R. Electric Conductivity of Stationary and Flowing Human Blood at Low Frequencies. *Annu. Int. Conf. IEEE Eng. Med. Biol. - Proc.* **1989**, *11* pt *5*, 1540–1542. https://doi.org/10.1109/iembs.1989.96329.

(32) Zhang, L. S.; Wong, G. T. F. Spectrophotometric Determination of H2O2 in Marine Waters with Leuco Crystal Violet. *Talanta* **1994**, *41* (12), 2137–2145. https://doi.org/10.1016/0039-

9140(94)00199-5.

(33) Kelly, A. M.; McAlpine, R.; Kyle, E. Venous PH Can Safely Replace Arterial PH in the Initial Evaluation of Patients in the Emergency Department. *Emerg. Med. J.* **2001**, *18* (5), 340–342. https://doi.org/10.1136/emj.18.5.340.

Chapter 6

Reagent-free phosphate chemiresistive sensor using carbon nanotube functionalized with cobalt phthalocyanines

1. Introduction

Phosphate is crucial for the growth of living beings including plants and humans. So, phosphorus is used extensively in crop fields to increase yield. Excess phosphorus from these crop fields ends up in the water bodies via water run offs [1,2]. Excessive phosphorus levels in the water bodies are responsible for rising incidences of algal bloom across the globe. Therefore, phosphorus is a strictly regulated parameter, and the wastewater treatment plants are required to monitor it regularly. Phosphate is measured using colorimetric systems with high accuracy and precision, but the method has narrow measuring range and need chemicals to operate resulting in generation of toxic waste [3]. Electrochemical sensors which are widely researched for phosphate monitoring due to their rapid response time, and simple fabrication process [4], but they need stable reference electrodes for reliable measurement. Miniaturized reference electrodes are known to drift over time which affects the electrochemical measurements [5]. Therefore, there is a need for solid state sensor for phosphate measurement which can work similar to electrochemical sensors without the need of reference electrode.

Chemiresistive sensors are surface sensitive sensing platform which measures the analyte concentration by change in resistance detected in the presence of analyte [6]. These sensors consist of a sensing film and two contact electrodes which records the change in resistance of the sensing film in presence of analyte. These sensors do not require a reference electrode for measurements. In past, these sensors have been used for gas sensing [7] and lately they have been used for sensing molecules like glucose, hydrogen peroxide and pH in liquid media [6].

Phthalocyanines are conjugated molecules which are thermally and chemically stable. These synthetic porphyrin analogues are known for the low-cost and biocompatibility resulting their use in multiple electrochemical sensors [8]. Thin films of phthalocyanine can be deposited by electrodeposition, self assembled monolayer, and spin coating [8]. Phthalocyanines have been used to detect phosphates using electrochemical sensors [9–15]. Cobalt phthalocyanine has been demonstrated as sensitive to dihydrogen phosphate within a working pH range of 4-7 in ion selective membranes [9,10]. Recently, substituted copper phthalocyanine was also used for phosphate detection in voltammetric [13–15] , impedimetric [12] and capacitive sensors [11]. However, all these sensors require reference electrodes for reliable measurements which poses a serious issue for sensor miniaturization. Phthalocyanines are used to manufacture hybrid materials with carbon nanomaterials like graphene and carbon nanotube using the π-π interaction [16]. These molecules are known to interact with the carbon nanomaterials using their 18-π electron system

Here, we report for the first time a proof of concept for a reagent-free solid state chemiresistive sensors for phosphate sensing in surface water samples. The sensor was fabricated using carbon nanotube as the sensing film and gold leaf as the contact electrodes. The sensor was functionalized with a self assembled monolayer of unsubstituted cobalt phthalocyanine as the active ligand for phosphate detection. The sensor exhibited a measuring range of 10^{-4} M to 10^{-2} M KH_2PO_4 in standard buffer solutions (20 mM bicarbonate buffer, pH 7.2).

2. Materials and methods

2.1 Materials

Copper phthalocyanine (#252980), cobalt phthalocyanine (#307696), poly (sodium 4-styrenesulphonate) (#243051), tetrabutylammonium tetrafluoroborate (#217964), dimethyl sulphoxide and sodium bicarbonate were purchased from Sigma-Aldrich and used without

modifications. Gold leaf was purchased from L.A. gold leaf wholesaler, USA and SWCNT ink dispersion was supplied by Nano-C, US (#CINK-200-P010100). Precleaned double sided frosted glass slides ((# 22-034-486) were purchased from Fisher Scientific, US.

The solution conductivity was measured using ExStick II EC400 and the pH was measured using a potentiometric pH probe Oakton pH 150.

2.2 Sensor fabrication and functionalization

The CNT sensors were fabricated using a previous protocol developed by our group [17]. The gold leaf patterning was done using a bench top craft cutter (Cricut, Provo Craft & Novelty Inc.) using a previous protocol [17]. The sensor fabrication process can be divided into four steps (Figure 6.1). The frosted glass substrate was cleaned using acetone followed by methanol to remove any organic contamination from the glass substrate (Step 1). The Nano-C ink was diluted using a 1:1 methanol and water mixture. The diluted Nano-C ink dispersion (4% v/v) was drop casted (300 µl every time) on the frosted glass substrate where the ink was contained within the frosted area using a parafilm-PET rectangular mask. The SWCNT film was cured for 60 minutes (Step 2). The copper tape was used as the external electrical connection. The patterned gold leaf was aligned and placed on top of the copper contacts and SWCNT film to form contact electrodes (Step 3). A xurographically patterned parafilm was used to passivate the contact electrode and to define the electrode area. The sensor was sealed by applying pressure after heating the parafilm at 70 ^{o}C for 20-30 s (Step 4).

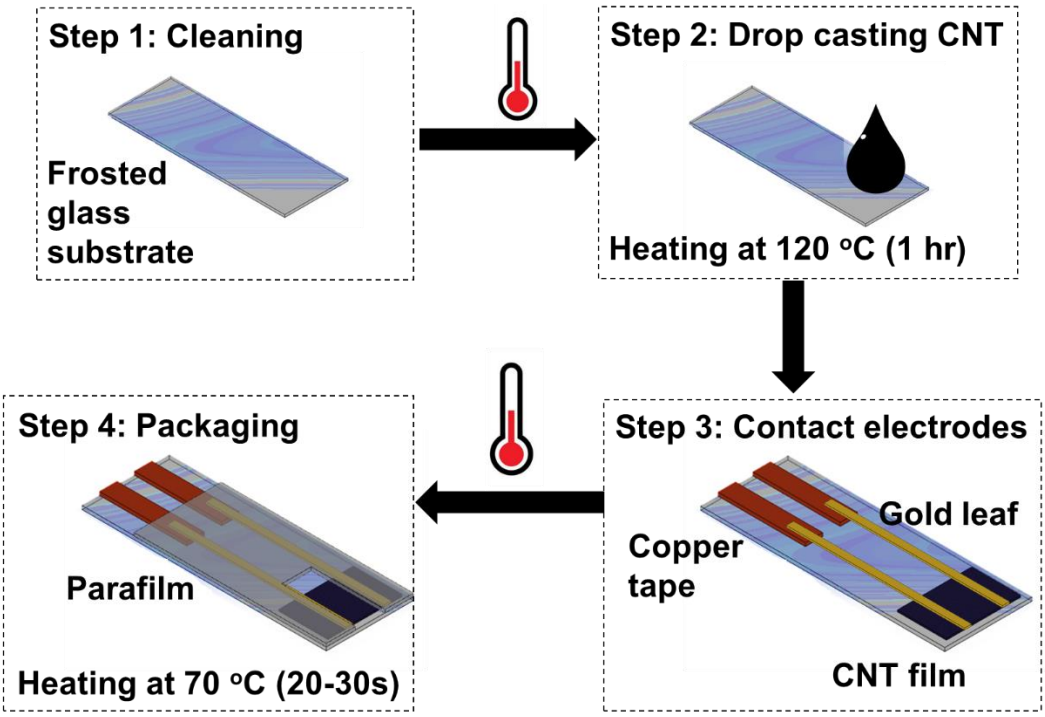

Figure 6.1 Overview of sensor fabrication process. Step 1: Cleaning the frosted glass substrate using solvents. Step 2: Drop casted CNT dispersion and heating the substrate for 60 minutes. Step 3: Contact electrode fabrication using copper tape and patterned gold leaf. Step 4: Sensor was packaged using a xurographically patterned parafilm.

Phthalocyanine are known to be insoluble or sparingly soluble in water and common organic solvents like methanol, ethanol and isopropanol [18]. The fabricated sensors were functionalized with cobalt phthalocyanines prepared in DMSO. The sensors were immersed in 2 mM phthalocyanine solution to form a self assembled monolayer until the current reaches a stable value (~3 hours). The sensors were rinsed with DMSO and dried overnight to remove the solvent. The sensors were heated at 50 ^{o}C for 60 minutes to remove any residual DMSO left after overnight drying at room temperature.

2.3 Electrochemical measurements and sensor characterization

All electrochemical measurements were performed using QUAD ISOPOD e-DAQ system in dip format. The measurements were performed in 20 mM bicarbonate buffer (pH 7.2, conductivity 1.75 mS/cm) to simulate the conductivity of fresh water (0.3 to 0.8 mS/cm) and natural water (0.5 to 3 mS/cm) [19]. The measured data was fitted into two adsorption isotherms, Langmuir [20] (Equation 1) and Freundlich [21] (Equation 2).

$$q = K_L \times \frac{K\,C}{1+KC} \quad (1)$$

$$q = K_F \times C^{1/n} \quad (2)$$

Where q is the relative sensor response at equilibrium, K is the Langmuir constant, K_L is the maximum theoretical adsorption on the film and C is the KH_2PO_4 concentration. n shows the extent of favorable adsorption on the electrode surface and K_F is the maximum adsorption capacity.

3. Results and discussion

3.1 Sensing functionalization

SWCNT film can undergo p-doping or n-doping depending on the dopants. The doping characteristics of the solvent (DMSO) and the active molecule (Cobalt phthalocyanine) was investigated. Two sensors were prepared with resistance values 4.13 ± 0.03 kΩ. The sensors were left in air for the first 5 minutes in air and then exposed to DMSO for 20 minutes. One sensor was switched to 1 mM solution of cobalt phthalocyanine prepared in DMSO while the other as left in DMSO (Figure 6.2, blue line). Both the sensors exhibited a decrease in current on exposure to DMSO which is due to n-doping of the SWCNT film with the solvent molecules. A further decrease was observed for the sensor exposed to cobalt phthalocyanine solution that can be attributed to the n-doping of the SWCNT film with phthalocyanine molecules.

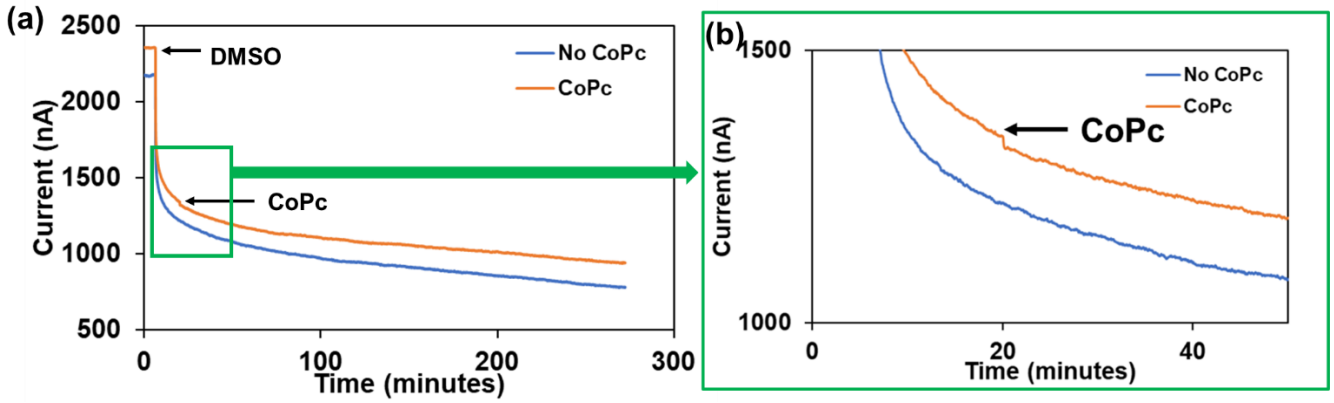

Figure 6.2 (a) Doping characteristics of the phthalocyanine and the DMSO molecules on SWCNT film. (b) Zoomed in image showing the decrease in current with introduction of cobalt phthalocyanine (Orange line).

3.2 Dynamic sensor response in standard phosphate solution

Dynamic sensor response was investigated to determine the measuring range of the sensor in standard phosphate solutions. Three sensors with resistance 4.34 ± 0.05 kΩ were fabricated to demonstrate the dynamic sensor response for different KH_2PO_4 concentrations. Four KH_2PO_4 stock solutions (1 mM, 10 mM, 100 mM and 1 M) were prepared to achieve the different KH_2PO_4 concentrations. The chemiresistive sensors were exposed to 20 mM bicarbonate buffer indicated as 1 (Figure 6.3a). The sensor was exposed to KH_2PO_4 concentrations (~200 minutes). The bicarbonate buffer solution was spiked with 100 µl of 1 mM KH_2PO_4 to attain a 1 µM KH_2PO_4 indicated as 2 (Figure 6.3a). Subsequently, the sensor was exposed to other four concentrations of KH_2PO_4 indicated as 3-6 after every 60 minutes. The calibration curve was plotted by averaging the current from the last 30 datapoints (30 s data) of the current response for each concentration (Figure 6.3b). The change in the current for each phosphate concentrations was measured with respect to current recorded for the 20 mM bicarbonate buffer (baseline current). The sensor response for 0.001 mM, 0.01mM, 0.1 mM, 1mM, 10mM KH_2PO_4 concentrations was 1% ± 0.5%, 2% ± 0.2%, 2% ± 0.3%, 4% ± 0.3%, and 7% ± 0.3%, respectively. The sensor provided a stable

response for a measuring range from 10^{-4} M to 10^{-2} M KH_2PO_4 concentrations. An increase in current response was observed for increase in phosphate concentrations. Further experiments are required to be performed to elucidate the sensing mechanism.

The sensor response data was fitted to Langmuir and Freundlich adsorption model for three KH_2PO_4 concentrations (0.1 mM, 1mM and 10 mM). The calculated Langmuir parameters K_L and K for the sensor response were 7.15% and 1.76 mM^{-1}, respectively with a R^2 and Root Mean Squared Error (RMSE) values of 0.9027 and 1.11, respectively. The calculated parameters for Freundlich adsorption model were K_F and n were 3.86 and 3.84 with a R^2 and RMSE values of 0.9973 and 0.1862, respectively. So, Freundlich isotherm showed a better fit than the Langmuir isotherm which can be due to the heterogeneous adsorption of the KH_2PO_4 molecules on the sensor surface. In addition, the n >1 also indicates strong affinity between KH_2PO_4 molecules and sensor surface [22].

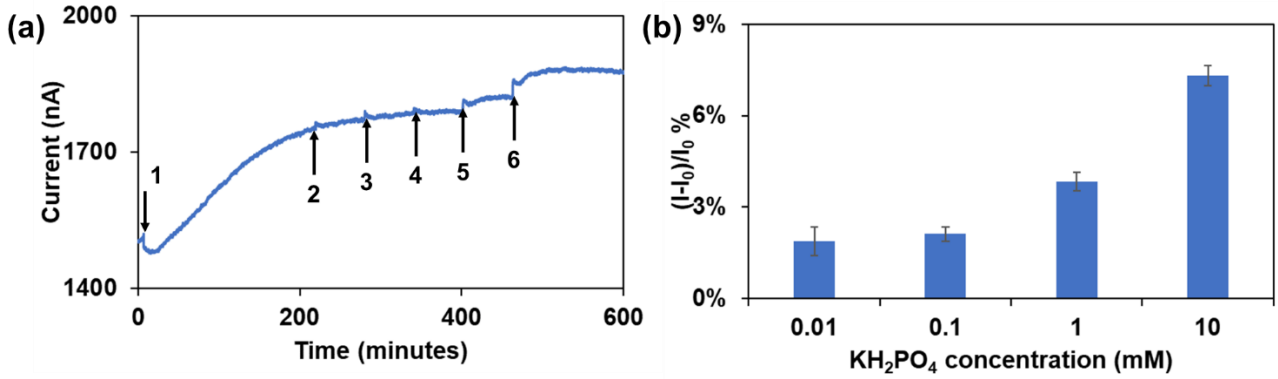

Figure 6.3 (a) Dynamic sensor response for SWCNT film functionalized with cobalt phthalocyanines. The numbers in the plot represent different solutions the sensor was exposed to during the experiment: (1) 20 mM bicarbonate buffer. The bicarbonate buffer was spiked with five different KH_2PO_4 concentrations indicated as 2 to 5 (0.001 mM, 0.01 mM, 0.1 mM, 1 mM and 10 mM, from low to high concentration). (b) Sensor response for four different KH_2PO_4 concentrations (n=3).

3.3 Effect of pH and conductivity

Conductivity and pH can affect the response of chemiresistive sensors. Here, we have investigated the effect of conductivity and pH change on bare SWCNT (Figure 6.4a) and functionalized SWCNT sensor (Figure 6.4b). The conductivity of natural waters lies between 0.5 to 3mS/cm [19]. Therefore, the effect of conductivity was tested with 20 mM bicarbonate buffer (conductivity 1.76 mS/cm, pH 7.2) and 50 mM bicarbonate buffer (conductivity 3.98 mS/cm, pH 7.2). The sensor was immersed in 20 mM bicarbonate for ~200 minutes. Then, the solution was switched to 50 mM bicarbonate buffer for 60 minutes. After 60 minutes, the solution was switched to a 20 mM bicarbonate buffer with pH 8. The sensor response for pH and conductivity changes was calculated with reference to sensor response for 20 mM bicarbonate buffer (pH 7.2). The bare SWCNT and functionalized SWCNT sensor exhibited -1.2% (Figure 6.4a, inset) and 0.2% (Figure 6.4b, inset) change with reference to 20mM bicarbonate buffer (pH 7.2), when the solution was changed from 20 mM bicarbonate buffer (1.76 mS/cm) to 50 mM bicarbonate buffer (conductivity 3.98 mS/cm). The functionalized sensors showed an insignificant change (0.2% current change) compared to bare SWCNT sensor (-1.2% current change). The change in current response due to conductivity can be attributed to the change in electrochemical double layer thickness. An increase in conductance can result in a more compact double layer leading to electrostatic gating effect [23]. The effect of electrostatic gating effect can lead to p-doping and n-doping depending on the substrate which can explain the current change directions for the bare and functionalized SWCNT.

The effect of pH was studied by changing the pH of 20 mM bicarbonate buffer from pH 7.2 to pH 8. The bare and functionalized SWCNT sensor showed -3.6% (Figure 6.4a, inset) and -1.6% (Figure 6.4b, inset) current change with reference to the 20 mM bicarbonate buffer at pH 7.2. A higher current change was observed for the bare sensor compared to the functionalized sensor.

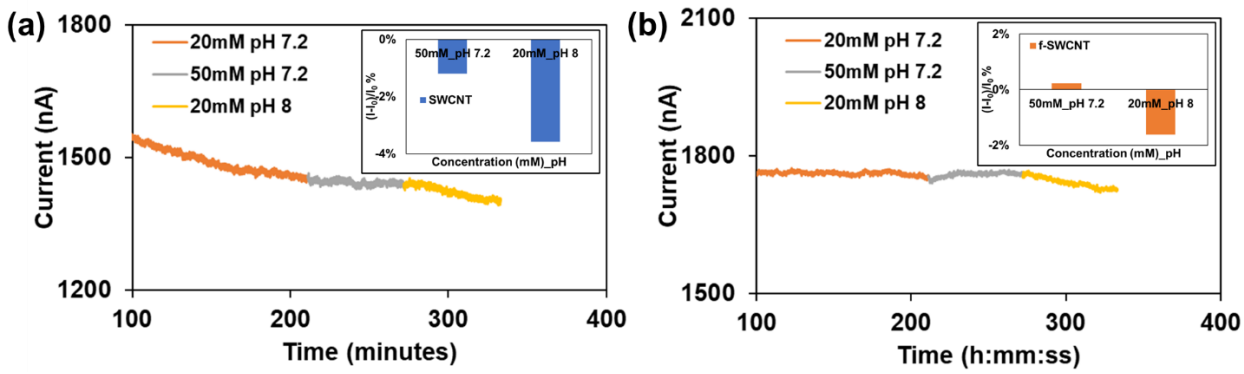

Figure 6.4 Effect of pH and conductivity on the sensor response. (a) bare SWCNT sensor. Inset plot shows the change in sensor response with reference to 20mM bicarbonate buffer (pH 7.2). (b) SWCNT sensor functionalized with cobalt phthalocyanine. Inset plot shows the change in sensor response with reference to 20 mM bicarbonate buffer (pH 7.2).

Hence, the bare SWCNT sensor showed higher sensitivity to pH and conductivity changes as compared to functionalized SWCNT sensors. However, experiments with more conductivity and pH range are required to performed to establish the working pH and conductivity range for the sensor.

3.4 Effect of interferents

The effect of interfering anions on sensor response was investigated by exposing to common anions like nitrates, sulphates and chlorides present in surface water samples. The interference was tested in presence of 10 mM phosphate solution prepared in 20 mM bicarbonate. The sensors were immersed in 20 mM bicarbonate, and it was allowed to achieve a stable current (~150 minutes). The solution was spiked with 10^{-2} M KH_2PO_4 solution (~60 minutes) and then the solution was subsequently spiked with three interfering anions in the given order sodium chloride (500 ppm), sodium nitrate (50 ppm) and sodium sulphate (500 ppm), respectively after every 60 minutes

(Figure 6.5a). The interfering anions concentrations were chosen based on the drinking water concentration of chlorides (<250 mg/l) [24], nitrates (0-18 mg/l) [25], and sulphates (200 mg/l) [26].

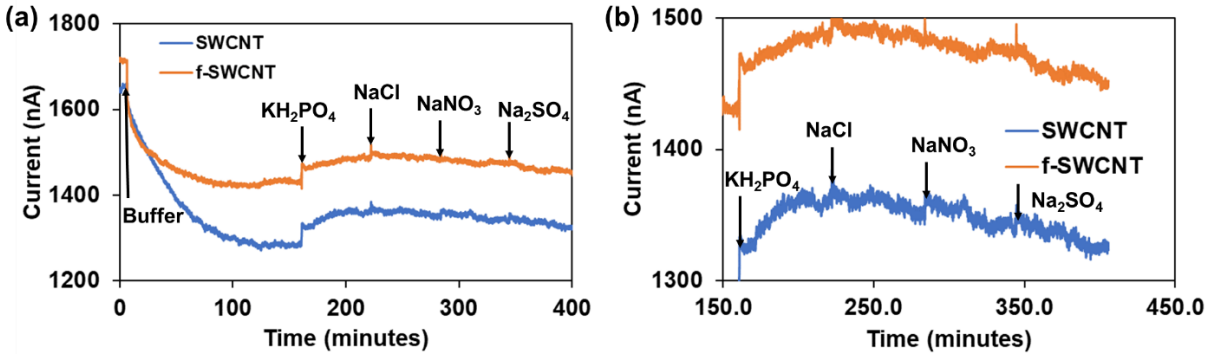

Figure 6.5 (a) Effect of interfering anions on the sensor response on bare (Blue line) and functionalized (Orange line) SWCNT sensor. 1: 20 mM bicarbonate buffer, 2: 10^{-2} M KH_2PO_4, 3: 500 ppm NaCl, 4: 50 ppm $NaNO_3$, and 5: 500 ppm Na_2SO_4. (b) Zoomed in plot (a) from 150 minutes to show the effect of interfering anions.

The sensor responses for bare and functionalized SWCNT sensor were 6.3% and 3.7%, respectively (Figure 6.5a). The bare sensor showed a negative response (response changed from 6.3% to 5.1%) for chloride while functionalized SWCNT did not showed ant significant change (response change from 3.7% to 3.6%). Based on the preliminary data, both bare and functionalized SWCNT sensor exhibited a negative response for nitrates and sulphates which can be due to the exposed SWCNT present on the functionalized sensor (Figure 6.5b). However, further investigation is needed to establish the working concentration of the interfering anions for the sensor.

4. Conclusion

A proof of concept for a solid state regent-free chemiresistive sensor was demonstrated for phosphate detection within 10^{-4} M to 10^{-2} M. The functionalized SWCNT sensor did not showed a significant change when exposed the pH and conductivity changes used in the study. Further, testing needs to be performed to establish the working pH and conductivity range for the sensor. The functionalized sensor was not affected by chloride concentration, but a negative response was observed for nitrates and sulphate. Therefore, sensor need further modifications to improve the selectivity of the sensor.

References

[1] P.J.A. Withers, P.M. Haygarth, Agriculture, phosphorus and eutrophication: A European perspective, Soil Use Manag. 23 (2007) 1–4. https://doi.org/10.1111/j.1475-2743.2007.00116.x.

[2] D.M. Anderson, P.M. Glibert, J.M. Burkholder, Harmful Algal Blooms and Eutophication: Nutrient Sources, composition and consequences, Estuaries. 25 (2002) 704–726.

[3] X. Zhu, J. Ma, Recent advances in the determination of phosphate in environmental water samples: Insights from practical perspectives, TrAC - Trends Anal. Chem. 127 (2020) 115908. https://doi.org/10.1016/j.trac.2020.115908.

[4] C. Forano, H. Farhat, C. Mousty, Recent trends in electrochemical detection of phosphate in actual waters, Curr. Opin. Electrochem. 11 (2018) 55–61. https://doi.org/10.1016/j.coelec.2018.07.008.

[5] E. Zdrachek, E. Bakker, Potentiometric Sensing, Anal. Chem. 93 (2021) 72–102.

https://doi.org/10.1021/acs.analchem.0c04249.

[6] V. Patel, P. Kruse, P.R. Selvaganapathy, Solid State Sensors for Hydrogen Peroxide Detection, Biosensors. 11 (2020) 1–32. https://doi.org/10.3390/bios11010009.

[7] R. Tang, Y. Shi, Z. Hou, L. Wei, Carbon nanotube-based chemiresistive sensors, Sensors (Switzerland). 17 (2017). https://doi.org/10.3390/s17040882.

[8] E. Demir, H. Silah, B. Uslu, Phthalocyanine Modified Electrodes in Electrochemical Analysis, Crit. Rev. Anal. Chem. 0 (2020) 1–37. https://doi.org/10.1080/10408347.2020.1806702.

[9] J. Liu, Y. Masuda, E. Sekido, Phosphate ion sensitive coated wire field effect transistor electrodes based on cobalt phthalocyanine with poly vinyl chloride as membrane matrix, 224 (1989) 145–151.

[10] J. Liu, Y. Masuda, E. Sekido, Response properties of an ion-selective polymeric membrane phosphate electrode prepared with cobalt phthalocyanine and characterization of the electrode process, J. Electroanal. Chem. 291 (1990) 67–79. https://doi.org/10.1016/0022-0728(90)87178-M.

[11] L. Barhoumi, A. Baraket, N.M. Nooredeen, M. Ben Ali, M.N. Abbas, J. Bausells, A. Errachid, Silicon Nitride Capacitive Chemical Sensor for Phosphate Ion Detection Based on Copper Phthalocyanine – Acrylate-polymer, Electroanalysis. 29 (2017) 1586–1595. https://doi.org/10.1002/elan.201700005.

[12] F. Zina, N.M. Nooredeen, S. Azzouzi, M. Ben Ali, M.N. Abbas, A. Errachid, Novel Sensitive Impedimetric Microsensor for Phosphate Detection Based on a Novel Copper

Phthalocyanine Derivative, Anal. Lett. 51 (2018) 371–386. https://doi.org/10.1080/00032719.2017.1322096.

[13] Z. Fredj, M. Ben Ali, M.N. Abbas, E. Dempsey, Determination of prostate cancer biomarker acid phosphatase at a copper phthalocyanine-modified screen printed gold transducer, Anal. Chim. Acta. 1057 (2019) 98–105. https://doi.org/10.1016/j.aca.2018.12.058.

[14] M. Talbi, A. Al-Hamry, M. Ben Ali, O. Kanoun, Carbon Screen Printed Electrodes Functionalized with Cu(II)Pc for Phosphate Detection, Proc. 17th Int. Multi-Conference Syst. Signals Devices, SSD 2020. (2020) 869–872. https://doi.org/10.1109/SSD49366.2020.9364241.

[15] B. Ali, T. McCormac, C. Maccato, D. Barreca, G. Carraro, Multilayer assemblies of a Cu-phthalocyanine with Dawson type polyoxometalates (POMs) for the electrocatalytic reduction of phosphate, J. Electroanal. Chem. 858 (2020) 113770. https://doi.org/10.1016/j.jelechem.2019.113770.

[16] T. V. Basova, A.K. Ray, Review—Hybrid Materials Based on Phthalocyanines and Metal Nanoparticles for Chemiresistive and Electrochemical Sensors: A Mini-Review, ECS J. Solid State Sci. Technol. 9 (2020) 061001. https://doi.org/10.1149/2162-8777/ab9fe8.

[17] V. Patel, P. Kruse, P.R. Selvaganapathy, A xurography based rapid prototyping method to fabricate and low-cost high quality metal thin film micropatterns using metal leaves, Mater. Today Commun. 30 (2022) 103132. https://doi.org/10.1016/j.mtcomm.2022.103132.

[18] F. Ghani, J. Kristen, H. Riegler, Solubility properties of unsubstituted Metal

Phthalocyanines in different types of solvents, J. Chem. Eng. Data. 57 (2012) 439–449.

[19] A.F. Rusydi, Correlation between conductivity and total dissolved solid in various type of water: A review, IOP Conf. Ser. Earth Environ. Sci. 118 (2018). https://doi.org/10.1088/1755-1315/118/1/012019.

[20] I. Langmuir, The constitution and fundamental properties of solids and liquids. Part I Solids, Jounal Am. Chem. Soc. 38 (1916) 2221–2295.

[21] H. Freundlish, Over the adsorption in solution, J. Phys. Chem. 57 (1906) 385–470.

[22] V. Sabna, S.G. Thampi, S. Chandrakaran, Adsorption of crystal violet onto functionalised multi-walled carbon nanotubes: Equilibrium and kinetic studies, Ecotoxicol. Environ. Saf. 134 (2016) 390–397. https://doi.org/10.1016/j.ecoenv.2015.09.018.

[23] I. Heller, S. Chatoor, J. Männik, M.A.G. Zevenbergen, C. Dekker, S.G. Lemay, Influence of electrolyte composition on liquid-gated carbon nanotube and graphene transistors, J. Am. Chem. Soc. 132 (2010) 17149–17156. https://doi.org/10.1021/ja104850n.

[24] WHO. SDE. WSH, Chloride in Drinking-water Background document for development, Guidel. Drink. Qual. - World Heal. Organ. 2 (2003) 9. http://www.who.int/water_sanitation_health/dwq/chloride.pdf.

[25] World Health Organization, Nitrate and nitrite in drinking water, WHO Guidel. Drink. Qual. 37 (2011) 227–231. https://doi.org/10.1159/000225441.

[26] WHO, Sulfate in Drinking-water Background document for development of WHO Guidelines for Drinking-water Quality. Available at http://www.who.int/water_sanitation_health/dwq/chemicals/sulfate.pdf (December 2015),

(2004).

Chapter 7

Conclusions and future direction

1. Contributions to knowledge

This thesis work was inspired by the current problems associated with phosphate monitoring for environmental and medical diagnostics. Here, solid-state phosphate sensor technologies were developed to enable in-field monitoring without the need of toxic chemicals. This was achieved by using two sensor technologies: potentiometric and chemiresistive sensors.

An *in situ* electrical pretreatment method was developed to pretreat the cobalt electrode in the phosphate solution itself. The pretreatment method eliminates the need for chemical pretreatment before measurement that reduces the time required the to perform the phosphate measurement. In addition, the pretreatment also enhances the sensitivity of the electrode to -91.4 mV/decade within a measuring range of 10^{-6} M to 10^{-3} M phosphate concentration. The method was also implemented for phosphate sensing in spiked samples of tap water, lake water and creek water samples which showed the pretreatment method works well in real water samples.

A rapid prototyping method was developed to pattern low-cost high quality thin metal films for applications including electrochemical sensing, chemiresistive sensors and high surface electrodes. The patterning method was to pattern features with both line width and pitch <100 µm and reliable conductive line features with < 250 µm. The resolution achieved using the pattern are sufficient for applications in the sensor manufacturing and biomedical devices. The method uses a simple bench top plotter cutter which enables it to be used in low resource settings. The method reduces the cost of electrode manufacturing to one-fifth compared to sputter coated gold electrodes.

The developed rapid patterning method was used fabricate thin metal contact electrodes for chemiresistive sensors. These thin film metal electrodes enabled us to fabricate low noise chemiresistors for H_2O_2 sensing. The chemiresistive sensors were fabricated with SWCNTs as the sensing substrate. The SWCNT sensor was functionalized with a self assembled layer of crystal violet to impart better selectivity to the sensor compared to bare SWCNTs. The thin self assembled film was electropolymerized to improve the stability of the sensor for multiple chemical resets. The H_2O_2 sensor showed a wide measuring range from 0.5 ppm to 1000 ppm which is suitable for multiple peroxidase assays for medical diagnostics such as glucose detection in blood, urine, and saliva, galactose in food products, and lactose in blood. The functionalized sensor showed good selectivity against common interferents like uric acid, urea, and glucose. The functionalized sensor was deposited with glucose oxidase to demonstrate the use of peroxidase assays and it was used to measure glucose in standard buffered solutions and human pooled plasma within a measuring range of 2 mM to 20 mM. The sensor also exhibited a good recovery (95% to 107%) for glucose measurements in human pooled plasma samples.

Finally, the knowledge gained from both the chemiresistive sensing and cobalt based potentiometric sensor was used to fabricate a reagent-free chemiresistive sensor for measuring phosphate. Cobalt/cobalt oxide is known to be selective to phosphate ions. SWCNT can be functionalized with π-π interactions with conjugated organic molecules. Phthalocyanine molecules were used to functionalize the SWCNT film for phosphate detection. This format was used to measure phosphate without the need of reference electrodes, and/ or enzymes. The measurements were performed using a small potential bias of 10 mV. The sensor showed a measuring range of 10^{-4} M to 10^{-2} M phosphate concentration.

2. Future directions

This thesis has developed two sensor technologies to realize *in-field* phosphate measurement without the use any chemicals. These technologies were used in different sample matrixes like tap water, lake water, creek water and human pooled plasma samples. However, extensive tests are required to validate these sensors for *in-field* measurements.

2.1 Electrical pretreatment method

Here, the electrical pretreatment method was demonstrated to enhance the sensitivity of the cobalt electrode for phosphate measurement. Numerous metal electrodes like Iridium, molybdenum and tungsten have been used to measure analytes like pH and phosphates. Similar to cobalt, the sensitivity of these electrodes is limited by Nernstian limit. So, the pretreatment method can be implemented with other metal electrodes to enhance their sensitivity.

Sensor are fabricated in all sizes varying from few centimeters to few micrometers or even smaller. The method can be implemented in multiple form factors to further investigate the versatility of the pretreatment method.

Finally, the sensors are needed to be tested in different environmental condition and sample matrixes. Although, the method was tested with real water samples like tap water, and surface water samples. However, the effect of other environmental parameters like temperature, organic molecules still need to be studied in detail. Further, the method can also be implemented with sensor performing measurements in medical diagnostics samples.

2.2 Solid-state chemiresistive sensors

In this thesis, chemiresistive sensors demonstrated the ability to measure H_2O_2 over a wide range and their application in peroxidase assays. The sensor was demonstrated in blood plasma. However, the sensor should be tested in other human fluids like urine, tear, and sweat.

This study used a single step enzyme to demonstrate the ability of sensor in peroxidase assays. However, multiple analytes require more than one enzyme to generate small detectable molecules like H_2O_2. So, the sensor sould be tested with multiple enzymes because a multiple enzyme cascade can pose problems like interferences from the intermediate compounds, and stability of the enzyme in presence of these intermediates.

2.3 Electropolymerized self assembled monolayer

In this thesis, the electropolymerization of self assembled monolayer was done in organic molecules free solution to manufacture thin and high stable films on the chemiresistive sensors. The self assembled monolayer was electropolymerized using potentiodynamically in the current study. However, electropolymerization can done using other method like potentiostatic and galvanostatic. So, a comparative study to elucidate the differences between the electropolymerized self assembled films is required to further study the effect of electropolymerization on sensing parameters. This would also help researchers to use this process where a stable thin film is required for applications.

Appendix 1

Supporting information for:

Enhancing the sensitivity of cobalt based phosphate sensor using current pretreatment

Vinay Patel [1], and P. Ravi Selvaganapathy [1,2*]

[1] School of Biomedical Engineering, McMaster University, Hamilton, ON, L8S 4K1, Canada

[2] Department of Mechanical Engineering, McMaster University, Hamilton, ON, L8S 4K1, Canada

(*) Corresponding author selvaga@mcmaster.ca

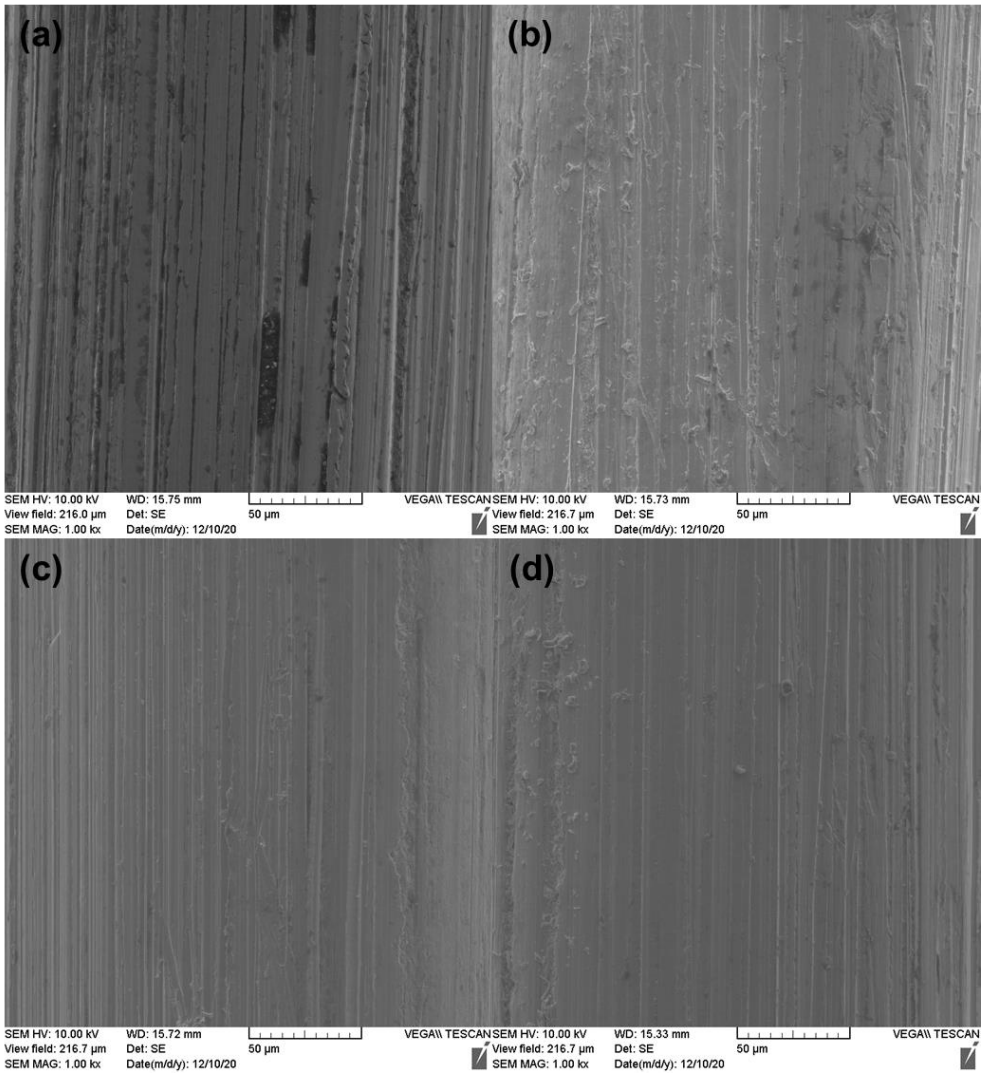

Figure S1 SEM images at 1000x with 50 µm scale bar (a) Cobalt wire polished with Silicon Carbide ultra fine 600, (b) Cobalt wire used for measurement phase in a 10 mM KH_2PO_4, (c) Cobalt wire pretreated with the negative current in a 10 mM KH_2PO_4 and (d) Cobalt wire pretreated with the negative current followed by the measurement phase in a 10 mM KH_2PO_4.

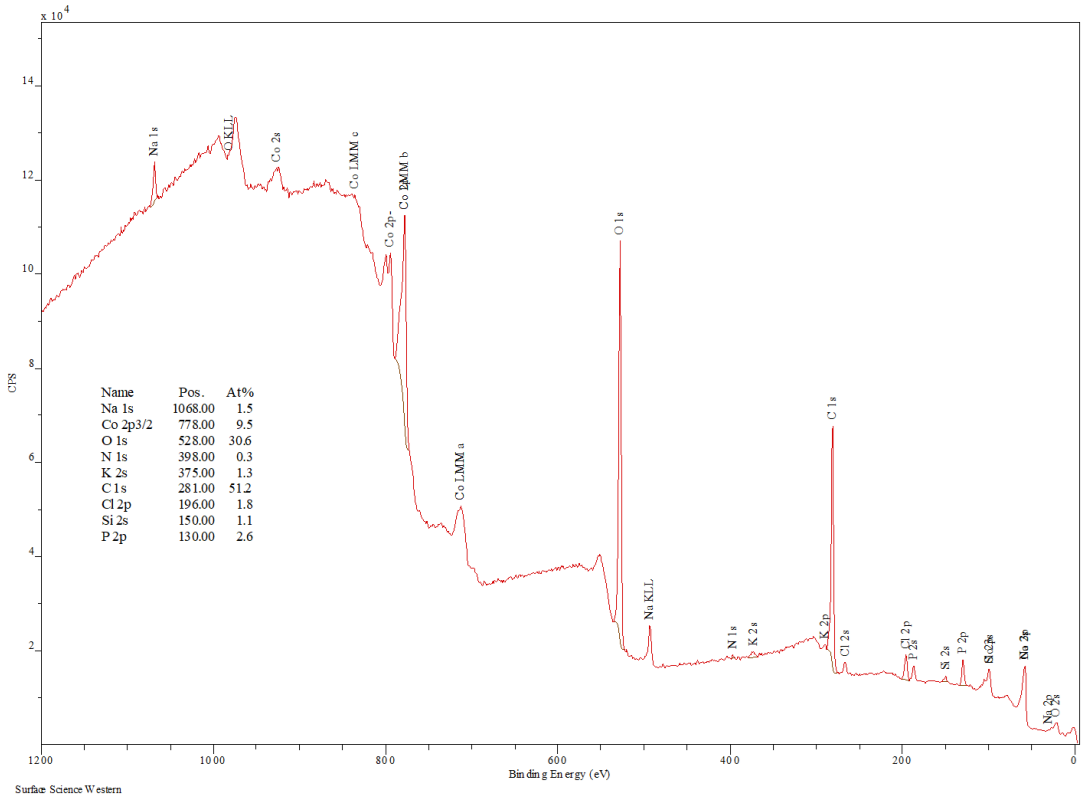

Figure S2 XPS survey spectrum for untreated cobalt electrode (Sample 1) after potentiometric measurments in 10^{-2} M KH_2PO_4 with 20mM NaCl as background electrolyte. The electrodes were stored in nitrogen just after the experiment to avoid air exposure.

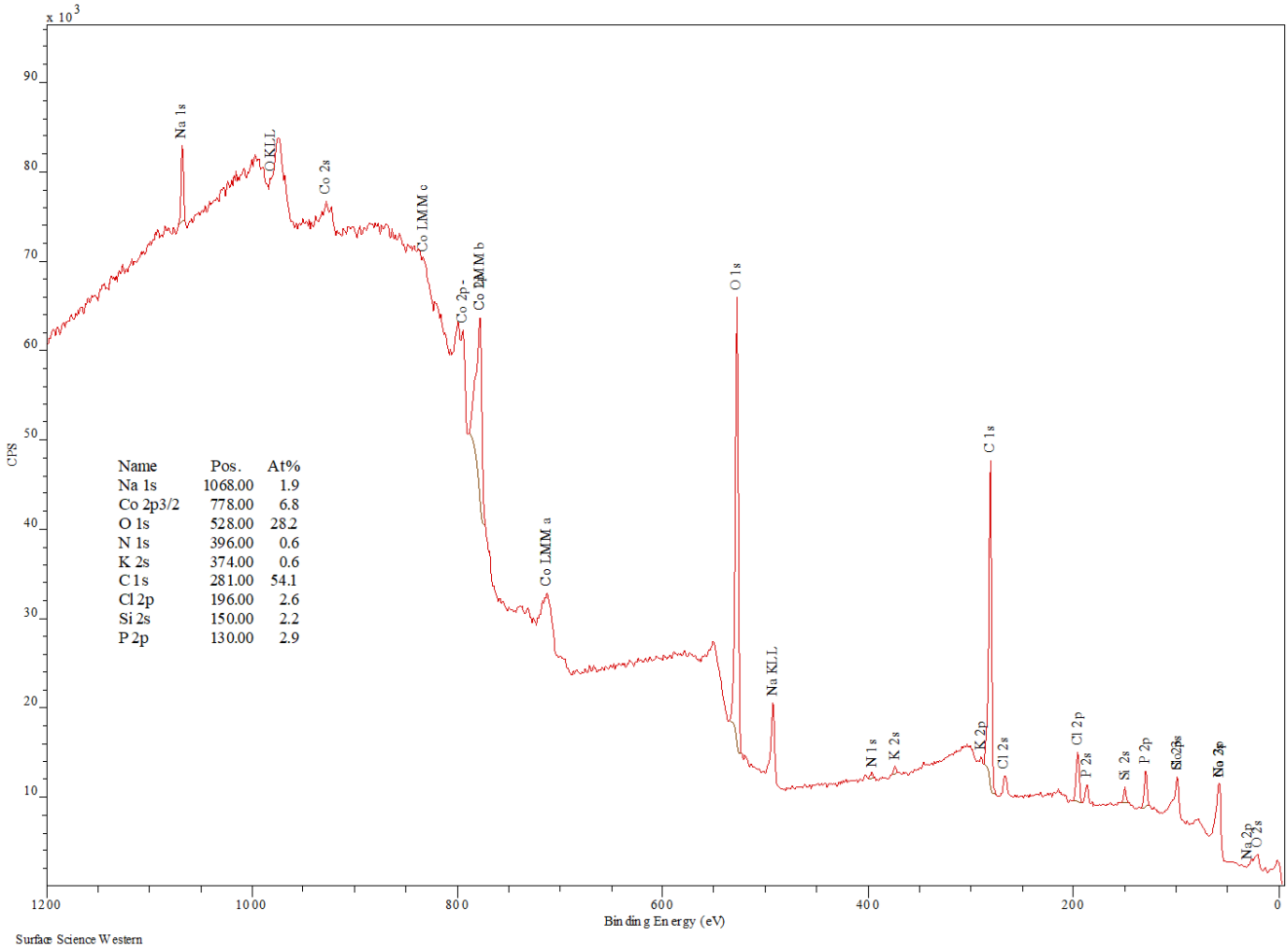

Figure S3 XPS survey spectrum for cobalt electrode after the electrical pretreatment (Sample 2) in 10^{-2} M KH_2PO_4 with 20mM NaCl as background electrolyte. The electrodes were stored in nitrogen just after the experiment to avoid air exposure.

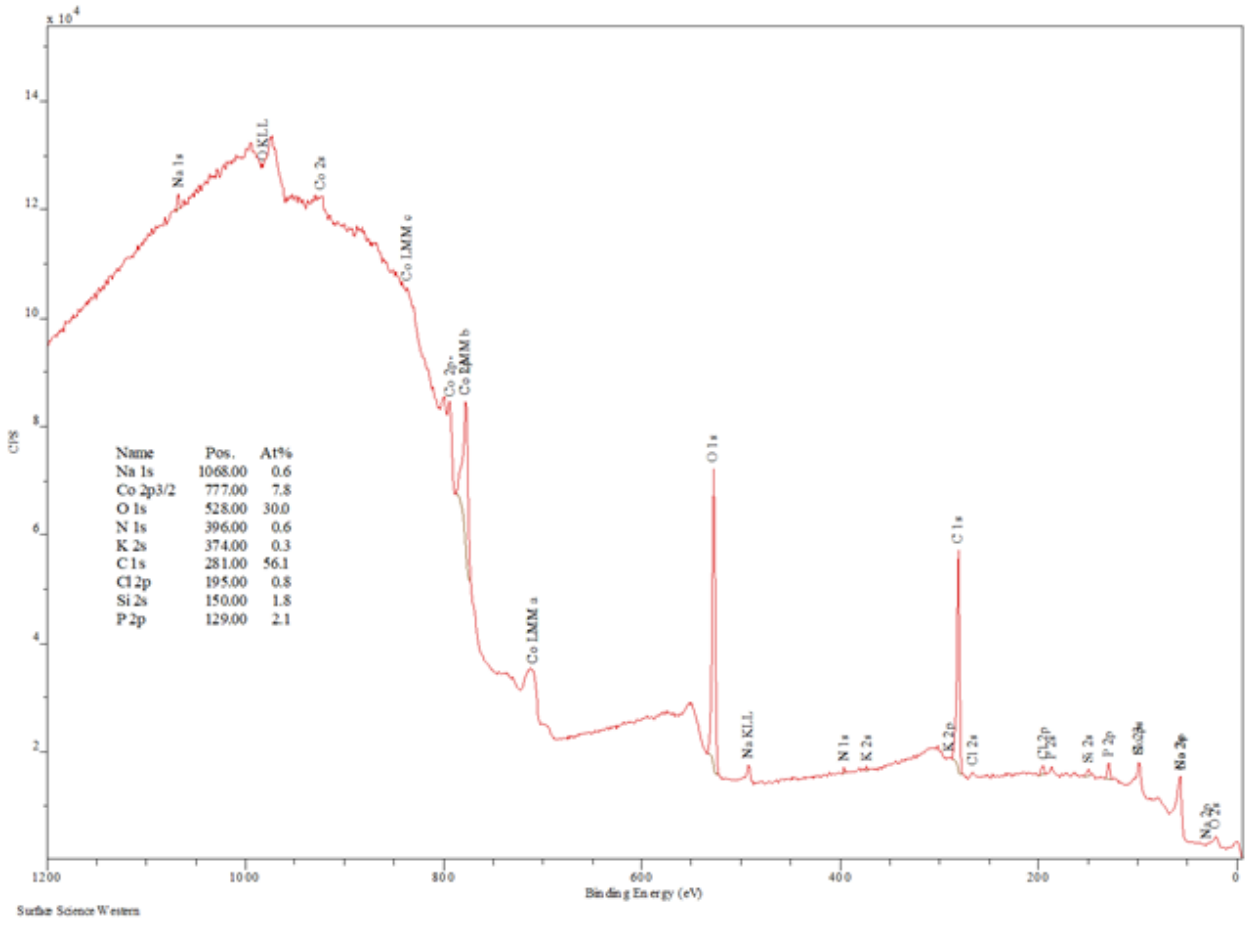

Figure S4 XPS survey spectrum for cobalt electrode after the electrical pretreatment followed by potentiometric measurement (Sample 3) in 10^{-2} M KH_2PO_4 with 20mM NaCl as background electrolyte. The electrodes were stored in nitrogen just after the experiment to avoid air exposure.

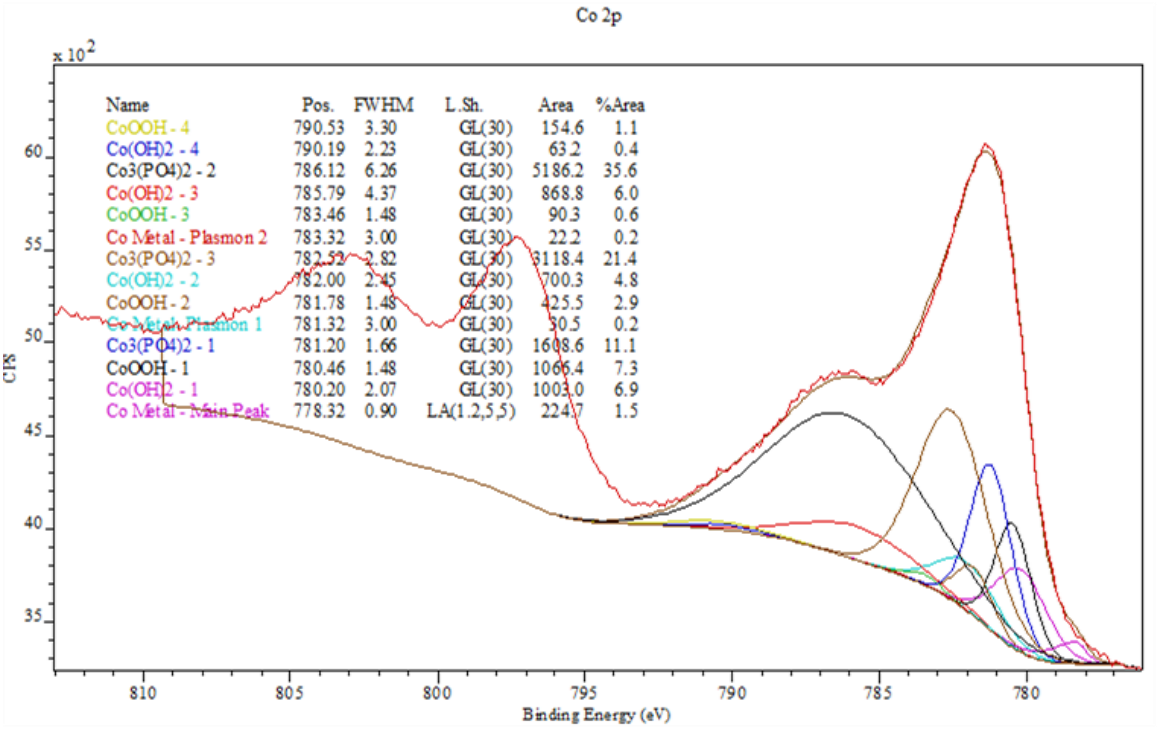

Figure S5 XPS High resolution spectra of cobalt (Co 2p) for untreated sensor (Sample 1).

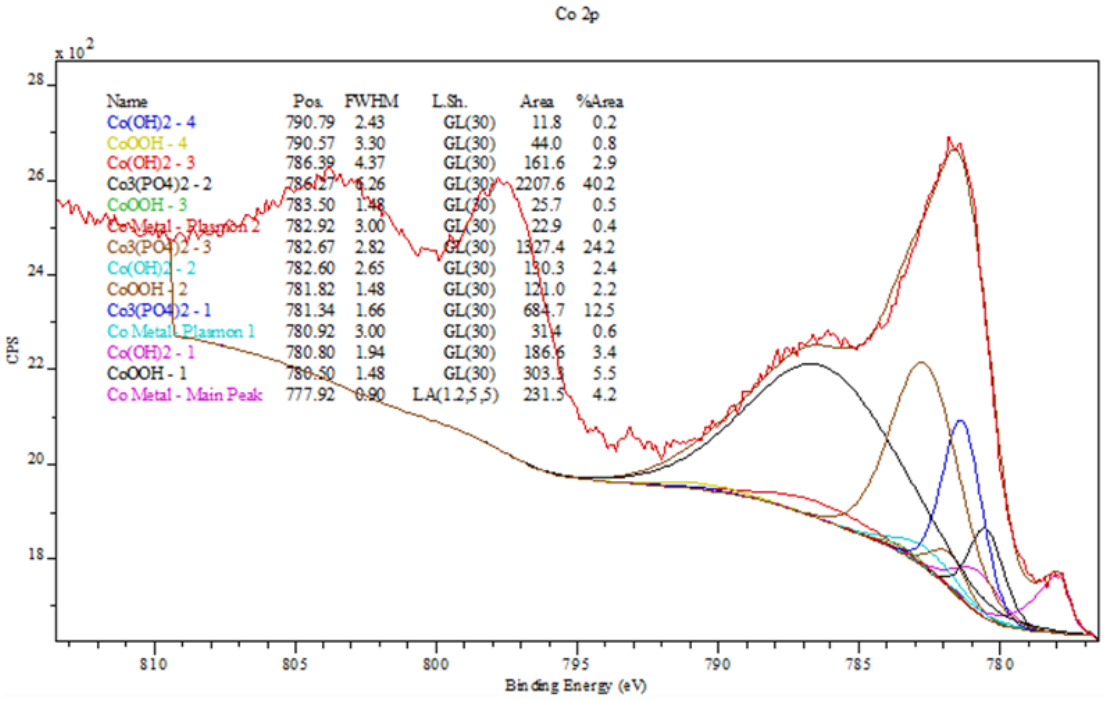

Figure S6 XPS high resolution spectra of cobalt (Co 2p) sensor after electrical pretreatment (Sample 2).

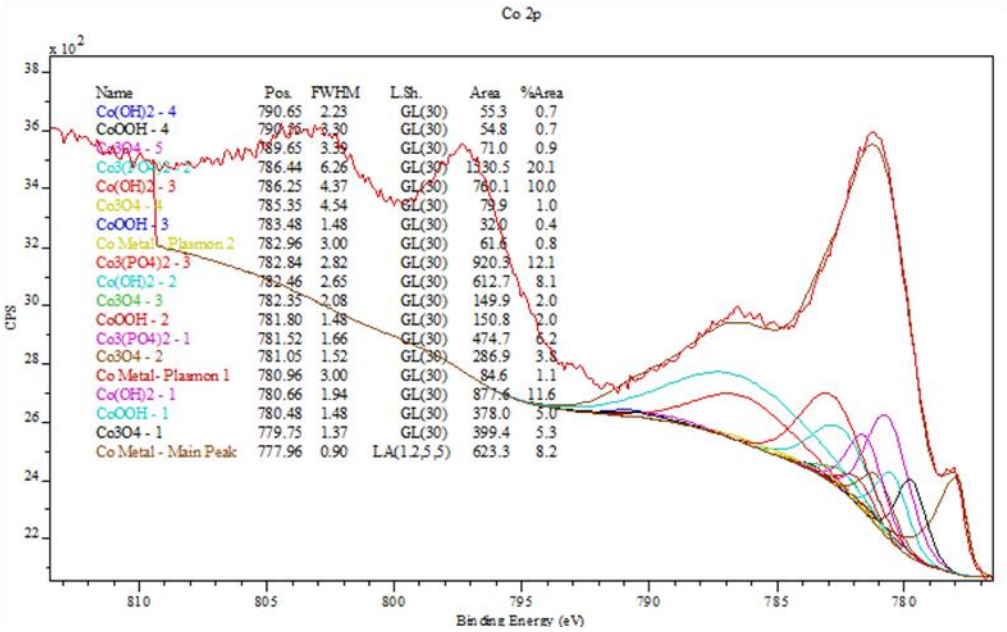

Figure S7 XPS high resolution spectra of cobalt (Co 2p) sensor after the electrical pretreatment followed by potentiometric measurement (Sample 3).

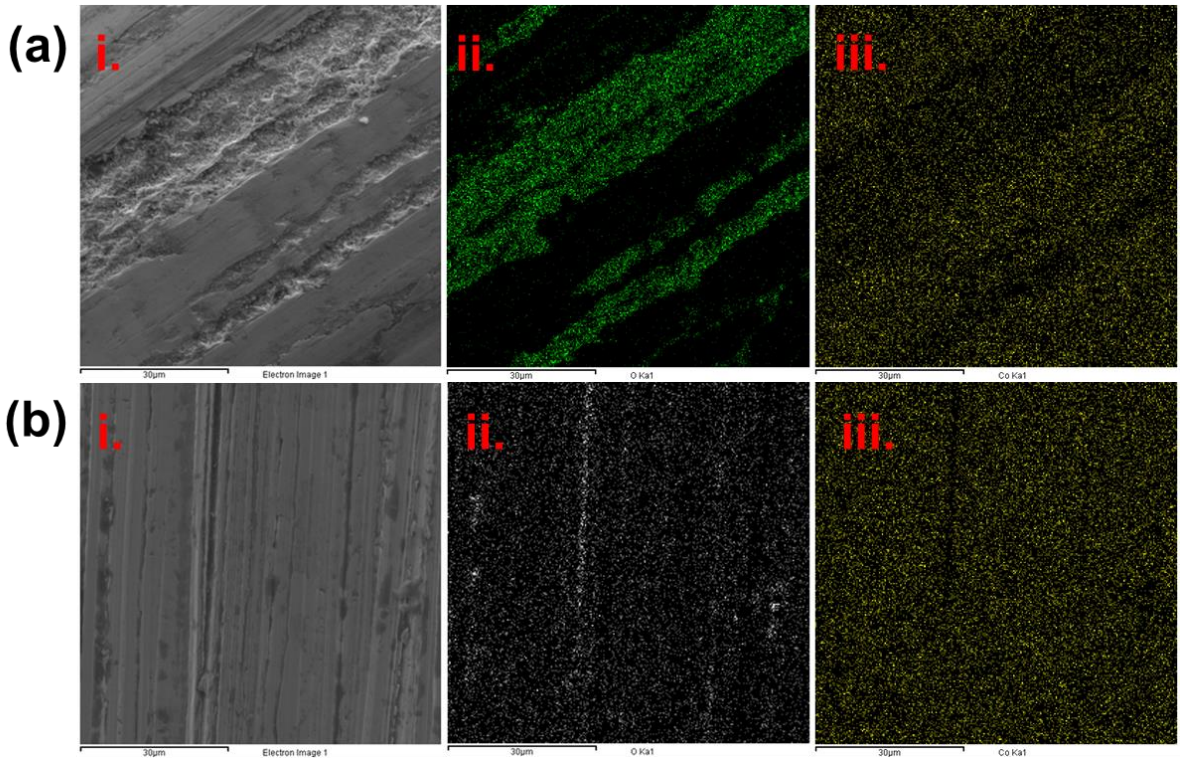

Figure S8 SEM-EDX mapping images i. SEM image of the wire ii. Oxygen map of the wire marked with green iii. Cobalt map of the wire marked in yellow (a) Unpolished cobalt wire (b) Polished cobalt wire

Protocol for testing phosphate with Orion Aquamate 8000, UV-Vis spectrophotometer using the Phosphomolybdic acid/ascorbic acid method

The measuring range of the protocol used was 0.05-4 mg/l PO_4. Therefore, the samples with phosphate values higher than the upper limit were diluted using DI water. The reagent vial was filled with the 10 ml of the sample and the blank was measured. Phosphate no. 1 tablet was added and crushed followed by phosphate no. 2 tablet. Once, both the tablets were dissolved. The sample was incubated for 10 minutes, and measurement was performed.

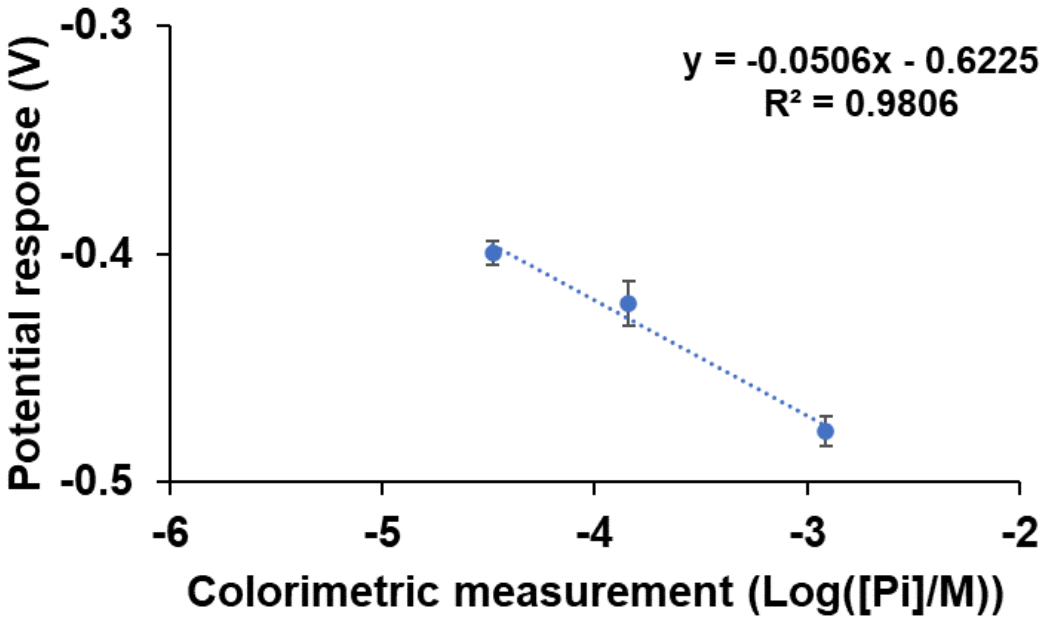

Figure S9 Zero current potentiometric response of the sensor in tap water. The samples were spiked with KH_2PO_4 to generate two different phosphate concentrations (0.01, 0.1 and 1 mM). Each data point in the plot represents average of three sensor data (n=3) and error bar represents the standard deviation of the data.

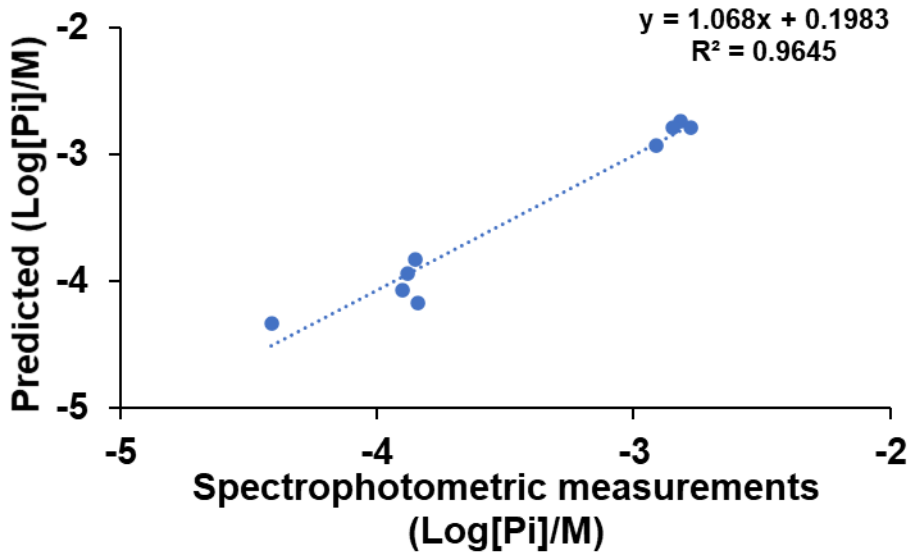

Figure S10 Correlation between the phosphate concentrations predicted from the sensor response (y-axis) and spectrophotometric measurements (x-axis).

Appendix 2

Supporting information for:

A xurography based rapid prototyping method to fabricate and low-cost high quality metal thin film micropatterns using metal leaves.

Vinay Patel [1], Peter Kruse [2], and P. Ravi Selvaganapathy [1,3*]

[1] School of Biomedical Engineering, McMaster University, Hamilton, ON, L8S 4K1, Canada

[2] Department of Chemistry and Chemical Biology, McMaster University, Hamilton, ON, L8S 4M1, Canada

[3] Department of Mechanical Engineering, McMaster University, Hamilton, ON, L8S 4K1, Canada

*selvaga@mcmaster.ca

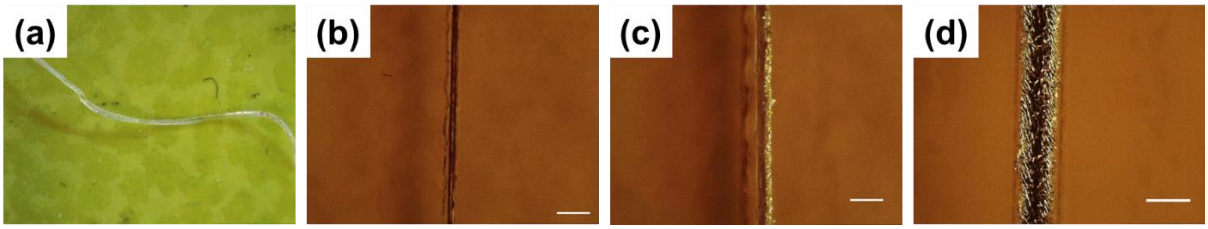

Figure S1 (a) Optical image of silver metal leaf linear pattern with design LW of 0.1 mm showing curling and non-uniform cutting. (b) Optical image of gold metal leaf linear pattern with square anchors on both ends with design LW of 0.1 mm showing the failure of the cutting process (Scale bar 200 µm). (c) Design LW of 0.2 mm (Scale bar 200 µm). (d) Design LW of 0.3 mm (Scale bar 200 µm).

Table T2 Summary of design and achieved LW (n=30) for the gold leaf patterned using xurography.

Designed LW (mm)	**Achieved LW (mm)**
0.1	0.035±0.004
0.2	0.080±0.005
0.3	0.228±0.026
0.4	0.349±0.015
0.5	0.429±0.032
0.75	0.602±0.031
1	0.886±0.078
1.25	1.146±0.039

Table T2 Summary of design and achieved pitch for the gold leaf patterned using xurography (n≥12).

Design pitch (mm)	**Achieved pitch (mm)**
0.1	0.092±0.002
0.2	0.143±0.02
0.3	0.236±0.02
0.5	0.45±0.03
0.75	0.75±0.03
1	1.07±0.02
1.25	1.24±0.04

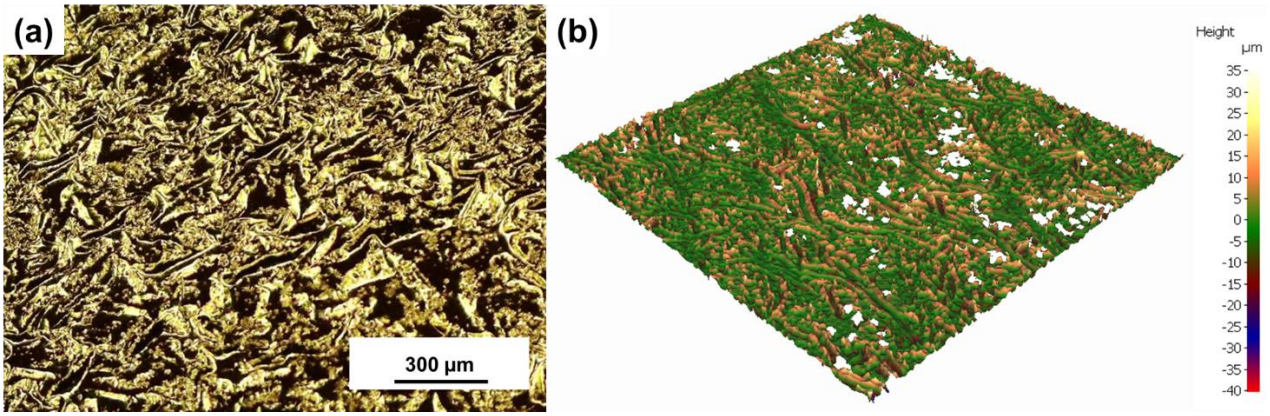

Figure S2 (a) Optical images of gold leaf on a paper backing as received from the supplier. (b) Optical images of gold leaf captured using white light interferometry.

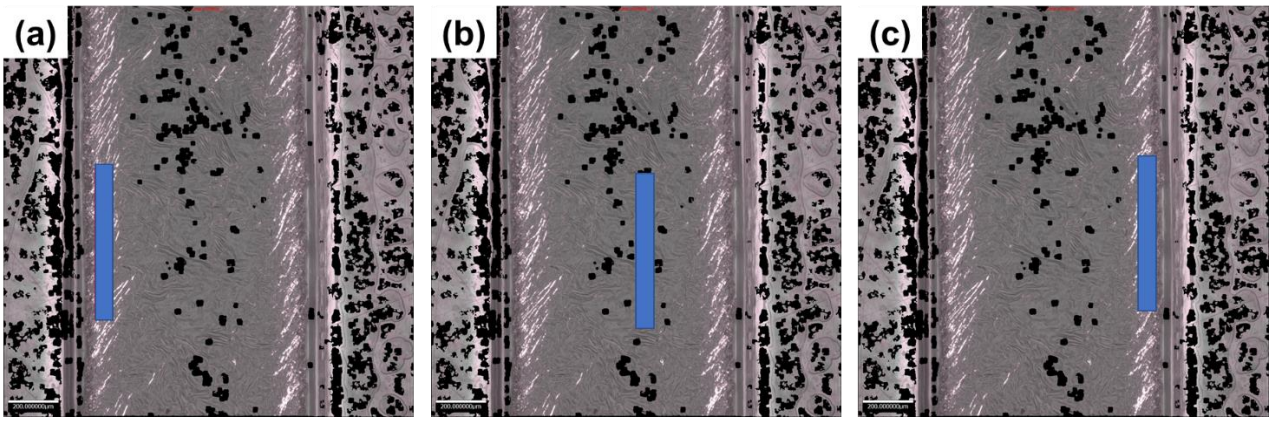

Figure S3 Optical images of linear pattern captured using white light interferometry. The blue shows the area used to calculate the surface roughness at various positions (a) left edge (b) middle (c) right edge.

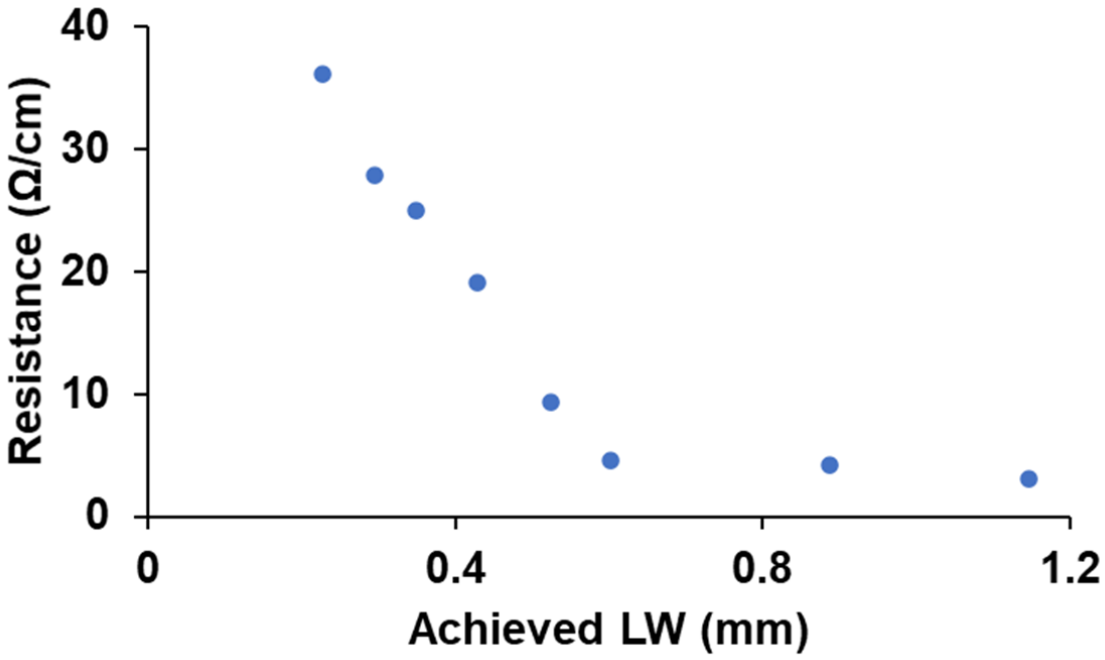

Figure S4 Plot showing the change in resistance/pattern length (Ω/cm) with achieved LW ranging from ~0.23 mm to 1.2 mm.

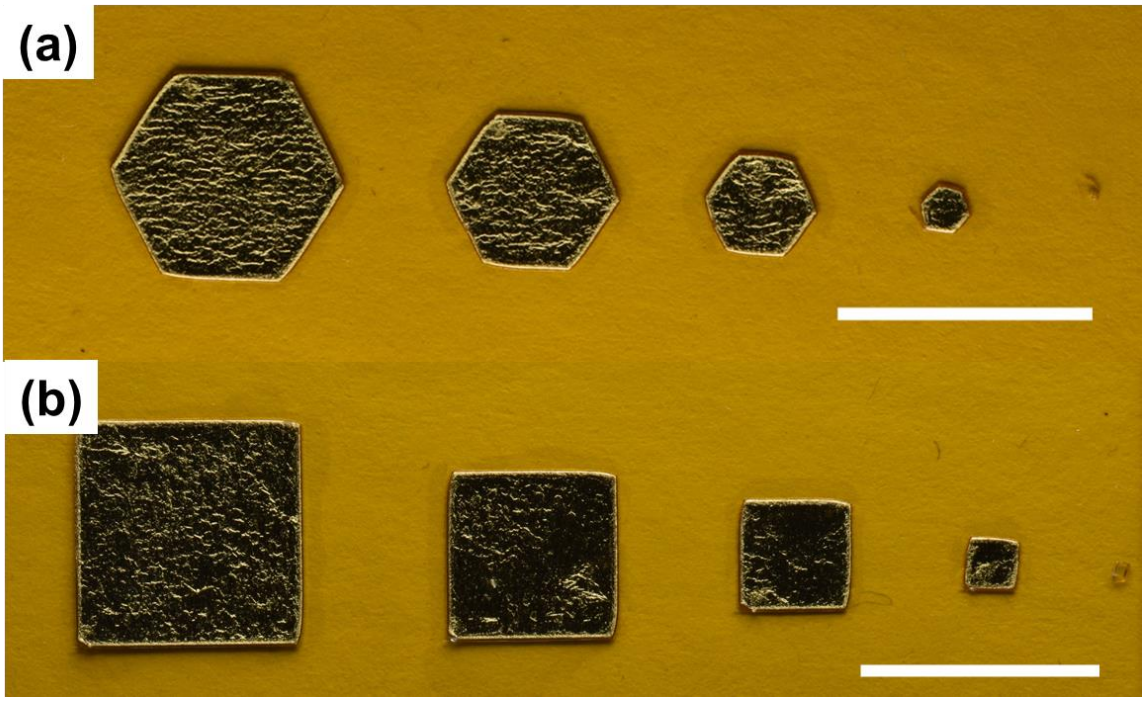

Figure S5 Image showing geometrical patterns like hexagon and rectangles patterned using xurography (Scale bar 1 cm).

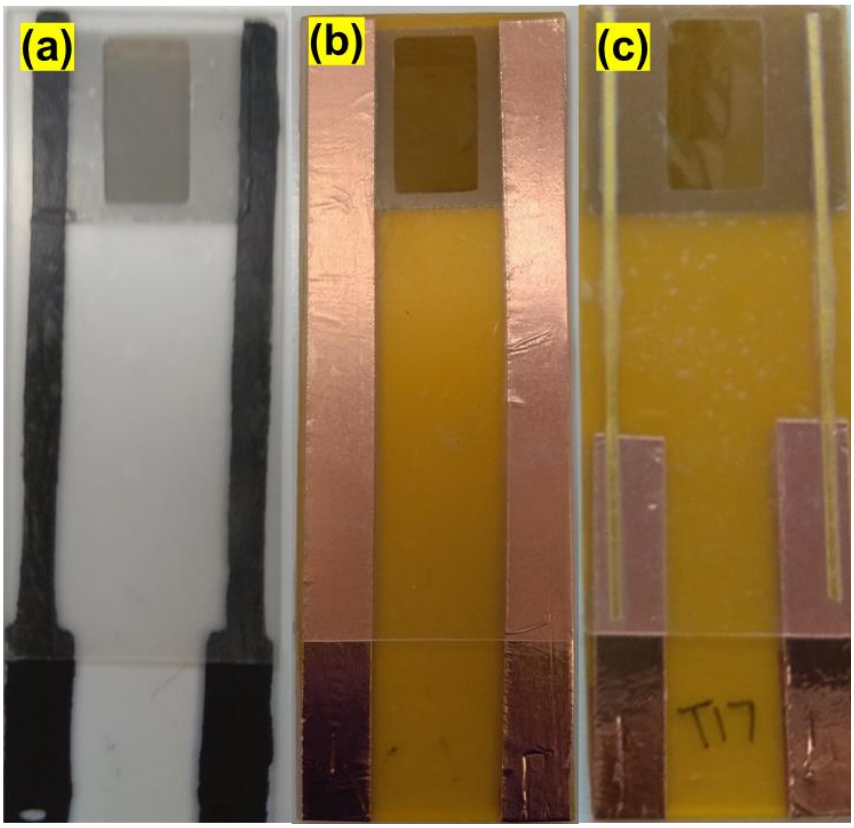

Figure S6 Electrode picture of GLC sensors with different contact electrodes (a) Carbon electrodes (b) Double sided conductive copper tape (c) Gold leaf electrodes (1 mm width).

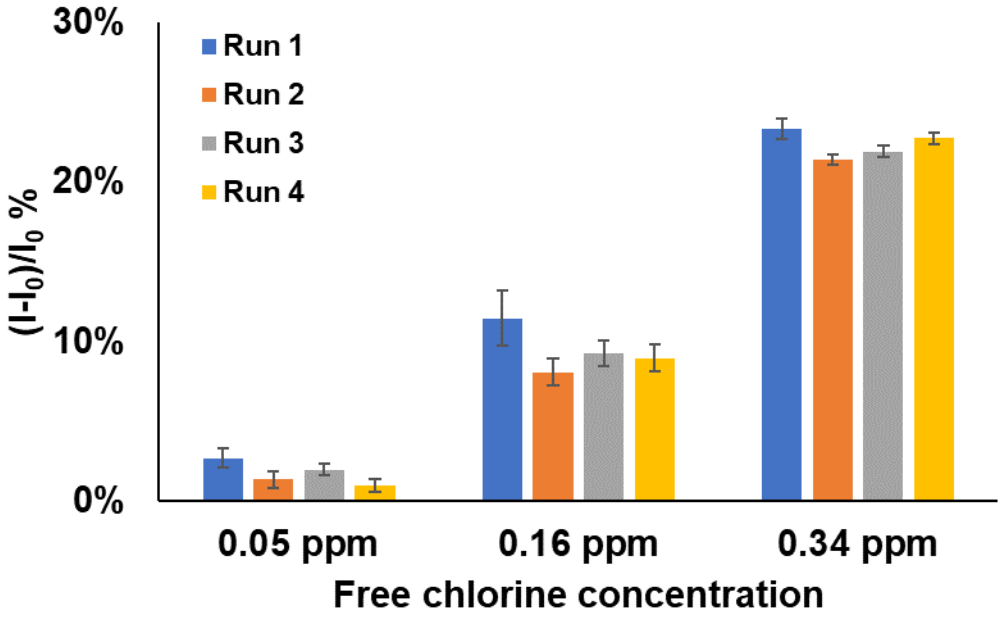

Figure S7 Sensor response for flexible chemiresistive sensor fabricated with gold leaf as contact electrode. The sensor was exposed to three free chlorine concentrations and then the sensor was chemically reset using the 0.1 M ascorbic acid.

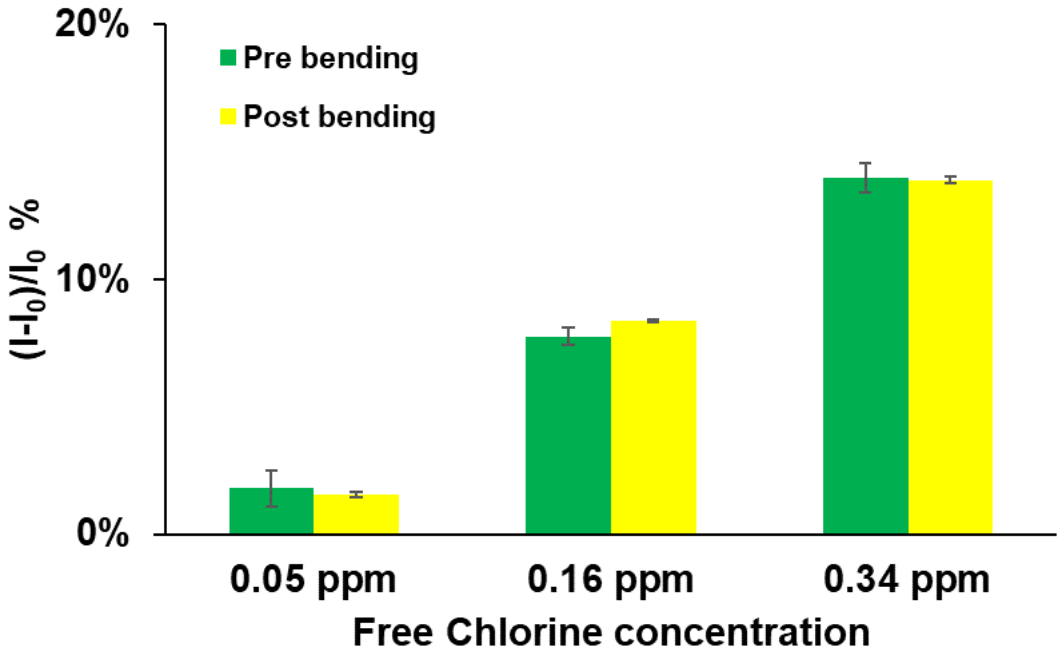

Figure S8 Sensor response for flexible chemiresistive sensor fabricated with screen printed carbon as contact electrode. The sensor was exposed to three free chlorine concentrations and the response was recorded pre (Green) and post bending (Yellow).

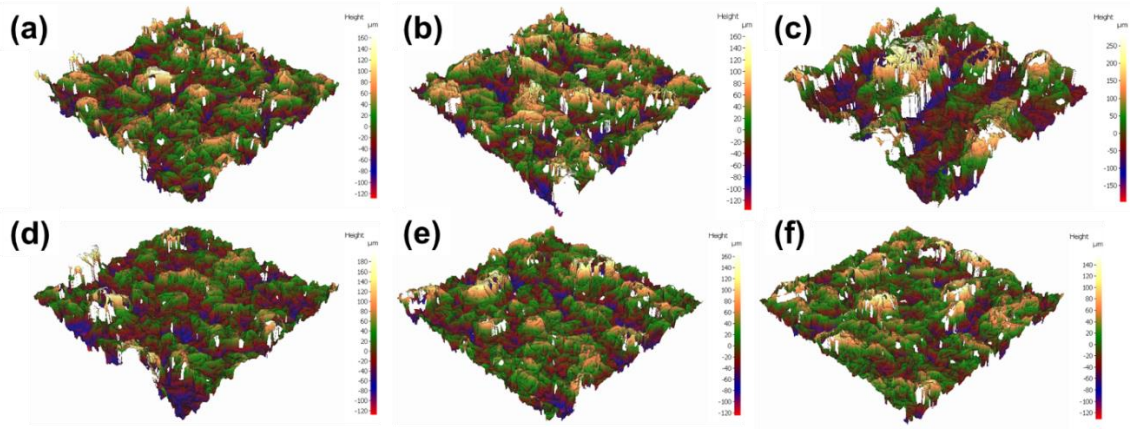

Figure S9 Surface profiles of wrinkled gold lead (a) to (c) Shrinking temperature 130ºC for different shrinking time (a) 5 minutes (b) 10 minutes (c) 15 minutes. (d) to (f) Shrinking temperature 160ºC for different shrinking time (d) 2 minutes (e) 5 minutes (f) 10 minutes.

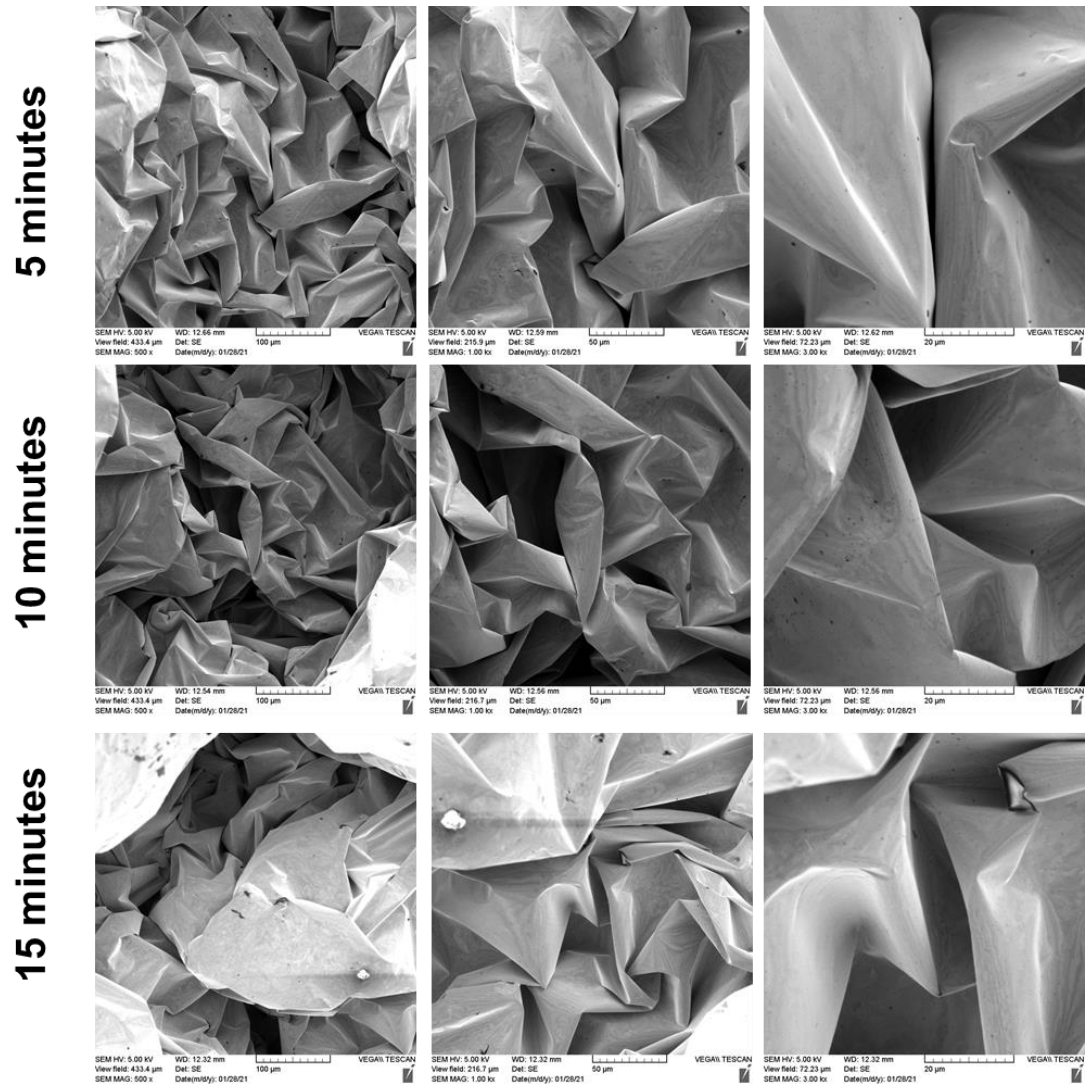

Figure S10 SEM images of wrinkled gold surfaces shrinked at 130 ºC and the time on each row represents the shrinking time for all three images in that row. Each row of images (Left to right) is arranged in decreasing order of scale from 100 µm (left) , 50 µm (middle) and 20 µm (right).

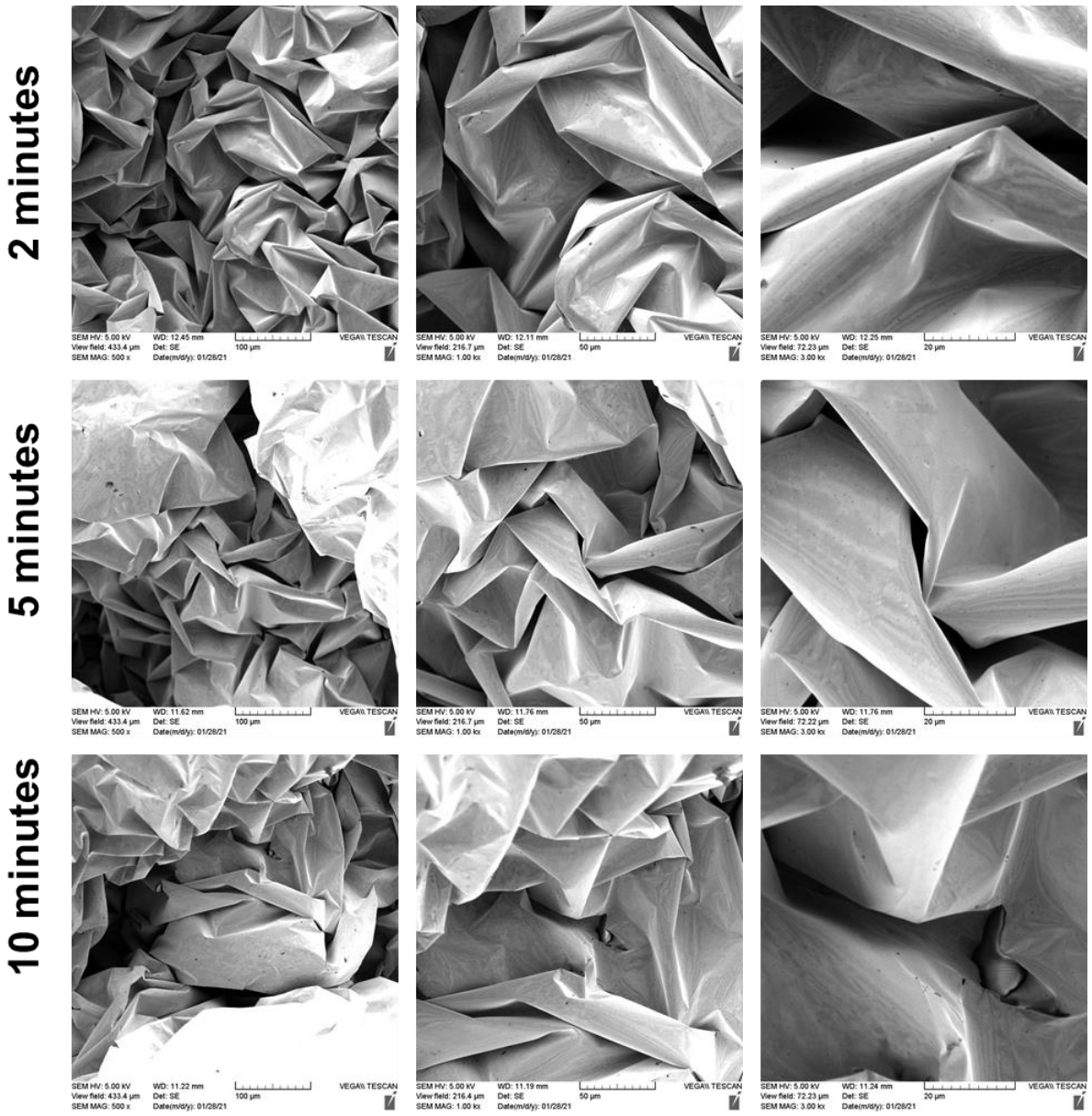

Figure S11 SEM images of wrinkled gold surfaces shrinked at 160 ºC and the time on each row represents the shrinking time for all three images in that row. Each row of images (Left to right) is arranged in decreasing order of scale from 100 µm (left), 50 µm (middle) and 20 µm (right).

Appendix 3

Supporting Information for:

A reagent-free hydrogen peroxide sensing using carbon nanotube chemiresistors with electropolymerized crystal violet and its applications in biological samples

Vinay Patel [1], Dipankar Saha[2], Peter Kruse [2], and P. Ravi Selvaganapathy [1,3*]

[1] School of Biomedical Engineering, McMaster University, Hamilton, ON, L8S 4K1, Canada

[2] Department of Chemistry and Chemical Biology, McMaster University, Hamilton, ON, L8S 4M1, Canada

[3]Department of Mechanical Engineering, McMaster University, Hamilton, ON, L8S 4K1, Canada

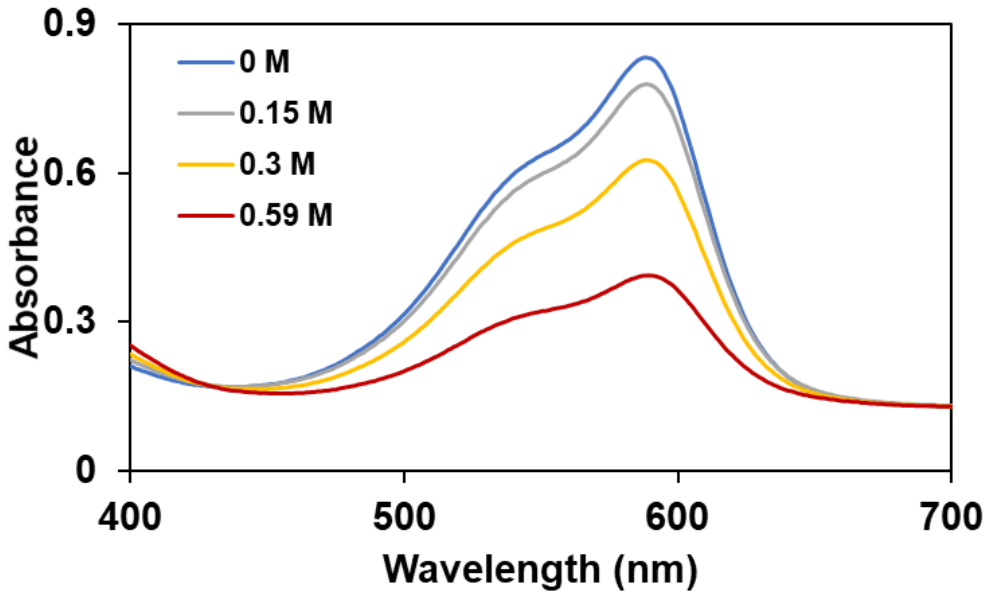

Figure S1 UV-Vis spectra of crystal violet (12 µM) in 0.1 M phosphate buffer (blue line) and in presence of three H_2O_2 concentrations.

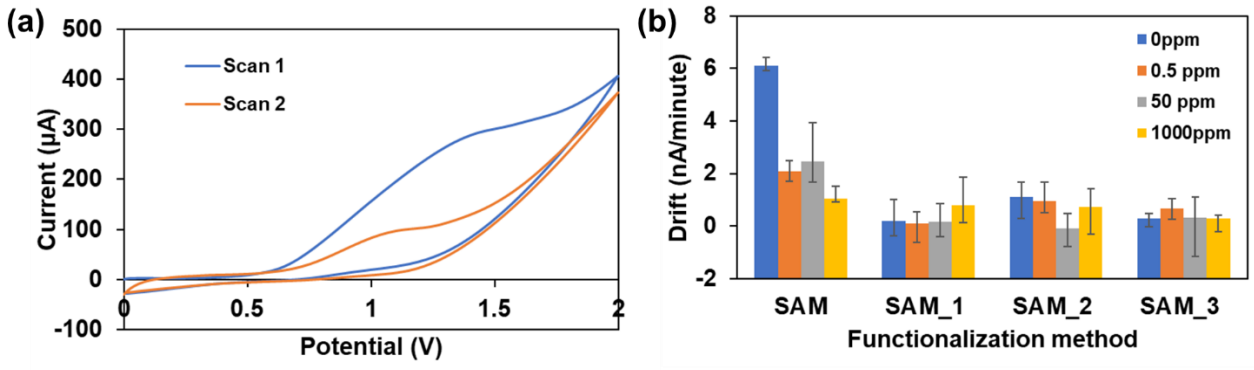

Figure S2 (a) Cyclic voltammetric scans for direct electropolymerization in 0.2 mM crystal violet and 0.1 M phosphate buffer. (b) Drift rate for different functionalization processes.

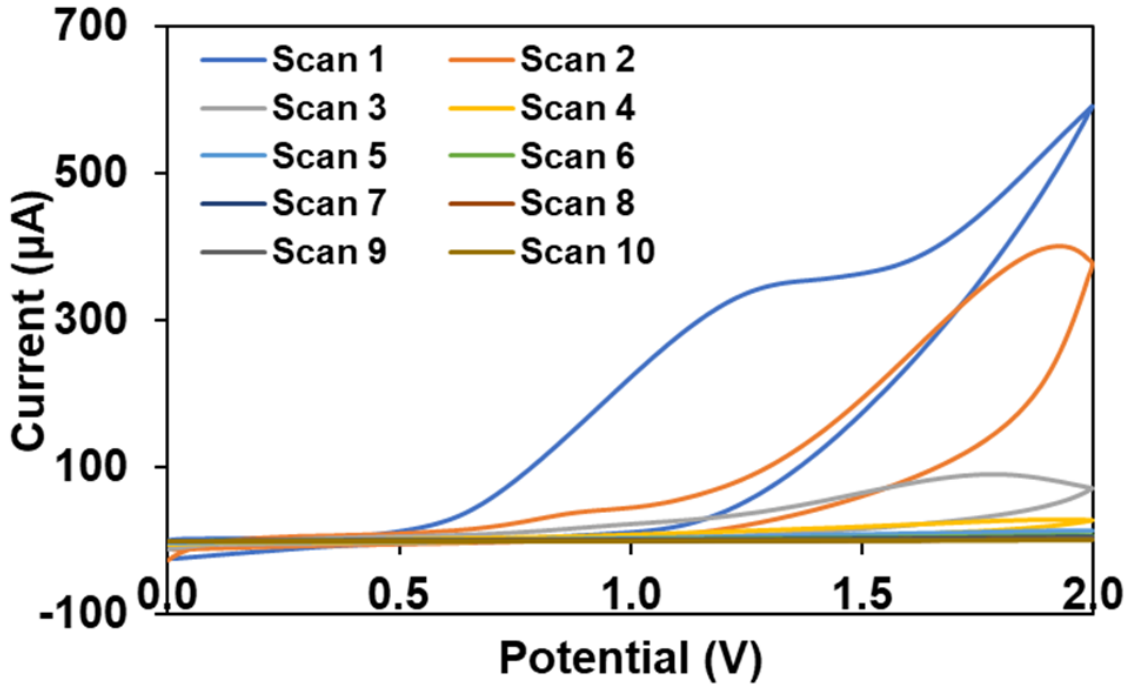

Figure S3 Cyclic voltammogram for electropolymerization of self assembled layer of crystal violet in 0.1 M phosphate buffer for scan cycles 1 to 10 scans.

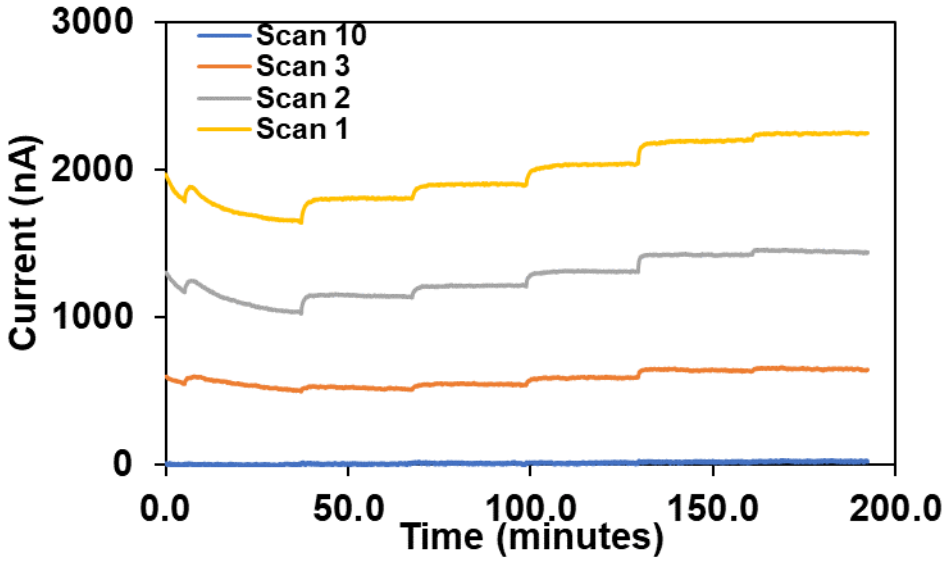

Figure S4 Effect of scan cycles on the conductivity of the SWCNT film.

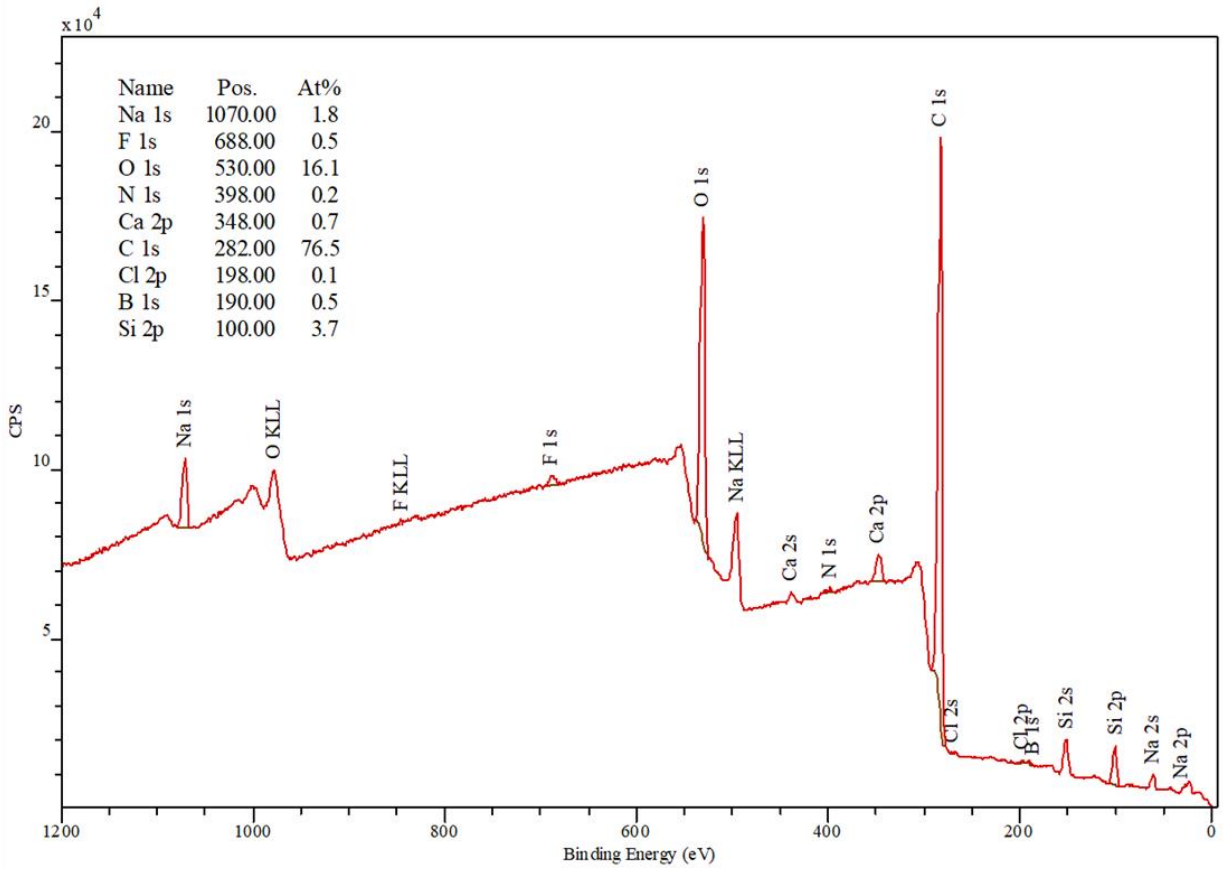

Figure S5 XPS Survey spectrum of Sample 1 (SWCNT film).

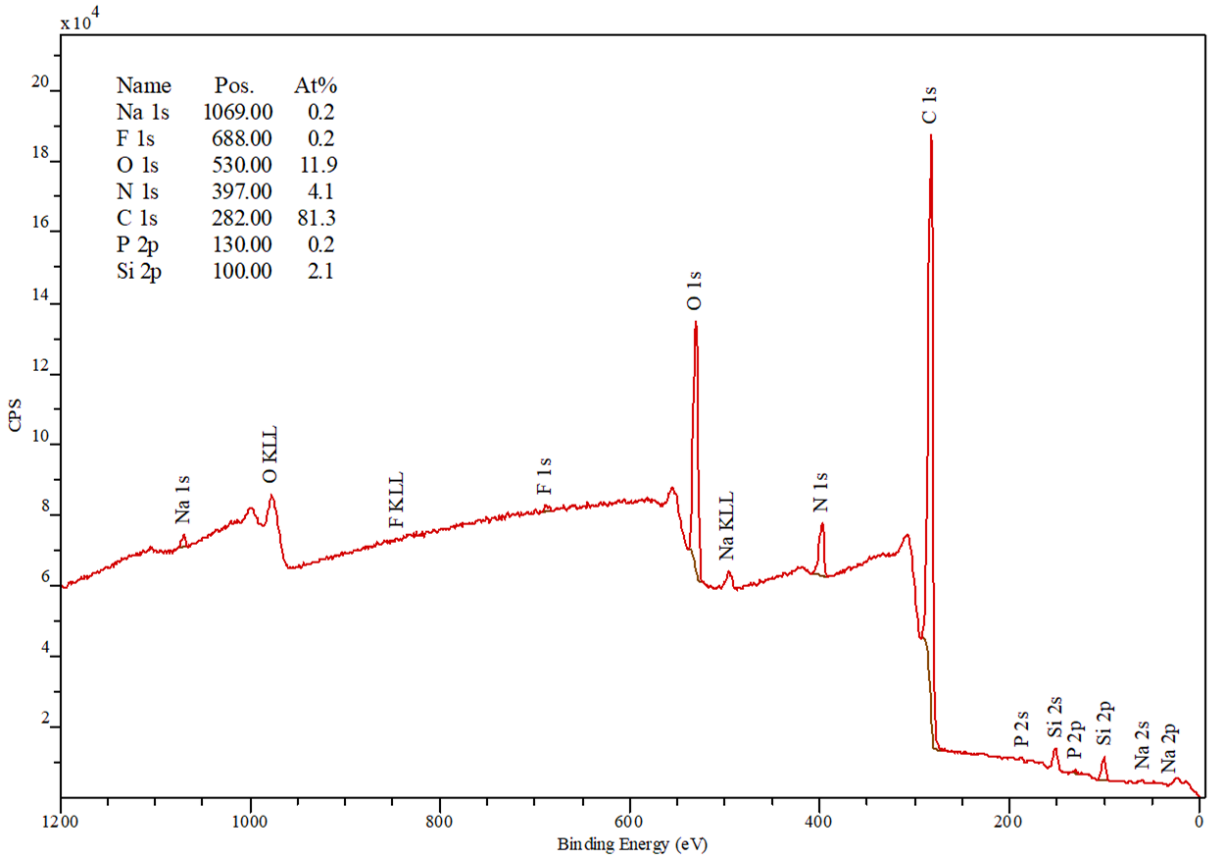

Figure S6 XPS Survey spectrum of Sample 2 (SWCNT film functionalized with SAM crystal violet).

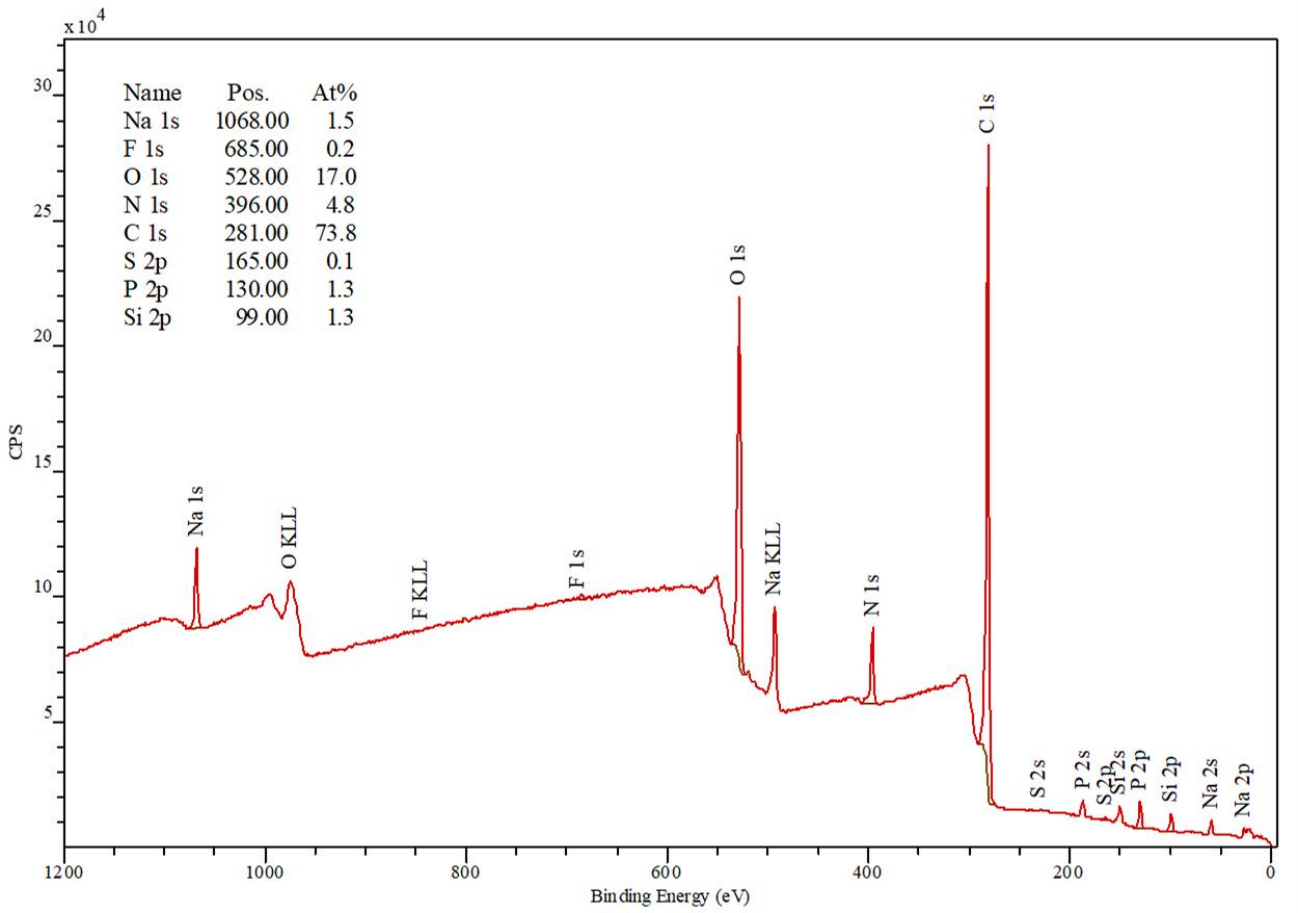

Figure S7 XPS Survey spectrum of Sample 2 (SWCNT film functionalized with SAM crystal violet).

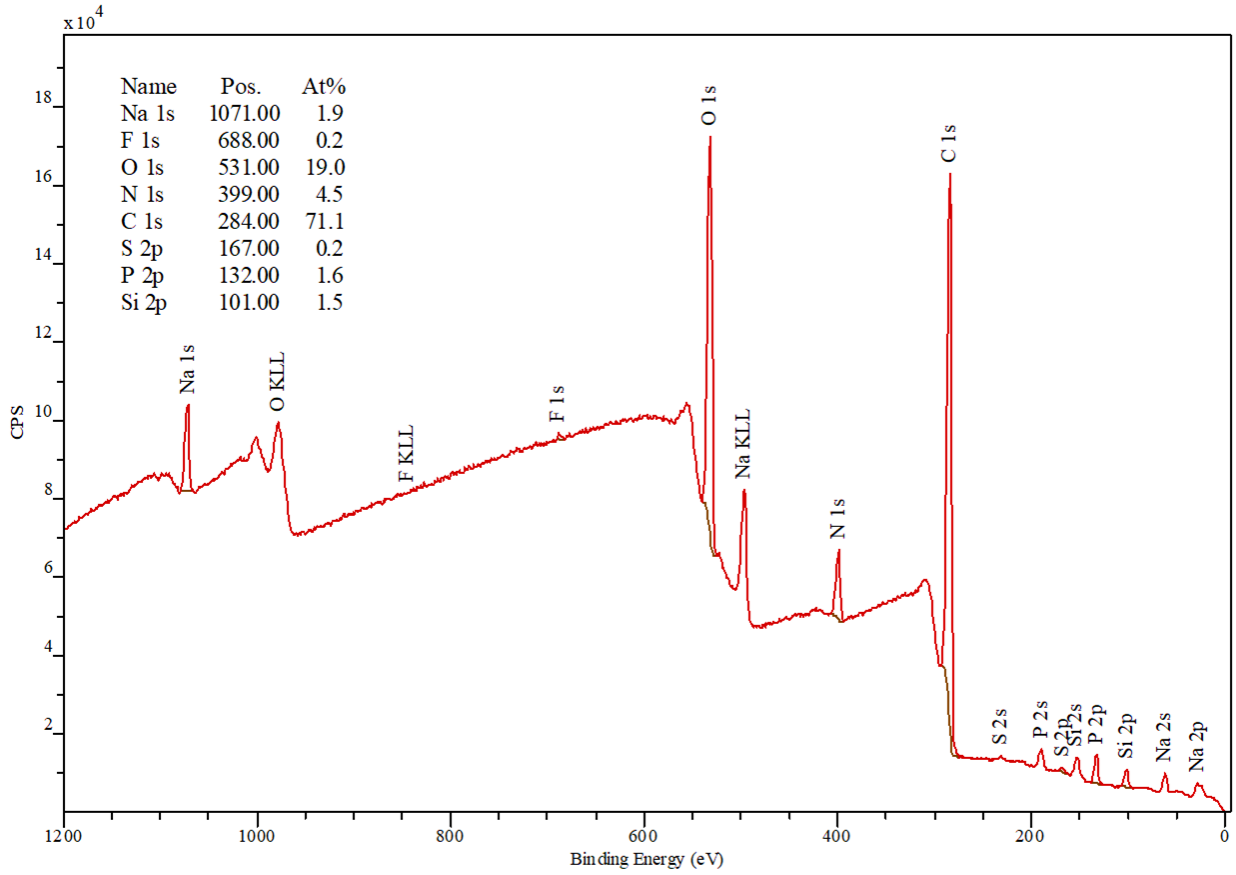

Figure S8 XPS Survey spectrum of Sample 2 (SWCNT film functionalized with SAM crystal violet).

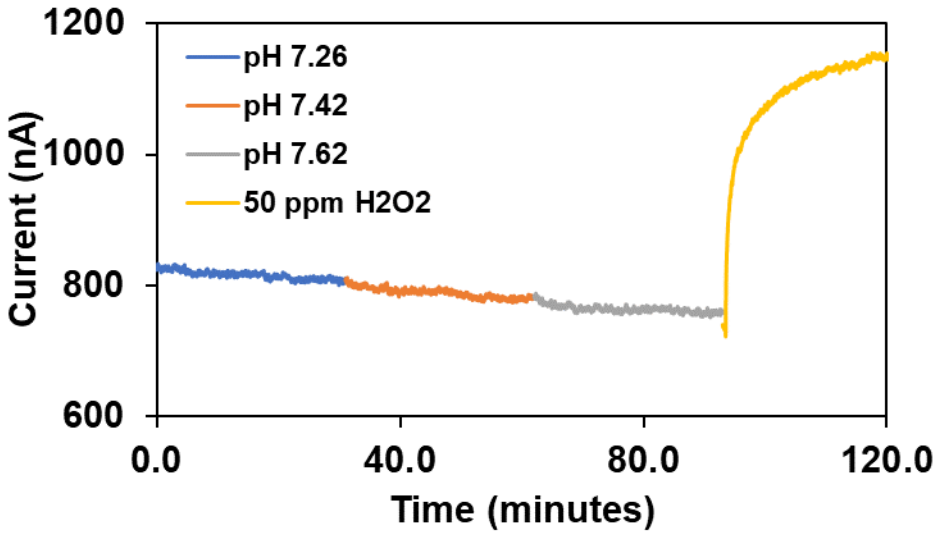

Figure S9 Current response of the sensor for three different pH solution followed by 50 ppm H_2O_2 solution.

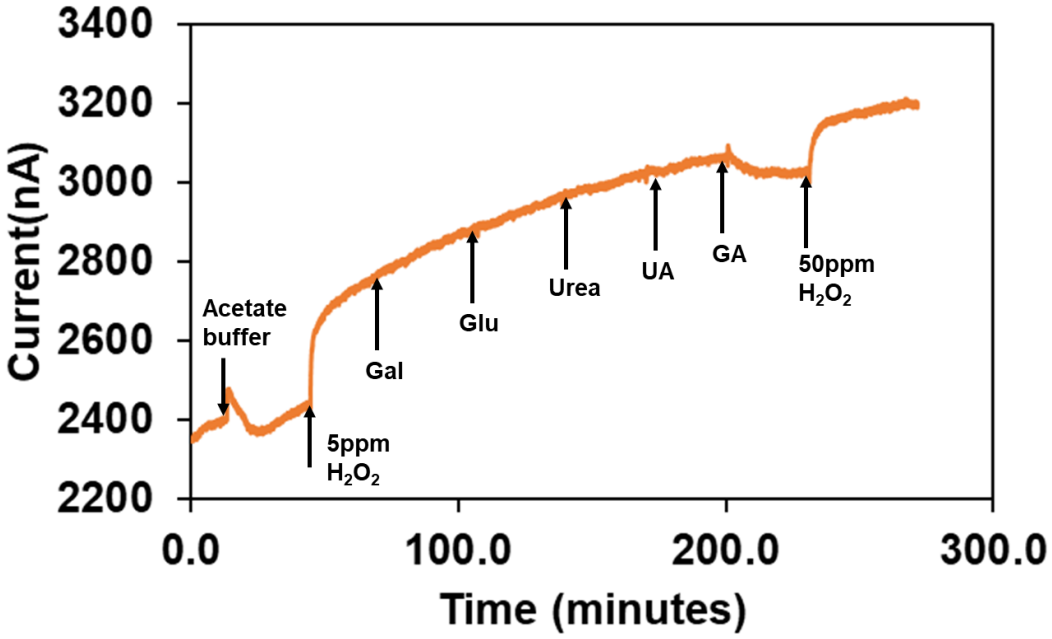

Figure S10 Effect of interfering species on the response of SWCNT sensors in presence of 5 ppm (0.15 mM) of H_2O_2. GA: Gluconic acid, Gal: Galactose, Glu: Glucose, and UA: Uric acid (n=3).